Hydrothermal carbonisation for the conversion of food waste to energy products

Jaime Eleazar Borbolla Gaxiola

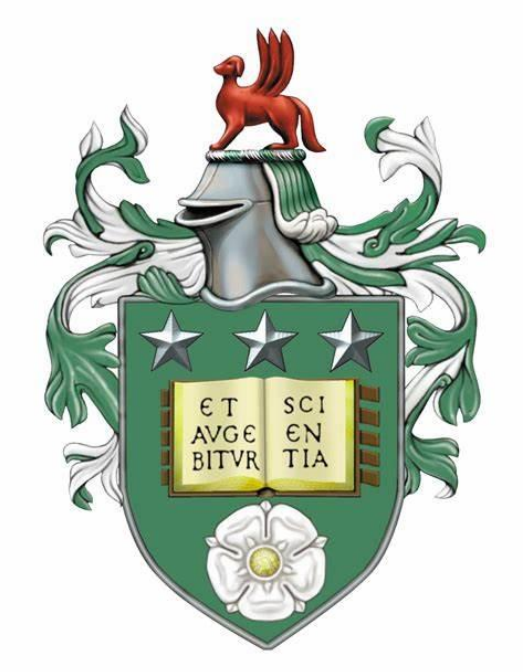

Submitted in accordance with the requirements for the degree of
Doctor in Philosophy in Chemical and Process Engineering

The University of Leeds
School of Chemical and Process Engineering

May 2022

The candidate confirms that the work submitted is his own and that appropriate credit has been given where reference has been made to the work of others.

Acknowledgements

I would like to thank firstly all the universal forces that allowed me to carry out my Ph.D. project in an institution such as the University of Leeds. It was truly a remarkable experience that I know will be treasured and undoubtedly held dearly in the years to come.

To my supervisors Dr Valerie Dupont and Dr Andrew B. Ross that were always open for consultation and support when needed. Even if I restrained myself from doing so more than I should have. I appreciate your tutelage and supervision.

To my wife Jessica that was always by my side, I felt her support and love at every step of the way, and even if we walked the same path, I am sure we had different experiences, you always understood that, and I thank you for it.

To my family, mother, father and sister, that even if we were separated by distance, your support was never in doubt. I could not wait to see you again.

Abstract

Food waste is an abundant biomass resource generated continuously all around the world. However, due to numerous technical challenges linked to the heterogeneous nature of food waste, its utilisation is neglected in large parts of the world and underutilised in others. An option for treating food waste is to feed it into synthetic fuel production plants. The core of the synthetic fuel route is a gasification stage to decompose biomass into light-weight gas molecules by partial combustion. However, food waste is not suitable to be treated by this technology due to its heterogenicity and high moisture content. In this regard, there is an emerging technology that locates itself as a potential link between food waste and the synthetic fuel route, hydrothermal carbonisation (HTC). The HTC is a thermochemical technology that consists of treating a solid feedstock submerged in water at sub-critical conditions. This technology can convert food waste into an enhanced solid fuel with coal-like properties, known as hydrochar. However, the HTC treatment of food waste is still significantly unexplored, marked by the lack of insight and studies focused on expanding the feedstock catalogue. Also, most of HTC studies have the one-response-at-a-time approach, which is counterintuitive with a technology known for the trade-off between its responses. Therefore, in this work the HTC of food waste was evaluated with a response surface methodology, using a central composite rotatable design for evaluating the effect of process parameters (temperature, reaction time, and solid load) and ultimately performing optimisation studies involving utilisation-responses and viability-responses. The results include the parametric analysis of the composition and fuel quality of hydrochar, the biomethanation properties of the process water and the validation of empirical models. Also, the HTC process optimisation includes energy efficiency and hydrochar responses with a desirability function.

Table of content

List of tables

List of figures

List of abbreviations

AD	Anaerobic digestion
ADF	Acid detergent fibre
ANOVA	Analysis of variance
BECCS	Bio-energy with carbon capture and storage
BMP	Biochemical methane potential
BTL	Biomass-to-liquid
CCRD	Central composite rotatable design
CCS	Carbon capture and storage
CHP	Combined heat and power
COD	Carbon oxygen demand
D	Desirability function
db	Dry basis
DOE	Design of experiments
DTG	Derivative thermogravimetric
ED	Energy densification
EJ	Exajoules
EMC	Equilibrium moisture content
EROI	Energy return of investment
EY	Energy yield
FAN	Free ammonia nitrogen
FC	Fixed carbon
FOG	Fat, oils and greases
FT	Fischer-Tropsch
FW	Food waste
GC	Gas chromatography
GHG	Greenhouse gas
Hf	Combustion stability
HHV	Higher heating value
HMF	Hydroxymethyl furfural
HRT	Hydraulic retention time

HTC	Hydrothermal carbonization
ISR	Inoculum-to-substrate ratio
kJ	KiloJoule
kWh	Kilowatt-hour
LCFAs	Long-chain fatty acids
LHV	Lower heating value
LPG	Liquified petroleum gas
MC	Moisture content
MSW	Municipal solid waste
NDF	Neutral detergent fibre
NOx	Nitrogen oxides
OCDE	Organisation for Economic Co-operation and Development
OFMSW	Organic fraction of the municipal solid waste
OLR	Organic loading rate
PID	Proportional integral derivative
PW	Process water
Q	Energy
R^2	Coefficient of determination
RSM	Response surface methodology
RT	Retention time
S	Combustibility index
SL	Solid load
SY	Solid yield
TC	Total carbon
TCD	Thermal conductivity detector
TGA	Thermo-gravimetric analyser
TIC	Total inorganic carbon
TOC	Total organic carbon

TS	Total solids
VFA	Volatile fatty acids
VM	Volatile matter
VSS	Volatile suspended solids
WV	Working volume
WWT	Wastewater treatment

Chapter 1. Introduction

Modern society is on all-time high energy consumption with a constant increase due to the population growth and the demand for goods. Energy supply and demand transcend the technical barriers and are interlinked to socio-economic issues. Moreover, main energy generation still heavily relies on fossil fuels, whose carbon emissions represent an environmental concern due to the relationship to the climate change phenomenon.

Great effort is thrown in recent decades searching for renewable alternatives to fossil energy. Harnessing energy from the sun, the air, the geothermal activity of the planet, and the mass of biological organisms inhabiting it. The development of these technologies has come a long way, and several have found commercial use, contributing to a significant share in the energy supply in some regions. However, renewable technologies still must compete with the fossil energy industry, which is already consolidated into society and the world economy.

Among the alternatives that could have an important share in the replacement of fossil fuels is the energy from biomass, or bioenergy. The potential of bioenergy lies in its wide abundance, and it is based on organic carbon. The latter shows its potential exploitation by thermochemical or biological technologies and infrastructure, while linked to the carbon cycle in a renewable manner. Nonetheless, the commercial implementation of bioenergy has been curbed by several issues. For instance, the polemical use of energy crops, which compete with the food market. Also, the seasonal availability fluctuation of different feedstock makes their application difficult. Moreover, more complex biomass sources present technological barriers that prevent their application in the current energy systems.

In addition, the next energy transition is encouraged to be developed in a multi-dimensional manner. Therefore, most recent efforts to incorporate bioenergy must be addressed considering the multiple implications not only related to technical feasibility but including societal concerns. The energy

trilemma illustrates this multi-dimensional implication consisting of three edges: 1) energy security involves the efforts to utilise the most domestic resources and diversify the renewable energy sources; 2) energy equity, points out the efforts for producing low-cost energy or policies to facilitate the economic access to energy for everyone; and 3) environmental sustainability, involving the efforts to decarbonise and diversify the energy sources (**Figure 1. 1**) [1]. This multi-dimensional approach for such as the energy trilemma allows the development of robust renewable energy systems, which are necessary to achieve the United Nations sustainable development goals, particularly goal 7 to “Ensure access to affordable, reliable, sustainable and modern energy for all” [2].

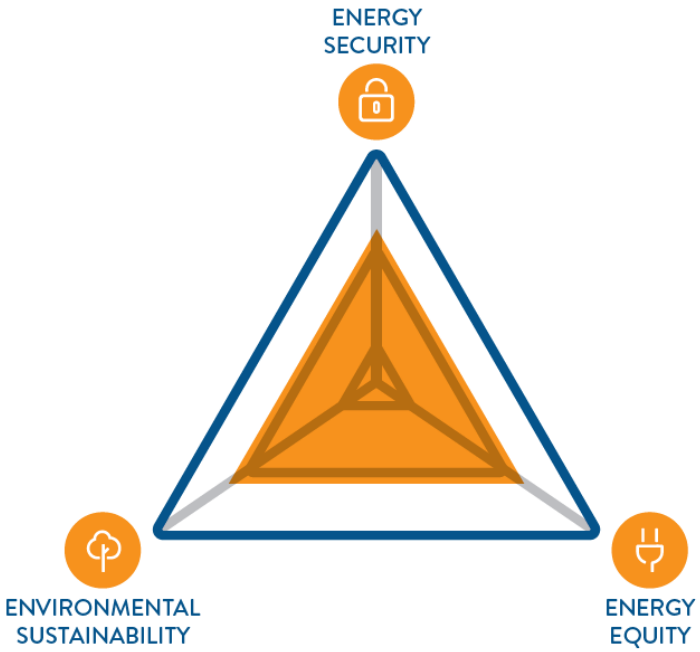

Figure 1.2 Basic scheme of the energy trilemma.

Based on the previous, the overall aim of this work is to address the utilisation of food waste as a biomass source for bioenergy production by employing hydrothermal carbonisation (HTC) as a pre-treatment technology, for further utilisation in the production of liquid fuels. The work evaluates the solid and liquid products, energetics, and utilisation options of food waste after being treated with HTC technology. Also, HTC products and energy analysis are evaluated with a multi-variable and multi-response statistical analysis for

enhanced insight into the effect of HTC parameters on the products of food waste for further statistical optimisation.

Regarding the energy trilemma approach on this project, for environmental sustainability, the obvious benefit is reducing the carbon emission by using renewable fuels from food waste instead of fossil fuels. Also, the proper disposal of conventional food waste is often energy consuming and carries an environmental impact causing pollution and the dispersion of pathogens. Regarding energy security, the conversion of raw biomass into hydrochar increases the densification and stability of the solid fuel, improving the storage ability. Moreover, the long period of storage of the solid fuel along with the continuous generation of food waste could address the supply of feedstock, thus reducing the fluctuation often related to biomass supply and assuring the production of biofuels. Also, in terms of energy equity, it is proposed that implementing an HTC process could allow the operation in decentralised units. Therefore, HTC could supply renewable fuels in remote regions that are off-grid with difficult access or distributions. Furthermore, the development of this technology and construction of process plants could provide jobs to the communities and added-value products to an abundant waste that is not in conflict with the food supply.

Food waste is a biowaste source with great utilisation potential and availability. For starters, it is estimated a worldwide generation of waste of 1.3 billons tons per year [3]. This statistic has not been updated to our knowledge by an official source and this one keeps being referenced. The most common methods for disposal of food waste include landfill and ocean dumping and given the large quantities produced, its disposal results in several inherent problems [4]. Both methods of disposal result in significant environmental impact due to the emission of greenhouse gases since approximately 45% of the carbon content in food waste is released in gaseous form after landfill [5]. A large fraction of the released carbon is in the form of methane, which has more than 20 times the greenhouse effect of carbon dioxide [6]. In addition, the decomposition of organic matter after dumping and landfilling causes nutrient imbalances in soil and water bodies. To counter these problems, several regions have developed more advanced methods of disposal with the most common being composting and anaerobic digestion (AD) [4]. However, these technologies

have their technical challenges such as long processing times and the need for pre-treatment of feedstock to achieve optimal conversion.

In recent years, hydrothermal carbonisation has positioned itself as a potential technology to valorise food waste, as it overcomes many of the technical challenges of using food waste (FW) as a feedstock in comparison to other technologies. HTC involves the treatment of biomass submerged in water at sub-critical conditions, at temperatures ranging from 160 to 280 °C, and autogenic pressures, resulting in a solid hydrochar and process water containing dissolved organics and inorganics. The solid product has coal-like properties and is commonly known as hydrochar, to differentiate from the biochar produced by dry-carbonisation technologies such as pyrolysis. The hydrochar exhibits superior properties to the original biomass, including enhanced stability, storage, and energetic value [7]. Moreover, there is a considerable volume reduction from the original feedstock that facilitate its further transportation, storage, and utilisation. The numerous advantages of HTC make it more suitable to treat food waste in comparison to other technologies, such as pyrolysis or gasification, because HTC does not require the energy-demanding drying process, which makes it more energetically favourable [8]. The utilisation of HTC to treat high moisture biomass can reduce its carbon footprint compared to other treatments without generating odour. HTC offers several advantages to biological treatments, such as a shorter process time, as it takes only hours instead of days. Also, HTC could employ FW with variable chemical composition, a factor that could significantly affect the performance of biological processes such as AD [8]. In addition, due to high temperatures and sub-critical water conditions, HTC eliminates pathogens and inactivates other potential organic contaminants [9].

In recent years, the use of HTC for the treatment of food waste has gained momentum, and experimental and literature reports are more numerous every year. Hydrochar from food waste covers different end-use purposes, including soil conditioner or fertilizer [10,11], adsorbents of metals [12], and nitrogen and phosphorus [13,14]. Nonetheless, the use of hydrochar from food waste as solid fuel either for combustion or gasification is still the major proposed end-use [5,15–22]. These experimental works along with the feasibility and

process evaluation [6,8,23,24] have made advances in the development of the technology for food waste valorisation or treatment.

However, it has been noted that most studies focus on expanding the feedstock options and evaluating often one variable at a time [25]. This suggests that the evaluation of how multiple variables and their interaction affect the HTC process represents a significant gap in HTC research. Filling this gap is an important step in continuing the maturation process of the technology. Thereby, studies and multi-response analysis could help develop opportunities for HTC technology application. Finding the optimal conditions is a crucial step for assessing the viability of HTC as a commercial technology and achieving its implementation as a biomass pre-treatment in larger processes. However, the optimisation of this process is hindered by the complexity of the HTC reaction and further complications due to the heterogeneity of food waste feedstock [26]. Thus, statistical and empirical models are a powerful tool to develop the optimization of the HTC process.

Previous studies have used response surface methods for understanding the effect of multiple variables on HTC parameters such as temperature, reaction time, solid load (the percent mass of dry solids in the HTC reactor), and pH [27–29]. However, studies on optimization are limited, while few graphical optimization studies have been reported for maximising hydrochar yields [30,31]. Nonetheless, this optimization approach is limited to one response at a time. In this regard, more recently, multiple-response numeric optimization of HTC is beginning to appear using the desirability method, although once more with limited responses and variables [32,33]. Therefore, combining end-utilization multi-responses with multi-variable optimization could provide a better insight into the HTC process and overcome the trade-offs of the reaction.

In summary, it is crucial to find how to utilise wet biomasses to address the energy trilemma. Food waste is an abundant waste worldwide with a significant energy content, which could be added to the already highly abundant lignocellulosic and woody biomass. However, this type of feedstock exhibits a technical challenge for the current technologies due to its diverse chemical composition, and high content of water. The latter challenges the

transformation, storage, and supply of this feedstock, thus reducing the capacity to harness its energy content. Hydrothermal carbonisation is a technology that has repeatedly shown excellent results for increasing the energetic density of wet biomass with good energy efficiencies. Nevertheless, there is still a knowledge gap on the effect of the process parameters on the products from processing the food waste and their proper optimization. Moreover, the optimization of the process could increase the attractiveness of utilising food waste via HTC in a ´tailored´ process for specific products.

1.1 Overall aim

This project attempts to bring insight into the effect of HTC process conditions on the products from hydrothermally treated food waste. The influence of the HTC parameters temperature, retention time, and the solid load of food waste on the products hydrochar and process water, and how these parameters impact their further applications. Moreover, finding proper conditions involving the product compositions and their energy content would advance the utilisation of food waste and the development and commercialization of HTC technology.

1.2 Objectives

1. Perform and design experiments for the understanding of the implementation of HTC as a pre-treatment of food waste for the conversion into energy-dense hydrochar.

    1a. Evaluate the effect of process conditions on the composition of hydrochar and perform a significance test of the parameters.

    1b. Perform individual response optimization by desirability function.

2. Evaluate the thermogravimetric properties of hydrochar and the effect of the process variables. For the assessment of utilising the hydrochar in thermochemical processes such as incineration or gasification.

3. Assess how the process parameters of HTC affect the liquid product of HTC (also referred to as ‘process water’).

3a. Evaluate the effect of HTC parameters on the composition of process water.

3b. Evaluate the effect of HTC parameters on the bio-methane production capability of process water.

4. Perform an energy analysis of different energy streams and how the process parameters affect the energy efficiency.

4a. Evaluate the effect of HTC parameters on the energy efficiency processing food waste process.

4b. Evaluate the impact of implementing biomethanation of process water on the energy efficiency of the HTC process.

4c. Evaluate the impact of the drying stage on the energy efficiency of the HTC process.

4d. Perform an optimisation test including energy efficiency responses.

5. Propose recommendations for future work in the areas of developing HTC technology and its application for food waste.

Chapter 2. Rationale for the research and literature review

2.1 On bioenergy and food waste

The energy obtained from biomass is often referred to as bioenergy and has an important role in the replacement of fossil fuels. Commercially, bioenergy found a partial share in the energy sector in the form of biofuels. These biofuels are now known as first-generation biofuels and are produced from energy crops. These types of biofuels are used in limited countries, including the United States of America, using bioethanol from maize, and Brazil, using bioethanol from sugarcane. However, even if the implementation of first-generation biofuels is in theory beneficial in environmental terms, it is now known that several implications compromise sustainability. The most evident problem with first-generation biofuels comes with the food vs fuel debate. In this debate, it is discussed that destining crops for energy production may harm food security. This concern is founded on the arguments that using food for energy purposes will affect food supply and food prices [34].

In addition to the widely discussed concern of food vs fuel, there are now identified various problems regarding first-generation biofuels that must be addressed when designing systems for second-generation fuels. Mohr and Raman [34] proposed a series of challenges facing the implementation of second-generation biofuels. Among these challenges are the large-scale land acquisition, GHG balance of exploiting forestry and agricultural biomass, biodiversity concerns, and local social impacts. Large-scale land acquisition recognizes the possibility of designating large parts of land for energy production could lead to violations of peoples' rights and livelihood. In the case of carbon emission balance, utilising resources from the forest, grasslands peatlands, and energy crops for energy production could lead to the reduction of carbon saving stocks. Also, intensive production of energy crops will require the consumption of large quantities of agricultural additives such as fertilizers, which are produced mainly from fossil sources. Regarding the local social impact concerns, they are based on not considering the local population for different projects, leading to displacements, land grabbing, impact on air quality, transport emissions, and aesthetics of local landscape [34]. As part of the lessons learned from first-generation biofuels, it is argued that the artificial

separation of economic, environmental, and social considerations when designing a bioenergy process must be avoided to maximize sustainability [34].

A big part of the generated biomass is a by-product of a waste of productive activity, sometimes referred to as ‘biogenic residues’ [35,36]. Biogenic residues could include livestock manure, agricultural residues such as straws, forestry wood residues, industrial and construction wood residues, municipal solid waste, and sewage sludge, to mention some [36]. This makes it a challenge to find a technology able to transform different biomass feedstock in the same process [37]. Hence the need for the development of feedstock-specialized technologies.

This scenario causes an unbalanced effort in researching technologies for specific biomass sources. Woody biomass is the most studied biomass source to the point that the term ‘biomass’ is often reserved for this type of source [38]. Following woody biomass is lignocellulosic biomass, which differs from woody biomass due to the lower content of lignin and has the advantage that most of their sources classify as wastes [39]. Nevertheless, they exist the called ‘non-lignocellulosic’ biomass sources. This biomass category includes sources with high abundance, many of which are from human activities. Such as Municipal solid wastes, sewage sludge from wastewater treatment, and animal manures from large livestock industries. As well as other non-lignocellulosic feedstock from the biotechnology industry such as algae and yeast biomass [40]. Thus, this type of biomass could be called biowaste [40].

The availability and energy potential of biowaste feedstock are not rigorously estimated. Among the reasons complicating the estimation of biowaste availability are the improper recording of data and the delay in the publication of collected data [41]. Another reason is the lack of a standardized estimation method for data generation [42]. This could explain the scarce number of studies on the availability and energy potential of biogenic residues. Nevertheless, the found studies suggest that the biogenic residues have significant potential to exploit. For instance, Brosowski et al. [41] estimated that the unused biomass in Germany represents close to 0.5 EJ, and corresponds mainly to logging residues, livestock manure, and cereal straw,

and calculated up to 1 EJ by adding the biomass currently in use. Also, Milbrandt et al. [42] estimated the availability and potential of ‘wet residues’ in the United States of America. They reported potential of 1 EJ from livestock manure, FOG (fats, oils, and greases), food waste, and sewage sludge. This shows the abundance and variety of biomass sources, as well as the opportunities for developing technologies to harness non-lignocellulosic feedstock.

The utilisation of abundant biogenic wastes, such as food waste, covers several of the mentioned challenges for second-generation biofuels. This approach exploits the energy contained in a waste that already has to be treated for environmental and health and safety reasons. Also, it opens the opportunity for a circular economy in communities. In addition, on the contrary of other alternative energy sources, even if we do not exploit the energy contained in the biomass, there is still the necessity to apply energy at its proper disposal to avoid environmental damage. However, aside from their great potential, energy from biowastes has several challenges to overcome. For starters, there is no technology or system which could efficiently transform all biomass sources [36], and current technologies used for wood and lignocellulosic biomass are inadequate for the more diverse and with high moisture content biowastes. Also, their low energy density increases the difficulty of transport and storage, which increases the cost of its logistics and limits their utilisation at an industrial scale [43]. Therefore, it could be necessary a treatment step prior to its utilisation, and the technology to implement them is not properly developed [40].

This project is focused on the use of food waste for energy production. Aiming to advance its feasibility to be used as feedstock for liquid fuels for the transport sector. Next will be discussed the food waste problem and the proposed route to transform and utilise it.

2.1.1 Food waste

According to the Food and Agriculture Organization of the United Nations (FAO), food waste (FW) is defined as any food destined for human consumption that is discarded. Whereas food loss encompasses the loss of quantity and quality of food during its production, mainly due to inefficiencies in the supply chain and logistics [44]. Food waste is generated either directly from agriculture, as a waste from the food industry, or from final consumers, often leading to large amounts of food waste entering municipal waste streams. An estimation calculated a worldwide food waste of 1.3 billion tons per year [3]. Food waste represents one-third of the total food production [45]. This number represents a significant fraction of the municipal solid waste, varying from country to country from 25 to 70% of the total mass [9]. These quantities of food waste are estimated to represent over 1 trillion USD loss [6]. This shows the high availability and supply of this waste resource.

In addition to the large quantities of food waste generated worldwide, its disposal brings up other inherent problems. The most common methods of disposal are landfill and ocean dumping [4]. These two methods of food waste disposal have a significant environmental impact on the biodegradability of food waste [5]. It is estimated that close to 45% of the carbon content in food waste is released in gaseous form after landfills [6]. A significant extent of the decomposed food waste is turned into methane, which presents more than 20 times the greenhouse effect of CO_2. It was estimated that by 2011, the methane released in landfills was the equivalent of 4.4 Gton of CO_2 per year [6]. In addition, the decomposition of organic matter after dumping and landfilling causes nutrient imbalances in soil and water bodies.

Therefore, food waste is a biomass source with great potential due to its high abundance and worldwide distribution and generation. Also, its treatment is already required for reducing the environmental impact and preventing health and safety issues.

2.1.2 Food waste utilisation

Although food waste has a great potential as feedstock. There are still major technical challenges hindering its exploitation for energy or chemical production. The main factors limiting the exploitation of food waste lay in the nature of the biomass itself. The nature of food waste includes a variable and heterogeneous composition, based on three major biomolecules (carbohydrates, proteins, and lipids). The high moisture content of food waste limits the technologies able to treat it without a drying stage, and its low energy content makes it unfeasible to utilise [9].

These features create numerous technical problems that limit the technologies for the efficient disposal or utilisation of food waste. The most common alternatives to dumping methods include composting and anaerobic digestion. However, these technologies have their technical challenges such as long process times and the need for pre-treatment of feedstock, such as the saccharification stage, for optimal operation of the biological system [4].

Among the possible technologies capable to exploit energy from food waste, transforming food waste into liquid fuel directly is a complicated task, most of them upgrade it into an energy carrier in gas or solid-state. Thus, to produce liquid fuels as the end-product of food waste utilisation, it is crucial to evaluate the integration of various technologies with several upgrading steps. Its low energy density is one of the major drawbacks of the exploitation of energy from food waste. To cope with this issue, biomass is proposed to be treated or transformed into a different material, with higher energy density or easier handling. This material transformation step is known as ‘upgrading’ [46]. The main advantage of the upgrading step is that it converts low-value biomass into a suitable material to be incorporated into current energy systems, working as a substitute for fossil energy carriers [46]. Therefore, upgrading food waste into a more attractive energy carrier could increase the utilisation and application options to exploit most of the energy contained in this feedstock.

The technologies for biomass upgrading vary according to the desired material, or fuel. It could be converted into liquid, gas, or solid fuels [47]. However, the upgrading step has its challenges, such as increasing the

complexity of the complete process, thus, increasing investment cost [46]. Due to the nature of food waste, technologies able to exploit energy from it are few and the effectiveness is limited. These technologies could be classified into two categories: biological and thermochemical [39].

Although biological and thermochemical conversion technologies have efficient and commercial applications for simpler feedstocks, both are limited when treating food waste. Biological technologies include fermentation and digestion processes, they use microorganisms as the catalyst for biochemical reactions. The drawbacks of biological conversion are long processing time, pre-adjustment of feedstock, only efficient for feedstock high in free sugars, and limited products. Anaerobic digestion is one of the mature technologies for treating food and other biowastes. However, even if this technology is mature for specific feedstocks, its utilisation for food waste is recognized to have several technical limitations, including operational bottlenecks, low food collection efficiency, unprofitable projects, difficulty in feedstock procurement, and high auto-consumption of the produced electricity and heat [48].

In the case of thermochemical technologies, common technologies dealing with wastes are incineration, pyrolysis, and gasification [9]. These technologies utilise high temperatures, pressures, and inorganic catalysts to transform feedstock directly into heat, in the case of incineration; bio-coal, bio-oil, and gases by pyrolysis; and synthetic gas by gasification [9,49]. These technologies required a pre-drying stage to transform efficiently the biomass. Thus, efficient treatment of food waste is heavily hindered by the high moisture content of food waste.

An option to commercially transform food waste would be to incorporate it into liquid fuels market. One approach to convert food waste into liquid fuels is via the route of synthetic fuels. This route includes several steps of fuel upgrading with a core, energy-intensive step of feedstock decomposition into syngas, this would be followed by much lower energy consuming catalytic synthesis into fuel. In this case, the well-known Fischer-Tropsch (FT) technology can synthesize a wide selection of liquid fuels for different transport end uses. Including food waste as feedstock in the synthetic fuel route could open great opportunities for commercializing bioenergy in the current market. However,

the utilisation of this technology to exploit energy from food waste is limited by the gasification stage. As mentioned earlier, the nature of food waste is a hurdle to the application of gasification. Nonetheless, there is an emerging technology able to overcome many of the challenges set by the complexity, heterogeneity, and water content of food waste: hydrothermal carbonisation (HTC). HTC is the main technology considered in this work as the first upgrading step for food waste. The implementation of HTC could allow the inclusion of food waste in production lines for liquid fuel. In this work, HTC is proposed as a pre-treatment of food waste that will enable the utilisation of food waste in a Biomass-to-Liquid process, including the gasification followed by the Fischer-Tropsch route.

2.1.3 Transport sector and the synthetic fuel route

The total energy consumption, transport energy included, will continue to increase in the next decades mainly due to the emerging markets in developing countries. The transport sector represents a major share of the total energy consumption globally. Twenty years ago, the energy from the transport sector already represented 21% of the total energy consumption worldwide, with a net energy value close to 86 EJ/yr. Also, the transport sector accounted for 14% of greenhouse emissions and around 25% of CO_2 emissions [50], or 37% of CO_2 emissions from end-use sectors with 7.2 Gt in 2020 [51]. It is argued that the de-carbonization efforts in the transport sector are lagging 10-30 years in comparison with other sectors. Liquid fossil fuels still represent 90% of the total transport energy demand [52]. This argument is supported by the fact that the shares of fossil sources in transportation have not changed in the last 25 years [52]. Therefore, de-carbonizing the transport sector is a global concern that must be addressed.

The transport sector has not had a significant technological transformation that allows a significant de-carbonization. it is subjected to several challenges preventing an easy transition out of the current system. For instance, the dependency on petroleum oil, accompanied by the volatility of the oil market and the geopolitical uncertainty that follows, and the pressure for reducing

greenhouse gas (GHG) emissions [53]. The next technological transition in the energy sector should address all these matters.

However, reducing the fossil fuel dependency in the transport sector presents titanic challenges, that could vary in political, socio-economic, or technical nature. First of all, it must be noted that the complete infrastructure for transport is built around the properties of fossil fuels such as energy density, stability, and combustion characteristics [50]. Among the outlooks for the next decades, the total consumption of these liquid fuels will continue to increase led by the non-OCDE countries (Organisation for Economic Co-operation and Development), especially for gasoline and diesel [52]. Also, it is envisioned that air transport will continue to increase worldwide [51,54]. Furthermore, is projected that liquid fuels will continue to be predominantly consumed in the transport sector due to their energy density, chemical properties, and cost [54]. Therefore, the usage of liquid fuels for the transport sector will continue increasing and will not easily transit into a different energy form. An overwhelming share of the liquid fuels consumed is produced from fossil oil. There are estimations that 98% of the energy consumed for transport comes from a fossil source, of it, gasoline and diesel make up the bigger share [51].

After decades of no visible direction of strategic decarbonizing efforts of the transport sector, in last years has been a forceful push for the electrification of the transport sector. On one side, is the idea of an abrupt electrification policy pushing for a planned ban of internal combustion vehicles in countries such as the UK, Canada, and EU by 2035. On the other side, is envisioned non-radical electrification, with estimations of electric vehicle stock representing 31% of the total passenger vehicles by 2050 [54].

A possible scenario is that although developed economies could achieve significant electrification of passenger private vehicles, developing economies will lag in the electrification effort, due to differences in purchasing power per capita and the investment necessary to modernize the electric infrastructure. Also, shipping and air transport will continue to gain relevance due to connected production lines and advanced logistics and will rely on liquid fuels. Therefore, betting all decarbonization efforts on electric vehicles would be unwise.

A sensible option for the near future to reduce the environmental impact of the transport sector is to produce non-fossil liquid fuel alternatives with properties similar to fossil fuels. For instance, it is argued that for decarbonizing a sector heavily dependent on fossil fuels, using bio-similar commodities as direct substitution is the most promising approach [55]. Thus, the use of biomass considered waste, or biowaste, has the potential as feedstock for bio-similar transport fuels without affecting the food market. Moreover, their utilisation could bring together different advantages, not only direct benefits such as reducing the dependency on oil and reducing the GHG emissions, but also energy independence for oil-importers countries and local jobs if domestic production of biowaste liquid fuels is promoted [50].

Synthetic fuel, or synfuel, is the term used for naming any liquid fuel synthesized from synthetic gas. Synfuel production commonly uses syngas from biomass gasification, the process is known as biomass-to-liquid (BTL). BTL systems consist of several sequential unitary processes such as biomass pre-treatment, gasification, syngas cleaning and conditioning, fuel synthesis, and fuel reforming [38].

Synthetic liquid fuels have the advantage of having similar chemical properties to current commercial liquid fuels. Thus, they represent a highly promising technology as they could work with the current infrastructure built for fossil fuels and be used in regular internal combustion engines [56]. In addition, the utilisation of synthetic liquid fuels has the environmental benefits of renewable sources of carbon such as reducing GHG emissions and reducing the dependency on petroleum oil. Furthermore, synthesizing liquid fuels from syngas could have a wide set of by-products. During the hydrocarbon synthesis stage olefins or waxes of different chain lengths are formed such that, after refining, they could be introduced into the bio-plastic industry [56]. This feature shows the versatility of the BTL system, with the possibility to incorporate a wide range of feedstock and produce several energy commodities.

At the core of BTL is the gasification stage, where the feedstock is converted into syngas. Gasification is an important technology with the capability of increasing the utilisation of solid fuels. It can be defined as the conversion of

solid fuel to light gas components by a thermochemical process [49]. By converting the solid fuel to a gas improves the handling along with the removal of undesirable material present in the original feedstock such as ash [57]. This gas produced, known as ‘syngas’, short for synthetic gas, or producer gas, can be used as a direct fuel in internal combustion engines for electricity generation, or cleaned for direct use in fuel cells or as a building block for further fuels and other fine chemicals [57,58]. Therefore, it widens the application of solid fuels, favouring their implementation in different energy markets.

Gasification has been used for a long time to seize energy from solid fuels. The application of gasification can be traced back to the gasification of coal during the 19th century, using it for public lighting [39]. And although its potential was slowed down due to the exploitation of the abundant oil, it has been resorted to in times of shortage of oil, such as during World War II, and the 1970’s oil crisis [59]. These repeated returns to gasification of solid fuel show the potential and reliability of the technology.

Although the commercial application of biomass gasification is increasing, most of the development has been made for wood biomass. Wood biomass gasification increased significantly in the last decade, particularly for combined heat and power (CHP) plants. However, the number of start-up plants for CHP from wood gasification is declining [60]. Instead, the technology including biomass gasification with the most start-up plants in recent years is liquid fuel production. With steady starting-up numbers of 2-3 since 2011, and with 4 planned for 2019 [60]. This shows that biomass gasification is increasing and diversifying the markets of application.

Disregarding the end-product, biomass gasification has been considered in the past as a promising technology for de-centralized units, able to produce power in small units for communities in remote locations or off-grid [59]. Also, it had the capacity to add income to farmers [61]. Thus, gasification has promising applications, particularly for developing countries. However, with the approach for second-generation liquid biofuel production, most of the efforts in implementing pilot or commercial plants are located in developed countries [60]. This suggests, that even if simple biomass gasification for heat

power production was not attractive for developed markets, the potential for liquid biofuels is a promising technology for dealing with wastes and generating renewable energy.

The principle of gasification can be summarised by subjecting a solid fuel at high temperatures with a limited supply of oxygen. The temperatures used in the process vary over a wide range of over 700 ºC with the regulation of oxygen load [49,58]. To produce synthetic gas, it is necessary to perform partial oxidation of the organic feedstock. For this, oxidant must be supplied in less quantity than that necessary for complete stoichiometric combustion [57].

Gasification is a complex process that involves several chemical reactions. These reactions are grouped into bigger reaction groups that vary depending on the criteria. For instance, Keche et al. [62], divided the process into oxidation and reduction. Oxidation, being an exothermic reaction, is where the products of partial oxidation are formed, including CO_2, CO, and H_2O. And reduction, where CO_2 and H_2O are partially reduced to CO and H_2. Nevertheless, a more descriptive classification is given by Ramzan et al. [49], where the process reactions are divided into: 1) Drying, as a sole reaction where water is evaporated. 2) Pyrolysis or devolatisation, where solid is broken down into smaller and volatile components. If the high molecular weight volatiles produced during this stage do not further react, they tend to condense downstream causing technical issues. 3) Combustion, where oxidation takes place, producing CO_2, CO, and H_2O. 4) Gasification or reduction, where H_2, CO, and CH_4 are generated. **Table 2.1** lists the main reactions during biomass gasification, exhibiting the complexity of the gasification reactions.

In general, during biomass gasification increasing temperature increases carbon conversion and gas yield, and enhances H_2 content, while decreasing gas heating values. The influence of temperature in the production of CO and CO_2 is difficult to predict due to the complexity of reactions where both species are involved, and both have endothermic and exothermic nature. The nature of biomass has a large impact on the performance of gasification. Moisture

content is the property that affects the most carbon conversion, cold gas efficiency, and heating value [63].

Table 2.1. Reactions of the gasification process.

Reaction	Reaction name	Heat of reaction
Heterogeneous reactions:		
Char combustion		
$C + 0.5O_2 \rightarrow CO$	Partial combustion	-111 kJ mol^{-1} CO
$C + O_2 \rightarrow CO_2$	Complete combustion	-394 kJ mol^{-1} CO_2
Char gasification		
$C + H_2O \leftrightarrow CO + H_2$	Steam gasification	+131 kJ mol^{-1} C
$C + CO_2 \leftrightarrow 2CO$	Boudouard reaction	+172 kJ mol^{-1} C
$C + 2H_2 \leftrightarrow CH_4$	Methanation of carbon	-75 kJ mol^{-1} C
Homogeneous reactions:		
$CO + 0.5O_2 \rightarrow CO_2$	CO partial combustion	-283 kJ mol^{-1} CO_2
$H_2 + 0.5O_2 \rightarrow H_2O$	H_2 combustion	-242 kJ mol^{-1} H_2O
$CO + H_2O \leftrightarrow CO_2 + H_2$	Water-gas shift reaction	-41 kJ mol^{-1} CO_2
$CH_4 + 2O_2 \rightarrow CO_2 + 2H_2O$	Methane combustion	-283 kJ mol^{-1} CO_2
$CH_4 + H_2O \leftrightarrow CO + 3H_2$	Steam-methane reforming	+206 kJ mol^{-1} CH_4
S and N reactions:		
$H_2 + S = H_2S$	H_2S formation	-20.6 kJ $mol^{-1}H_2S$
$0.5N_2 + 1.5H_2 \leftrightarrow NH_3$	NH_3 formation	45.9 kJ mol^{-1} NH_3

Adapted from [57,64].

Syngas utilisation requires a gas cleaning stage that is crucial for proper performance and could represent a significant percentage of the cost and energy consumption. The gas cleaning stage consists of the removal of nitrous and acid species, (for example, H_2O and NH_3), as well as heavy tars

generated during gasification which their condensation downstream causes fouling and slagging. This is argued to represent 50 to 65% of the entire plant cost [53]. The catalytic synthesis of synfuels is responsible for the high purity of synfuels and is a key stage of the process. Fischer-Tropsch catalytic reaction (FT) is used as the fuel synthesis stage and is able to produce synthetic diesel, gasoline or jet fuel [65]. The capacity to produce a wide range of hydrocarbons of linear chain, free from sulphur, nitrogen and aromatics, makes the FT the most promising technology for the production of biofuel for the transport sector. One of the main features of the FT synthesis is the multiple products that could be obtained. Among the products we can find methane, ethane, liquified petroleum gas (LPG) (C3-C5), gasoline (C6-C12), diesel (C13-C22), and waxes (C23-C33) [60]. In this regard, the production in a BTL plant could be modified according to the market.

FT reaction is a catalytic-polymerization process used to convert syngas into linear chain hydrocarbons with a carbon content ranging from C1 to C50. The General chemical formula for the reaction is shown in **Eq. 1** in the case of alkane production [50].

$$(2n+1)H_2 + nCO \rightarrow C_nH_{(2n+2)} + nH_2O \qquad \textbf{Eq. 1}$$

The polymerization reaction kinetics is governed by the Anderson-Schulz-Flory model, the model equation and the logarithmic representation are shown in Eq. 2 and Eq. 3:

$$W_n = n(1-\alpha)^2\alpha^{n-1} \qquad \textbf{Eq. 2}$$

$$\log C_n = \log(\ln \alpha^2) + n \log \alpha \qquad \textbf{Eq. 3}$$

Where W_n is the weight percentage of any product with 'n' carbon atoms, α is the probability of chain growth. For the logarithmic equation, $C_n = w_n/n$ which represents the mole fraction. Plotting C_n vs n must give a straight line [50].

Fischer-Tropsch reaction has its specific operation conditions, and they dictate the composition of the syngas and the produced synfuels. FT reaction can be operated in a 'one pass' or a recycled system. One pass operation could allow the implementation of a CHP system for electric power generation, while the recycle system is aimed at maximising fuel production [66]. This shows that the operation of the FT could be adjusted depending on the necessities of each specific plant. Nevertheless, the possibility of adjusting the operation could be limited by the gasifying agent. If the syngas is diluted with N_2, the one-pass operation is recommended, as a recycle from additional passes would increase the dilution [66]. Therefore, air gasifying should be limited to one pass operation if no extra conditioning is considered. The optimal operation conditions of the FT reactor based on the catalyst used (Iron or Cobalt) are shown in **Table 2. 2**.

Table 2.2 Syngas composition and process parameters for FTS using iron and cobalt catalyst (adapted from [60]**).**

	Fe catalyst	**Co catalyst**
Pressure (bar)	10 – 40	7 – 12
Temperature (°C)	300 – 350	200 – 240
H_2/CO (mol/mol)	0.6 – 1.7	2 – 2.15
H_2/CO_2 (mol/mol)	1	3

While the selection of catalyst and process conditions are important for the FT synthesis, several studies of the BTL process are focussed on the previous process of pre-treatment and gasification of biomass. These steps limit the syngas characteristics that could be obtained from biomass. Therefore, improving the early stages could enhance the performance of the overall plant. The stages of pre-treatment, gasification, and gas cleaning could account for 75% of the investment cost [67]. This shows the importance of developing and optimising these previous process stages.

2.2 Hydrothermal carbonisation

Hydrothermal carbonisation (HTC) is a more than a century-old technology that revived interest in recent years due to its characteristics [68]. It consists of the treatment with water at sub-critical conditions, high temperatures, and autogenic pressures, resulting in solid fuel. During the HTC process, the generation of a coal-like solid product occurs, with enhanced stability, storage, and more energetic properties than its original solid fuel [7]. This solid is commonly known as hydrochar, to differentiate it from biochar from dry-carbonisation technologies.

The products formed during hydrothermal carbonisation could be classified into three groups based on their physical state. First, are the solids, which include the unreacted ash, and the carbonaceous product hydrochar [69]. Hydrochars have lower hydrogen and oxygen content than the original feedstock, commonly expressed as H/C and O/C ratios. For this reason, the HTC process could be described with dehydration and decarboxylation as the dominant reactions [7]. However, this is an oversimplification of a complex process of multiple reactions of decomposition and condensation. There are works recognizing the capacity of the HTC process to reduce the oxygen content of a wet sample as an attractive option to upgrade several biomass sources for energy purposes in the past three decades [70]. The reactions occurring during HTC are numerous. Water at a sub-critical state during HTC causes a wide spectrum of decomposition and synthesis reactions [71]. Three products are identified during biomass carbonisation: light ‘permanent’ gases, a liquid phase, and a solid product [72]. The permanent gases are referred to as non-condensable light molecular weight compounds such as H_2, CO, CO_2 and CH_4. The gas phase has the lowest mass yield of the three and is mostly composed of CO_2. The liquid could be in one or two phases, water, and tar. And the solid phase, which is the hydrochar. Due to the multiple condensation and polymerization reactions, the products could result in numerous compounds [72]. This illustrates the complexity of the hydrothermal carbonisation mechanism.

2.2.1 General HTC advantages

The main advantage of HTC for food waste conversion is the capacity to improve the energy densification of a biomass feedstock without the requirement of a drying step, making it a very versatile technology. The HTC has proven a successful energy densification improvement on a wide range of different feedstock, including lignocellulosic biomass such as Miscanthus [73,74] sewage sludge [30,75], agricultural waste such as stalks [76,77], corn stover [78], olive stone [27], different pure food waste sources such as tomato peel [79], spent coffee grains [80], fish waste [31]; anaerobic digestate [32] and microalgae [28], among others. This illustrates the wide range of feedstock that could be treated by HTC and successfully increase the energy density of the original feedstock without the previous drying process.

Another large benefit of implementing the HTC process is the capacity to remove impurities from hydrochar. These impurities present in food waste cause technical problems with certain technologies, like gasification. Therefore, reducing the amount of impurities from hydrochar could increase the utilisation of food waste. These impurities include nitrogen and sulphur compounds, alkali metals, and tars. This removal is mostly due to the solubilisation of the different undesirable compounds into the liquid product of HTC also known as ‘process water’.

Sulphur compounds are known for their role in the poisoning and deactivation of catalysts [79], which makes them undesirable for the FT process. Hence, its removal increases the applicability of hydrochar from food waste in the gasification route. Reza et al. [37] reported the removal of up to 90% of the original sulphur content in different lignocellulosic feedstock. Also, Zhuang et al. [81] reported the removal of 38.2%, 27%, and 36.1% at 240 °C for 30 min for sewage sludge, penicillium mycelia waste, and peat waste, respectively. This shows that HTC achieves an efficient removal of sulphur content for lignocellulosic feedstock conversion to hydrochar, but also achieves a significant removal for different non-lignocellulosic feedstock.

Regarding the nitrogen content, its removal aims to reduce the NOx emissions from the downstream use of hydrochar. Zhuang et al. [81] reported the removal of 66.2%, 20%, and 27.6% of N for sewage sludge, penicillium

mycelia waste, and peat waste, respectively at 240 °C. Wang et al. [14] reported a nitrogen removal from hydrochar of 22.3% and demonstrated the elimination of amino groups. This is followed up by an increase of heterocyclic N-compounds, pyridinic-N. This indicates the removal of nitrogen from hydrochar is related to the deamination of biomass and is also followed by an increase of heterocyclic N-compounds.

The other impurities removal consideration is the content of alkali metals and heavy metals reduction from feedstock to hydrochar. It has been reported that HTC decreases considerably the content of heavy metals by 72-93% for lignocellulosic feedstock [37]. However, they found a low removal for alkali metals, which are in low concentration in this type of feedstock. On the other hand, Smith et al. [82] evaluated the impurities removal from a wide range of feedstock and corroborated this behaviour in the lignocellulosic feedstock. Nevertheless, they found that for non-lignocellulosic feedstock, HTC achieved a significant removal of both alkali and heavy metals from feed to hydrochar. This shows that HTC has a major contribution to the reduction of undesirable components of non-lignocellulosic feedstock, which could increase the utilisation of waste and hydrochar.

Regarding the energy consumption, it is suggested that HTC as pre-treatment could decrease the energy consumption at the different process stage of wet biomass utilisation. For instance, HTC has lower energy requirements than other carbonisation technologies such as dry-pyrolysis and torrefaction [27]. This suggests that its implementation could decrease the energy consumption during the pre-treatment stage and improve plant energy efficiency. In addition, the capability to treat high moisture content biomass is accompanied by an improved dewaterability of the produced hydrochar. Escala et al. [83] proved that the HTC of sewage sludge followed by a subsequent drying process consumed less energy than the direct drying of sewage sludge, saving 99 kWh of thermal energy and 8.5 kWh of electric energy per ton of sewage sludge. This indicates that HTC could make energetically feasible the carbonisation of high-moisture content feedstock. This feature has been addressed only in the mentioned study, and it could be worth further exploration to confirm this capability for food waste too. Nevertheless, it demonstrates that the HTC is an efficient option for the thermal treatment of

wet wastes, without even taking into consideration the produced hydrochar and the energy that could be further harnessed from it.

In a related aspect, HTC could improve the performance of non-central operational units. For instance, Briesemeister et al. [84] proposed HTC as a pre-treatment step for a CHP plant due to the improvement in dewaterability and grindability between raw feedstock and hydrochar product. This, suggest that the application of HTC could decrease the energy consumption for drying and grinding steps of biowaste, and could reduce the energy consumption in processes that require intensive particle size reduction such as fluidized or entrained-flow gasification. Biomass-adjusting process (for example, thickening and drying), are highly energy-consuming and affects the overall process efficiency of solid biowaste conversion to syngas [36,40]. HTC has lower energy requirements and it is attractive to use in small-scale decentralised units [85]. This property of the HTC process permits the utilisation of a wider range of biomass sources than other mentioned carbonisation technologies. Therefore, making it a technology with great potential to treat non-lignocellulosic biomass.

Also, some signs utilising HTC as food waste pre-treatment have indicated that this approach could improve its implementation on processes involving combustion or gasification. Regarding the utilisation of hydrochar or combustion purposes, hydrothermal carbonisation decreases the energy activation for the early gasification stage. Feng et al. [12], reported the reduction of energy activation devolatilization of raw sewage stage from 231.0 KJ/mol to 209.8 for hydrochar at 200 ºC, and 185.7 KJ/mol at 260 ºC. Erlach et al. [86] compared the implementation of HTC as a pre-treatment of wood biomass for gasification against the direct gasification of the feedstock with entrained flow gasifier and fluidized bed gasifier. They found that the implementation of HTC slightly decreased the overall energy efficiency of the process due to higher energy consumption and a mass loss into the liquid phase. Nevertheless, the HTC as pre-treatment of wood showed several advantages over the other systems, with only a slight difference in energy efficiency. The model including HTC as pre-treatment of the wood shows better energy efficiency at the gasification stage. Also, the gas composition was high on CO and H_2 (50% and 24% respectively), while the lowest was on

CH_4. In addition, HTC lowered the content of tar and H_2S, along with increasing molecular N_2. This shows that HTC improved the performance of the gasification stage.

2.2.1.1 hydrochar gasification

The gasification of hydrochar, in comparison with other biochars, is an area that is still widely unexplored, and its utilisation for different feedstock is still unknown. Gasification studies with hydrochar are scarce, not to mention studies comparing different biochar gasification.

Gai et al. [87] studied the comparison of the gasification profiles of hydrochar and pyrochar from sewage sludge, where pyrochar is char from pyrolysis. They concluded that hydrochar syngas was higher in H_2 production achieving a maximum of 57% of H_2 of the syngas composition, with CO as the second component with over 15%. Although the energy content of the syngas was overall higher than pyrochar, the energy consumption of producing and gasifying hydrochar was lower than the pyro char. In addition, the syngas composition from hydrochar, had higher H_2 and CO, as well as lower CO_2 than the pyrochar syngas, showing that HTC could be better suited for further processes, such as Fischer-Tropsch synthesis. Therefore, it indicates that the gasification of hydrochar could bring advantages for energy consumption and syngas composition for use in larger processes like biomass-to-liquid plants.

Examples of hydrochar gasification are shown in **Table 2.3**. In this compilation, are included studies involving hydrochar gasification and combustion, due to the scarcity of pure gasification studies. It is evident that examples of gasification of hydrochar are scarce, with around half of the studies using a thermo-gravimetric analyser (TGA) for the decomposition studies, being the other half of gasification studies focusing on the syngas production. However, most of the compiled studies lacked a proper experimental design or gas composition, which prevents them from evaluating optimal conditions for gasification.

It is notable that most of the studies have been made in fixed bed reactors. With this technology, the gasification of hydrochar from non-conventional feedstock has been explored, including sewage sludge [87–89], olive biomass [90], and spent grains [91]. The fixed bed technology, as mentioned earlier, is

not the ideal option for biomass or hydrochar gasification. However, these studies are focused on exploring the behaviour of different feedstocks, that were overlooked in raw biomass gasification studies, and it is only in recent years that they have been considered as possible feedstocks for gasification with pre-treatment technologies such as HTC. Also, fixed bed technology has numerous units in operation worldwide due to its low cost, thereby implementing hydrochar into already built infrastructure could facilitate its commercial implementation. Thus, it is a technology and a market worth considering.

Nevertheless, another gasifying technology that has been considered is the entrained flow gasifier. Tremel et al. [92], proposed a mild HTC for the entrained flow gasification of wood chips. The main arguments for the study were: first, entrained flow is a potential solution for the high tar production during biomass gasification, second, this type of gasification for woody/lignocellulosic material is limited due to a highly energy-intensive feedstock pulverization requirement, and a pulverized product that results ineffective for pneumatic transport. They found that the HTC as pre-treatment decreases significantly the energy necessary for pulverisation. Also, the gasification of the hydrochar showed a similar behaviour as lignite gasification with higher conversion at lower temperatures. This indicates that the hydrochar could be used in entrained flow gasification facilities designed for lignite.

Table 2.3. Compilation of previous studies of hydrochar gasification or combustion.

Feedstock	HTC variables	HTC responses	Gasifier	Gasification variables	Gasification responses	Reference
Beech wood chips	None	Carbon yield Energy yield Grindability properties	Entrained flow	Temperature Residence time	Gas quality Carbon conversion Overall conversion	[92]
Spent grains from a brewery	None	Chemical composition	Fixed bed Updraft	Feed rate Equivalence ratio airflow rates	Syngas composition DTG profile Cold gas efficiency	[91]
Olive biomass	None	Mass yield	Fixed bed	Temperature Feedstock Steam Flow	Syngas composition	[90]
Karanj fruit hulls	None	Mass yield	TGA	Temperature Heating Rate	DTG profile	[93]
Sewage sludge	None	Chemical composition Surface morphology	Fixed bed	Temperature Feedstock Steam:Biomass	Syngas composition	[87]
Sewage sludge	None	Chemical composition Surface morphology	Fixed bed	Temperature Steam:Biomass Catalyst	Syngas composition	[89]

Table continues

Feedstock	HTC variables	HTC responses	Gasifier	Gasification variables	Gasification responses	Reference
Green waste	None	Chemical composition Ash behaviour	Entrained flow	Air/fuel eq. ratio Temperature Steam addition	Syngas composition Carbon Conversion Cold gas efficiency	[94]
Sewage sludge	Temperature Catalyst	Mass yield Chemical composition	TGA	Temperature	DTG profile	[88]
Sewage sludge	Temperature	Surface morphology Pore volume Specific surface area	Fixed bed	Feedstock	Syngas composition Tar composition	[95]
Macroalgae Sugar cane bagasse Grape marc	Temperature	Chemical composition Energy densification	Fixed bed	Feedstock Catalyst	DTG profile	[96]
Algae Sunflower stalk Poultry litter	Temperature Feedstock BM:W	Mass yield Energy densification	TGA	Temperature Feedstock	DTG profile	[25]
HTL char Pine sawdust	None	Chemical composition	TGA	Heating Rate	DTG profile	[97]

In addition, as the gasification of hydrochar showed higher reactivity at lower temperatures, it was proposed to perform gasification at temperatures lower than the ash melting point. They concluded that hydrochar gasification must explore other feedstock more economically viable for HTC, as well as the necessity to explore the industrial feasibility of the technology.

A second study including the gasification of hydrochar in an entrained flow gasifier was reported by Briesemeister et al. [98]. In this study, the gasification of hydrochar from green waste is evaluated in a pre-commercial gasification system. As they evaluated the gasifier, the parameters were the air to fuel equivalence ratio and the steam addition. They found positive results in terms of lower tar generation and higher carbon conversion. They concluded that is necessary to further investigate the steam addition effect with other variables. Also, they recognize that the pre-heating of the air is highly reflected in the cold gas efficiency, and must be explored higher than 300 °C. Moreover, they saw the need to evaluate heat-recovery technologies and overall system efficiency. Therefore, this suggests that the gasification of hydrochar could be technically viable in a commercial small-scale entrained flow unit.

One consideration for hydrochar gasification is the severity of the process and its effect on the hydrochar nature and further gasification. Higher temperatures and residence time increase the formation of fixed carbon during the HTC process, which increases the HHV (higher heating value) of the hydrochar. However, Ulbrich et al. [99], using TGA of hydrochar of spent grains, reported that high severity process conditions decreased the reactivity of devolatisation reaction in CO_2 atmosphere, and has the inverse response to temperature and residence time than fixed carbon generation.

The gasification reactivity is a crucial attribute for a shorter residence time in the gasification stage and affects the overall efficiency of the process. Based on the thermogravimetric analysis, Feng et al. [95] observed the gasification of hydrochar in two visible sections. The first section happened at temperatures between 200 and 550 ºC and is attributed to the devolatilisation stage. The next stage, considered the steam gasification process, occurred from 550 to 1000 ºC. However, it is necessary to evaluate if this feature improves the complete gasification performance.

Gai et al. (2016), comparing pyrochar and hydrochar gasification, reported that, as temperature increases, the H_2 yield increased considerably from 32.9% at 750 ºC to 55.6% at 950 ºC, and lowered slightly to 52.5% at 1050 ºC. In the case of CO and CO_2, it was reported that CO_2 decreased as temperature increased from close to 20% at 750 ºC to 12% at 1050 ºC. On the contrary, CO slightly increased from around 15% at 750 ºC to 18% at 1050 ºC. Methane being the lowest compound was around 5% at 1050 ºC.

2.3 HTC Reaction on food waste

The previously mentioned features of HTC show us the potential for treating and enhancing numerous properties of food waste (FW). However, studies on HTC-FW are less numerous than on feedstocks such as sewage sludge, AD digestate, or lignocellulosic biomass. Nonetheless, FW as a feedstock has a particular composition with important variability in comparison to the mentioned type of feedstock. Therefore, understanding how the HTC process affects FW will allow us to improve the valorisation of the feedstock and the applicability and commerciality of the HTC technology.

The variability of biochemical composition is an important factor when performing HTC on food waste. As it is known to cause variability in the properties of the products, complicating the development of general mathematical models of HTC for food waste. One way to standardize the composition variability is to consider the three major biomacromolecules present in food waste: carbohydrates, protein and lipids. However, how the different biomolecules interact and affect the HTC products is still unclear as this mechanism is still required to be elucidated.

Of the three biomacromolecules, carbohydrates have the most studies on their mechanism, due to the spotlight on woody and lignocellulosic biomass. The mechanisms involve the breaking of polymers into di- or monomers of sugar (glucose, xylose, fructose, etc) due to hydrolysis. Hydrolysis is possible because of the presence of H^+ and OH^- ions in water in subcritical conditions [100]. Monomers produced, hexoses or pentoses, suffer a dehydration reaction resulting in furan compounds, hexoses are converted into hydroxymethyl furfural (HMF) and pentoses into furfural [101], 5-methyl

furfural is also possible [100]. Further dehydration could result in the appearance of organic acids: acetic, formic, propionic, levulinic and lactic are among the acids found in experiments [100]. Other products of further dehydration include aldehydes, acetaldehydes, acenylacetones, glycealacetone, glyceraldehyde, pyruvate, and pyruvaldehyde [102].

At the same time that hydrolysis and dehydration reactions occur, polymerization reactions are also taking place. The polymerization process is proposed to be by condensation reactions [100], linking two molecules while one water molecule is released. These new compounds form cyclic compounds and aromatization reactions take place. In particular intermolecular dehydration and tautomerization of keto-enol groups are the two reactions likely to occur during the aromatization process [100].

Thus, the structure of hydrochar has a different matrix than biochar obtained by dry carbonization methods. Due to the previously proposed mechanism routes, it was believed that hydrochar was formed only by furan-rich core, in comparison with biochar that is arene-rich. However, it was further proposed that the hydrochar matrix is formed by three-unit furanic structures as the motive, not discarding the possibility of small arene structures in co-existence [103]. Furthermore, furanic polymers are formed as early as 180 °C, and the degree of aromatization increases with the intensity of the process [104].

Therefore, the aromatization of polymers like cellulose appears to follow a second route. In this route, the aromatization starts in the cellulose matrix by intermolecular dehydration without following the hydrolysis and furanic route [104]. This reinforces the co-existence of two motives of cyclic hydrocarbons in the core of hydrochar from polysaccharides. However, the proportions of furan and arene aromatics are not defined and they are most likely to vary from one feedstock to another. Browns et al. [69], proposed that the hydrochar from glucose has two possible structures:1) 1 furan and 3 arenes motives linked by aliphatic chains, corroborating the structure proposed by Falco [104]; 2) aromatic cluster formed with 6 to 8 arenes motives with carbonyl groups on the surfaces.

Regarding protein, one of the main interests of its mechanism routes is the content of nitrogen. Studies exploring the mechanism involving protein are

less than those of carbohydrates. Like carbohydrates, protein polymers start breaking by hydrolysis forming peptides and aminoacids. Proteins start to transfer from the solid feedstock into the liquid phase at temperatures from 150 °C [105]. The aminoacids are further degraded and their breakdown shows above 200 °C. The breakdown of aminoacids was related to the generation of volatile fatty acids (VFA), principally acetic, propionic, and butyric acid. It was reported that humic substances almost disappear completely under these conditions [105]. Also, aminoacids suffer reactions of deamination, producing NH_4^+-N [14].

At the same time, aminoacids in presence of carbohydrates, common in food waste feedstock, will react with the reducing-end of sugars by the Maillard reactions. These reactions can generate pyridines, pyrrolidine, pyrrolidinedione, pyrrolidinone and derivatives in the process water of the HTC reaction [14]. It has been reported that Maillard products found in process water decrease as temperature increases due to the lower availability of sugars, which are degraded at higher temperatures. However, at higher temperatures the nitrogen from protein is incorporated into the stable furan/arene structure of hydrochar in form of pyridine-N [14]. Therefore, protein has high reactivity with carbohydrates during HTC, and could lead to Maillard products within process water at low temperatures and incorporated into the furan/arene matrix at higher temperatures.

However, the participation of protein in the degree of carbonization is not fully elucidated. Li et al. [106], evaluated different compositions of synthetic food waste. They found that food waste containing only lignocellulosic and sugar promotes the generation of hydrochar with higher fixed carbon. When protein is added to lignocellulosic waste, fixed carbon decreases while HHV remains the same as with sugar. This indicates that the presence of protein does not promote the generation of fixed carbon, and even if it is incorporated into the hydrochar matrix it generates structures with less aromaticity. Also, it is noted that proteins tend to coagulate and clump due to denaturalization, decreasing the surface area [107]. This suggests that if the feedstock has a considerable protein content, a degree of homogenization could be recommended to enhance the interaction between protein and sugars.

In the case of lipids, even if they are highly energetic compounds, their participation in the carbonization process is not clear. The stability of fatty acids could be a factor inhibiting the carbonization of lipids. It is reported the stability of triglycerides is up to 190 °C, and the appearance of free fatty acids starts from 220 °C and a minimum of 30 min [107]. This shows the stability of lipids at low intensity of HTC. Furthermore, it has been reported that free fatty acids by themselves do not produce solid products even up to hydrothermal liquefaction conditions (300-350 °C) [108]. This suggests that, due to their stability, lipids could not participate in the carbonisation reaction, or could even inhibit the production of hydrochar.

However, it has been suggested that fatty acids might react with aminoacids and carbohydrates at low temperatures and participate in the polymerization and aromatization as temperature increases, producing heterocyclic compounds such as indoles and quinolines [109]. Nevertheless, even if the mechanism for the reaction of lipids in HTC is not clear, their presence in the feedstock has been evaluated. When lipids are added to a lignocellulosic sample, fixed carbon decreased significantly resulting in high volatile matter values after HTC. However, even if the volatile matter was higher when lipids were added, the hydrochar with lipids showed the highest HHV values [106]. In addition, in combustion analysis, samples with lipids showed behaviours related to high volatile matter such as lower ignition temperature and forward pyrolysis region. The high volatile matter follows a high presence of unreacted, unsaturated free fatty acids on the hydrochar [106]. This indicates that fatty acids do not show reactivity with lignocellulosic biomass and the presence of protein may be necessary to increase the interactions between biomacromolecules.

2.3.1 Previous studies of HTC treated food waste

Despite the advantages of HTC for the valorisation of FW, the number of studies on FW is much less than on feedstocks such as lignocellulosic or woody biomass and sewage sludge. However, interest in the application of HTC for the valorisation of FW is increasing rapidly in the research community, as illustrated by a sharp increase in journal articles in recent years (**Figure**

2.1). Evidencing the gained momentum of this application of the HTC technology.

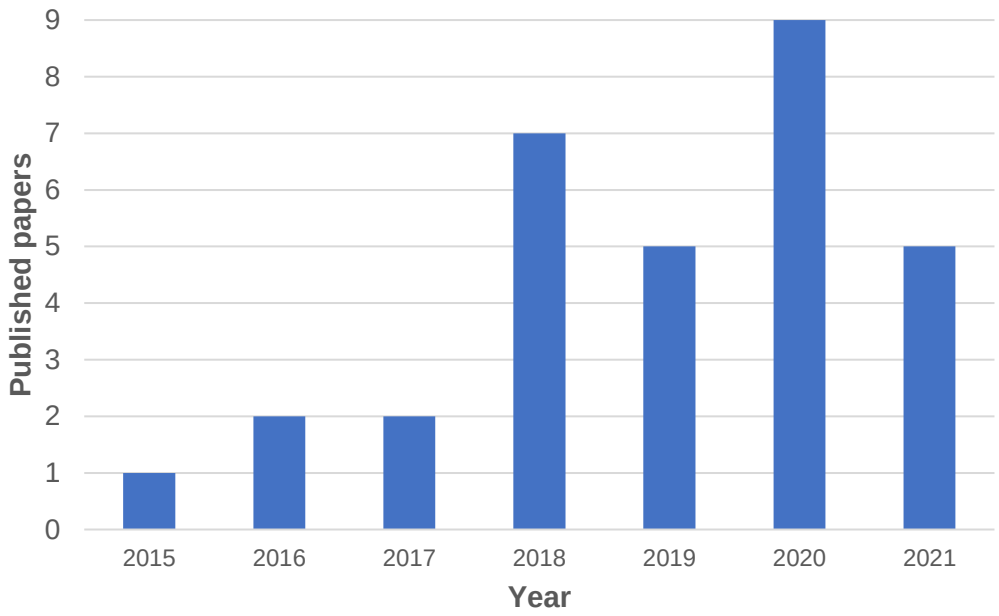

Figure 2.1. Number of papers on HTC of food waste published in journals in recent years

Hydrochar has several proposed applications, with the most investigated being for the production of solid fuel. lists the studies reported in the literature where the focus is on producing and evaluating the characteristics of hydrochar as a solid fuel for either combustion or gasification. Due to the dehydration and decarboxylation reactions occurring during HTC, the resulting bio-coal has an improved heating value and reduced volume, enhancing its energy densification. The production of solid fuels from HTC was the first reported use of the hydrochar, hence this application is mentioned in the earliest reports of HTC [85,110], with a proven coalification effect on a wide selection of feedstocks. The overwhelming efforts for solid fuel in comparison to other utilisation of HTC-FW are illustrated in **Figure 2.2**, where solid fuel represents 66% of the efforts followed by nutrient recovery with 13%.

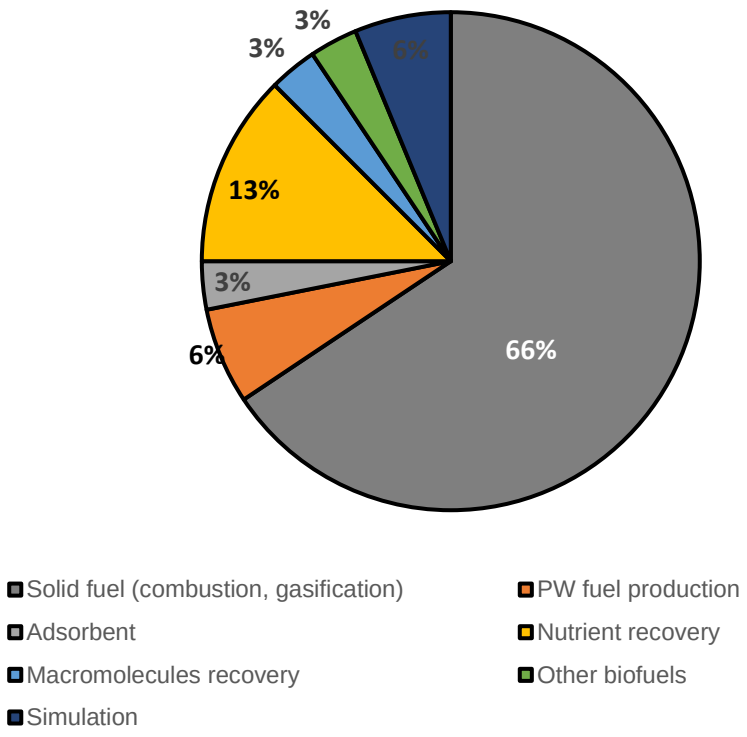

Figure 2.2 End-product for HTC of food waste on previous studies

Several studies have investigated the HTC of single food wastes or homogeneous food wastes. These waste streams tend to be associated with an industrial processing step and are categorised in this study as pre-consumer food waste. These studies include Olive stone [27], tomato peel waste [79], fish waste [31], watermelon peel [10], sweet potato waste [111], lemon peel waste [112] and beet pulp [22]. In all these studies, HTC improves the solid fuel quality of the feedstock, indicating that HTC has potential for the treatment of organic waste at industrial sites.

2.3.1.1 Hydrochar for solid fuel

Utilising hydrochar from FW as a solid fuel can replace fossil fuels in both power generation and domestic heating, reducing its carbon footprint and reducing the environmental and health-related effects of its disposal. The use of hydrochar as a solid fuel can be utilised for direct combustion, co-combustion with fossil coal, or as an energy carrier for combined heat and power CHP or gasification. In a food waste-to-energy review, Pham et al. [9]

remarked that HTC produces a solid hydrochar containing between 45 to 93 wt % of the carbon content in the hydrochar with an energy content of 15 to 30 MJ/kg dry solids. Also, the carbon loss into the aqueous phase ranged between 10 to 40 wt %. FW generally produces a higher HHV hydrochar than other feedstocks such as sewage sludge, digestate, and agricultural residues due to its lower ash content and higher fat content with HHV as high as 30 MJ/kg being reported. However, FW generally produces lower yields of hydrochar and there are high levels of COD as organics are solubilised into the process waters.

Most of the studies published to date focus on using hydrochar as a solid fuel for direct combustion. In these studies, hydrochar is characterized in terms of its energy content and evaluated by combustion behaviour analysis [5,21,111], as well as combustion kinetics [106,113]. A common way of analysing the combustion characteristics of the resulting hydrochar is to determine its comprehensive combustibility index (S) [113] as illustrated in **Eq. 20**. The comprehensive combustibility index links the ignition and burnout temperatures of the solid fuel and the rate of mass loss and gives a quantitative assessment of the combustion reactivity. The utilisation of hydrochar from FW has also been considered for conversion by gasification [18] and steam gasification [15].

Many recent studies have investigated the combustion behaviour and kinetics of HTC during co-processing. Saqib et al. [5] evaluated the combustion behaviour of hydrochar using thermo-gravimetric analysis (TGA) in air, comparing the different temperatures of pure hydrochar and blends with coal at different ratios. Combustion of hydrochar from FW was shown to have a lower activation energy than that of coal. They also found that hydrochar combustion showed two reaction zones, with similar behaviour to raw biomass, in comparison to the single burnout zone for coal. This behaviour could be due to the presence of lipids and fats in FW which show minimal decomposition during HTC.

Wang et al. [21] also evaluated the combustion behaviour and gas emission of hydrochar produced at temperatures ranging from 180 to 260 °C for 1 h. They found that HTC lowers the combustibility index (S) in comparison to raw

FW. This indicates that hydrochar would improve the stability of the flames during combustion. There was also a reported reduction in pollutant emissions after HTC treatment, associated with the reduction of inorganics in the solid fuel. Li et al. [106] evaluated the influence of the FW composition on the combustibility index of the hydrochar indicating an improvement when sugar and protein are present. The combustibility index increases when lipids are present in the feedstock due to the higher volatile matter in the resulting hydrochar. Mazumder et al. [114] reported that the co-processing of FW with coal waste increases the energy output of HTC and found that co-HTC increases the energy content of the resulting hydrochar/coal blend. It also resulted in a desulphurization and dichlorination of the coal waste, reducing its potential emissions. They also observed a synergistic effect on the combustion behaviour of the mix, showing similar behaviour to raw coal combustion.

2.3.1.2 Hydrochar for soil amendment, soil conditioner and fertilizers

Other potential applications of hydrochar, include its use as a soil conditioner for improving soil quality. Bamminger et al. [115] compared biochar (from pyrolysis) and hydrochar, both derived from maize for the stability and effect on microbial and enzymatic activity in soil. The two types of char and their mixture were incubated with the soil for 57 days where hydrochar amended soil showed the highest respiration rates and maximum increase in microbial activity. It was reported that 15% of the hydrochar was mineralized in 8 weeks and proved to be superior to biochar generated from pyrolysis. Hydrochar significantly improved the consumption of soil organic carbon, which is the main source of energy for soil microorganisms. Easy availability of soil organic carbon improves the organic carbon uptake by plants. Whereas Busch et al. [116] reported that hydrochar exhibited negative effects such as total inhibition of germination above 5% v/v addition when evaluating chromosomal aberrations in the pollen cells of Tradescantia. The hydrochar was prepared from different feedstock (maize silage, food leftovers, digestate from biogas plant, grass cut, sewage sludge). Post-treatment of hydrochar before soil application has been reported following water washing, chemical treatment with H_2O_2 and biological treatment via composting along with other

compostable materials (organic waste) in a 1:3 ratio by weight to facilitate microbial degradation of organic pollutants. Genotoxic effects were not observed after treatment with H_2O_2 and composting, along with no germination inhibition after composting. Therefore, biological and chemical post-treatments were found to be satisfactory in completely eliminating the toxic effects of hydrochar. An important area of research is the effect hydrochar has on the volatilisation of ammonia when added to the soil. There are conflicting reports of the effect of hydrochar application on ammonia volatilisation. Chu et al. [117] showed that sewage sludge-derived hydrochar inhibits ammonia volatilisation, improving soil nitrogen whereas Liu et al. [118] observed the opposite and the additional hydrochar does increase ammonia volatilisation. Subedi et al. [119] also indicate that the soil amended with hydrochar increases ammonia emissions compared to the control after the application of pig slurry. The impact of hydrochar on ammonia volatilisation is therefore unclear and likely to be affected by hydrochar pH and feedstock composition.

Regarding hydrochar produced from food waste the information is not as extensive and germination or *in situ* analysis are still lacking. The utilisation of hydrochar from food waste for nutrient recovery for later use in soil amendment and fertilizers has been explored with the favourable nutrient recovery of nitrogen [10,14] and phosphorous [13] and positive results of leaching properties of hydrochar [11]. They estimate that between 1 and 2.3% of the phosphorous and nitrogen-based fertilizers could be used and replaced with hydrochar produced from currently landfilled wastes in the US alone [11]. Process water recirculation showed no increase in the content of S or N, thus, neither on the emissions of SO_2 and NOx following combustion of the hydrochar [111]. This indicates that the content of S and N in hydrochar is not affected by the recirculation of process water despite the improvement in energy content. The most abundant nutrients are nitrogen, potassium, phosphorus, calcium, sodium and magnesium, with lower concentrations of other metals. The fate of inorganics and nitrogen has been studied in detail [82,120,121] however their release is dependent upon the feedstock composition and reaction severity. Generally, the higher the temperature, the more the nitrogen is converted to soluble ammonia, and the lower the

temperature, the more phosphate is released into the water phase. The levels of phosphate in the hydrochar are generally related to the levels of a counter ion such as calcium content.

Idowu et al. [11] evaluated the fate of primary and secondary nutrients from FW during HTC. They observed that in a similar way to other feedstocks, most of the potassium and sodium are solubilised into the process water. While nitrogen, calcium and magnesium remained largely in the solid product. In the case of phosphorus, the largest transfer into the water phase was observed at mild process conditions and reintegration into the solid phase at higher temperatures and longer retention times. Idowu et al. [11] argued that nitrogen is unlikely to be released to any great extent from the hydrochar, due to its bonding within the hydrochar matrix, reporting that just over 50% of the initial nitrogen content remains in the hydrochar, even after increasing process severity. This agrees with Wang et al. [14], who evaluated the fate of nitrogen of FW after HTC at temperatures ranging from 180 to 260 °C. They found that the deamination occurs as the temperature increases but it stalls at 220 °C.

2.3.1.3 Hydrochar for absorbent use

Other proposed applications of hydrochar focus on its adsorbent capacities, in particular for heavy metals and nutrients. A comprehensive review of the sorption capacity of heavy metals using hydrochar was conducted by Mihajlovic [122]. Hydrochar from coconut shells, has been used for the adsorption of heavy metals from wastewater [123]. This research concluded that the coconut shell was a feasible feedstock to be used to adsorb copper, nickel and zinc from aqueous solutions. In a different study, Ronix et al. [124] evaluated the adsorbent capability of hydrochar made from coffee husk to remove methylene blue dye. They found that hydrochar showed good monolayer adsorption for methylene blue. Moreover, they reported that most adsorption occurs by physisorption, while the process was endothermic and spontaneous. These studies, indicate that hydrochar has the potential to be utilised as an adsorbent.

One crucial aspect of the implementation of HTC technology for FW is the viability of scaling up. A few studies have focussed on the viability of HTC [6,8,24]. These studies evaluated small de-centralized HTC plants with

hydrochar production, however, there is no further process integration or feedstock dependent analysis. Tradler et al. [24] proposed the use of decentralized HTC units being applied for industrial and communal use, they argued that if hydrochar is incorporated into the energy market, small-scale HTC for restaurants or industries would be a cheaper option than the current disposal cost, and the HTC plant could pay for itself in a few years. They also concluded that it is also necessary that the products from HTC comply with current standards, for instance, product quality for the production of solid fuels. McGaughy and Reza [6] evaluated experimentally and by modelling the energetic performance of HTC on FW. They argue that, in comparison to previous studies, the hydrothermal carbonisation of FW has the potential to be energy-positive and to achieve energy savings. They identify that most of the energy savings come from the hydrophobic nature of the hydrochar and its increased HHV. They concluded that future research on the HTC of FW should be focused on optimising energy recovery and process optimisation for specific product applications.

2.3.2 Previous HTC plants

The characteristics of the HTC make it an interesting option for the pre-treatment stage in a larger plant, specifically a biomass-to-liquid plant. Some of these features have been explored and suggest that HTC could benefit the BTL process in different aspects such as: energy consumption, hydrochar quality, and feedstock options. While the number of studies on HTC has increased in recent years, the implementation of HTC in an integral process has not been fully explored. Currently, there is a handful of studies where HTC is proposed and evaluated as a part of a plant design. Moreover, analysis in Aspen Plus as a tool to simulate the flow diagram of an operative plant is scarce.

One of the first approaches to integrating HTC was reported by Erlach et al. [125], where they couple the HTC with combined heat and power production (CHP). In this study, HTC was used as an upgrading step for improving different biomass properties. Including energy densification (HHV increase), minerals removal, and increase mechanical dewaterability. They evaluated the standalone HTC, and the standalone CHP, and compare the HTC-CHP to

the CHP coupled with the wood pelletizing stage (WP-CHP). Regarding the Aspen Plus simulation, the HTC is modelled as a black box, with experimental data input for biomass and hydrochar, the HTC operation conditions were 220 °C for 4 h. The main product of the study was the pelletized hydrochar, and CHP was used as an energy recovery unit, that utilises part of the heat produced during HTC along with additional feeding for the boiler. They reported that the separated HTC module achieved 81.1 % energy efficiency based on HHV. When the sum of HHV, net electricity, and district heat were considered, the overall energetic efficiency resulted in 60.8% using wood, and 59.7% using biodegradable waste. In this first approach, they concluded that the hydrochar pellets could be produced at a comparable cost to wood pellets. In addition, the CHP plant eliminates the need for complex heat recovery in the HTC plant.

Later, Erlach et al. [86] reported a second approach incorporating HTC in a bio-energy with carbon capture and storage (BECCS) system. They evaluated the energy efficiency, exergy analysis, and techno-economic analysis of the HTC plant, coupling it with an entrained-flow gasifier and a fluidized bed gasifier, both with a CCS unit. Comparing them against direct wood gasification and direct coal gasification. The schematics of the process are shown in **Figure 2.3**.

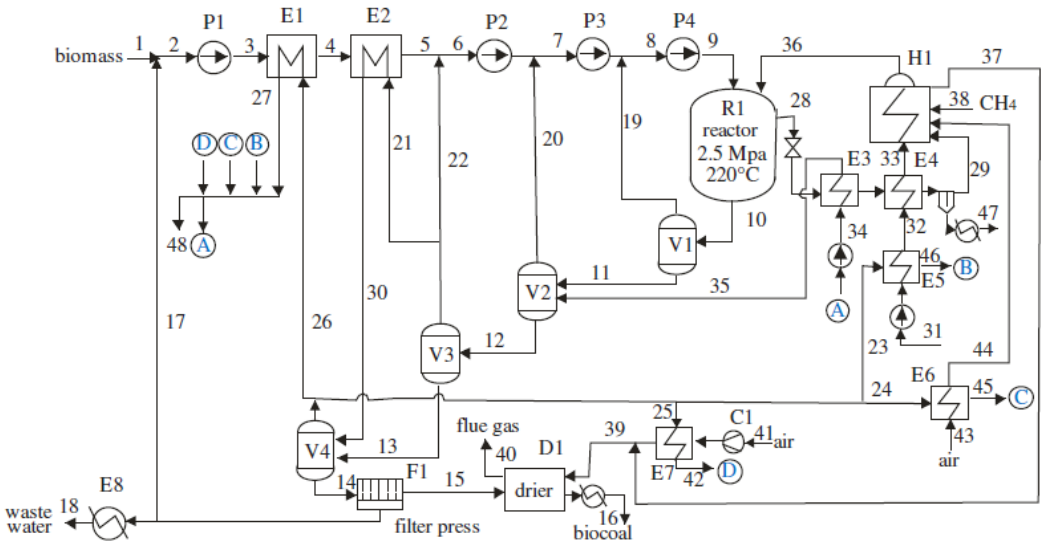

Figure 2.3 Flowsheet of a BECCS process with production of hydrochar [86]**.**

Regarding the Aspen Plus simulation, HTC was again modelled as a black box with data from previous studies. The operation conditions were 220 °C and 4 h. They found that the exergetic efficiency was higher for hydrochar gasification (65.1%), in comparison with the direct gasification of wood for both fluidized bed (59%) and entrained flow (58%). However, when considering the complete process, with the losses and extra energy of the HTC, the exergetic efficiency drops to 54.4%. Regarding the CCS-IGCC system, the hydrochar gasification showed a 27.7% electrical efficiency and a 72.7 % of carbon capture rate. This is lower than that obtained with fluidized bed gasification of wood with 28.6% electrical efficiency and 84.5% of carbon capture rate. These lower results are associated with the carbon loss as gas and dissolved into the water during HTC. The notion that this carbon loss in the process water reduces the HTC potential for carbon capture and the energy efficiency, indicates that energy recovery from the process water should be incorporated into the simulation, although it could improve if the carbon in the process water is treated. It is worth mentioning that the operating conditions used for the gasification of the three feedstocks (wood, hydrochar, and bituminous coal) were the same. They suggest that using optimized conditions for each feedstock is crucial to improve the cold gas efficiency. Also, the improvement of milling was considered one of the motivations for using HTC. However, this aspect was overlooked and not incorporated in the simulation, neglecting the possible handling benefits from HTC hydrochar.

One of the main motivations of this study is using HTC as biomass pre-treatment, to increase the suitability for entrained, downdraft, and updraft gasification. The solid feed particle size requirements for entrained gasification being the most stringent, this is proposed by facilitating the milling and feeding it by conventional pneumatic transport.

The following year, in a study by the same research group, Stemann et al. [126] proposed the use of HTC as a pre-treatment for wastes of the palm oil industry. This study was planned for producing hydrochar pellets in an HTC-pelletization plant-based where the palm oil industry is located, and to evaluate its techno-economical production and commercialization. For starters, the same flowsheet from previous studies was used, with the same HTC conditions of 220 °C and 4 h. Overall energetic efficiency (based on

HHV) of 71.2% was obtained. Of the energy input, 92.3% was from the entering biomass, 1.5% electricity, and 6.2 boiler fuel, in this case, raw biomass was used. Also, it is important to note that 28.8 of the input energy is lost in the organic load of the process water. They ran several simulations evaluating the recirculation of process water into the HTC reaction. They found that with the recirculation, the energy efficiency increases to 77%, along with the solid yield (77%). Other noteworthy results were that HTC could be mechanically dewatered to 32%, between a third and a half of the carbon content of process water was acetic acid, K was completely removed from solid during HTC, while only 30% of N dissolved. While they considered the proposal feasible, it had numerous challenges and uncertainties in the market. Also, it had to be compared to other simpler waste treatment technologies, for example, composting or briquetting.

Another study of HTC plant design was reported by Briesemeister et al. [84] as shown in **Figure 2.4**. This study proposed to incorporate HTC as biomass pre-treatment in a combined heat power production (CHP) plant, using an entrained-flow reactor for the gasification of hydrochar. A new flowsheet for the HTC plant is presented. However, it is evident that some of the elements of the previous study remained, mentioning the 4 sequential flash reactors to depressurize and recirculate heat.

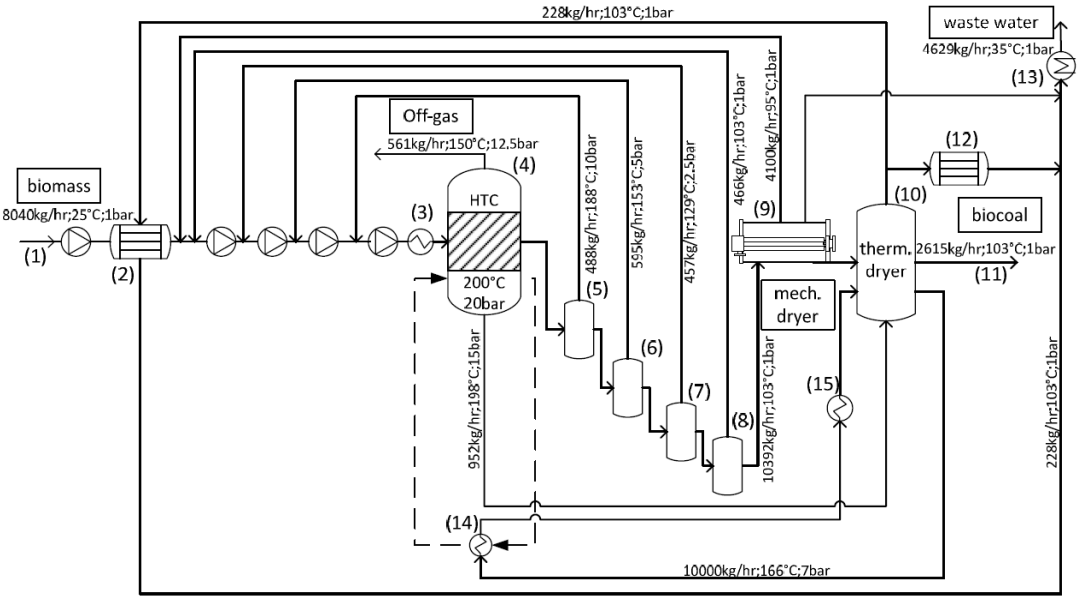

Figure 2.4 Flowsheet of an HTC process with heat recovery (reported by [84]**.**

In the Aspen Plus simulation, no model was proposed for HTC and is represented as a black box with process data obtained from Suncoal Industries. For this design, the overall energy efficiency of the HTC plant was 86.92, higher than the previously reported studies. For the gasification stage, it was simplified by operating at atmospheric pressure and air as the gasification medium. However, it lacked details on the representation of gasification in the Aspen Plus simulation. They concluded that the complete plant resulted in an overall electrical efficiency of 25.4% and overall thermal efficiency of 42.67%, which are comparable to the efficiencies of current biomass utilization technologies. Also, they highlighted the capability of using biomasses that are not currently in use, due to their nature and the limitation of the technology.

As a perspective, due to the trade-off between quality and quantity of the hydrochar, it is foreseeable that the optimization of the process is a necessary step. The optimization should include operation parameters such as temperature and residence time, but also parameters incorporating production, logistics, and utilization. For instance, including energy efficiency into the optimization along with utilization responses would progress the development of HTC technology. In this regard, previous studies do not include the utilisation of process water, this process water contained considerable content of solubilized matter and its utilisation would increase the efficiency of the HTC plant. Moreover, including the impact of process water utilisation on the optimization analysis would bring important information. In this study, it is evaluated the utilisation of process water for biogas production via anaerobic digestion (AD) and will be considered as energy recovery within the process plant.

2.3.3 Anaerobic digestion of process water for energy recovery

Anaerobic digestion has been implemented for the treatment of municipal solid waste (MSW) for over 80 years. In the last few decades, different national and international legislations have promoted AD, resulting in a growth of scientific and industrial research. During AD, the organic carbon suffers a series of oxidation-reduction reactions for its conversion into CO_2 and CH_4,

the most oxidised and reduced forms of carbon, respectively [127]. AD is considered a promising technology for the treatment of high moisture and energy-dense organic waste biomass. The versatility of AD relies on its capacity to use a wide range of substrates, even high moisture and complex biomass that represent a challenge for other technologies [128].

AD involves the breakdown and transformation of complex organic matter in the absence of oxygen within a four stages process. Firstly, during hydrolysis, facultative and strictly anaerobic bacteria produce exoenzymes that break down large macromolecules, such as carbohydrates, protein, and fats into smaller constituents like sugars, amino acids, and long-chain fatty acids (LCFAs) [129]. Hydrolysis takes place within a wide range of pH (4-11), with an optimum performance at pH 6-8. The hydrolytic microorganisms are strongly resistant to fluctuations in the digester and the presence of toxic or inhibitory compounds. Secondly, during acidogenesis, these products are transformed into C1-C5 volatile fatty acids (VFAs), such as propionic, butyric, acetic acid, and ethanol. The acidogenic bacteria has a fast growth rate, thus this is the quickest step of the process. The VFAs are quickly generated, mainly acetic and butyric acid, reducing thus the pH. The optimal range for acidogenesis is pH 5.5-6.5, whereas pH environments below 4 could change the metabolic pathway to the more inhibitory propionic acid. Thirdly, in acetogenesis, the VFAs are consumed by homoacetogenic microorganisms to produce acetic acid, CO_2 and H_2. Acetogens are strict anaerobes, with an optimal work at acid-weak pH 6.0-6.2, and a slower kinetic than the previous acidogenesis. The accumulation of H_2 products increases the partial pressure of the system which inhibits the bacteria involved in acetogenesis. Therefore, it is imperative to have a synergistic relationship between acetogenesis and the last step of methanogenesis to quickly consume the by-products and avoid inhibition [130]. Fourthly, in methanogenesis, these intermediaries are transformed into methane via two principal biochemical pathways: (i) acetotrophic pathway is the primary and follows the reaction $CH_3COOH \rightarrow CO_2 + CH_4$; (ii) hydrogenotrophic pathway follows $CO_2 + 4H_2 \rightarrow CH_4 + 2H_2O$. The optimum pH of methanogens is near neutrality (pH 7.0-7.2), hence they are extremely sensitive to pH variations and high concentrations of other by-products, such as VFAs, and free ammonia nitrogen (FAN) [129].

The term biogas ‘digester’ refers to the vessel or reactor where the reactions involved in AD take place. The operation of AD systems involves a digester set at certain growth conditions (temperature, pH, nutrient supplementation) that influence the microorganisms and in consequence their performance. Controlling the operating parameters of organic loading rate (OLR) and retention time (RT) allows sufficient contact time between the microorganisms and the substrate [128]. There are different types of digesters and configurations with particular optimal thriving conditions. The single-stage system is the simplest configuration where all reactions take place in the same vessel. This simplicity facilitates the operation and reduces the costs, although it requires long RT (30-60 d). The two-stage system separates the hydrolysis and methanogenesis in two different digesters. This configuration is more robust and allows the implementation of shorter HRT and higher OLR. The three-stage system employs more digesters to separate the hydrolysis, acidogenesis/acetogenesis, and methanogenesis steps. However, this configuration does not provide considerable improvements in comparison to the two-stage, and it requires a more complex operation and investment [130].

The decomposition of biomass generates biogas comprised of an average of 55-65% methane, followed by carbon dioxide and traces of other gases. AD performance is highly influenced by the substrate composition, adequate amount of nitrogen represented by an appropriate C/N ratio (16-25), micronutrients, and operating conditions [129]. The methane yields are dependent on the composition of the digested biomass. For instance, the theoretical methane yield is considerably higher for lipids and protein than carbohydrates, with values of 1014, 740, and 370 mL CH_4/g VS, respectively, although the hydrolysis rate of the carbohydrates is considerably faster than that of the others. Further, foaming could occur when digesting lipids, while large concentrations of protein could result in toxic TAN levels. [128].

Even though AD is a well-established technology, it still faces several operational challenges that affect its commercialisation. The digestion of recalcitrant substrate, the presence of inhibitory compounds, the instability of the digestate due to sub-optimal operating conditions, and the instability of the microorganisms that affect their synergy. Several strategies have been proposed to overcome these drawbacks, with a recent interest in coupling AD

with a thermochemical pretreatment. This would enhance the biodegradability of recalcitrant biomass and increases energy recovery from the digestate [131]. Pre-treating biomass by HTC avoids the necessity of an initial energy-intensive drying step, which donates HTC a greater potential to be coupled with AD than other treatments like pyrolysis. It has been suggested that low HTC temperatures produce a more diluted liquid product with less inhibitory compounds than that produced by pyrolysis [132]. The AD of biomass treated by HTC has repeatedly proven to be a promising alternative for improving AD performance. The valorisation of HTC process water for methane production via AD has been reported for several feedstocks including algae, digestate, sewage sludge, and orange pomace, although there is little work for food waste (FW) (**Table 2.4)**. FW is an excellent candidate for AD, due to its large availability, and energy content. However, the AD of FW still requires significant research and development to be widely implemented. The cost for transportation of FW and operation by AD still faces several technical, social, and economic challenges. In addition, the accumulation of volatile fatty acids (VFAs), low buffer capacity and foaming compromise the stability of the digester [128]. Even so, FW generates higher methane yields (300-1100 mL CH_4/g VS) than other substrates like lignocellulosic biomass, sewage sludge and animal manure. Therefore, AD is an effective solution for the treatment of FW, since this biomass offers a balanced nutrient composition formed by carbohydrates, lipids and protein that have proven to be advantageous for AD [128].

Table 2.4. Summary of the literature reports for the use of HTC process water as a substrate for anaerobic digestion.

Feedstock	HTC conditions	Digester	AD conditions	Methane yield	Reference
Sewage sludge	200 °C, 6 h, citric acid	30 L reactor, WV 26 L	OLR 1-5 g COD/L·d 37 °C	0.14-0.71 L CH_4/L·d	[133]
Orange pomace	190 °C, 2 h	100 mL syringe	1 g COD/L, 42 °C	214 mL CH_4/g COD	[134]
	225 °C, 2 h			209 mL CH_4/g COD	
	260 °C, 2 h			195 mL CH_4/g COD	
Macroalgae *Saccharina latissima*	Control	AMPTS	37 °C, 30 days, ISR 2	200 mL CH_4/g VS	[135]
	150 °C, 1 h			217 mL CH_4/g VS	
	200 °C, 1 h			202 mL CH_4/g VS	
	250 °C, 1 h			196 mL CH_4/g VS	
Sewage digestate	Control	120 mL glass bottle	ISR 1, 10 g VSS/L, 37 °C, 21 days	175 mL CH_4/g COD	[136]
	160 °C, 30 min			260 mL CH_4/g COD	
	220 °C, 30 min			277 mL CH_4/g COD	
	250 °C, 30 min			226 mL CH_4/g COD	
Food waste	Control	120 mL glass bottle	Inoculum 15 g VS/L, ISR 2, 35 °C,	228 mL CH_4/g COD	[137]
	200 °C			140 mL CH_4/g COD	
	230 °C			154 mL CH_4/g COD	
OFMSW	Control	135 mL glass bottle	ISR 2, 35 °C, 30 days	149 mL CH_4/g COD	[20]
	180 °C, 1 h			205 mL CH_4/g COD	
	220 °C, 3 h			166 mL CH_4/g COD	
	250 °C, 6 h				
Sewage sludge	208 °C, 1 h	120 mL glass bottle	ISR 2, 35 °C, 40-45 days, 10[a] and 25[b] g COD/L	122-165[a] mL CH_4/g COD	[138]
				91-228[b] mL CH_4/g COD	

VSS volatile suspended solids, OFMSW organic fraction of municipal solid waste, ISR inoculum-to-substrate ratio, WV working volume, COD carbon oxygen demand.

2.4 Optimization of HTC process

In general terms, it is agreed that higher yields of solids are obtained when working with low or mild temperatures and short reaction time, while at higher temperatures and longer residence time, a significant mass loss occurs. Nevertheless, with more intensive conditions, the produced hydrochar has a higher density and energy content [25,86]. Therefore, increasing the process conditions, such as temperature and reaction time, improves the hydrochar quality while reducing the solid yield. For example, Lohri et al. [139] found that HTC has the best energy efficiencies working under mild conditions. Achieving the highest energy efficiency at 190 ºC, 28.9 bar and 8 h of residence time. Nevertheless, this study was focused on energy efficiency, thus the hydrochar produced had high volatile matter (60%), low fixed carbon, and heterogeneous combustion. This indicates that HTC at mild conditions has the highest energy efficiencies, although it produces a low-quality char. Based on the past premise, for evaluating HTC performance it must be taken into consideration how the char is planned to be used, and the process optimal conditions are necessary to explore the viability of the technology.

As shown previously, there are several factors affecting the hydrothermal carbonization process. These factors include process conditions such as temperature, residence time, pressure, pH, water:solid ratio. There are also, factors inherent to feedstock, for example, biomass type and chemical composition. Because of the complexity of HTC reactions and multiple factors involved in the process, it is difficult to generate a mathematical model that encompasses the previously mentioned challenges and could be used as a general model for multiple applications. This complicates the optimization of the HTC process.

In this scenario of an impossibility of a general HTC model, one option to progress the optimization of the HTC process is to employ a multiple-factor experimental analysis. Such experimental analysis could be used to develop empirical models. These empirical models can allow simulation and process optimization based on experimental data. However, empirical models have usage limitations, as they can only be applied within the margins of the studied conditions. Therefore, these models are useful for studying and optimizing

complex processes such as HTC of food waste. To develop and empirical model, it is necessary to plan the experiments to cover the process conditions of interest and assure statistical rigour. To comply with these requirements, a design of experiments (DOE) can be used. A DOE involves the planning and running of experimental sets and allows the determining effects of process variables on the system Mäkelä, [140]. Pertinent DOE allows the generation of empirical models and its application for optimisation.

When working towards an experimental optimisation, there are various steps to follow in order to generate an efficient DOE with pertinent factors and variables. A first step is to perform a screening design to evaluate numerous independent variables affecting the process and would allow us to filter out non-significant factors with simple designs and fewer runs, such as the Plackett-Burman design [141]. After the factors to evaluate are defined, it is convenient to perform an approximation analysis to find the factors range where the optimum region is located. One technique used in this step is the method of steepest ascend, in which a first order regression model is generated based using **Eq. 4**. a fist order surface response is generated and then proceeds to follow the direction on which the response increases more rapidly. The method continues until the response do not increase any further and it is considered that the optimum region was located [141,142].

$$y = \beta_0 + \sum_{i=1}^{k} \beta_i x_i \qquad \textbf{Eq. 4}$$

Where y represents the response of interest, x_i represents the variable and β is the calculated regression coefficient. Once the factors and their levels are defined it is possible to perform a response surface methodology (RSM) with a full quadratic regression model to perform the optimisation. For HTC analysis, the implementation of RSM is a good option. RSM can be used to develop a functional relationship between a response of interest and the selected variables [143]. Among the benefits of RSM is the ability to develop statistical models that include the effect of selected variables in first-degree, interaction and second-degree parameters. The general equation used for second degree models is shown in **Eq. 5**.

$$y = \beta_0 + \sum_{i=1}^{k} \beta_i x_i + \sum_{i<j} \sum \beta_{ij} x_i x_j + \sum_{i=1}^{k} \beta_{ii} x_i^2 + \in \quad \textbf{Eq. 5}$$

Where y represents the response of interest, $x = x_1, x_2, \ldots x_k$ represents the variable and β is the calculated constant parameter. Using the model is it possible to evaluate the relationship between responses and variables and predict response values. On can also determine the significance of the effect of different variables and find optimum settings of variables for desired values of the response of interest [143].

The RSM methodology is a statistically-based optimization technique that consists of a number of elements: 1) an adequate DOE for proper data collection; 2) Linear regression modelling, in case the tested region contains curvature, it can be used for finding the optimal point of a parameter; 3) Analysis of variance (ANOVA), it is used for comparing mean values of the data and allows the validation of the regression model or the determination of the significance of various model elements. The results obtained are based on the assumption that residual, or error data, has a normal distribution and population variances are equal; 4) residual testing, it is used to verify the normality assumptions, and if not, some transformation techniques can be used, such as Shapiro-Wilks; 5) comparative testing, in principle, the ANOVA null hypothesis states that mean values of the tested population are equal, then, if at least one of the means is statistically different the null hypothesis is rejected [142].

ANOVA can be used mainly for two purposes. First, rejecting the null hypothesis with respect to the entire regression means that the model adequately describes the process. Second, using ANOVA to evaluate individual parameters rejecting the null hypothesis for an individual parameter indicates that the parameter has a significant effect on the evaluated response. Therefore, the parameter should the included in the model [142].

The main effects and interactions effects variances are compared to the error variance for the significance test. Using the F-test, F0 is calculated with the variance of a given factor against the error variance and compared to

tabulated F distribution values. The higher the F0 value, the higher the probabilities that the factor has a significant effect on the response are. As an alternative, p-values can be used. P-value represents the probability that F0 is the result of a population that corresponds to a null hypothesis. Hence, if the p-value is low the probability of a null hypothesis decreases [142].

Once the correlation models are generated, the RSM method could be used to perform the optimization of the HTC process. During the optimization, test the correlation models are utilised to find the set of process conditions (variables) for optimal responses. The multiple models generated during the RSM method could be employed to conduct a multi-variable and multi-response optimization using the 'desirability function' approach. The desirability method was proposed by Derringer and Suich (Derringer and suich) and consists of converting the response model $(\hat{y})$, into individual functions, called desirability functions (d), which are included in a composite desirability function (D). This composite function is an arithmetic or geometric mean and is used to define the optimization goals: maximize, minimize or target [144].

Desirability function approach is used for multiple response optimizations because it is easy to use, easy to understand, has flexibility for decision making and is incorporated in many software packages [144].

Chapter 3. Methodology

3.1 Introduction

The extent of the project covered the hydrothermal carbonisation (HTC) of food waste for further food waste valorisation and hydrochar utilisation. This chapter first describes the materials used, the origin of the food waste samples, and how they were treated by hydrothermal carbonisation. For the HTC, the reactor used is described, along with the processing conditions established by a design of experiments (DOE). Then, it moves on to describe the methodologies used for the characterisation of the HTC products, hydrochar, and process water. Followed by the outline of the mass and energy balance equations and other considerations for determining the energy efficiency of hydrochar. Also, the use of a thermogravimetric method for establishing the combustion properties of the hydrochar. And finally, the application of the food waste process water as a substrate for the anaerobic digestion (AD), would allow the valorisation of HTC as a pre-treatment for AD.

All chemicals used for experiments and analysis were of analytical grade and used as received. All analyses were performed in duplicate to strengthen the representativity of the results.

3.2 Food waste collection

Food waste was collected from a hall of residence canteen at the University of Leeds. The food waste had the accumulation of three meals for two days, comprised of significant amounts of eggs, sausages, cooked vegetables, cooked potatoes, bread, and fresh fruit, as observed during the initial visual inspection. The sample was blended to a more easily handled size with a Nutribullet® blender and mixed to homogenization. The homogenized sample was stored in 1.5 kg bags and frozen at -20 °C to preserve its initial composition. Food waste was characterised by proximate and ultimate analysis, as well as biochemical analysis, and further used in HTC experiments.

3.3 Hydrothermal carbonisation

HTC reactions were carried out in a high-pressure reactor of 600 mL (Parr Instrument Company, Germany) (**Figure 3.1**). Biomass was loaded fresh into a glass liner, and the moisture content was adjusted to the desired solid load values for the different runs. The glass liner containing the sample submerged in water was placed into the HTC reactor vessel and turned on. The reactor counted with a heating jacket surrounding the reactor vessel that heated the sample until it reached a set temperature, only then the reaction time was started. The temperature was regulated by a proportional integral derivative (PID) controller at a heating rate of approximately 8 °C/min. After the reaction time ended, the heater was turned off, and the reactor was taken out of the furnace and left to cool down at room temperature until the temperature went below 40 °C. The gaseous phase produced during the treatment was vented through the fume cupboard.

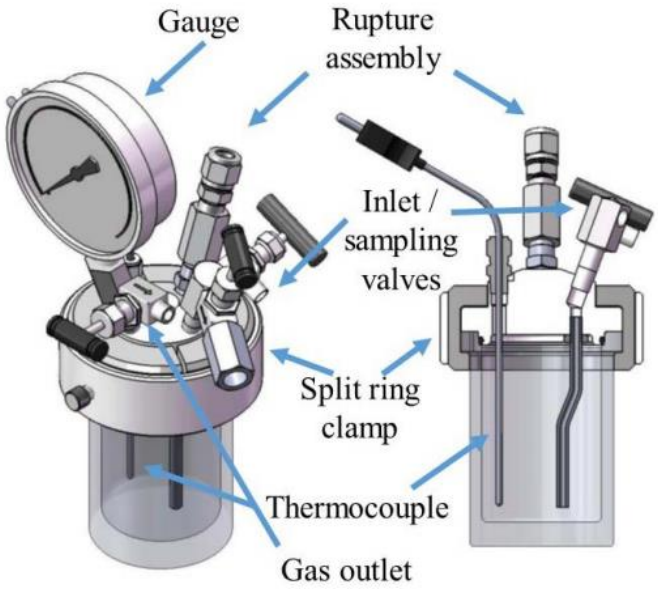

Figure 3.1 Schematic of 600 mL HTC Parr reactor and its components (Smith, 2018).

The reactor was opened once it reached a manageable temperature, and the hydrochar was separated from the process water using 150 mm filter paper (Whatman, UK) and vacuum filtration for 1 min. The liquid filtered called ‘process water’ was frozen at -20 °C for further analysis. The solid fraction

‘hydrochar’ was oven-dried at 60°C overnight and manually ground in a mortar and stored in a zip-lock sealed bag. The weight of the materials, the sample, and the products were recorded for calculating the product yields.

3.4 Design of experiments and statistical analysis

To evaluate the effect of different process conditions on the HTC products the surface response methodology (RSM) was utilised. The design of experiments (DOE) consists of a central composite design with rotatable points. The design evaluated the linear, quadratic, and the two-way-interaction of 3 continuous variables: temperature, reaction time, and solid load. The complete design was composed of 8 cubic or factorial points, 6 central points, and 6 axial points . High and low levels values for each variable were temperature (240 and 180 °C), reaction time (60 and 20 min), and solid load (25 and 15 wt.%). The values for the central points were the middle point between the higher and lower level of each parameter (210 °C, 40 min, and 20 % solid load). Axial points were added to the design to incorporate quadratic analysis into the models, extend the analysed surface area, and add rotatability to the design. In a rotatable design the variance of the predicted response remains unchanged when the design is rotated about the centre and provides equal precision of estimation in all directions. This feature is particularly useful for DOE with optimisation purposes. In this case, the axial points were calculated by $\alpha = \left(n_f\right)^{1/4}$, where n_f is the number of factorial points in the DOE (8), resulting in a coded value of α=1.682 [142].The full run set is shown in **Table 3.1**. The order of the runs was sorted randomly to conduct the experiments.

The values for each variable were selected based on different considerations. For temperature, 180 to 240 °C (and axial points of 160 and 260 °C) cover most of the HTC temperature reaction region, lower temperatures mean that HTC conditions are not reached, and higher temperatures go beyond HTC conditions, reaching hydrothermal liquefaction conditions. Regarding reaction time, DOE screens from 6 min up to 73 min in the longest run. This is relatively short considering the integration of HTC in a larger process, where the shorter times make it more viable economically, thus, longer reaction times are not considered. In the case of solid load, the final range analysed was from 11.5

to 28.5 wt%. This range covers the variation of moisture content in real food waste while still achieving submerged conditions for the sample.

Table 3.1. Full set of runs in the DOE (1: Higher level value, -1: Lower level value, 0: centre point value, α: axial point value).

Coded values			Actual values		
Temperature (°C)	Reaction time (min)	Solid load (%)	Temperature (°C)	Reaction time (min)	Solid load (%)
-1	-1	-1	180	20	15
1	-1	-1	240	20	15
-1	1	-1	180	60	15
1	1	-1	240	60	15
-1	-1	1	180	20	25
1	-1	1	240	20	25
-1	1	1	180	60	25
1	1	1	240	60	25
-α	0	0	159.5	40	20
α	0	0	260.5	40	20
0	-α	0	210	6.4	20
0	α	0	210	73.6	20
0	0	-α	210	40	11.6
0	0	α	210	40	28.4
0	0	0	210	40	20
0	0	0	210	40	20
0	0	0	210	40	20
0	0	0	210	40	20
0	0	0	210	40	20
0	0	0	210	40	20

For the statistical analysis, the software Minitab® was used because it facilitates the planning, creation, and further evaluation of the DOE. This same software allowed the carrying out of the ANOVA analysis, a valuable statistical tool for regression model evaluation and different factor significant testing. A full quadratic regression model was used to fit the experimental data as shown in **Eq. 5**.

$$y = \beta_0 + \sum_{i=1}^{k} \beta_i x_i + \sum_{i<j} \sum \beta_{ij} x_i x_j + \sum_{i=1}^{k} \beta_{ii} x_i^2 + \in \qquad \textbf{Eq. 5}$$

Where y is the response variable, β_0 is the overall mean effect, β_i is the effect of factor x_i, β_{ij} denotes the effect of the interaction between two factors $x_i x_j$, and β_{ii} is the quadratic effect of a factor x_i^2, $\in$ is the random error.

The validation of both analyses (ANOVA and regression model) was carried out by a hypothesis test based on the Fischer F-test that considers the variance ratio distribution. For the regression model hypothesis test, the variance of the model against the variance of the residual (error) was evaluated and compared to tabulated values of the F-statistic (**Eq. 6**).

$$F_0 = \frac{MS_{mod}}{MS_{err}} \qquad \textbf{Eq. 6}$$

The null hypothesis (H_0) stated that all coefficients of the regression model were equal to zero and the model is noise (**Eq. 7**). Against the alternative hypothesis (H_1) where at least one coefficient is different from zero (**Eq. 8**) [140]. The null hypothesis is rejected if F calculated (F_0) is higher than F tabulated (F_{tab}) (**Eq. 9**).

$$H_0: \beta_{1\ldots}\beta_k = 0 \qquad \textbf{Eq. 7}$$

$$H_1: \beta \neq 0 \qquad \textbf{Eq. 8}$$

$$F_0 > F_{tab,\alpha=0.05,v1,v2} \qquad \textbf{Eq. 9}$$

Where $v1, v2$ represent the degrees of freedom of the model and the error, respectively. In this DOE the degrees of freedom were 9 for the model and 10 for the error. If the null hypothesis is rejected the model is validated. and it can be concluded that at least one of the variables has a significant contribution to the model.

The factor significance test was used with a similar approach where each factor variance is evaluated against the error variance, while F tabulated

considers the degrees of freedom for each effect of 1 for $v1$, according to **Eq. 10**, **Eq. 11**, and **Eq. 12**. This would allow the visualisation of the linear, quadratic or/and interaction effect of each factor has statistical significance, and their effect causes a variation on the response higher than the error variance.

$$H_0: \beta = 0 \qquad \textbf{Eq. 10}$$

$$H_1: \beta \neq 0 \qquad \textbf{Eq. 11}$$

$$F_0 > F_{tab,\alpha=0.05,v1,v2} \qquad \textbf{Eq. 12}$$

Also, another significant indicator is the probability of significance p-value, which considers the probability of F_0 being higher than F_{tab}. Thus, it can be used as a single value without the necessity of relative comparison of the F-values. Those parameters with p-values > 0.05 were considered insignificant.

The significance test was performed on all responses of interest to bring insight into the effect of HTC parameters on the composition and quality of hydrochar.

3.5 Solids characterization

3.5.1 Proximate analysis

The proximate analysis allows the characterisation of both raw biomass and hydrochar to obtain the fractions of volatile matter (VM), fixed carbon (FC), ash, and moisture content. These fractions are indicative of the energy densification during HTC and allow the calculation of the heating values based on established correlations.

Proximate analysis was carried out with the thermogravimetric analyser (TGA) (Mettler Toledo TGA/DSC 1). For this method, 10 mg of homogenised sample was loaded into an Alumina 70 µL ceramic crucible and then placed in the TGA equipment. The temperature was ramped from 25 to 900 °C at a heating

rate of 25 K/min, initially under a constant flow of nitrogen (50 mL/min), and finally, switch to an airflow. The equipment was heated from 25 to 105 °C, at this temperature, it was held for 10 min to assure the removal of moisture, this section was used to calculate the moisture content. Heating was resumed until the system reached a temperature of 900 °C, and was held for 10 min to allow the release of volatile matter. After that, the nitrogen flow was switched to air and the system was held once more at 900 °C for another 15 min. The change in the gaseous phase assured the total combustion of the fixed carbon fraction. Finally, the remaining produced comprised the inorganic fraction, considered ash. The proximate composition of the samples was thus calculated based on the difference in mass loss during each heating stage. The analysis was done by a duplicate for each sample.

3.5.2 Ultimate analysis

The objective of the ultimate analysis was to determine the elemental composition of the samples of study, by allowing the quantification of the main elements carbon, hydrogen, oxygen, nitrogen and sulphur (C, H, O, N, S). This technique utilised the instrument elemental analyser (Thermo Instruments Flash EA 1112 Series). In this method, 2.5 to 3.0 mg of sample was weighed in tin foil capsules (Elemental Microanalysis D1009) and crimped for removing the presence of air. The encapsulated sample was then combusted along with two standard samples (Elemental Microanalysis, Devon, UK) as listed in **Table 3. 2**.

Table 3.2 Composition of the standards (Elemental Microanalysis) used as a reference for the ultimate analysis.

Standard	Description	Ultimate (% wt, db)				
		C	H	N	S	O
B2044 BBOT	2,5-Bis(5-tert-butyl-2-benzo-oxazol-2-yl) thiophene (BBOT) OAS	72.53	6.09	6.51	7.44	7.43
B2276 Oatmeal	Oatmeal Organic Analytical Standard	47.76	5.72	2.09	0.16	-
B2306 Coal	Coal Standard Sulphur Range 2.04%	-	-	-	2.03	-

The elemental composition was determined by the conversion of the different elements to their oxides, carbon to CO_2, nitrogen to NOx, sulphur to SO_2, and hydrogen to H_2O. These compounds were measured and quantified by a gas

chromatographer using a thermal conductivity detector, while oxygen was determined by difference.

3.5.3 Biochemical analysis

The biochemical analysis was performed in the School of food sciences of the University of Leeds. Neutral detergent fibre (NDF), acid detergent fibre (ADF) and lignin were determined using the Gerhardt Fibrecap system C. Gerhardt GmbH & Co. KG, Germany) complying with the van Soest methods [145,146]. Where NDF is the sample's remaining fraction after treating with a neutral detergent solution, NDF includes hemicellulose, cellulose and lignin fractions. The ADF fraction is obtained after a following acid detergent digestion and consists of cellulose and lignin fraction, while hemicellulose fraction is removed by filtration. Finally, lignin is determined after treating the ADF fraction with a sulfuric acid solution, where cellulose is removed. Total oil was determined using the Soxtec method [147]. Total protein content was determined using a nitrogen-to-protein using the DUMAS method using a conversion factor of 5.13.

3.5.4 Solid fuel responses

The solid yield was calculated considering the solid fraction remnant in the hydrochar in relation to the initial solid fraction in raw food waste, as stated in **Eq. 13**.

$$Solid\ yield\ (\%) = \frac{Dry\ mass_{hydrochar}}{Dry\ mass_{food\ waste}} \cdot 100 \qquad \textbf{Eq. 13}$$

The quality of the char was also evaluated based on its fuel characteristics. The IGT correlation was used to calculate the higher heating value (HHV) (**Eq. 14)**, a parameter highly used for coal fuels [148].

$$HHV\ \left(\frac{MJ}{kg}\right) = 0.341\ C + 1.323\ H + 0.0685 - 0.01.53\ A - 0.1194(O + N) \qquad \textbf{Eq. 14}$$

Where C, H, A, O, and N represent the percentage of carbon, hydrogen, ash, oxygen, and nitrogen, respectively, in the sample.

For a more accurate estimation of the available energy in the hydrochar, the lower heating value (LHV) was also calculated, accounting for the energy associated with the evaporation of the moisture content. The correlation shown in **Eq. 15** [8] was employed for calculating the LHV.

$$LHV\ \left(\frac{MJ}{kg}\right) = HHV - 0.212\ H - 0.0245\ M - 0.0008\ O \qquad \textbf{Eq. 15}$$

Where H, M and O represent hydrogen, moisture, and oxygen percentage, respectively. The energy densification (ED) ratio was used for evaluating the improvement in the heating value of food waste after carbonisation (**Eq. 16**). Also, the energy yield (EY) was determined to assess the energy content remaining in the hydrochar as a percentage of the feedstock energy content (**Eq. 17**).

$$Energy\ densification = \frac{LHV_{hydrochar}}{LHV_{food\ waste}} \qquad \textbf{Eq. 16}$$

$$Energy\ yield\ (\%) = \frac{Dry\ mass_{hydrochar}\ .\ LHV_{hydrochar}}{Dry\ mass_{food\ waste}\cdot\ LHV_{food\ waste}} \cdot 100 \qquad \textbf{Eq. 17}$$

To evaluate the impact of HTC conditions on the proportion of elemental compounds in hydrochar, the content yield of each elemental response from CHNS analysis in relation to the feedstock content was assessed using **Eq. 18**.

$$X\ yield_{hydrochar}(\%) = \frac{Dry\ mass_{hydrochar}\ \cdot X_{hydrocahr}\ (\%)}{Dry\ mass_{food\ waste}\cdot\ X_{food\ waste}(\%)} \qquad \textbf{Eq. 18}$$

Where X would be substituted by C, H, N, S, O, and ash. The different yields were used to analyse the recovery or removal of the different elements.

3.5.5 Equilibrium moisture content

Equilibrium moisture content (EMC) experiments were conducted to assess the hygroscopic properties of the hydrochar and how it is affected by the

process conditions. This parameter is of relevance because a low hygroscopicity hydrochar would re-adsorb and absorb less moisture after drying, benefiting the storage, transport and further processing.

Particle size was homogenized, using a mesh of 500 and 250 microns, and approximately 1 g of samples was weighed in a crucible. The samples were then placed in a closed chamber of 35 x 50 cm, accompanied by a saturated NaCl solution was placed to generate a relative humidity of around 75 %. The principle of the experiment consisted in placing the samples inside a chamber with constant relative humidity, letting the hydrochar adsorb and absorb moisture. Consequently, weighing the sample to record the hydrated weight, and finally drying and weighing the sample for the mass balance as stated in **Eq. 19**.

This experiment was not focused on obtaining the adsorption isotherms, but to assess the hygroscopicity of the hydrochars generated in the DOE and locating the conditions zone where moisture adsorption is minimized. Instead, the adsorbed moisture is represented as the percentage of dry mass, using the following equation [149]:

$$EMC\ (\%) = \frac{m_{wet} - m_{dry}}{m_{dry}} \cdot 100 \qquad \textbf{Eq. 19}$$

3.5.6 Humic compounds content

The content of humic and humic-like compounds generated during HTC was evaluated gravimetrically with an alkaline extraction from hydrochar. One gram of hydrochar sample was placed in a 50 mL centrifuge tube and added NaCl 0.1 M in a 1:20 (wt:vol). The mix was placed in a shaker bath at 40 °C for 2 h. After the bath, samples were centrifuged at 3100 x g for 15 and the supernatant was decanted into a separated tube. The pH of the supernatant was lowered to 2 with concentrated H_2SO_4 and stored at 4 °C for 24 h.

After letting the sample rest for 24 h, it was separated into a solid phase containing humic-like acid compounds and a clear phase containing fulvic acids and non-humic compounds. For the solid phase separation, samples

were filtered with filter paper (Whatman), rinsed with NaCl 0.1 M, and further freeze-dried.

The content of humic-like molecules was calculated as a percentage of initial hydrochar mass as in **Eq. 20**.

$$\%HA = \frac{Mass\ of\ freeze\ dried\ HA}{Mass\ of\ hydrochar} \cdot 100 \qquad \textbf{Eq. 20}$$

3.6 Thermogravimetric analysis

A thermogravimetric analysis (TGA) was performed to evaluate the effect of HTC on the devolatilization of hydrochar. At the same time, this technique allows the evaluation of the combustion properties and the performance of hydrochar as a solid fuel for combustion.

The TGA experiments were conducted in a thermogravimetric analyser (Mettler Toledo TGA/DSC-1). 10 mg of homogenised sample was loaded in 70 µL Alumina crucibles. The combustion method consisted of ramping the temperature from 35 to 900 °C at a constant heating rate of 10 K/min accompanied by air at a flow rate of 50 mL/min. The temperature and weight loss were measured to create the thermogravimetric (TG) and first derivative thermogravimetric (DTG) curves.

Combustion parameters were determined as points on the DTG and TG curves and were used for the calculation of the comprehensive combustibility index (S) (**Eq. 21**) and combustion stability index (H_f) (**Eq. 21**). These indexes provide a numerical assessment of the combustion behaviour correlating the various parameters determined from the DTG and TG curves.

Comprehensive combustibility index:

$$S = \frac{(DTG)_{max} \cdot (DTG)_{mean}}{T_i^2 T_b} \qquad \textbf{Eq. 21}$$

Where $(DTG)_{max}$ represents the maximum weight loss rate (%/min), and $(DTG)_{mean}$ the average weight loss rate (%/min). The ignition temperature T_i

(°C), is the temperature at which the combustion reaction commences. It has been argued that the ignition temperature is not a physical property of the solid fuel [19], thus, T_i was determined with the graphical tangent-method [19,150,151]. Burnout temperature T_b (℃) is the temperature of end of combustion, it was determined as the temperature at which the reactivity goes below 0.5 percent of weight loss per minute (%/min), inspired by the method used by Śliz and Wilk [150] and Zhang et al. [151].

Combustion stability index:

$$H_f = T_p \ln\left(\frac{\Delta T_{1/2}}{DTG_{max}}\right) \cdot 10^{-3} \qquad \textbf{Eq. 22}$$

Where T_p represents the temperature of the highest reaction rate (DTG_{max}), and $\Delta T_{1/2}$ is the temperature range where DTG/DTG_{max}= 0.5. For the stability index, a lower value means higher combustion stability.

3.7 Process water characterization

3.7.1 Chemical oxygen demand

COD technique was used to determine oxidable organic matter content in water, it was carried out with Hach® test kits EZ7004 of high range 100 - 10,000 mg/L O_2 of dichromate digestion method. For adequate quantification, the samples were diluted at 1:20 with distilled water.

3.7.2 Total organic carbon

Total organic carbon (TOC) and total inorganic carbon (TIC) comprise the total carbon (TC) forms found in water samples. The samples were filtered (0.2 µm) and analysed in the high-performance Analytik Jena TOC Analyzers multi N/C® Series. The principle of the technique consists of injecting the water sample into the analyser where it is heated up to 1000 °C and accompanied by pure oxygen to allow the combustion of the carbon compounds into carbon dioxide. The resultant gas is then passed through an inbuild gas chromatography (GC) column coupled to a thermal conductivity detector (TCD) for the quantification of the TC. To differentiate the TOC from the TIC,

the sample is initially acidified to transform the TIC into carbon dioxide and purged by passing oxygen through the water sample. TC determination is then measured directly in the multi N/C® analyser with a flow injection method. The TOC corresponds to the difference between TC and TIC.

3.7.3 Total solids

The quantification of total solids (TS) was carried out gravimetrically according to APHA (2005). A clean crucible was ignited at 550 °C for 1 h in a muffle furnace, allowed to cool down, transferred to a desiccator and weighed (B) for the mass balance. 5 mL of process water was weighed in the crucible (C) and put in the drying oven at 105 °C overnight. The crucible with the dried sample (A) was weighted and total solids were calculated according to **Eq. 23**. All samples were run in duplicate.

$$Total\ solids\ (^{g}/_{kg\ pw}) = \frac{A - B}{C - B} \cdot 1000 \qquad \textbf{Eq. 23}$$

Where:

A = Dry crucible

B = Empty crucible

C = Crucible with process water

3.7.4 Total nitrogen

Total nitrogen was determined with the Hach Total Nitrogen TNTplus® 828 Vial Test (20-100 mg N/L), using the DR3900 Laboratory Spectrophotometer for water analysis.

3.7.5 Gas chromatography by derivatisation method

The composition of the process water was analysed for VFA and cyclic compounds by gas chromatography (GC), using the Shimadzu GC-2010 Plus with GCMS-QP2010SE mass spectrometer and an RTX®-5 column. The process water sample compromised the safety of the GC equipment; thus, a

derivatisation method was utilised to adequate the process water sample for GC analysis.

The derivatization was performed using the methodology reported by Madsen [152], it consisted in taking 200 µL of process water sample and mixing it with 40 µL of 5 % w/w sodium hydroxide solution, 200 µL of methanol, and 50 µL of pyridine. 25 µL of methyl chloroformate were added to the mix and vortexed for 30 s, this step was repeated one more time. Then, 400 µL of chloroform containing 4-bromotoluene (20.8 µg/mL) were added immediately and vortexed for 10 s. After that, 400 µL of sodium bicarbonate (50 mM) was added and vortexed for 10 s. Finally, the aqueous layer was removed by micropipette, and the solvent layer was placed in the GC vial with an insert.

The GC was set with an inlet temperature of 280 °C, while the used program started at 40 °C with a 5 min hold, then a ramp at 10 °C/min to 100 °C, followed by another ramp at 4 °C/min to 280 °C, and 10 °C/min to 300 °C with a hold of 10 min.

3.8 Anaerobic digestion

3.8.1 Anaerobic sludge inoculum

Inoculum from an anaerobic reactor operated at mesophilic conditions (37 °C) was provided by the wastewater treatment (WWT) plant Esholt in Bradford, West Yorkshire. The inoculum was stored at 4 °C until used and was replaced every three months to guarantee its viability. Before use, the inoculum was homogenised by filtration through a 1 mm mesh, and its COD content was recorded.

3.8.2 Anaerobic digestion reactor

The anaerobic digestion experiments were performed in the Bioprocess™ Automatic Methane Potential Test System (AMPTS II) (Lund, Sweden) (**Figure 3. 2**). The AMPTS II system consisted of three main components, (i) a thermostatic water bath with a capacity for fifteen reactors of 500 mL; (ii) a carbon dioxide fixing unit connected to each reactor where an alkaline solution (NaOH 3M) solubilised the gaseous CO_2 into Na_2CO_3 allowing the passage of the CH_4 to be measured; (iii) a multi-flow gas volume measuring device

working under the principle of liquid displacement and buoyancy generates a digital pulse of the measured gas. The Bioprocess Control Software automatically normalised the measured gas to standard conditions (0 °C, 1 atmosphere), quantifying it by an integrated data acquisition system.

Figure 3.2 Automatic Methane Potential Test System (AMPTS II) by BioProcess Control, equipment used in determining biomethane yield potential from HTC process water.

3.8.3 Biochemical methane potential

It was carried out using the instrument automatic methane potential test system (AMPTS II) (Bio-process Control, Sweden). The tests were set in 500 mL reactors with a working volume of 400 mL filled with inoculum and process water for a final concentration of 10 g COD/L and 5 g COD/L respectively, ending with a proportion of 1:2 substrate/inoculum. After the inoculation, the reactors were flushed with nitrogen to assure anaerobic conditions. A blank control with only distilled water and inoculum was added with every batch by duplicate to account for the residual methane emissions of the inoculum. The reactors operated at 37 °C for 4 weeks and the biomethane produced was measured.

Once the reactors were set up, the AMPTS II system automatically calculated the cumulative biochemical methane potential (BMP) using **(Eq. 24**).

$$BMP = \frac{Volume\ CH_4 from\ sample\ (mL) - Volume\ CH_4 from\ blank\ (mL)}{g\ COD\ of\ substrate\ fed} \quad \textbf{Eq. 24}$$

3.8.4 BMP kinetics

The experimental BMP data was used to calculate the kinetics of the methanation process. The logistic growth model was used to fit the experimental data by nonlinear regression. The re-parameterization of the logistic model for microbial growth was reported by Zwietering (1990) and for biogas production by Pramanik (2019). Three kinetic parameters were calculated: BMP_{final}, for the biogas potential of the substrate; R_m, for the maximum production rate; and λ, for the lag phase. For a better fitting, the logistics equation was modified to a double logistics inspired by Lipovetsky (2010). The equation employed is shown in **Eq. 25**.

$$BMP(t) = \frac{BMP_{max,1}}{1 + exp\left[\frac{4 \cdot R_{m,1} \cdot (\lambda_1 - t)}{BMP_{max,1}} + 2\right]} + \frac{BMP_{max,2} - BMP_{max,1}}{1 + exp\left[\frac{4 \cdot R_{m,2} \cdot (\lambda_2 - t)}{BMP_{max,2}} + 2\right]} \qquad \textbf{Eq. 25}$$

Where $BMP_{max,1}$ and $BMP_{max,2}$ (mL CH_4/g COD) represent the biomethane potential for substrates 1 and 2 respectively. $R_{m,1}$ and $R_{m,2}$ (mL CH_4/day) represent the maximum production rate for substrates 1 and 2, respectively). Finally, λ_1 and λ_2 (days) represent the lag phase for substrates 1 and 2.

3.8.5 Design of experiments for anaerobic digestion

A smaller DOE was created for the AD experiment, it consisted of a factorial design with three factors governing the HTC process parameters: temperature, reaction time, and solid load. The design of the experiment consists of a composite design with 2 replicates, also, 4 central points are added for error evaluation, for a total of 24 reactors used (**Table 3.3**). The main purpose of the DOE is to evaluate the effect of HTC process parameters and the creation of a statistical empirical model of BMP for food waste based on HTC conditions. For this, MiniTab® 19 software package was employed. This DOE allowed the generation of correlation models with linear and interaction effects.

Table 3.3 Full DEO run set for the BMP of process water

Coded values			Actual values		
Temperature (°C)	Reaction time (min)	Solid load (%)	Temperature (°C)	Reaction time (min)	Solid load (%)
-1	-1	-1	180	20	15
1	-1	-1	240	20	15
-1	1	-1	180	60	15
1	1	-1	240	60	15
-1	-1	1	180	20	25
1	-1	1	240	20	25
-1	1	1	180	60	25
1	1	1	240	60	25
0	0	0	210	40	20
0	0	0	210	40	20
0	0	0	210	40	20
0	0	0	210	40	20

3.9 Energy efficiency

3.9.1 Energy balance

Calculation of energy efficiency assesses the energy content that remains in the hydrochar after the HTC processing of food waste. However, energy efficiency calculation could vary depending on the considerations and assumptions that we define for the analysis. Therefore, energy yield (%) is calculated considering only the chemical energy in food waste and hydrochar (**Eq. 11**), while energy efficiency (%) takes into consideration various energy inputs including food waste energy (Q_{fw}), electric energy consumption (W_{el}), and drying energy (Q_{dry}), and the pre-heating energy for heating the sample to the temperature of interest (Q_{pht}). As outputs were considered hydrochar energy (Q_{hc}), energy from process water (Q_{pw}) in form of methane and

simplified energy recovery (Q_{rec}), the general equation for energy balance was **Eq. 26**.

$$Q_{th,fw} + W_{el,HTC} + Q_{th,pht} + W_{el,press} + Q_{th,dry} = Q_{th,hyc} + Q_{th,biogas} + Q_{th,rec} + Q_{loss} \quad \textbf{Eq. 26}$$

$$Q_{th,pHt} = Cp_{fw} \cdot (\Delta T) \quad \textbf{Eq. 27}$$

Where Cp_{fw} represents the heat capacity of food waste, calculated with an empirical correlation based on the solids contained in food [156].

$$Cp_{fw} = 0.837 + 3.348X_{water} \quad \textbf{Eq. 28}$$

$$Q_{dry} = H_{ev\,water} \cdot m_{water\ in\ wet\ hydrochar} \quad \textbf{Eq. 29}$$

Where Q_{dry} stands for water evaporation energy, and W_{el} for electric consumption of the HTC unit.

3.9.2 Energy consumption estimation

For estimating the energy consumption, commonly it is considered the power rating of the heater, and the total time of the run. Total time includes heating time and residence time. However, it is possible that using the power rating of the heater could overestimate the total energy consumption, particularly if the heating device has a PID temperature controller. In this regard, a series of HTC experiments were run using a similar rig with an electric meter adapted. Energy consumed during HTC runs is shown in plot **Figure 2. 5**.

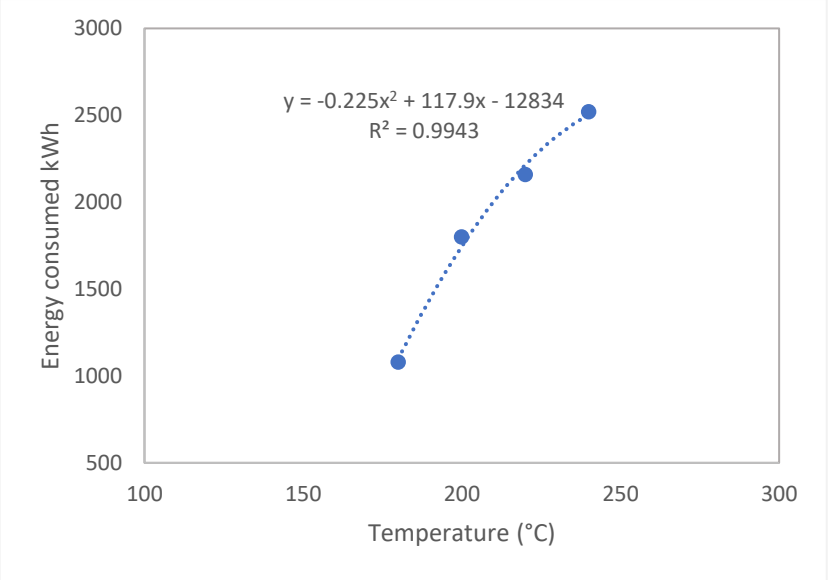

Figure 3.3 Energy consumption during the heating phase of HTC runs measured with an electric meter.

During these runs, the division of energy consumption during heating and during residence time was recorded manually. Two simple models were developed to calculate the electric energy consumption during the heating stage of the HTC reactor **Eq. 30**.

$$Heating_{el}\ (kJ) = \ -0.225T^2 + 117.9T - 12834 \qquad \textbf{Eq. 30}$$

Where T represents the final temperature of the HTC reaction. Also, electric energy consumed during the reaction time was calculated by **Eq. 31.**

$$Reaction\ time_{el}\ \ (kJ) = 1080 \cdot \left(\frac{t\ (min)}{60}\right) \qquad \textbf{Eq. 31}$$

Where t represented the reaction time of HTC after it reaches the final temperature. The final electric energy consumption was calculated by **Eq 32**. However, if the energy analysis is conceived without start-up energy consumption, only $Reaction\ time_{el}$ was considered for energy efficiency calculations.

$$W_{el} = Heating_{el}\ + Reaction\ time_{el} \qquad \textbf{Eq. 32}$$

3.9.3 Energy efficiency

Energy efficiency was calculated to determine the percentage of energy input that remains in the energy outputs. Different energy efficiencies were calculated based on different variations of the energy streams for better insight into the process. The general equation used for energy efficiency calculations is shown in **Eq. 33**.

$$Energy\ efficiency\ (\%) = \frac{Total\ energy\ outputs}{Total\ energy\ inputs} \cdot 100 \qquad \textbf{Eq. 33}$$

3.9.4 Return of energy invested

Return energy invested (REI) allows the assessment of the usable energy of the HTC process by considering only the consumed energy. Thus, due to the wet waste nature of food waste, the chemical energy contained in the food waste is not considered an input for calculating REI (**Eq. 34**).

$$REI = \frac{Total\ energy\ outputs}{Total\ energy\ inputs - Q_{fw}} \cdot 100 \qquad \text{Eq. 34}$$

Chapter 4. Multi-variable analysis and significance test of HTC solid hydrochar

4.1 Introduction

Analysis of HTC considering the effect of multiple factors on different responses is a necessary approach to bring insight into the process. In this work, the response surface methodology (RSM) was employed using a central composite rotatable design (CCRD) for statistical analysis of the effect of process parameters, model regression, and significance test on each response. These regression models are further used to find optimization zones for each response and conduct multi-objective optimization of the process, using the desirability method.

In this chapter, the name of the run is shown in parenthesis with the three parameters, e.g. (X/Y/Z), where X is the temperature (°C), Y reaction time (min), and Z solid load of food waste (%). First, the composition of proximate, ultimate, and biochemical analysis of the food waste feedstock is discussed. In this chapter are analysed the responses of the solid product of HTC, the hydrochar, while the analyses of process water are evaluated in **Chapter 5**. For solid products, the responses are separated into two groups: hydrochar composition and hydrochar quality. Hydrochar composition responses evaluate how the process factors influence the proximate and ultimate analysis of hydrochar. Meanwhile, the hydrochar quality assesses the effect of the process factors on the hydrochar responses more related to its utilisation, such as energetic responses (heating value (MJ/kg), energy densification (ED), energy yield (EY) (%) or elemental yields (C, N, ash yield (%)). Followed by an individual optimisation of the responses and a multi-response optimisation with the objective of evaluating how the individual optimisation is compromised when a multi-response optimisation is carried out.

This chapter is aimed to comply with **Objective 1**: Perform a design of experiments for the understanding of the implementation of HTC as a pre-treatment of food waste for the conversion into energy-dense hydrochar.

1a. Evaluate the effect of process conditions on the composition of hydrochar and perform a significance test of the parameters.

1b Evaluate the effect of process conditions on the fuel quality of the hydrochar and perform a significance test of the parameters.

1b. Perform response optimisation by desirability function of hydrochar qualities.

And **Objective 2**: Evaluate the thermogravimetric properties of hydrochar and the effect of the process variables. For the assessment of utilising the hydrochar in thermochemical processes such as incineration or gasification.

4.2 Food waste composition

Food waste compositions, as mentioned previously, vary depending on the source or type of waste. In this work, the selected feedstock was household or restaurant food waste, also called post-consumer food waste. However, for the sake of comparison and assessing the scenarios for HTC utilisation, the sample was considered as pre-consumer food waste or industrial food waste.

Food waste was collected, processed, and stored as described in the methodology section. **Table 4.1** shows the results for the proximate and ultimate analysis of the food waste, as well as the biochemical analysis. Among its particularities, the low fixed carbon (FC) value of 4.9% found in the feedstock is noteworthy, which is accompanied by a high volatile matter (VM) content of 92.9%. To put into context, literature on most food waste feedstock reported the volatile matter in a range of 80 - 90 %, and a fixed carbon ranging from 10 to 15 % with cases going up to 18 or 20 %. The closest proximate analysis to the present study is from Gupta et al. [157], with a VM of 93.2 % and a FC of 5%. For elemental composition, the low sulphur content of 0.09 % was noted, although it is expected from food waste. In the literature, sulphur in food waste ranged from 0.09 to 0.16 %, and numerous studies reported it as below the limit of detection during analysis. Both nitrogen and hydrogen contents fell in the average range for food waste with 2.54 and 8.43 % respectively. Carbon content represented the highest percentage with 52%,

with an oxygen content of 44%. These values were also found in the expected range of C and O % found in the literature review conducted for this work, with C varying from 40 to 55 % and O from 30 to 54%. Therefore, although this feedstock has shown a particularly low fixed carbon value, this difference is not reflected in the elemental composition.

Regarding biochemical composition, total lipids resulted in a 19.70%, this is an above-average value for food waste, and it is expected to impact positively on heating values for raw food waste and hydrochar. Protein estimation was 15.9% calculated from total nitrogen. The biochemical composition of food waste used in HTC studies is rarely reported. Thus, the comparison references of how the biochemical composition of food waste impacts the hydrochar composition or the HTC process outputs are greatly limited.

Table 4.1. Characterization of food waste.

Analysis	**Weight (%db)**
Neutral detergent fibre (NDF)	15.2
Amylase NDF	4.9
Acid detergent fibre (ADF)	6.8
Total lipids (Soxtec)	19.7
Acid detergent lignin (ADL)	3.1
Total protein[a]	15.9
Volatile matter	92.9
Fixed carbon	4.9
Ash	2.3
C	47.5
H	7.7
N	2.3
S	0.1
O	40.1

[a]Determined from total Nitrogen

Raw food waste was further treated by hydrothermal carbonization, the process products were evaluated in solid and liquid fractions. For evaluating solid products, or hydrochar, and how the parameters affect them, the responses were divided into composition [volatile matter (%), fixed carbon (%), carbon (%), hydrogen (%), and oxygen (%) content]; and solid fuel quality [yield (%), energy densification, O/C and H/C ratios, carbon efficiency (%), nitrogen efficiency (%), and equilibrium moisture content (%)].

4.3 Hydrochar composition

The effect of process factors on hydrochar composition was analysed to search for patterns and be able to correlate their role in each hydrochar response. These effects were further evaluated statistically in terms of significance and the reliability of the regression model. Fuel quality responses were evaluated with significance test and regression model reliability in the same manner, but they were also individually optimized for maximum or minimum values. A summary of the analysis of variance and the significant test of all effects for all responses is shown at the end of the sub-section.

The effect of process parameters on hydrochar composition was evaluated for fixed carbon, volatile matter, carbon, hydrogen, oxygen, and nitrogen content. These composition parameters could provide information on the HTC process mechanism as well as an indirect indicator of hydrochar quality and utilisation options where the hydrochar could be applied. The summary of composition for the complete DOE is shown in **Table 4. 2**.

Table 4.2. Proximate and ultimate analysis results of hydrochar from food waste (raw biomass), full DOE runs. SL is solid load, VM volatile matter, FC fixed carbon, all % on a mass basis.

Temp. (°C)	Time (min)	SL (%)	VM (%)	FC (%)	Ash (%)	C (%)	H (%)	O (%)	N (%)
Food waste			92.9	4.9	2.3	47.5	7.7	40.1	2.3
180	20	15	83.6	15	1.4	63.2	7.4	26.8	3.6
240	20	15	75.2	23.4	1.8	69.3	8.3	19.1	3.5
180	60	15	78.3	19.6	1.5	63.6	7.1	26.3	4
240	60	15	76.4	22.6	1.4	71.2	7.5	17.8	3.6
180	20	25	79.4	18.6	1.5	59.3	7.2	31.6	3.8
240	20	25	73.9	24.9	1.5	67.9	7	21.8	3.6
180	60	25	78.8	20.7	0.8	61.6	7.1	29.7	3.9
240	60	25	72.5	25.4	2	68.6	8	19.6	3.7
159.5	40	20	82.4	14.4	2.4	52.1	6.6	38.7	3.2
260.5	40	20	73.4	22.9	3.7	72	8.6	13.3	3.7
210	6.4	20	79.7	16.3	4.1	65	8.6	20.6	3.7
210	73.6	20	74.5	23.4	2.1	67.5	8.7	21.7	3.3
210	40	11.6	75.2	23.4	1	68.5	7.1	22.2	3.4
210	40	28.4	72.9	24.9	1.8	64.8	6.9	25.2	3.6
210	40	20	77.2	19.4	3.5	66	8.4	20.8	3.4
210	40	20	78.1	18.5	3.4	67.4	8.6	20	3.3
210	40	20	80.2	16.1	3.7	67.1	8.5	18.7	3.7
210	40	20	74.6	22.9	2.5	68.1	7.7	21.5	3.4
210	40	20	76.1	19.5	4.4	66.3	7.9	19.5	3.4
210	40	20	74.7	23.8	1.3	66.4	6.9	23.8	3.8

4.3.1 Fixed carbon, volatile matter and ash of hydrochar

Fixed carbon, volatile matter and ash content are the main parameters from proximate analysis of coal and biochar. They give a first estimation of the hydrochar structure and behaviour in processes such as combustion or gasification. Fixed carbon (FC) is the fraction of hydrochar that remains after both the volatile fraction and ash content have been removed. Fixed carbon has a recalcitrant structure, with a high degree of aromatization, as it resists thermal devolatilisation at temperatures as high as 900 °C [158]. It has been estimated that 90 wt% of the FC fraction of the hydrochar is comprised of carbon, although there are also small quantities of H, O and S present in FC.

In general terms, FC increases as process conditions increase (high temperature and longer reaction times). This is also illustrated in the main plot effect (**Figure 4.1**) where FC increased when temperature and reaction time increased. The highest FC values were found at (240/60/25) and (240/20/25) with 25.37 and 24.94%, this seems to indicate that temperature had a larger effect than reaction time. However, these values are relatively low in comparison to other studies found in the literature. For instance, Bhakta Sharma et al. [16] and Wang et al. [14] reported 48 and 45.5% FC, respectively, working with mixed post-consumer food waste at 250 and 260 °C, respectively. Nonetheless, values around 20% are also reported in the literature. For example, McGaughy and Reza [6] reported 22.42% FC working at 260 °C with post-consumer FW. In the same manner, Lucian et al. [20] reported 19.4% FC at 250 °C for 6 hours, working with the organic fraction of municipal solid waste (OFMSW). Therefore, relatively low values of FC (<30%) are not uncommon when working with FW. One reason for these relatively low values could be the presence of lipids in the FW feedstock. Li et al. [106] reported that the addition of lipids in food feedstock decreases the values of FC%. Most importantly, these FC values remained low even after intense HTC conditions, in comparison with samples with only carbohydrates, or carbohydrates and protein. Hence, it is highly possible that the reported high FC % were produced from food waste feedstock with significantly low lipid content.

In addition, solid load shows an important role in the generation of FC. At the highest temperature run (260/40/20), FC only reached 22% and the highest solid load run (210/40/29) produced a relatively high FC of 24.89%. This is observed in **Figure 4.1**, where FC reached its highest values at the largest solid load. However, FC decreases as SL was reduced, reaching a minimum of around 20% SL, and starts increasing again as SL keeps reducing.

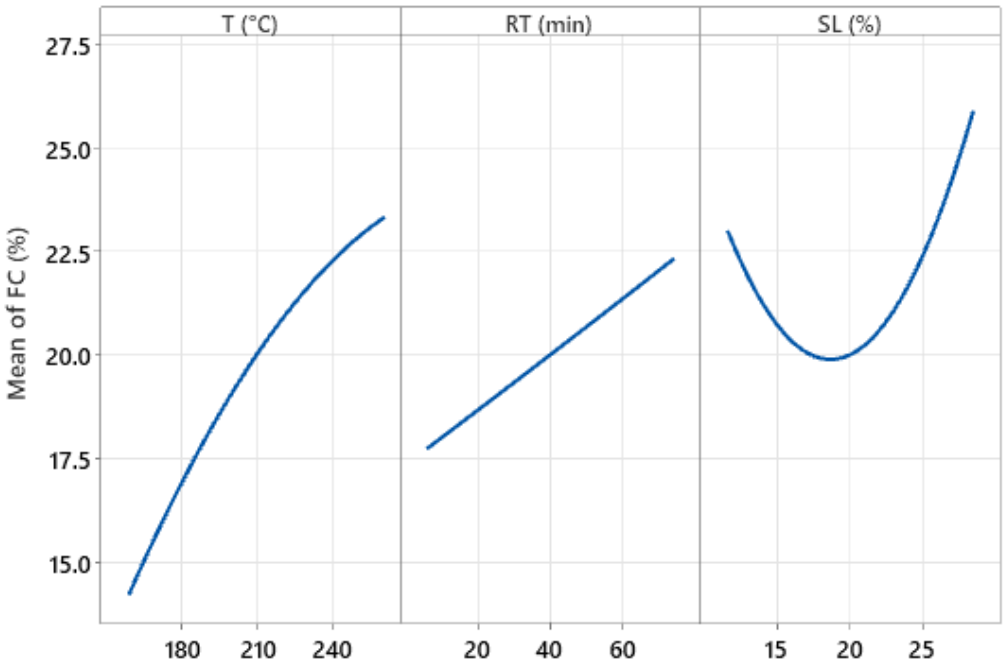

Figure 4.1 Main effects plot on Fixed Carbon (%).

As mentioned in the methodology, a significance test was conducted to evaluate which factors were statistically significant. First of all, the regression model of fixed carbon was significant with a $F_{(9,10)} = 3.86 > F_{tab} = 3.02$, or in p-value terms p = 0.023 (p < 0.050 = significant) with a $R^2 = 0.77$. The full regression model is shown in the following equation:

$$\boldsymbol{FC}\ (\%) = \boldsymbol{-16.4 + 0.356\,T + 0.410\,RT - 2.16\,SL + 0.000477\,T*T + 0.00002\,RT*RT + 0.0614\,SL*SL - 0.00149\,T*RT - 0.00032\,T*SL - 0.00151\,RT*SL}$$

Contour plots generated with the regression model are shown in **Figure 4.2**, where fixed carbon increases with temperature and reaction time. In contrast, solid load exhibited a lower fixed carbon generation at values close to 20% SL, and higher values at both low and high ends of solid load.

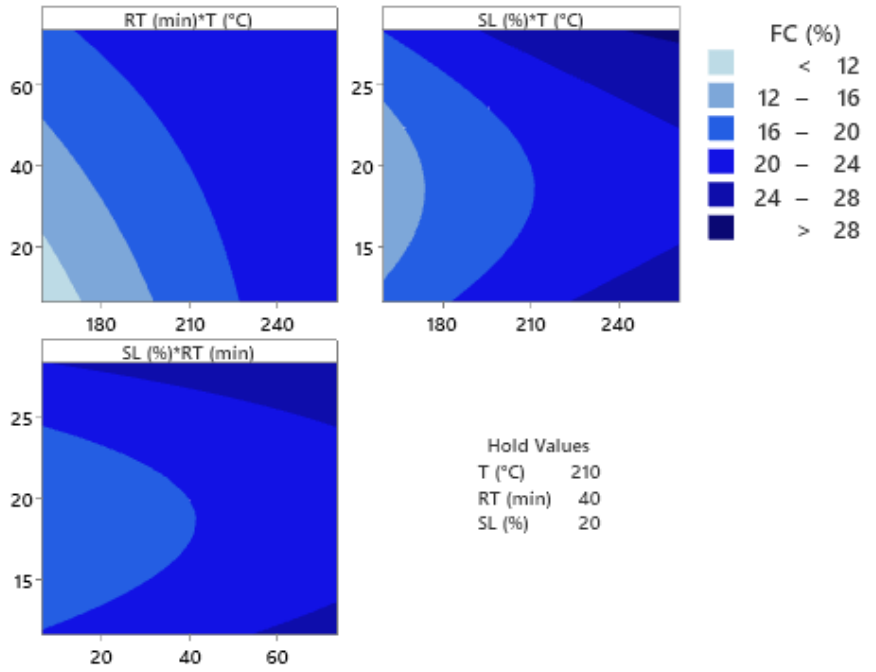

Figure 4.2 Contour plots of fixed carbon (%)

The significance test was also applied to individual effects, and Pareto charts were used for a visual representation of the significant effects as shown in **Figure 4.3**. The standardized individual effect is shown in the Pareto chart. The statistical significance of the effect is marked with a reference line; hence, those significant effects are represented when crossing the reference line. It was observed that for FC%, temperature had the main effect, which was linear ($F_{(1,10)}$ = 19.08, p = 0.001). Solid load showed a significant quadratic effect ($F_{(1,10)}$ = 6.60, p = 0.028). Reaction time fell below the limits of statistical significance in this work with $F_{(1,10)}$ = 4.84, just under tabulated F-values of 4.96, with p = 0.053. Therefore, the null hypothesis cannot be discarded. This result was not visible from the main effects plot **Figure 4.1**.

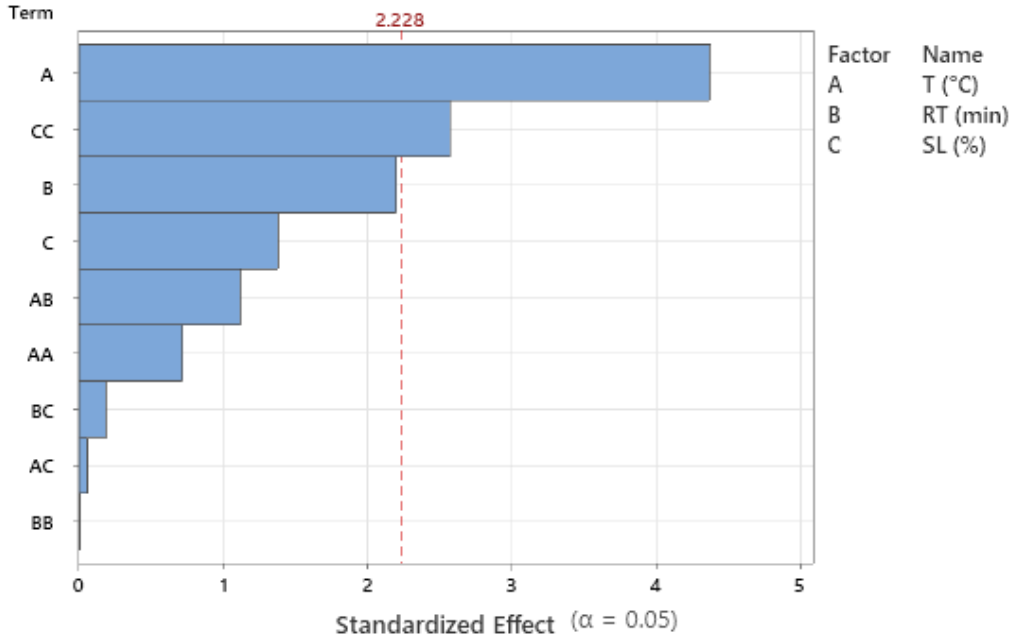

Figure 4.3 Pareto chart of standardized effects on Fixed Carbon (%).

Volatile matter is the fraction of hydrochar that is released by devolatilization during HTC. This fraction ignites easily and burns for a short duration [159]. Thus, as expected, it shows an inverse behaviour to fixed carbon. Volatile matter variation ranged from 72 to 83% on the full DOE run set, with the highest values found at run (180/20/15) with 83.55% followed by (160/40/20) with 82.37 %. This was expected as both runs have the lowest intensity in the DOE. Contrarily, the lowest values of VM were found at (240/60/25) followed by (210/40/29) with 72.54 and 72.92%, respectively. This difference is minimal, while the intensity of temperature and time were considerable. Thus, this could indicate that solid load has a significant effect on the content of VM. Nonetheless, these VM values are rather high in comparison to some studies in the literature, where VM% has been reported as low as 38.91% [160] or 39.7% [15]. In this regard, the high VM values obtained in this study reflect the presence of lipids in the sample, which restricts the samples to lower VM values even at higher process conditions, as explained in the fixed carbon section. However, VM values of 60.2% [20], 62.87% [161], and 75.5% [6] have been reported while working with temperatures >250 °C and reaction times >1 h. The latter illustrates that high VM could be common when working with

food waste as a feedstock since the FW sample would likely contain a considerable amount of lipids.

Regarding the effects of the process conditions on VM, the main effects plot (**Figure 4.4**) shows that both temperature and reaction time had a linear effect with a slight, levelling off curvature, decreasing VM as temperature and time increase. Instead, solid load showed a clear quadratic effect, increasing VM% as solid load reduced, reaching a maximum around 17 %SL, and declining at lower SL.

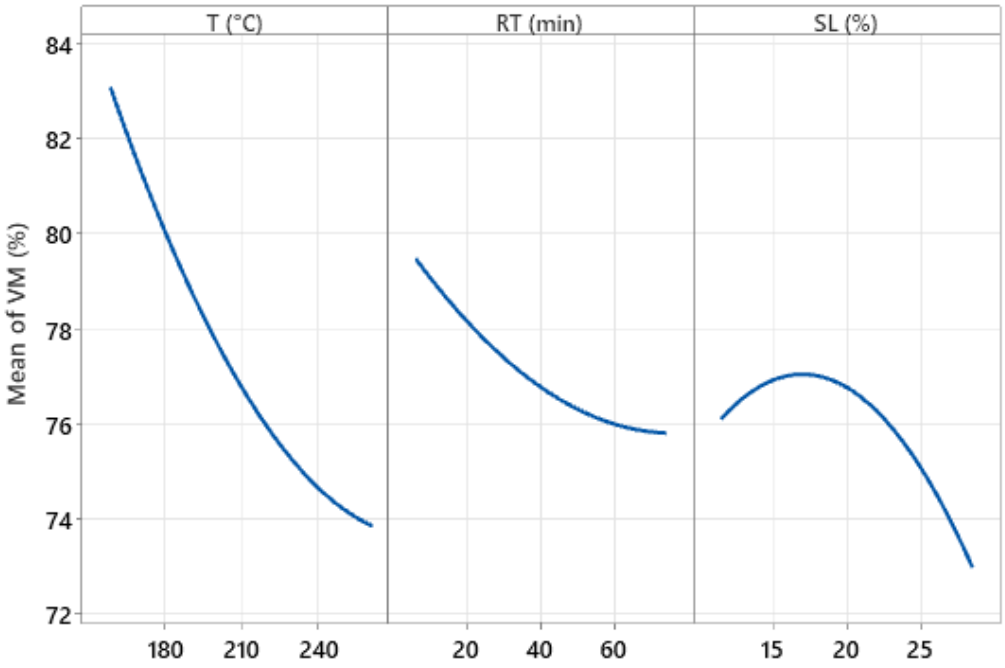

Figure 4.4 Main effects plot on Volatile Matter (%).

Regarding the statistical analysis, the regression model was significant for the ANOVA of volatile matter, with $F_{(9,10)}$ = 4.70 and p = 0.012, With an R^2 = 0.8087. The full regression model is shown next:

$$\boldsymbol{VM}\ (\%) = \mathbf{125.8} - \mathbf{0.385}\,\boldsymbol{T} - \mathbf{0.418}\,\boldsymbol{RT} + \mathbf{1.22}\,\boldsymbol{SL} + \mathbf{0.000650}\,\boldsymbol{T}*\boldsymbol{T} + \mathbf{0.00075}\,\boldsymbol{RT}*\boldsymbol{RT} - \mathbf{0.0309}\,\boldsymbol{SL}*\boldsymbol{SL} + \mathbf{0.00120}\,\boldsymbol{T}*\boldsymbol{RT} - \mathbf{0.00131}\,\boldsymbol{T}*\boldsymbol{SL} + \mathbf{0.00262}\,\boldsymbol{RT}*\boldsymbol{SL}$$

The generated contour plots are displayed in **Figure 4.6** and show that volatile matter decreased as temperature increases. However, neither reaction time nor solid load appeared to play a significant role. This was confirmed by the individual significance test shown in the Pareto chart (**Figure 4.5**), where the temperature was the only variable with a significant effect ($F_{(1,10)}$ = 28.46, p = 0.000). Meanwhile, the linear effect of time and solid load were insignificant by a small margin.

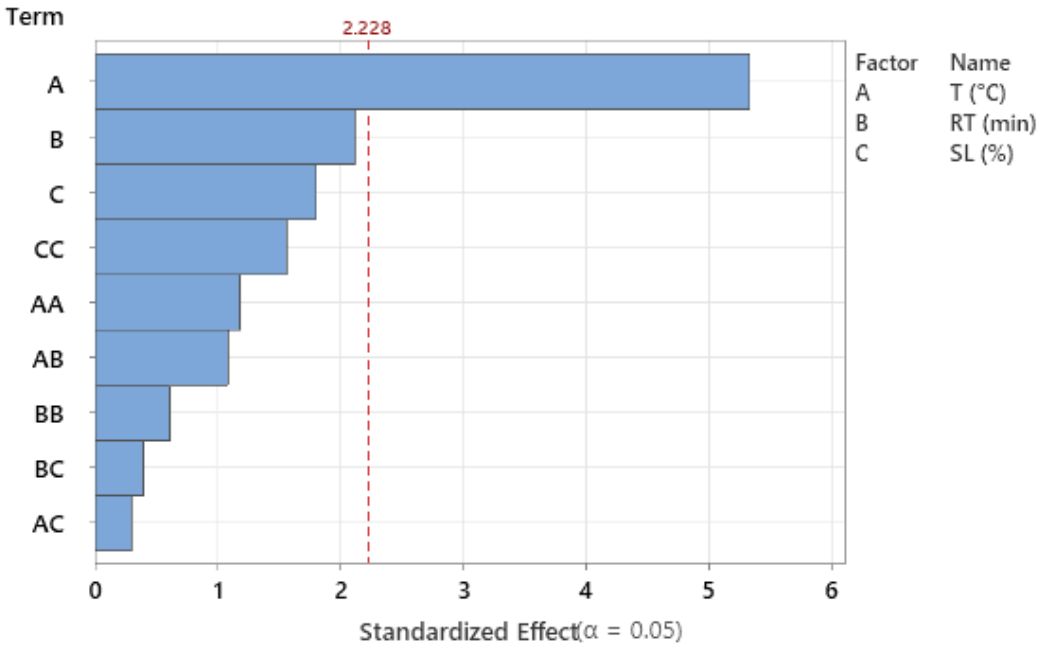

Figure 4.5 Pareto chart of standardized effects on Volatile Matter (%).

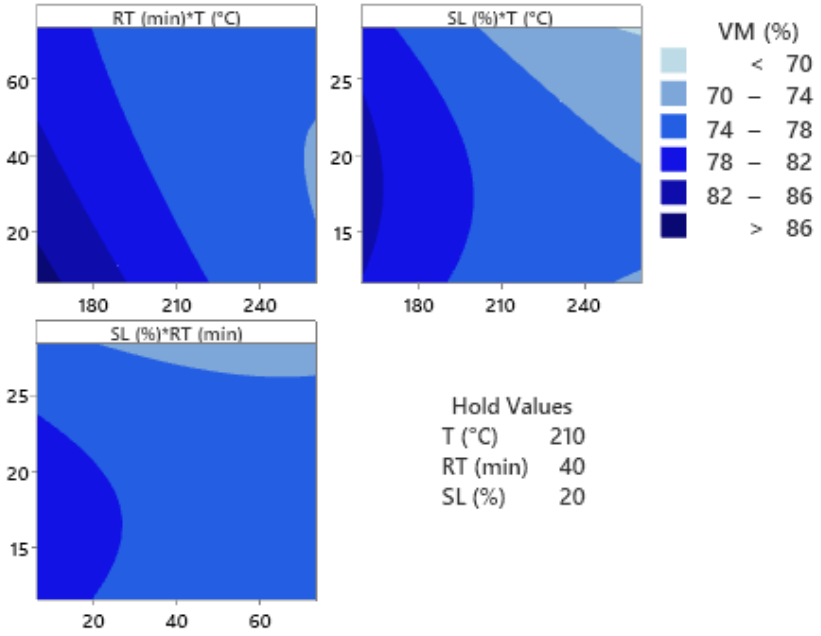

Figure 4.6 Contour plots of volatile matter (%).

The ash content of the hydrochar products was found in a range from 0.81 to 4.31%. There seems to be a trend where ash % is dependent on solid load, and lower ash values were achieved at either high or low solid load, while middle SL (20%) seems to promote higher ash content. Nonetheless, the low values, in combination with an unclear trend, did not permit an adequate statistical analysis. Ash content exhibited a lack of significant effect, and the regression model was not significant, exhibiting a low fitting $R^2 = 0.26$.

In addition to the proximate analysis, the effect of the HTC process on the elemental composition of hydrochar is assessed in the next section. This is useful to evaluate the fate of elemental N, and to assess the carbonization degree as well as the energy content by combined C, H and O contents.

4.3.2 Carbon, hydrogen, oxygen and nitrogen composition of hydrochar

In the case of elemental composition, there is limited information on the effect of different factors on their distribution. Carbon content (C%) ranged from 52 to 72%. Results show an increase in C% as temperature increases, reaching

a maximum value of 72% at (260/40/20) and the lowest value of 52.12% at (160/40/20), both runs were the highest and lowest temperature in DOE run set, respectively. Therefore, this suggests that %C is linked to temperature independently of reaction time and the solid load of food waste. The range of C% obtained in this study falls in that found in the literature review, from 48 to 73 %. The highest C% was reported by Saqib et al. (2018) with 73%, Gupta et al. [157] with 72.1%, Álvarez-Murillo et al. [27] with 72.03%, and Chen et al. [10] with 72.11%. Therefore, the C% in the present study is a relatively high value among other food waste feedstock works.

Figure 4.7 illustrates the dominance of temperature over the other factors. Temperature exhibits a large mean linear effect on C% ending in a slight curvature, increasing C% with temperature. In contrast, both time and solid load show a linear effect with no apparent significance. C content increases as reaction time increases and solid load were reduced.

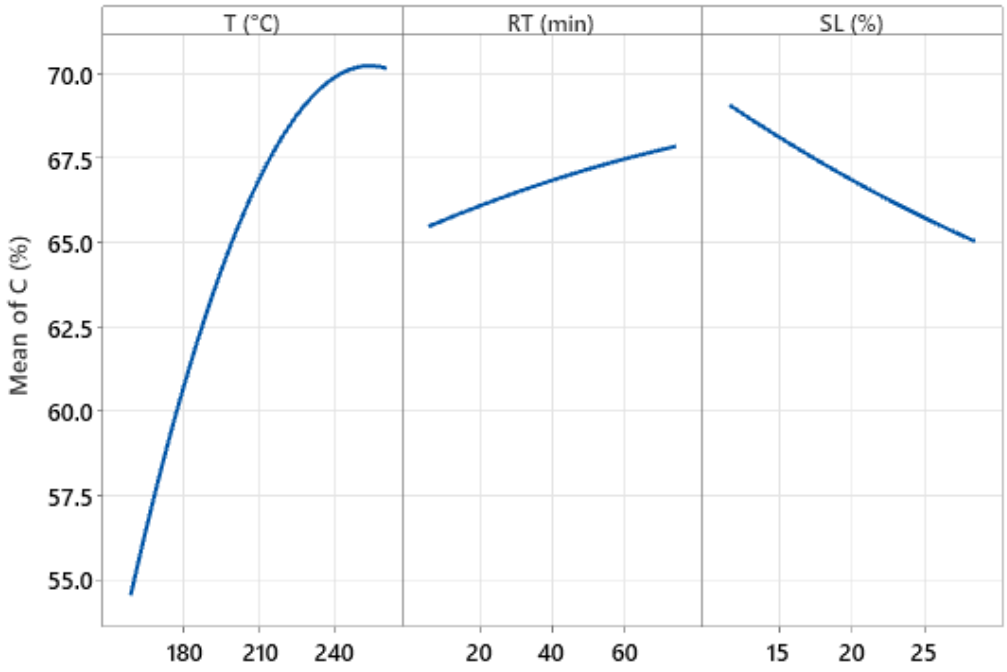

Figure 4.7 Main effects plot on carbon content (%).

The ANOVA reveals a significant regression model of C (%) with $F_{(9,10)}$= 17.31, p = 0.000 and a correlation coefficient of R^2 = 0.93. The full regression model is shown next:

$$\boldsymbol{C}\ (\%) = \mathbf{-29.9} + \mathbf{0.847}\,\boldsymbol{T} + \mathbf{0.037}\,\boldsymbol{RT} - \mathbf{0.74}\,\boldsymbol{SL} - \mathbf{0.001728}\,\boldsymbol{T} * \boldsymbol{T} - \mathbf{0.000157}\,\boldsymbol{RT} * \boldsymbol{RT} + \mathbf{0.0029}\,\boldsymbol{SL} * \boldsymbol{SL} - \mathbf{0.000039}\,\boldsymbol{T} * \boldsymbol{RT} - \mathbf{0.00166}\,\boldsymbol{T} * \boldsymbol{SL} - \mathbf{0.00093}\,\boldsymbol{RT} * \boldsymbol{SL}$$

The generated contour plots for C% are shown in **Figure 4.8**, where C% in hydrochar increases as temperature increases. According to the plots, maximum C% could be achieved at temperatures above 230 °C, enhanced by reaction times higher than 40 min and solid loads below 20 %.

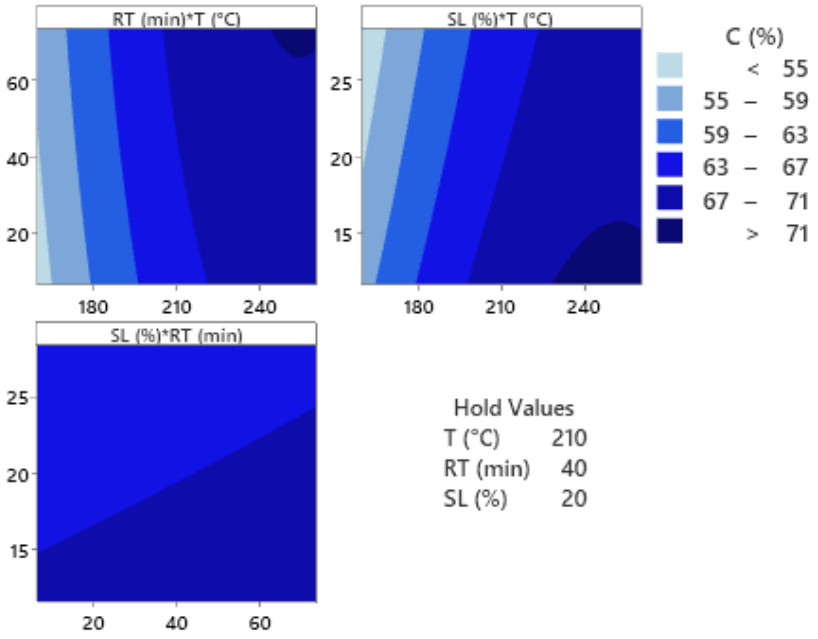

Figure 4.8 Contour plots of carbon content (%)

Individual parameters affecting C% are shown in the Pareto chart (**Figure 4.9**), where temperature exhibited both significant linear and quadratic effects with $F_{(1,10)}$ = 128.13, p = 0.000 and 15.47, p = 0.003, respectively. Solid load displayed a significant linear effect $F_{(1,10)}$ = 8.58 and p = 0.015, whereas the reaction time did not exhibit significance in any of the effects involved.

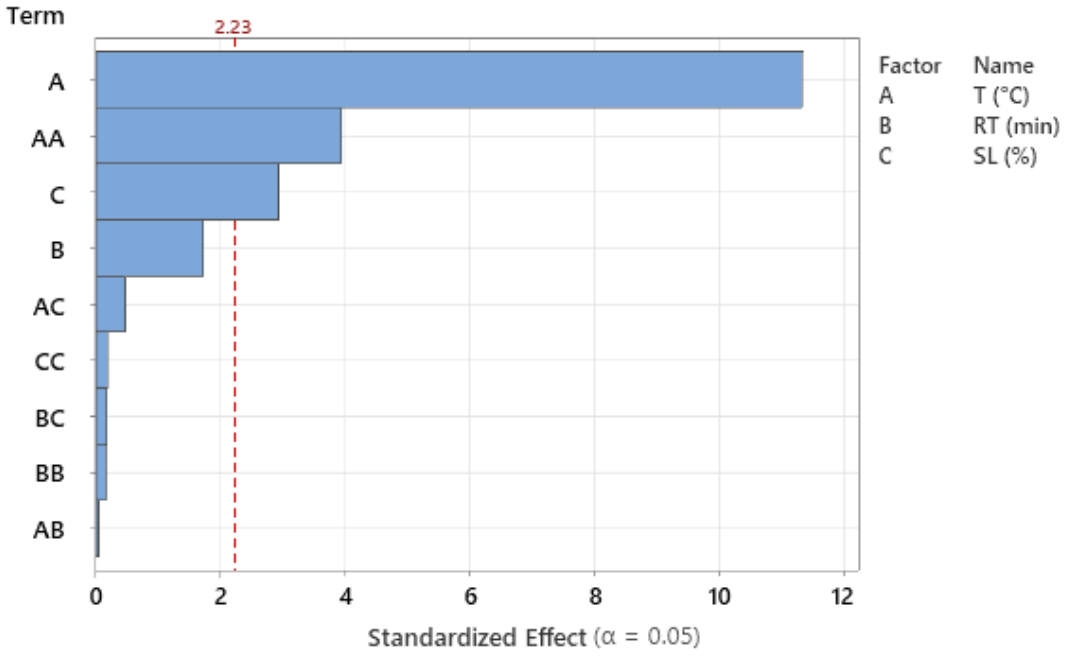

Figure 4.9 Pareto chart of standardized effects on C (%).

In contrast to carbon, H% showed little variation through the conditions of the DOE run set. Hydrogen content ranged from 6.64 to 8.68%, with no conclusive pattern. The lowest values were found at conditions (160/40/20); however, maximum values did not reveal a general pattern. The highest H% values were achieved at (260/40/20) with 8.64%, (219/73/20) with 8.68% and (210/06/20) with 8.60%. These runs were coincidently axial points within the DOE set, with extreme points of temperature and time, meanwhile, the rest of the DOE area showed just a small variation. This could indicate a major role of the solid load. According to the main effects plot (**Figure 4.10**) temperature yielded both linear and quadratic effects, increasing H% with temperature. Reaction time showed a low quadratic effect with a minimum H% at 40 min, while solid load appeared to have a highly quadratic effect with a maximum at 20 % SL.

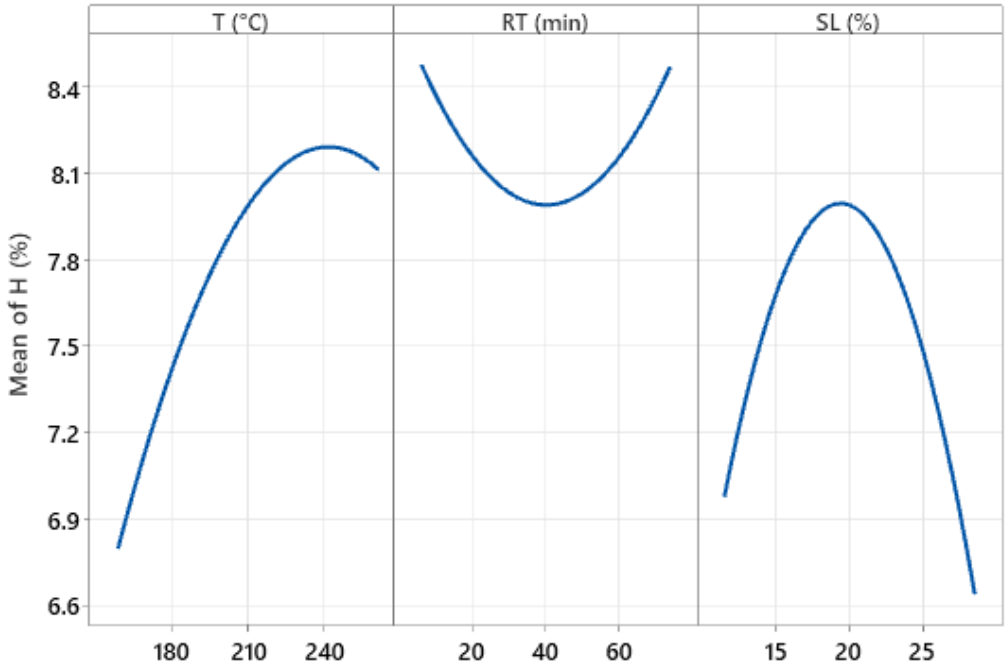

Figure 4.10 Main effects plot of hydrogen content (%).

Regression model for H% showed no significance with $F_{(9,10)} = 2.11$, $p = 0.130$ with a regression coefficient of $R^2 = 0.65$. This could be attributed to the fact that hydrogen content variation between runs was too low to differentiate from error.

$$\boldsymbol{H}\ (\%) = -\mathbf{8.5} + \mathbf{0.1048}\,\boldsymbol{T} - \mathbf{0.1027}\,\boldsymbol{RT} + \mathbf{0.641}\,\boldsymbol{SL} - \mathbf{0.000206}\,\boldsymbol{T}*\boldsymbol{T} + \mathbf{0.000419}\,\boldsymbol{RT}*\boldsymbol{RT} - \mathbf{0.01638}\,\boldsymbol{SL}*\boldsymbol{SL} + \mathbf{0.000104}\,\boldsymbol{T}*\boldsymbol{RT} + \mathbf{0.00048}\,\boldsymbol{T}*\boldsymbol{SL} - \mathbf{0.00236}\,\boldsymbol{RT}*\boldsymbol{SL}$$

However, even when the regression model was not statistically significant, it was observed that H% increases with temperature, as shown in **Figure 4.11**. This would indicate that hydrogen is retained while oxygen is removed from the hydrochar. Also, a solid load of around 20% yielded higher H%. In the case of the significance of individual effects, the variable solid load exhibited a significant quadratic effect ($p = 0.021$). Also, the temperature displayed a significant linear effect ($p = 0.031$), while reaction time did not have any significant effect (**Figure 4.12**).

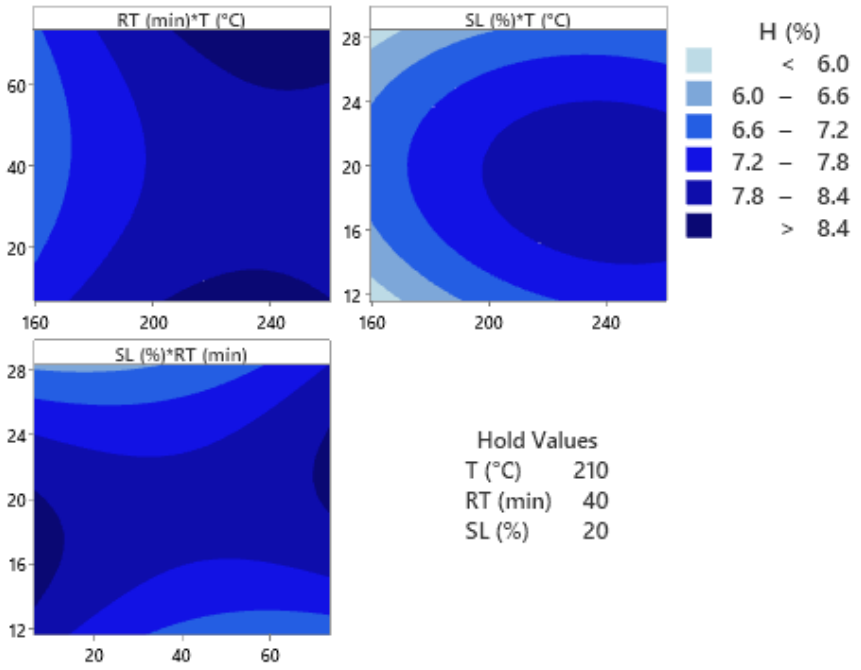

Figure 4.11 Contour plots of Hydrogen content (%)

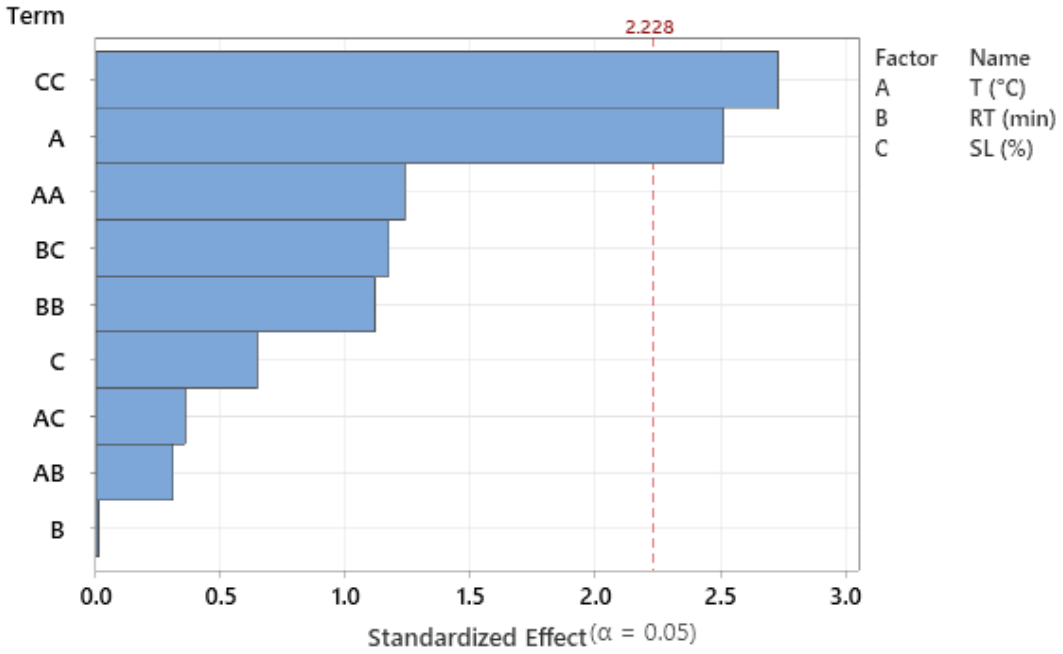

Figure 4.12 Pareto chart of the standardized effects on hydrogen content (%).

Oxygen content is an important response of HTC, due to its relation to the extent of carbonization, it is desirable a large removal of oxygen and thus low O%. Low oxygen content means a more reduced hydrochar, thus it could release more energy during combustion, reflected in higher heating values. Oxygen content varied from 38% at (160/40/20) down to 13.33% at (260/40/20). This carried a considerable reduction of O% at high temperatures from the original 40% in the raw food waste. In comparison, the reduction in O% at the lowest temperature was minimal, even if the reaction time was relatively long (40 min). This demonstrates the clear effect of temperature on oxygen content. The literature review indicates that the removal of oxygen in this work was relatively high. In comparison, other mixed post-consumer food waste feedstock hydrothermally treated at similar conditions reported O content of 15 to 25% [5,15,16,24,157], nevertheless, similar values have been reported by Lucian et al. [20] with 14% or Mazumder et al. [114] with 12.8%.

The main effects plots show an important influence of temperature with a clear linear effect, decreasing the oxygen content as temperature increases (**Figure 4.13**). Reaction time exhibits clear low importance, while solid load displays a curvature effect with no clear significant effect on O% with a minimum at 18 % SL.

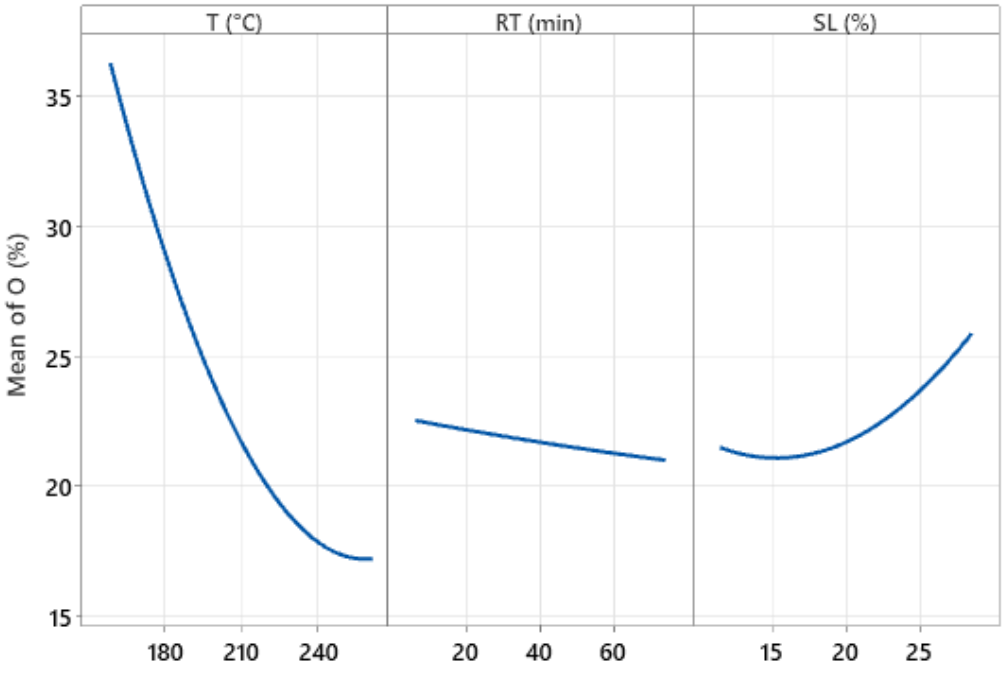

Figure 4.13 Main effects plot on oxygen content (%).

The regression model showed significance with $F_{(9,10)} = 11.67$, $p = 0.000$, and a $R^2 = 0.91$. The full regression model is shown below:

$$\boldsymbol{O\ (wt\ \%) = 136.4 - 0.936\,T + 0.110\,RT - 0.12\,SL + 0.001941\,T*T + 0.00006\,RT*RT + 0.0275\,SL*SL - 0.00029\,T*RT - 0.00274\,T*SL + 0.00380\,RT*SL}$$

The generated contour plots indicate that oxygen content decreases as temperature increases, drastically from 160 up to 220 °C, and beyond this temperature, the decrease of O% slows down **Figure 4.14**. Time does not impact the O%, while solid load seems to enhance O% removal at an SL of 15 to 25 %.

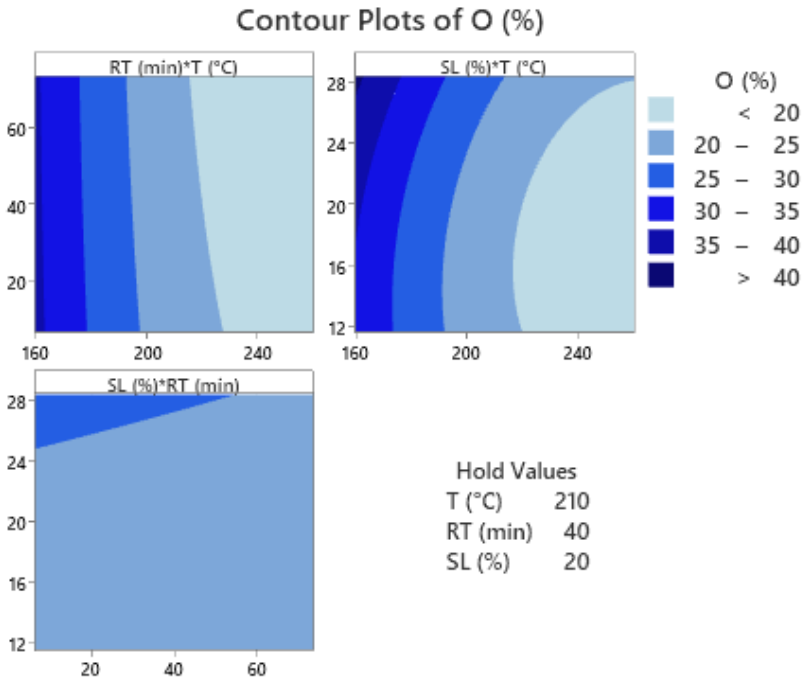

Figure 4.14 Contour plots of Oxygen content (%)

Regarding individual parameters, temperature was the only significant factor, exhibiting significance in linear ($F_{(1,10)} = 87.3$, $p = 0.000$) and quadratic effects ($F_{(1,10)} = 10.2$, $p = 0.010$). The linear effect of solid load on O% was closely under the limit of significance. In addition, solid load showed an important

influence on both its linear and quadratic effects (**Figure 4.15**). However, they fell below the statistically meaningful limit to be considered significant.

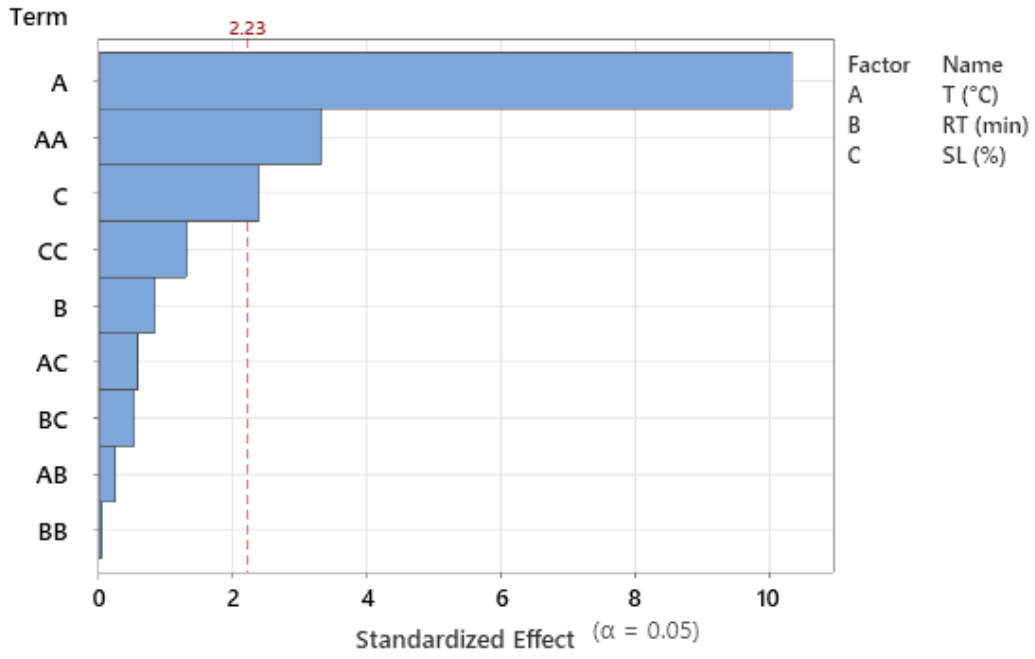

Figure 4.15 Pareto chart of standardized effects on oxygen content (%).

Nitrogen content is an important response for assessing fuels, as it relates to the generation of nitrogen compounds emissions, such as NOx. However, in this work, N (%) remained without considerable variation in the hydrochar throughout the experimental conditions set. Nitrogen content ranged from 4.05% at (180, 60, 85) to 3.24% (160, 40, 80). This does not mean that there was no nitrogen removal, as this would be reflected in combination with the solid yield, and is assessed in a later section. However, the N% in hydrochar did not vary widely in the experiment.

As illustrated in the main effect plot (**Figure 4.16**), the three factors yielded a quadratic effect. With a minimum N% at the middle point of each factor 210 °C, 40 min and 17 %SL. However, the mean variation of the effects is remarkably low.

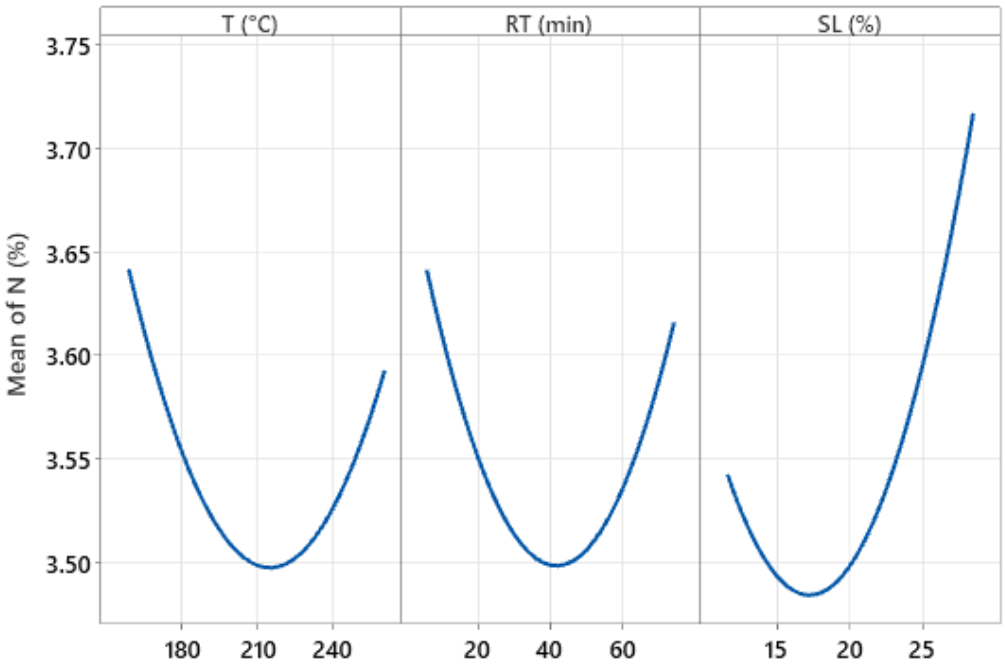

Figure 4.16 Mean effects plot on nitrogen content (%).

The regression model was not significant and resulted in a R^2 of only 0.17. This insignificance could be attributed to the little variation between the different runs, falling in the range of error. The regression model is shown next:

$$\boldsymbol{N\ (wt\ \%) = 5.44\ -\ 0.0174\,T + 0.0218\,RT - 0.059\,SL + 0.000045\,T * T + 0.000112\,RT\ * RT + 0.00181\,SL * SL - 0.000098\,T * RT + 0.000087\,T * SL - 0.000531\,RT * SL}$$

The marked quadratic effect evident in the main effects plot is also observed in the contour plots (**Figure 4.17**), where the marked onion patterns reflect a quadratic effect on the three factors. A zone with minimum N% is highlighted in the contour plots at mid temperatures and reaction time, with a low solid load.

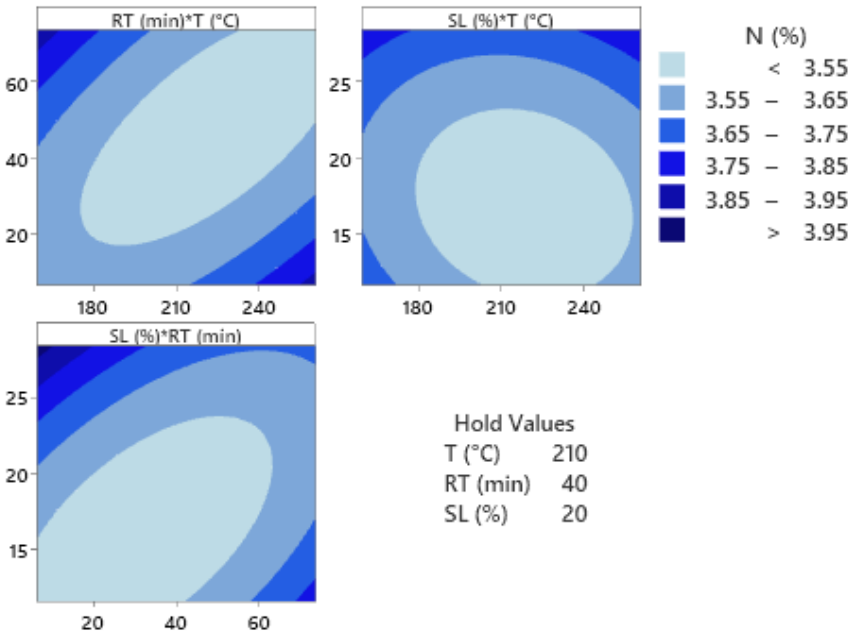

Figure 4.17 Contour plots of Nitrogen content (%)

None of the individual effects showed significance in **Figure 4.18**, where all are well below the reference line. Nonetheless, the highest effects were both linear and quadratic effects of solid load, this indicates a potential role in nitrogen removal.

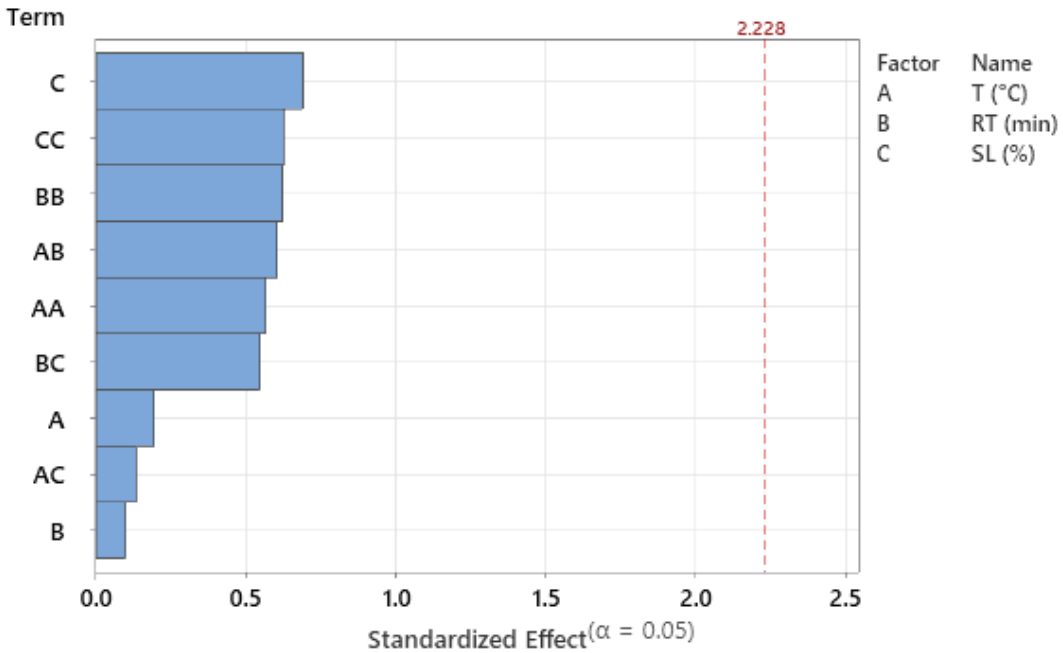

Figure 4.18 Pareto chart of the standardized effect on nitrogen content (%).

4.3.3 Summary and discussion

The ANOVA results for proximate and elemental responses are summarized in **Table 4.3** and **Table 4.4**. The regression model was significant for FC%, VM%, ash%, C% and O%, while H% and N% models were non-significant, mainly due to little variation between runs. Models in the literature do not evaluate hydrochar composition for proximate or elemental distribution. Therefore, to the author's knowledge, these are the only statistical models assessing hydrochar composition for hydrochar from food waste to date. The R^2 values indicate the percentage of variation that is explained by the model, the higher the R^2 the better the model fits the data, ranging from 0 to 1. The models for FC and VM (%) showed decent R^2 values, while Ash (%) had a relatively low R^2. The R^2adj represents the percentage of variation explained by the model adjusted by the number of predictors, this is useful when comparing models with different number of terms. However, in this work all models contained the complete terms.

Table 4.3 Summary of ANOVA for proximate analysis responses

	Response		
	Fixed carbon (%)	Volatile matter (%)	Ash (%)
R^2	0.77	0.80	0.53
R^2 *adj*	0.57	0.63	0.12
R^2 *pred*	0.40	0.26	0.00
F_0	3.86	4.7	1.29
F_{tab}	3.02	3.02	3.02
p-value	0.023	0.012	0.034
Model	-16.4+ 0.356 T+ 0.410 RT- 2.16 SL+ 0.000477 T*T + 0.00002 RT*RT+ 0.0614 SL*SL - 0.00149 T*RT- 0.00032 T*SL- 0.00151 RT*SL	125.8 - 0.385 T- 0.418 RT+1.22 SL + 0.000650 T*T + 0.00075 RT*RT - 0.0309 SL*SL+ 0.00120 T*RT- 0.00131 T*SL+ 0.00262 RT*SL	--4.1 + 0.0140 T - 0.0501 RT + 0.535 SL - 0.000066 T*T- 0.000135 RT*RT - 0.01643 SL*SL + 0.000178 T*RT+ 0.00052 T*SL + 0.00085 RT*SL

Table 4.4 Summary of ANOVA for elemental analysis

	Response			
	C (%)	H (%)	O (%)	N (%)
R^2	0.93	0.65	0.91	0.17
R^2 *adj*	0.88	0.34	0.83	0.00
R^2 *pred*	0.59	0.00	0.50	0.00
F_0	17.31	2.11	11.67	0.24
F_{tab}	4.96	4.96	4.96	4.96
p-value	0.000	0.130	0.000	0.980
Model	-29.9+ 0.847 T + 0.037 RT- 0.74 SL- 0.001728 T*T - 0.000157 RT*RT+ 0.0029 SL*SL - 0.000039 T*RT - 0.00166 T*SL - 0.00093 RT*SL	-8.5 + 0.1048 T- 0.1027 RT + 0.641 SL- 0.000206 T*T+ 0.000419 RT*RT- 0.01638 SL*SL+ 0.000104 T*RT+ 0.00048 T*SL - 0.00236 RT*SL	136.4 - 0.936 T+ 0.110 RT - 0.12 SL+ 0.001941 T*T + 0.00006 RT*RT + 0.0275 SL*SL - 0.00029 T*RT- 0.00274 T*SL + 0.00380 RT*SL	5.44 - 0.0174 T+ 0.0218 RT- 0.059 SL+ 0.000045 T*T + 0.000112 RT *RT+ 0.00181 SL*SL- 0.000098 T*RT+ 0.000087 T*SL- 0.000531 RT*SL

Temperature, reaction time and solid load were evaluated by their linear, quadratic and interaction effects and were considered with significant effect if $p < 0.05$. The p-values for each parameter are summarized in **Table 4.5**. Temperature was the most important factor affecting the composition, with a significant ($p < 0.050$) linear effect for FC, VM, C, H, and O%; It also yielded a significant quadratic effect for C and O contents. In contrast, reaction time was not statistically significant for any of the parameters. Although it showed important linear effect for FC ($p = 0.053$) and VM ($p = 0.060$), it was not so for the elemental responses. Regarding solid load, it carried significance for linear effect on C% ($p = 0.015$) and quadratic effect on FC, Ash and H% with $p = 0.028$, 0.014 and 0.021, respectively.

Table 4.5 Summary of significance test for model and individual effects for proximate and elemental responses. Significant p-values in bold.

	Prob>F tab									
Factor	**Model**	**β_1 (T)**	**β_2 (RT)**	**β_3 (SL)**	**β_1^2**	**β_2^2**	**β_3^2**	**$\beta_1*\beta_2$**	**$\beta_1*\beta_3$**	**$\beta_2*\beta_3$**
FC (%)	**0.023**	**0.001**	0.053	0.198	0.488	0.990	**0.028**	0.290	0.954	0.854
VM (%)	**0.012**	**0.000**	0.060	0.101	0.265	0.557	0.150	0.304	0.773	0.702
Ash (%)	0.346	0.362	0.344	0.762	0.420	0.415	**0.014**	0.849	0.774	0.981
C (%)	**0.000**	**0.000**	0.116	0.015	**0.003**	0.877	0.858	0.966	0.649	0.864
H (%)	0.130	**0.031**	0.991	0.533	0.244	0.290	**0.021**	0.763	0.728	0.267
O (%)	**0.000**	**0.000**	0.638	0.061	**0.010**	0.740	0.097	0.864	0.595	0.714
N (%)	0.98	0.85	0.92	0.51	0.58	0.55	0.54	0.56	0.89	0.59

Therefore, temperature and solid load were significant factors affecting the composition of hydrochar within the conditions range used in this work. This suggests that the reaction mechanisms, such as hydrolysis, polymerization, condensation, decarboxylation, and dehydration, were mainly governed by temperature, whereas, within the reaction time range, time played no important role. There was also evidence that solid load, played a crucial role, probably facilitating the reaction. This is worth noting, as most modelling and mechanisms studies on HTC are conducted, or assumed to occur, in low solid load (<10%), while practical studies for treating wet wastes have considered minimizing the addition of water to increase environmental viability. This discrepancy requires further addressing.

Most of the models generated for the composition of hydrochar were found significant and with adequate R^2, except for ash, H, and N (%). However, even if the regression model was not able to prove significance on these responses due to their low range falling in the error variation, they showed a lack-of-fit > 0.050, thus, indicating that they could have a prediction value. Therefore, the

regression models generated for the composition of hydrochar could be employed in further simulation studies and to develop a robust empirical HTC model.

The role of the process conditions on the hydrochar quality responses is evaluated in the next section. This time, in comparison to the analysis of the composition, the modelling could be utilised for optimization assessments, of the individual or multiple responses.

4.4 Hydrochar quality

The effect of process parameters on the composition of hydrochar from food waste was analysed previously. The responses used for the assessment of hydrochar fuel quality or HTC process performance are evaluated in this section. This section contains several different responses, which are grouped in subsections: hydrochar energetics, H/C and O/C ratios, and nutrient efficiencies, followed by the summary and discussion. The analysis here includes the statistical evaluation of the regression models and the significance tests of the different parameters. In addition, the optimization assessments are included for individual and multiple responses.

4.4.1 Hydrochar yield, heating values and energy yield

In this subsection are grouped responses based on hydrochar characteristics as a solid fuel, particularly to be used in combustion, as gasification is analysed in a different section. This subsection includes responses on solid yield (SY) (**Eq. 12**), higher heating value (HHV) (**Eq. 13**), lower heating value (LHV) (**Eq. 14**), Energy densification (ED) (**Eq. 15**), and Energy yield (EY) (**Eq. 16**). **Table 4. 6** provides the results obtained for the complete DOE set.

Table 4.6 Full DOE results on hydrochar energetics responses.

Temp. (°C)	Time (min)	SL (%)	SY (%)	HHV (MJ/kg)	LHV (MJ/kg)	ED	EY (%)
Raw food waste			-	21.3	19.5	-	-
180	**20**	**15**	47.9	27.1	25.5	1.31	62.8
240	**20**	**15**	51.8	31.3	29.5	1.52	78.6
180	**60**	**15**	53.1	26.9	25.3	1.3	69.1
240	**60**	**15**	49.2	31.2	29.6	1.52	74.9
180	**20**	**25**	66.2	24.7	23.2	1.19	78.8
240	**20**	**25**	55.3	28.9	27.3	1.4	77.6
180	**60**	**25**	63.3	25.6	24.1	1.24	78.2
240	**60**	**25**	57.1	30.6	28.9	1.49	84.8
159.5	**40**	**20**	88.1	20.9	19.5	1	88.1
260.5	**40**	**20**	50.7	33.5	31.6	1.62	82.4
210	**6.4**	**20**	57.7	30	28.2	1.45	83.6
210	**73.6**	**20**	51.7	30.6	28.7	1.47	76.2
210	**40**	**11.6**	47.3	29.1	27.6	1.42	67.1
210	**40**	**28.4**	63.8	27.2	25.7	1.32	84.3
210	**40**	**20**	57.6	30.1	28.3	1.45	83.7
210	**40**	**20**	53.2	30.7	28.9	1.48	78.9
210	**40**	**20**	57.3	30.9	29.1	1.49	85.6
210	**40**	**20**	57.1	29.5	27.8	1.43	81.7
210	**40**	**20**	53.9	29.8	28.1	1.44	77.9
210	**40**	**20**	55.6	27.9	26.4	1.36	75.4

Solid yield (SY) represents the percentage of mass from food waste that remains in the solid phase after the HTC process. It assesses the mass yield of hydrochar product and its relation to the original mass of food waste. It is a crucial parameter, as it impacts directly on the energetic efficiency and further commercialization of the process.

The maximum SY was 88% at (160/40/20) (**Table 4.6**) due to the low intensity of the run, where 160 °C did not promote the solubilisation of solids into the liquid phase. Moreover, the sample went through undesirable changes since considerable browning and hardening were observed, suggesting that caramelisation reactions took place. At these process conditions, the sample handling became more difficult, and impeded proper filtration, thus, making the dewatering and drying more difficult, and negating the benefits of HTC. Maximum hydrochar yield at the lowest temperatures is a trend reported in a

previous multi-factor study [30]. However, in the latter work, the yield it is particularly high, as other studies have reported lower solid yields at even lower temperatures. For instance, Mahmood [8] reported 65.73% SY working with post-consumer FW at 150 °C for 20 min, or Gupta et al. [157] with 52% SY at 160 for 5 h. This could indicate that the sample of the current work could have some biochemical particularity that could have promoted caramelisation reaction, such as a higher proportion of free sugars. However, 88% SY is an extreme point even within this DOE. Aside from this point, SY varied from 66% at (180/20/25), down to 47% at (210/40/12), suggesting that the solid load has a major role in SY.

As the temperature increased, solid yield decreased abruptly from 88% to a range between 50-60 % SY in most of the DOE conditions. This is easily observed in **Figure 4.21**, where the area between 50 and 60% SY takes most of the contour plots. At maximum temperature, a solid yield of 50.7% was found at (260/40/20). The lowest solid yield of 47.3% was obtained at (210/40/12), followed by 47.9 % at (180/20/25). These results could be attributed to the high amount of water used in runs, comprising a solid load of 12 and 15%, respectively. This indicates that low solid load could have facilitated the solubilisation of solids into the liquid phase. However, similar values between runs with considerably different process conditions suggest that the consideration of the three parameters in combination is necessary. For instance, the 180 °C temperature in (180/20/25) promoted higher solubilisation of solids in comparison to 160 °C. The relatively short reaction time of 20 min appears to allow effective solubilisation without promoting the re-polymerization of hydrochar in comparison to (180/60/25), where SY showed a modest increase up to 53% by significantly increasing RT from 20 to 60 min while maintaining temperature and solid load. This trend of RT is inverse at higher solid load runs, with a fall of SY from (180/20/5) with 66% to 63% at (180/60/25). One possible explanation could be that because of the higher solid load, maximum solubilisation was not achieved at a short reaction time and progressed with time. However, this behaviour appears to reverse at higher temperatures due to the increase in reaction rates for solubilisation and polymerization. In summary, low SL (25%) enhances SY at low temperatures and mitigates it at high temperatures.

Regarding the parametric analysis, temperature and solid load yielded a linear effect on SY. Thereby, SY declines as temperature increases and solid load reduces, while reaction time had a quadratic effect (**Figure 4.19**). This is corroborated in the individual significance test, illustrated in the Pareto chart (**Figure 4.20**), where temperature exhibited significant linear and quadratic effects ($p > 0.050$). The solid load had a significant linear effect, while reaction time did not show significance on any of its effects.

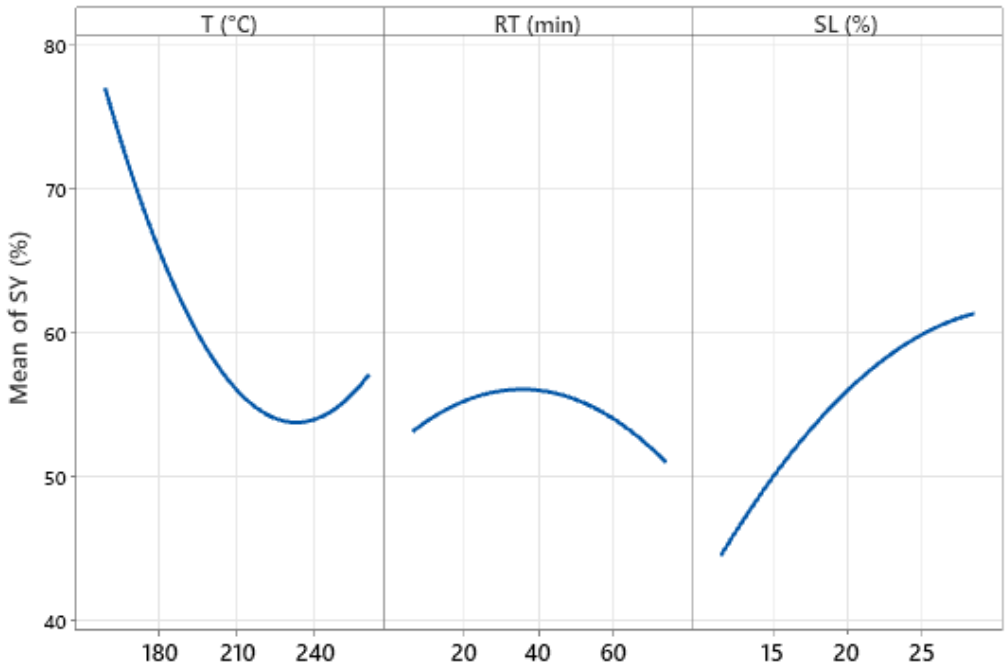

Figure 4.19 Main effects plot on solid yield (%).

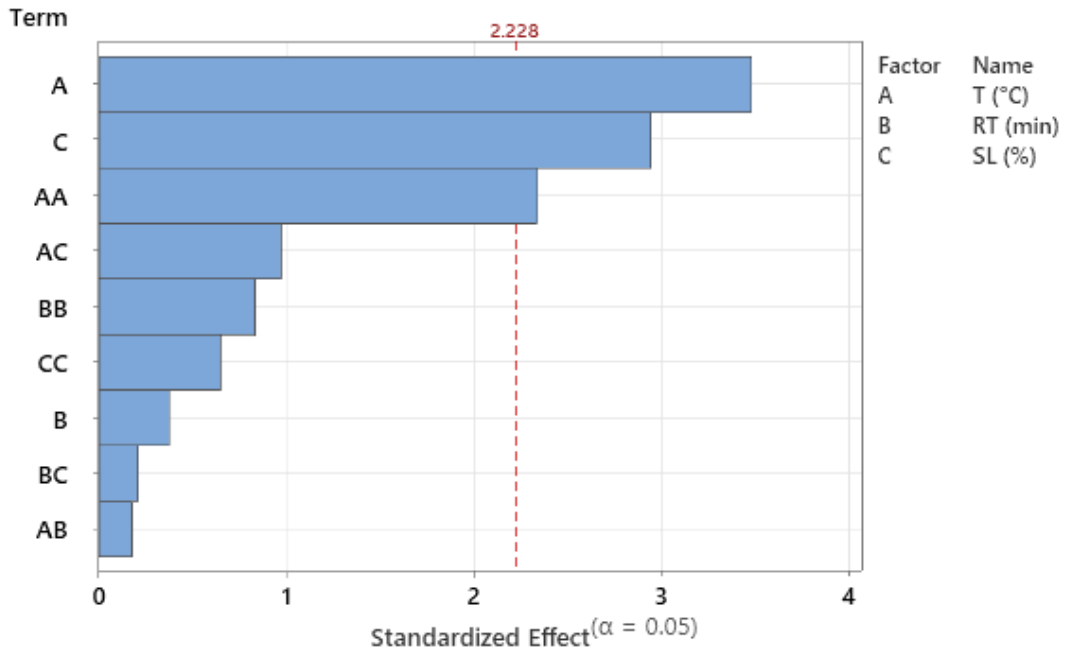

Figure 4.20 Pareto chart of the different effects on solid yield (%).

However, significant parameters affecting the HTC process seem to vary depending on the feedstock. For example, Kannan et al. [31], found that temperature and reaction time had a significant effect on the hydrochar yield, while the solid load was insignificant, working with fish waste. Also, the temperature had both significant linear and quadratic effects, agreeing with the effect of temperature in this work. Stutzenstein et al. [32], working with anaerobic digestate, also found temperature significant along with pH and the interaction of temperature and reaction time. In the current work, none of the interactions exhibited a significant effect on SY. In a different study, Toptas Tag et al. [25] found that temperature and time were significant on algal biomass and sunflower stalks, while the only temperature was significant for poultry litter. In any of these studies, solid load showed statistical significance. However, there are other examples where solid load showed significance. Volpe and Fiori [162], working with olive pulp found that the solid load had a significant effect. In a similar manner, it was reported by Sabio et al. [79] that the solid load showed a significant effect on the HTC of tomato peel. Therefore, there is an evident variation depending on the feedstock. Interestingly, both latter mentioned works used pre-consumer food waste, or

a single-food feedstock, suggesting that SL could be significant to other food waste related feedstock. Nevertheless, no significant test for HTC of mixed post-consumer food waste was found, and therefore a direct comparison on the same feedstock could not be conducted.

Regarding the statistical analysis, the regression model was significant (p = 0.041) with a R^2= 0.74. This is a better correlation fitting than previously reported by Danso-Boateng [30] with R^2= 0.66 using CCRD with 2 factors (temperature and reaction time). The regression model equation is shown next:

$$\boldsymbol{SY}\ (\%) = \mathbf{175} - \mathbf{1.674}\,\boldsymbol{T} + \mathbf{0.469}\,\boldsymbol{RT} + \mathbf{5.87}\,\boldsymbol{SL} + \mathbf{0.00426}\,\boldsymbol{T}*\boldsymbol{T} - \mathbf{0.00342}\,\boldsymbol{RT}*\boldsymbol{RT} - \mathbf{0.0425}\,\boldsymbol{SL}*\boldsymbol{SL} - \mathbf{0.00065}\,\boldsymbol{T}*\boldsymbol{RT} - \mathbf{0.0143}\,\boldsymbol{T}*\boldsymbol{SL} - \mathbf{0.0046}\,\boldsymbol{RT}*\boldsymbol{SL}$$

Previously mentioned patterns are observed more easily on the generated contour plots (**Figure 4.21**), where, as temperature increases and solid load reduces, hydrochar yield drops. In comparison, time does not seem to affect the process, corroborating the significance test. However, as mentioned previously, SY correlates inversely to fuel quality. Thus, it should be addressed with an optimization approach.

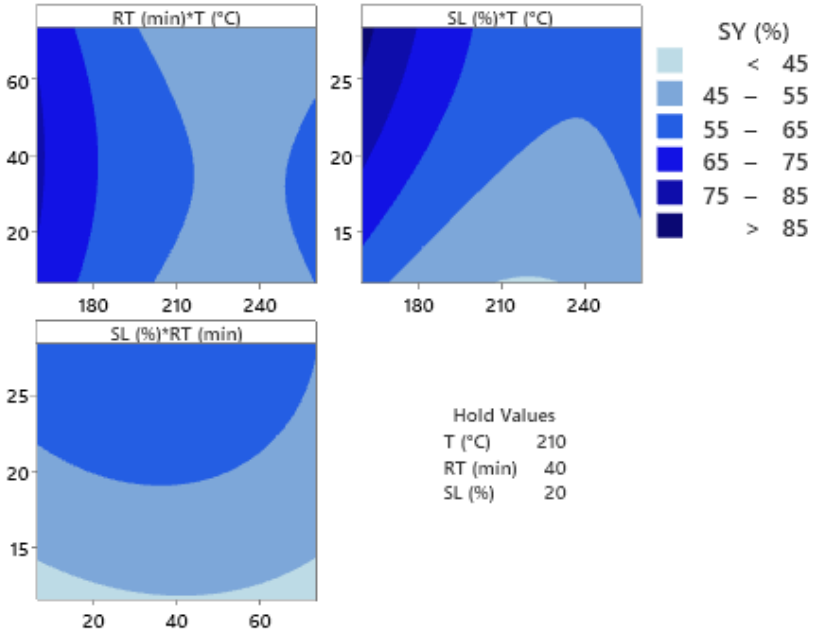

Figure 4.21 Contour plots of solid yield (%)

A higher heating value is an indicator of the energy contained in hydrochar that could be released during combustion [159], when the heat of product water condensation is recuperable. For the application of hydrochar, a lower heating value would provide an estimation of the usable energy without considering the condensation energy of water, representing most practical combustion processes. However, HHV is the standard response used in hydrochar studies. Thus, for the sake of comparison with other studies, HHV is used in the effect of parameters study. Hence, as heating value gives us the estimation of energy content per mass unit, it is a crucial response when analysing hydrochar for energetic purposes.

In general, HHV increases as HTC temperature increases, and maximum HHV was found at (260/40/20) with 33.48 MJ/kg, whereas minimum HHV was at (160/40/20) with 20.93 MJ/kg. Maximum HHV follows maximum temperature and maximum oxygen removal in hydrochar. On the contrary, minimum HTC temperature resulted in the lowest HHV and, unexpectedly, even achieved an HHV lower than the original food waste (21.29 MJ/kg). The second-lowest HHV value was at (180/20/25) with 24.71 MJ/kg, lower than a similar run at a lower solid load (180/20/15) which had an HHV of 27.11 MJ/kg.

This could be due to the effect of a larger solid load preventing a higher degree of coalification at low temperatures. The obtained HHV values are within the common range for hydrochar from food waste in the literature.

The main effects plots revealed an important effect of temperature, mainly linear, increasing HHV with temperature (**Figure 4.22**). Reaction time had a negligible effect. Solid load exhibited a quadratic effect with no clear importance. The individual significance test confirmed that temperature had the main effect, with statistical significance on linear and quadratic effect. Solid load also showed significance for its linear effect. Reaction time did not carry significance on any of its effects (**Figure 4.23)**. These results are similar to those reported by Sabio et al. [79], where temperature and SL had positive effect on HHV while RT did not for tomato peel. Vole and Fiori [162] reported that SL had an effect on HHV only at temperatures > 180 °C.

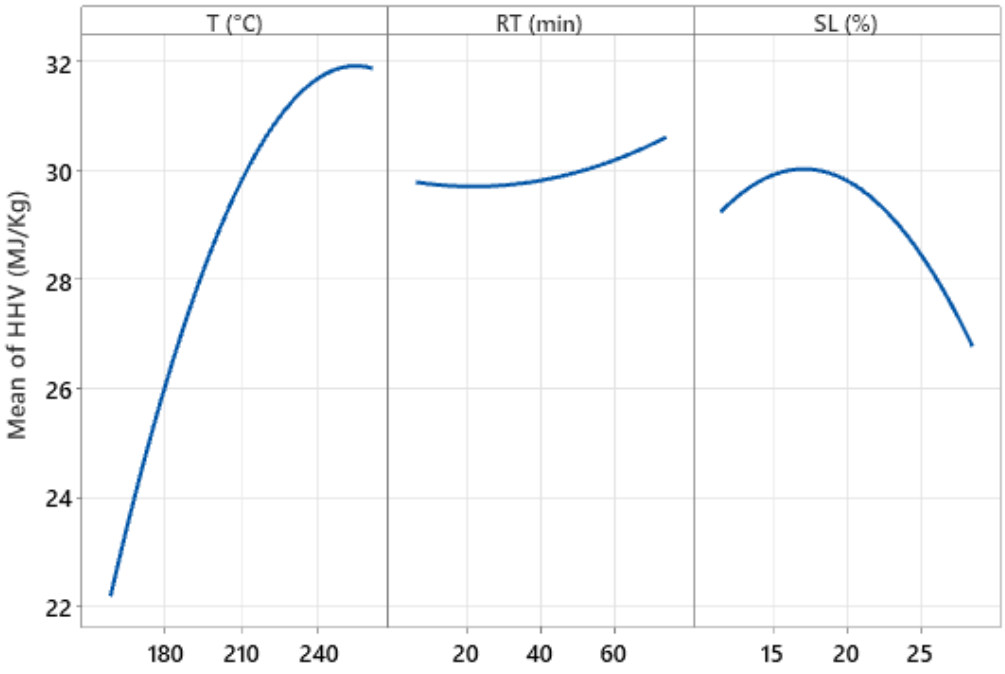

Figure 4.22 Main effect plot of the three factors on HHV (MJ/kg).

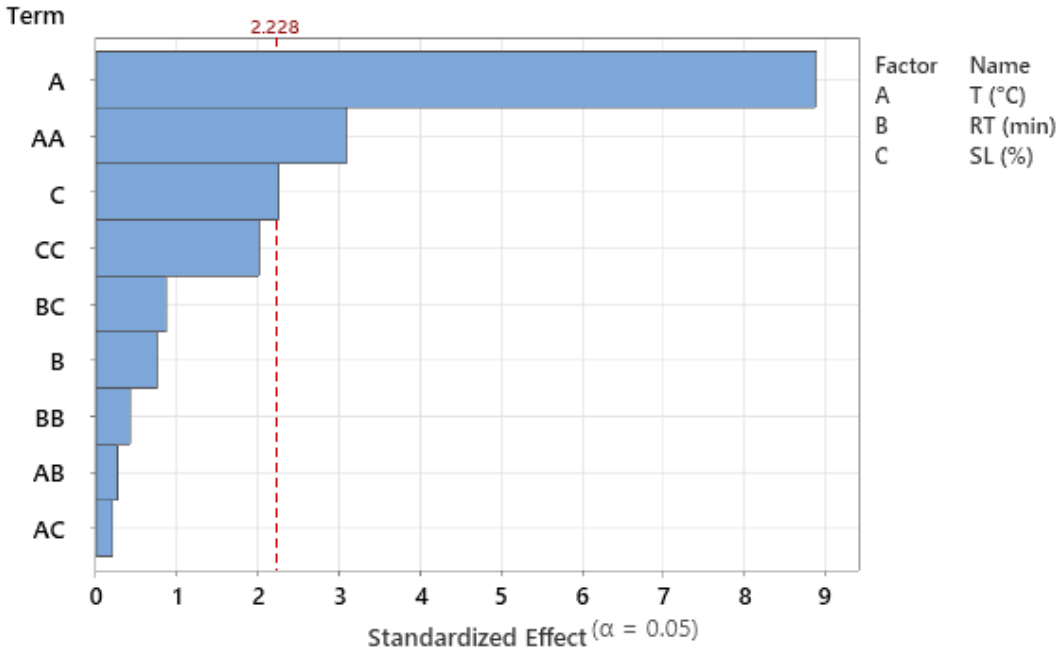

Figure 4.23 Pareto chart of the different effects on higher heating value (MJ/kg)

Regarding the regression model fidelity, ANOVA displayed a correlation coefficient of R^2 = 0.90. The full regression model equation is shown next:

$$HHV\left(\frac{MJ}{kg}\right) = -37.6 + 0.526\,T - 0.126\,RT + 0.593\,SL - 0.001070\,T * T + 0.000329\,RT * RT - 0.0251\,SL * SL + 0.000188\,T * RT + 0.00058\,T * SL - 0.00363\,RT * SL$$

The generated contour plots illustrating the effect of the process parameters are displayed in **Figure 4.24** and show that HHV increases with temperature. Higher HHV was found between 15 to 20 % SL. In contrast, reaction time had no impact on the contour plots.

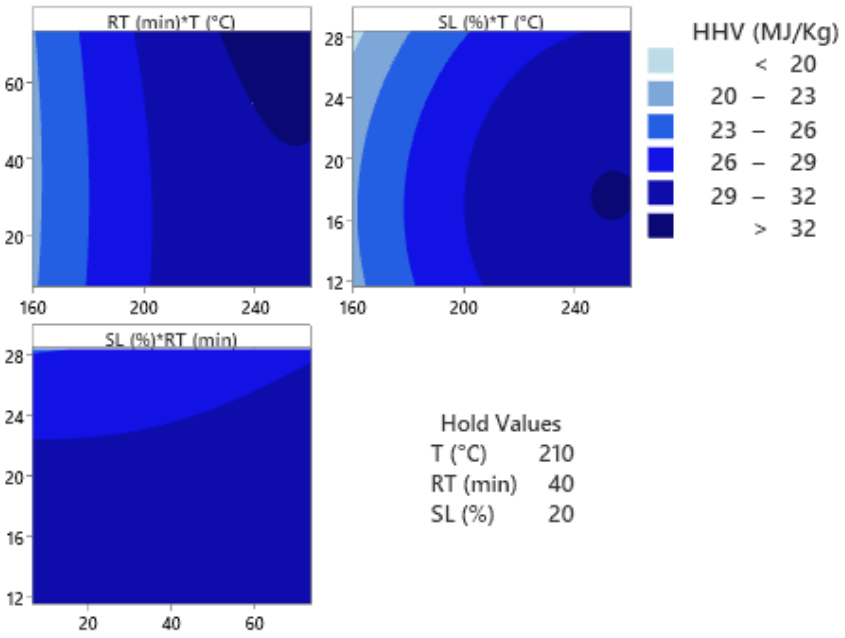

Figure 4.24 Contour plot of higher heating value (MJ/kg)

Energy densification (ED) is an indicator of the increase of the calorific value of the hydrochar relative to the raw food waste. Temperature is expected to be the most important factor, for ED is calculated directly from the ratio between HHVs in hydrochar and food waste (**Eq. 15**). The highest ED values were obtained at (260/40/20) with 1.62, followed by (240/60/15) and (240/20/15) both yielding 1.52. On the lowest value side, (160/40/20) produced an ED of 1. These values are among the range of ED by HTC commonly found in the literature for food waste. Saqib et al. [5] have reported higher ED values previously with 1.83. Nevertheless, the HHV was lower than that in the present work. Therefore, the high HHV of the raw feedstock is responsible for the lower values of ED in the current work.

For the runs with higher solid load (240/20/25) and (240/60/25), ED values were slightly lower at 1.40 and 1.49, respectively. This suggests that temperature and solid load had an important effect on ED, while reaction time was not relevant. This is also evident in the main effect plots (**Figure 4.25**), where the temperature has the largest effect, mainly linear with a slight curvature. Reaction time does not appear to have any effect on ED. Solid load has a quadratic effect with no clear importance. Regarding the significance

test, temperature showed significant linear and quadratic effects (**Figure 4.26**), the solid load had significance for its linear effect, but reaction time was not significant for any of its effects, as foreseen.

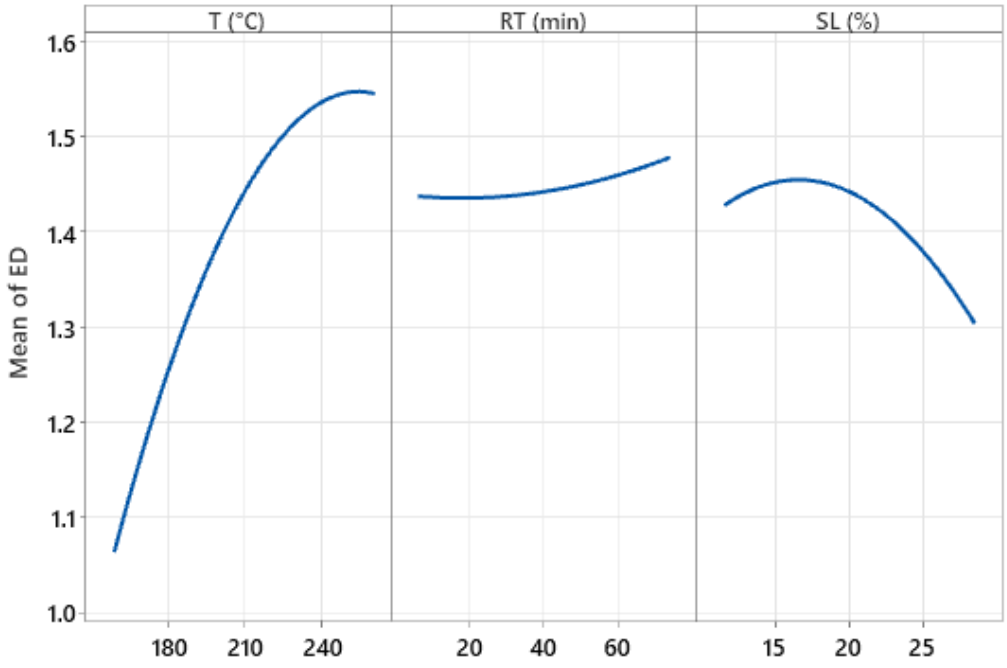

Figure 4.25 Main effect plots for Energy Densification ratio.

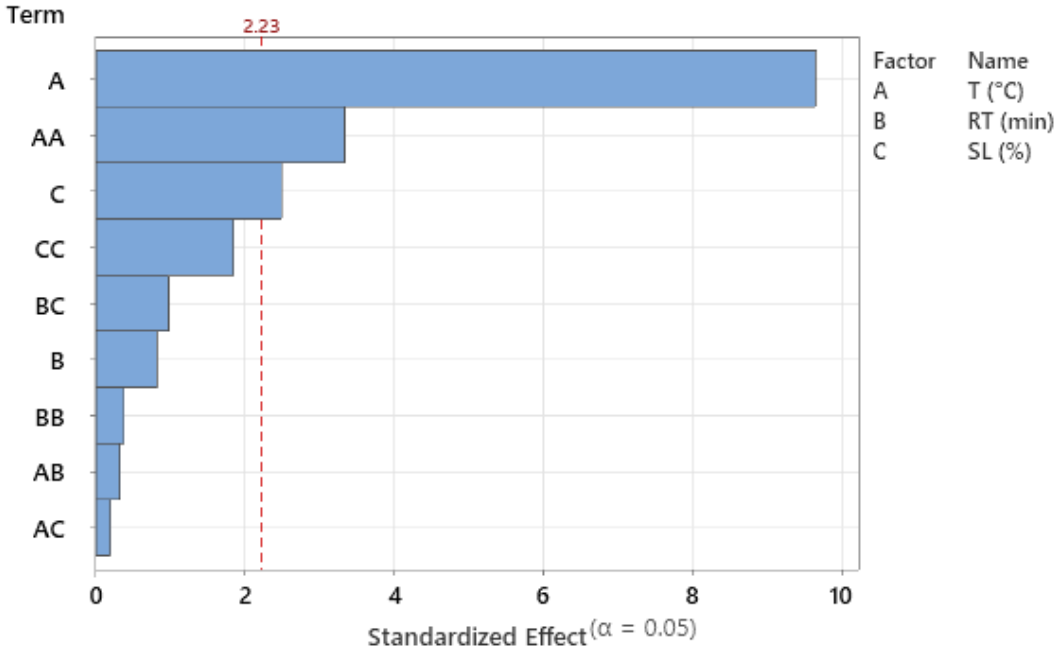

Figure 4.26 Pareto chart of the different effects on Energy Densification.

The regression model had an excellent R^2 = 0.91 and statistical significance ($p < 0.000$). The full regression model equation is shown next:

$$\boldsymbol{ED = -1.818 + 0.02602\,T - 0.00642\,RT + 0.0222\,SL - 0.000053\,T * T + 0.000014\,RT * RT - 0.001056\,SL * SL + 0.000010\,T * RT + 0.000025\,T * SL - 0.000187\,RT * SL}$$

On the generated contour plots in **Figure 4.27**, can be located the zones with higher energy densification. The area with the highest energy densification (>1.5), is located with temperatures higher than 230 °C and a solid load below 25%. Reaction time has a negligible effect on the contour plots s (**Figure 4.27**).

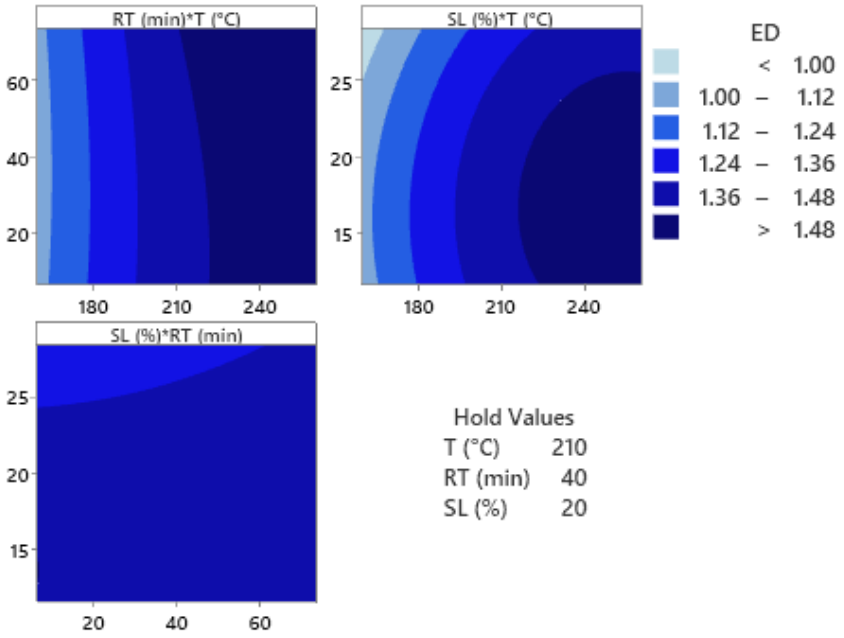

Figure 4.27 Contour plots of energy densification of hydrochar

Energy yield (EY) response assesses the percentage of chemical energy that remains in the hydrochar from the original food waste (**Eq. 16**). It is an energy efficiency assessment that only considers the chemical energy of cold solid product and feedstock. For the estimation of energy yield, the heating value

and the solid yield are considered, two responses that behave inversely to the same process conditions. Hence, optimization is particularly interesting. The highest value of EY was found at (160/40/20) with 88%. This is due to the significantly higher solid yield in comparison to the rest of DOE runs. However, as explained before, hydrochar at (160/40/20) showed poor fuel and handling characteristics. Therefore, it must not be considered optimum for this feedstock. Aside from that point, energy yield ranged from 62.7% at (180/20/15) to 84.8 % at (240/60/25). In comparison, the EY obtained in this study was higher than in the majority of the reported studies for hydrochar from food waste. In the present literature review, the reported range for EY was between 20 and 65 %, working with different food waste feedstock and process conditions [16,22,112,114,161]. Only one study was found with a similar EY to the present study, with 84% [12]. Indicating that the area of the process conditions used in the present study covers an adequate process set of conditions to obtain high EY, resulting in a balance between solid yield and HHV.

The main effect plots are shown in **Figure 4.28** where energy yield decreases with temperature, reaction, and solid load. The temperature has a higher, linear effect. Also, temperature carries a small quadratic effect at the highest temperatures, when EY shows a slight increase. Both reaction time and solid load have a linear effect with no clear significance. However, on the Pareto chart, only the linear effect of the solid load had statistical significance ($p < 0.050$). Thus, as solid load has a great impact on hydrochar yield, it could be inferred that solid yield dominates the effect of the heating value on the EY.

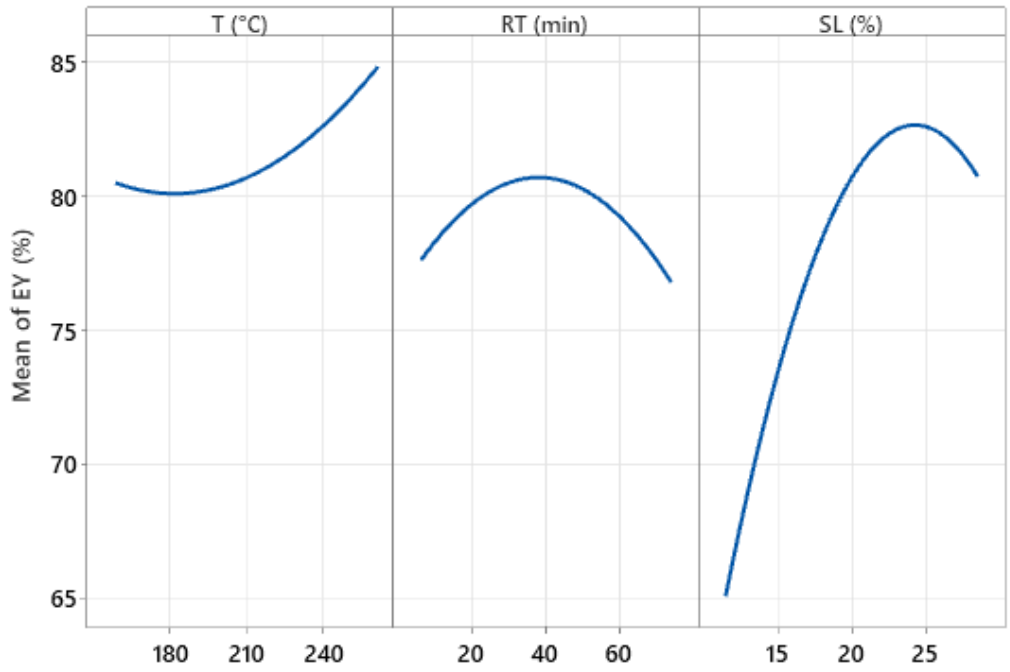

Figure 4.28 Main effect plot for the three factors on Energy Yield (%).

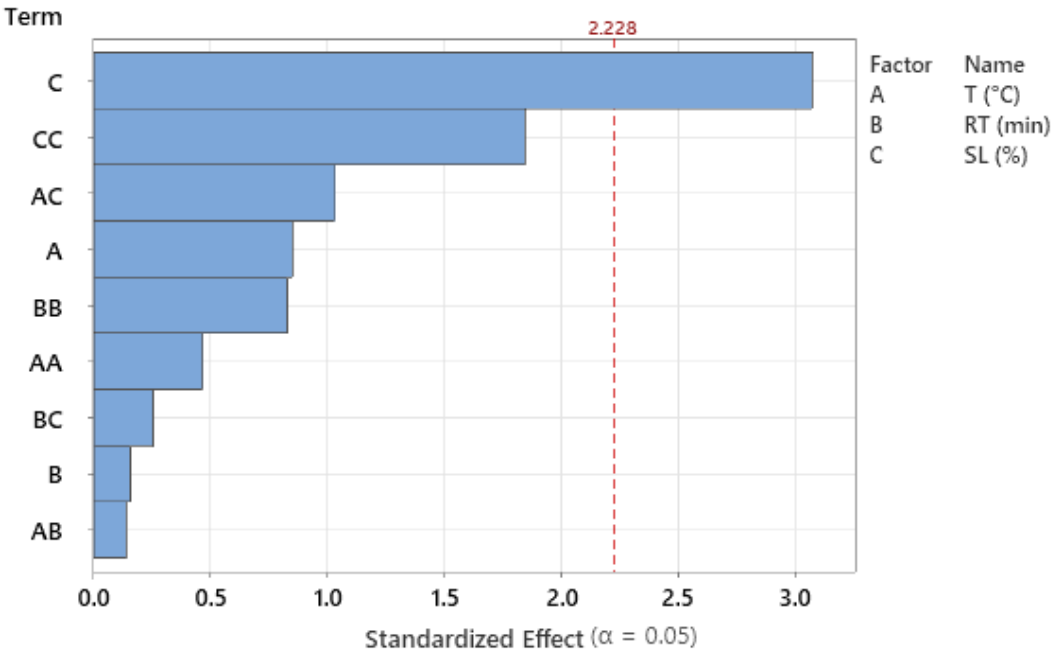

Figure 4.29 Pareto Chart of the different effects on Energy yield (%)

The regression model had a correlation factor of R^2=0.61. Also, the model exhibited no statistical significance (p = 0.197). The full regression equation is shown next:

$$\begin{aligned} \boldsymbol{EY}\ (\%) = &-\mathbf{17} + \mathbf{0.012}\,\boldsymbol{T} + \mathbf{0.226}\,\boldsymbol{RT} + \mathbf{7.87}\,\boldsymbol{SL} + \mathbf{0.00076}\,\boldsymbol{T} * \boldsymbol{T} \\ &- \mathbf{0.00302}\,\boldsymbol{RT} * \boldsymbol{RT} - \mathbf{0.1078}\,\boldsymbol{SL} * \boldsymbol{SL} - \mathbf{0.00046}\,\boldsymbol{T} * \boldsymbol{RT} \\ &- \mathbf{0.0135}\,\boldsymbol{T} * \boldsymbol{SL} + \mathbf{0.0050}\,\boldsymbol{RT} * \boldsymbol{SL} \end{aligned}$$

For better appreciation of the effects of process parameters, contour plots are displayed in **Figure 4.30**. In general, EY rises with temperature. Also, higher EY is shown at mid reaction times (around 40 min) in comparison with short or long reaction times. This was particularly important when working with middle temperatures (180 – 200 °C) and could suggest an optimal zone between heating value and hydrochar yield. However, as the temperature keeps increasing energy yield is less dependent on time. Longer reaction time yielded lower EY, due to the higher solubilisation of solids resulting in low hydrochar yield. Also, long reaction times could decrease the efficiency of the process if energy consumption during the process is taken into consideration, and thus should be kept at a minimum. Higher EY was obtained at a greater solid load (20-30%). However, it decreases dramatically as solid load goes below 20 %. This could be due to as temperature increases higher heating values are countered by lower hydrochar yield.

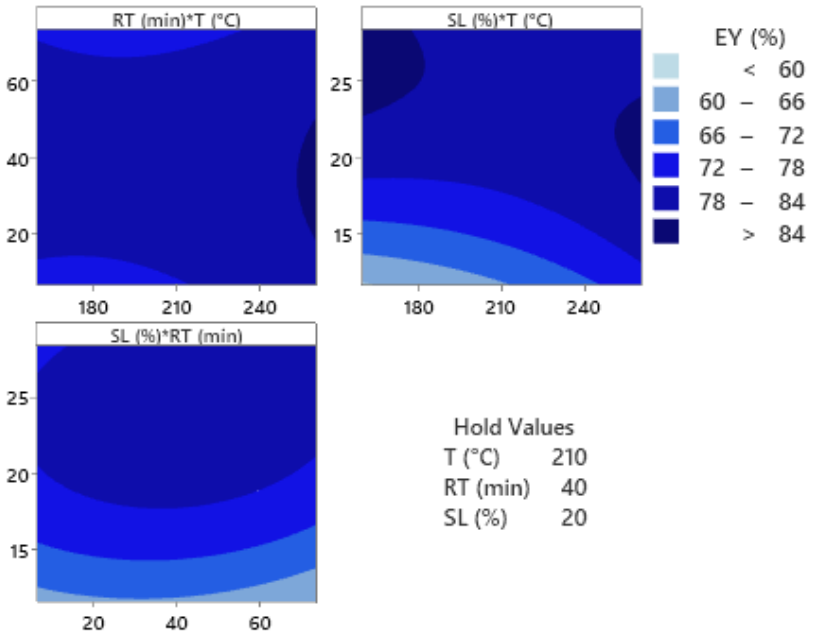

Figure 4.30 Contour plots of energy yield (%).

4.4.2 H/C and O/C ratios

Previously, the significance of the HTC process conditions effects on carbon, hydrogen, and oxygen elemental content in hydrochar was analysed. However, as the CHNO content provides a first glance of the solid fuel enhancement, the relations between H/C and O/C are a more standardized estimation of the coalification degree of the solid fuel. A compilation of the values of O/C and H/C for the complete DOE run set is displayed in **Table 4.7**.

Table 4.7 Values of H/C and O/C of the complete DOE run set.

Temp. (°C)	Time (min)	SL (%)	H/C	O/C
Raw food waste			1.94	0.64
180	20	15	1.4	0.32
240	20	15	1.43	0.21
180	60	15	1.35	0.31
240	60	15	1.26	0.19
180	20	25	1.45	0.4
240	20	25	1.24	0.24
180	60	25	1.38	0.36
240	60	25	1.39	0.21
159.5	40	20	1.53	0.56
260.5	40	20	1.44	0.14
210	6.4	20	1.59	0.24
210	73.6	20	1.54	0.24
210	40	11.6	1.24	0.24
210	40	28.4	1.28	0.29
210	40	20	1.53	0.24
210	40	20	1.53	0.22
210	40	20	1.52	0.21
210	40	20	1.35	0.24
210	40	20	1.42	0.22
210	40	20	1.24	0.27

Van Krevelen plots are used to describe the progression of the carbonization process and as indicators of dehydration and decarboxylation reactions. The Van Krevelen plot of the DOE run set of this work is shown in **Figure 4.31**. Raw food waste had a H/C close to 2 and an O/C of 0.64, and it is located in the upper right corner in **Figure 4.31**. Moving in the left direction of the plot, are scattered all the points in the DOE set.

As mentioned previously, intense process conditions promote HTC reactions. Hence, higher temperatures and longer times resulted in lower H/C and O/C ratios. However, the combination of parameters indicated results suggesting that not only higher temperatures and long times are necessary for a major carbonisation degree, but that solid load could play an important role. All high–temperature runs yielded a high decrease in O/C. However, the behaviour of H/C seems unrelated to any parameter.

Among the DOE runs, the points that reached the highest carbonization degree, based on Van Krevelen plot, were (240/60/15) with 1.26 H/C and 0.19

O/C, followed by (240/20/25) with 1.24 H/C and 0.24 O/C. On the other hand, the highest temperature run (260/40/20) showed the lowest O/C value of 0.14, due to the high effect of temperature on oxygen removal. However, H/C remained higher at the maximum temperature with a value of 1.44. This same pattern is observed with the rest of the runs at high temperatures (240/20/15) and (240/60/25), where O/C values were low, but H/C did not decrease to the same degree. The O/C values are common for different types of feedstocks after the HTC process, although the most intense runs displayed a rather low O/C value. However, H/C is high in comparison to those found in other feedstock (i.e. lignocellulosic biomass), but is rather common for food waste.

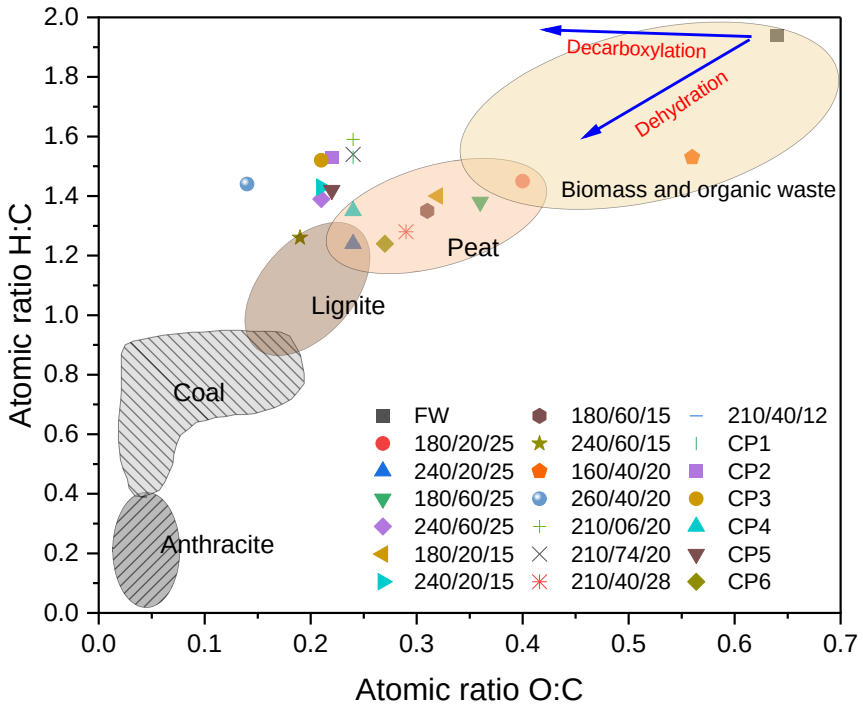

Figure 4.31 Van Krevelen diagram of the full DOE run set (points C1 - C6 represent central points)

The effect of process parameters on H/C is shown in the main effect plots (**Figure 4.32** and **Figure 4.34**). H/C decreases as temperature rises with a low inclination slope, indicating a low relevance of temperature over the H/C ratio (**Figure 4.32**). Reaction time shows a quadratic effect, with minimum values of H/C at mid reaction time (45 min). A quadratic effect was also

observed for solid load, with maximum values of H/C at 20%SL, yielding low values at both highest and lowest SL. Also, SL seems to have the largest role of the three factors. This is corroborated in the significance test, where only the quadratic effect of SL carried statistical significance (**Figure 4.33**).

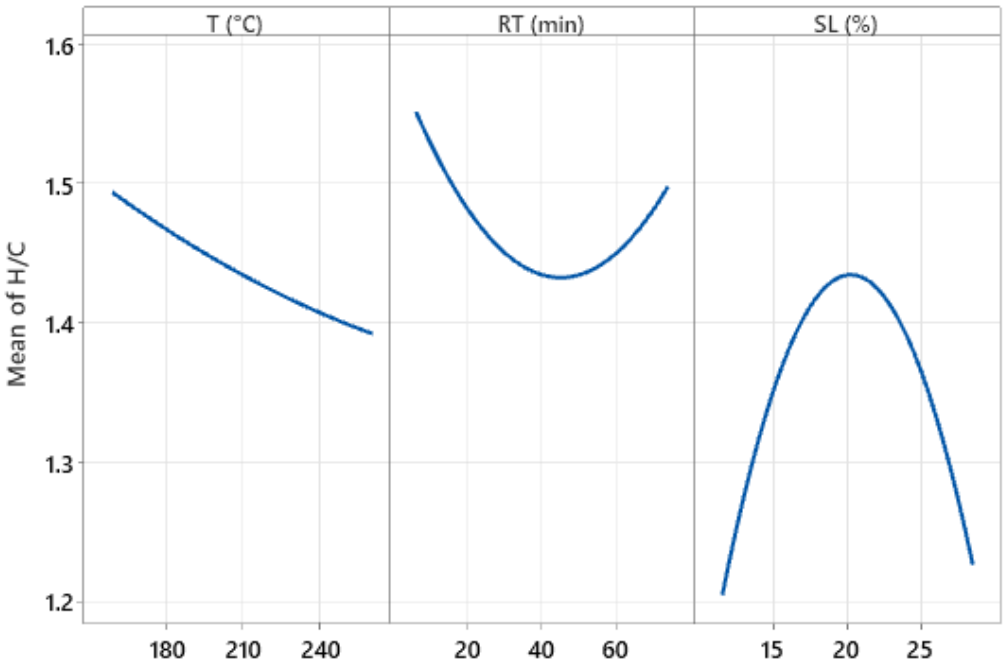

Figure 4.32 Main effects plot for H/C ratio.

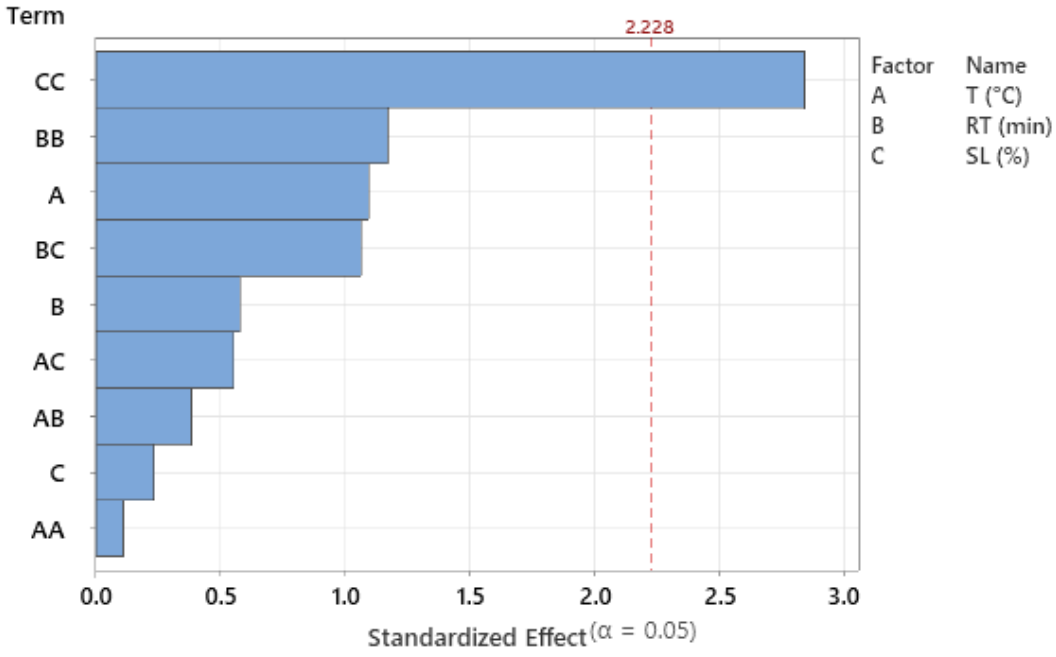

Figure 4.33 Pareto chart of the standardized effects on H/C ratio.

O/C values showed a strong relation to temperature. This is expected because both C% and O% decreased with temperature and were mainly influenced by this factor. **Figure 4.34** shows that temperature is the main factor affecting the O/C ratio. According to the significance test (**Figure 4.35**), the temperature was the only significant factor, with both significant linear and quadratic effects.

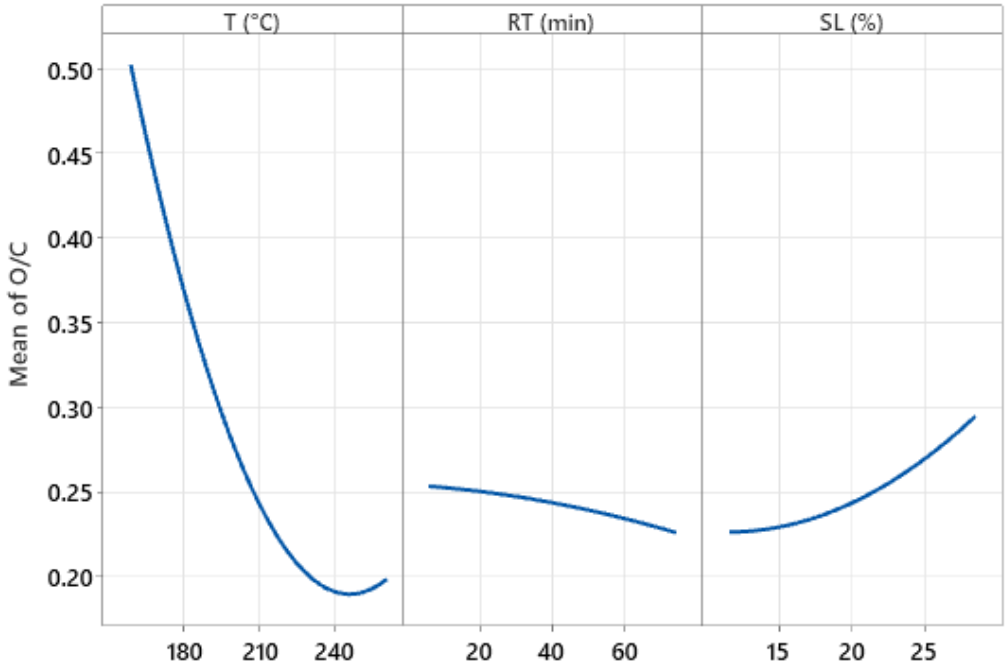

Figure 4.34 Main effects plot for O/C plots.

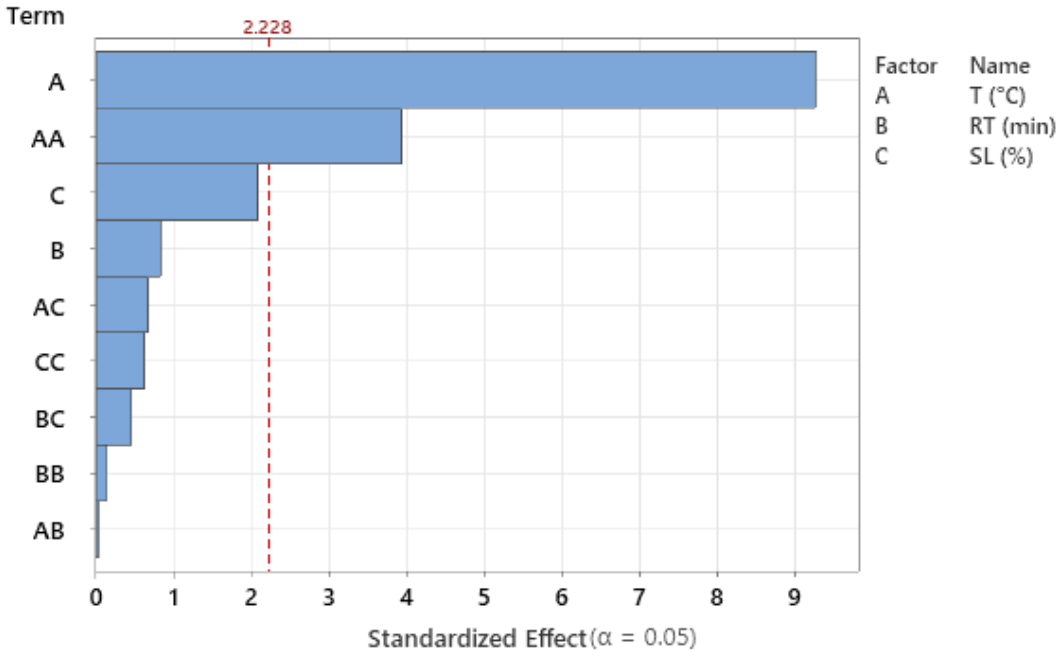

Figure 4.35 Pareto chart of the standardized effects on O/C ratio.

4.4.3 Carbon, nitrogen, sulphur and ash yields

The yields or mass efficiencies of carbon, nitrogen, sulphur, and ash contained in the hydrochar are assessed in this section. The reason for assessing the yields of these elements is due to their potential emission during the combustion or gasification of hydrochar. For starters, it must be pointed out that the initial food waste feedstock is relatively low in these components. Nitrogen content in raw food was 2.54%, sulphur 0.09%, and ash 2.28%. Based on these values, it is foreseen that hydrochar from food waste will contain lower content of these components than those in coal. Therefore, the effect of HTC process parameters on the mass yields of carbon, nitrogen, sulphur, and ash of hydrochar from food waste is evaluated in this section. A summary of the results is shown in **Table 4.8**.

Table 4.8 Mass efficiencies of carbon, nitrogen, sulphur and ash (%) for the full DOE .

Temperature (°C)	Time (min)	SL (%)	CY (%)	NY (%)	SY (%)	AY (%)
180	**20**	**15**	31.4	72.7	ND	47.9
240	**20**	**15**	37.3	77.1	44.2	51.8
180	**60**	**15**	34.9	90.5	ND	53.1
240	**60**	**15**	36.7	74.8	ND	49.3
180	**20**	**25**	67.1	100	ND	66.2
240	**20**	**25**	65.1	85.4	46.1	55.3
180	**60**	**25**	66.7	100	94.2	63.3
240	**60**	**25**	68	88.5	ND	57.1
159.5	**40**	**20**	62.5	100	79	87.5
260.5	**40**	**20**	50.6	80.2	ND	50.4
210	**6.4**	**20**	51.6	89.8	76.9	57.4
210	**73.6**	**20**	47.5	70.7	ND	51.3
210	**40**	**11.6**	26	67.9	ND	47.3
210	**40**	**28.4**	81	97.1	67.6	63.8
210	**40**	**20**	52.3	81.2	ND	57.2
210	**40**	**20**	49	73.5	ND	52.9
210	**40**	**20**	53	90.5	52.4	57
210	**40**	**20**	52.9	81.8	48.2	56.8
210	**40**	**20**	49.5	78.2	ND	53.6
210	**40**	**20**	51.1	88.4	ND	55.6

*ND = non-detectable

4.4.3.1 Carbon yield

Carbon yield (CY) response is an indicator of the carbon stored in hydrochar. CY is estimated as the percentage of carbon from feedstock remaining in the hydrochar after the hydrochar process. Moreover, is an important response for assessing the carbon capture and carbon emissions capacity of the hydrothermal carbonization of food waste.

Similar to solid yield, the general tendency is that as process conditions get more intensive, the HTC process transfers a larger fraction of carbon into the liquid phase. Nonetheless, the highest CY value was at (210/40/29) with 81.6%. This could be related to the minimum MC and hence, higher solid load. In contrast, the lowest carbon yield resulted at (210/40/12) with the minimum solid load. Therefore, SL seems to have a higher effect on CY than temperature and reaction time. In addition, an increase of CY at mid reaction times (around 40 min) is noted (**Figure 4. 36**). This could be due to a re-polymerization process after the initial hydrolysis. This increase in CY is later negligible as time increases, possibly due to the increase in decarboxylation reactions (**Figure 4.36**).

Regarding the significance test, only the linear effect of solid load yielded statistical significance (**Figure 4. 37**), followed by the quadratic effects of temperature and time. However, these did not reach significance. The regression model for CY was not significant with a $R^2 = 0.65$ and a $p = 0.137$, even with a large linear effect of solid load. The full regression model is shown below:

$$\begin{aligned} \boldsymbol{CY}\ (\%) = \mathbf{74.7} - \ & \mathbf{0.670}\,\boldsymbol{T} + \mathbf{586}\,\boldsymbol{RT} + \mathbf{5.43}\,\boldsymbol{SL} + \mathbf{0.00223}\,\boldsymbol{T} * \boldsymbol{T} \\ & - \mathbf{0.00416}\,\boldsymbol{RT} * \boldsymbol{RT} - \mathbf{0.0364}\,\boldsymbol{SL} * \boldsymbol{SL} - \mathbf{0.00093}\,\boldsymbol{T} * \boldsymbol{RT} \\ & - \mathbf{0.0135}\,\boldsymbol{T} * \boldsymbol{SL} - \mathbf{0.0032}\,\boldsymbol{RT} * \boldsymbol{SL} \end{aligned}$$

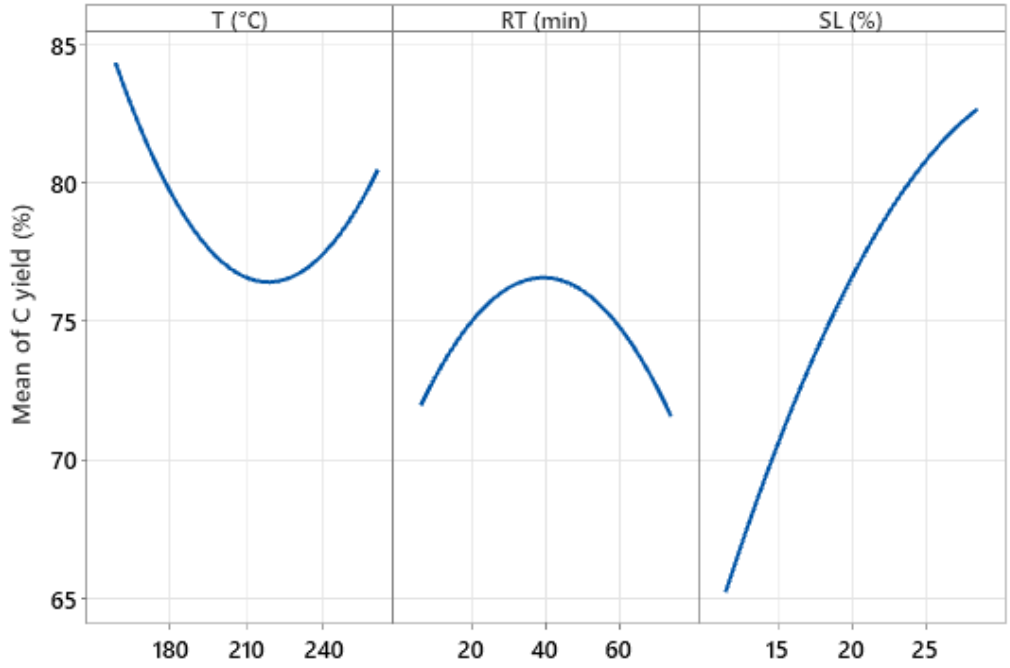

Figure 4.36 Main effects plot on Carbon yield (%).

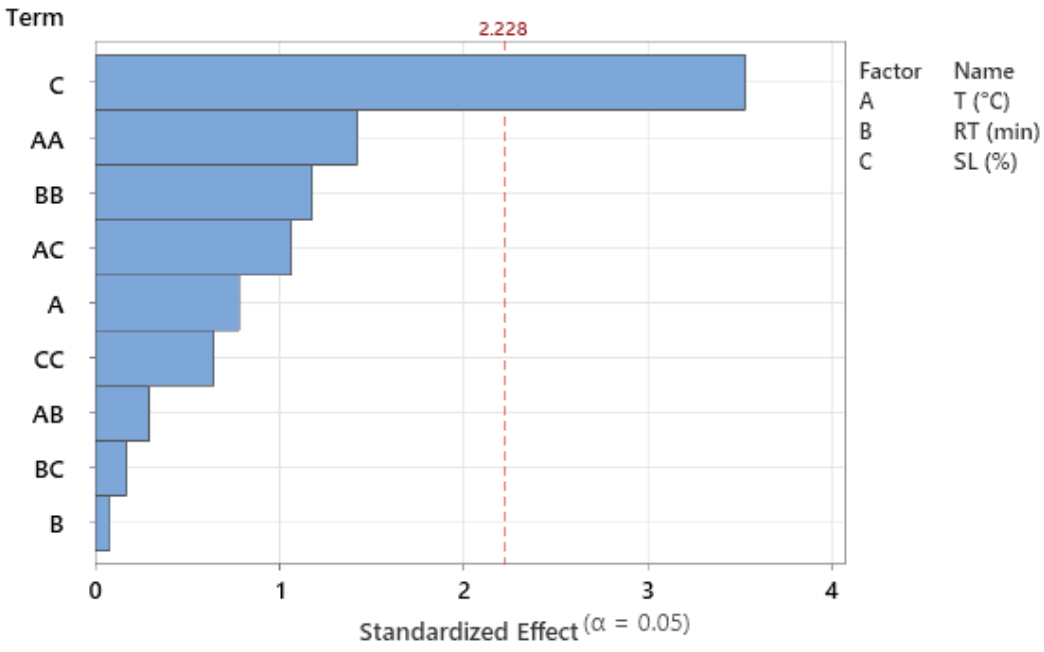

Figure 4.37 Pareto chart of the standardized effects on Carbon yield (%).

In **Figure 4.38** are displayed the contour plots of carbon yield, and it is appreciable that the effect of both temperature and reaction time have

no conclusive pattern on CY. Whereas SL shows a greater effect, with higher CY ay higher SL, and low temperature seem to enhance it. It was noted that even if temperature plays a major role on the solubilisation of solids during HTC, it was not significant for CY.

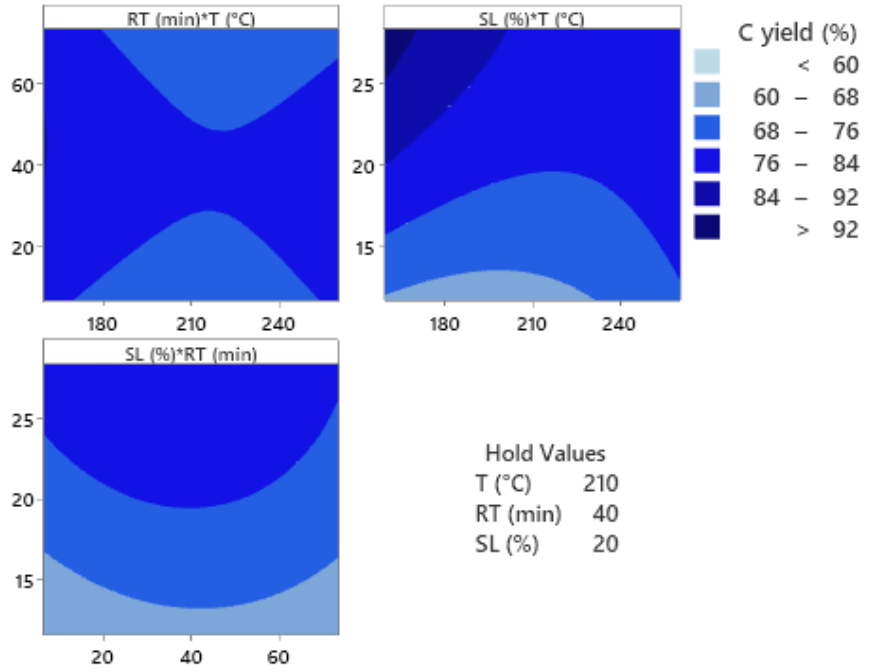

Figure 4.38 Contour plots of carbon yield (CY%).

4.4.3.2 Nitrogen yield

Nitrogen yield (NY) is defined as the nitrogen content remaining in hydrochar after HTC. It is an important response, as it indicates potentially lower NOx emissions at the moment of hydrochar utilization compared to the original food waste [14]. As opposed to carbon yield, here the desired goal is to decrease nitrogen content in the hydrochar compared to the HTC feed source.

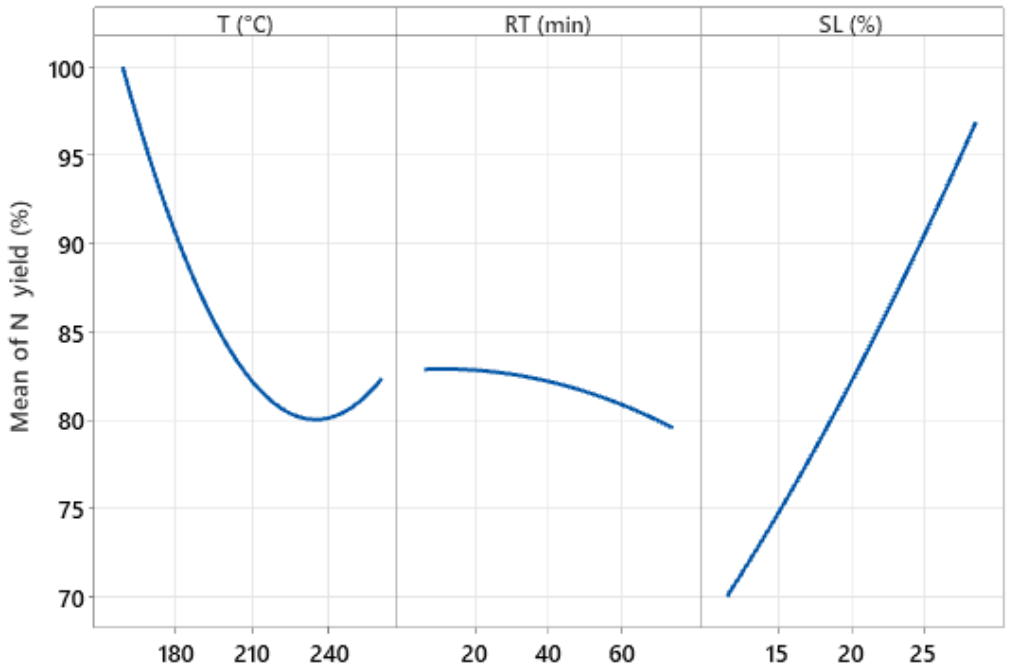

Figure 4.39 Main effects plot on nitrogen yield (NY).

The lowest NY was 67% at (210/40/12). This could be attributed to the lowest solid load, enhancing solubilisation of nitrogen. However, in comparison to carbon, the second-lowest NY was found at (210/73/20) with 70%. This indicates that longer reaction times improve the solubilisation of nitrogen. Another explanation could be that nitrogen has a lower re-polymerization rate than carbon. Nonetheless, the highest NY was found at low-temperature runs (160 to 180 °C) to the point that in various runs it was impossible to detect any decrease in nitrogen content. This indicates that even if solid load and reaction time affect the extent of nitrogen solubilisation, it requires a higher temperature for it to begin.

According to the significance test, solid load and temperature were statistically significant, as illustrated in the Pareto chart (**Figure 4. 40**). For both factors, the linear effect was the only significant effect, SL being the main one with p = 0.002, followed by temperature with p = 0.022. The regression model carried significance (p = 0.040) with a R^2 = 0.74. The full regression model is displayed below:

$$\boldsymbol{N\ yield}\ (\%) = \mathbf{153}\ -\ \mathbf{1.237}\ \boldsymbol{T} + \mathbf{1.07}\ \boldsymbol{RT} + \mathbf{4.09}\ \boldsymbol{SL}\ +\ \mathbf{0.00346}\ \boldsymbol{T} * \boldsymbol{T}\ -\ \mathbf{0.00085}\ \boldsymbol{RT} * \boldsymbol{RT} + \mathbf{0.00175}\ \boldsymbol{SL} * \boldsymbol{SL} - \mathbf{0.00355}\ \boldsymbol{T} * \boldsymbol{RT} - \mathbf{0.0124}\ \boldsymbol{T} * \boldsymbol{SL} - \mathbf{0.00154}\ \boldsymbol{RT} * \boldsymbol{SL}$$

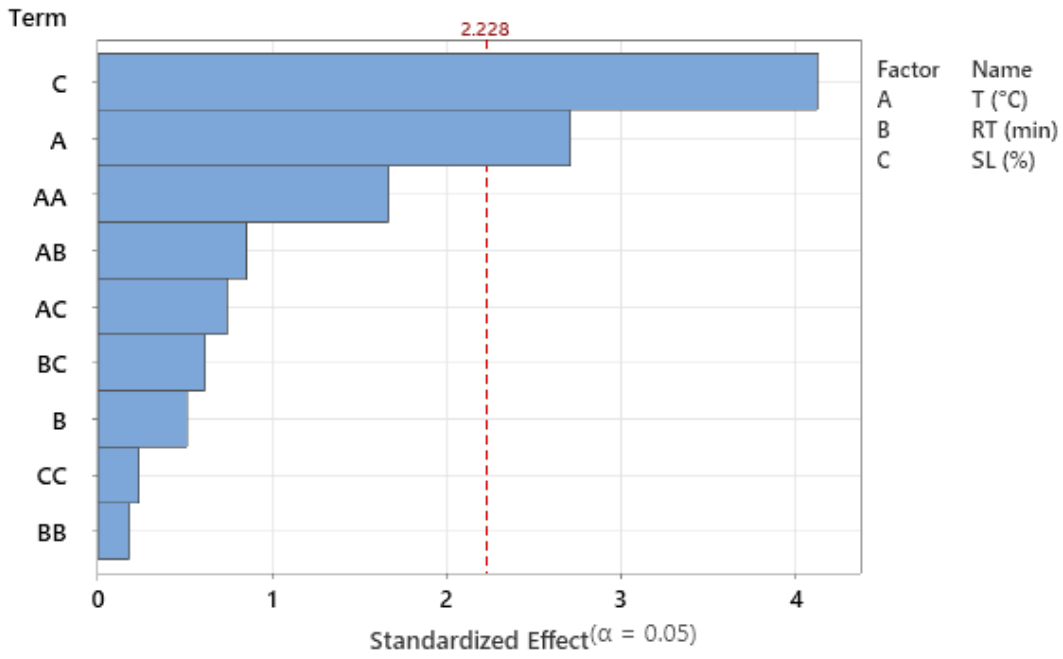

Figure 4.40 Pareto chart of the nitrogen yield

Using the contour plots in **Figure 4.41** is visible that the combination of high temperature and long reaction time, particularly over 210 °C and 40 min, yields the lowest NY. Also, the importance of solid load is evident, showing a decrease of NY under 80% when the solid load is below 18%. Thus, high solubilisation conditions promote nitrogen removal. Nonetheless, in comparison with carbon yield, solubilisation of N requires more intensive process conditions, and its re-polymerization rate is not as high.

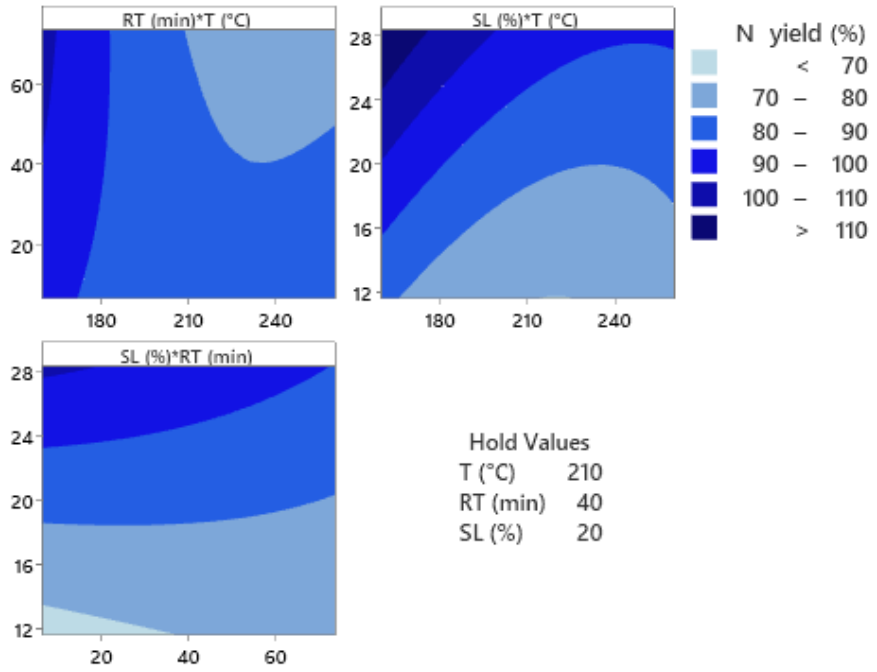

Figure 4.41 Contour plots of nitrogen efficiency (%).

4.4.3.3 Sulphur yield

The removal of sulphur from hydrochar is an attractive feature of HTC. In this work, the initial sulphur content in food waste was already low (0.09% db). Hydrochar samples showed a sulphur yield (SY) ranging from 94 to 44%. However, close to half of the samples fell below detectable values of sulphur content. This is understandable due to the low initial content in addition to the removal. Nonetheless, it was not possible to determine a behaviour or analyse the effect of the process conditions.

4.4.3.4 Ash yield

Ash is the fraction of the sample that remains after the devolatilisation of volatile matter and fixed carbon. In general, it contains a great proportion of the inorganic content of food waste. Therefore, the removal of ash content from hydrochar is desirable for reducing inorganic compound emissions. Here, ash removal is assessed with the ash remaining in hydrochar via the ash yield (AY).

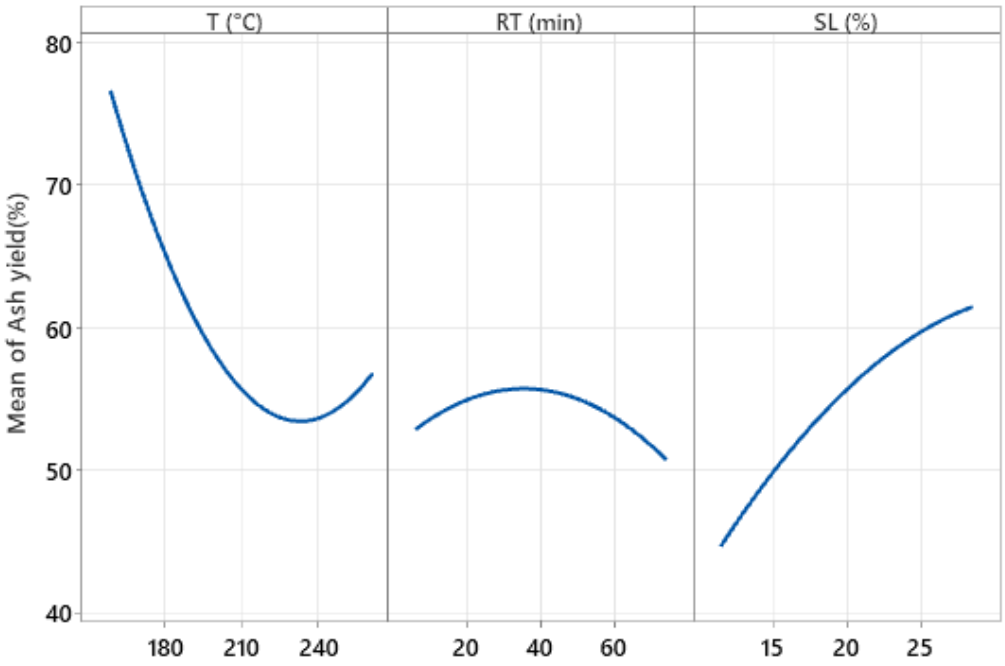

Figure 4.42 Main effects plot on Ash yield (AY).

Results show that ash removal started even at the lowest temperature (160 °C), for an AY of 87% at (160/40/20). However, the lowest AY was found at (210/40/12) with 47.3%, indicating the importance of solid load in food waste processing. Although AY showed a considerable decrease even in lower and mild conditions, high temperatures yielded the lowest AY values. This indicates that temperature plays a major role in the solubilisation of ash.

Regarding the significance test, the Pareto chart (**Figure 4.43**) shows that temperature was the most impactful factor, with statistical significance of the linear and quadratic effects. In addition, solid load showed a significant linear effect.

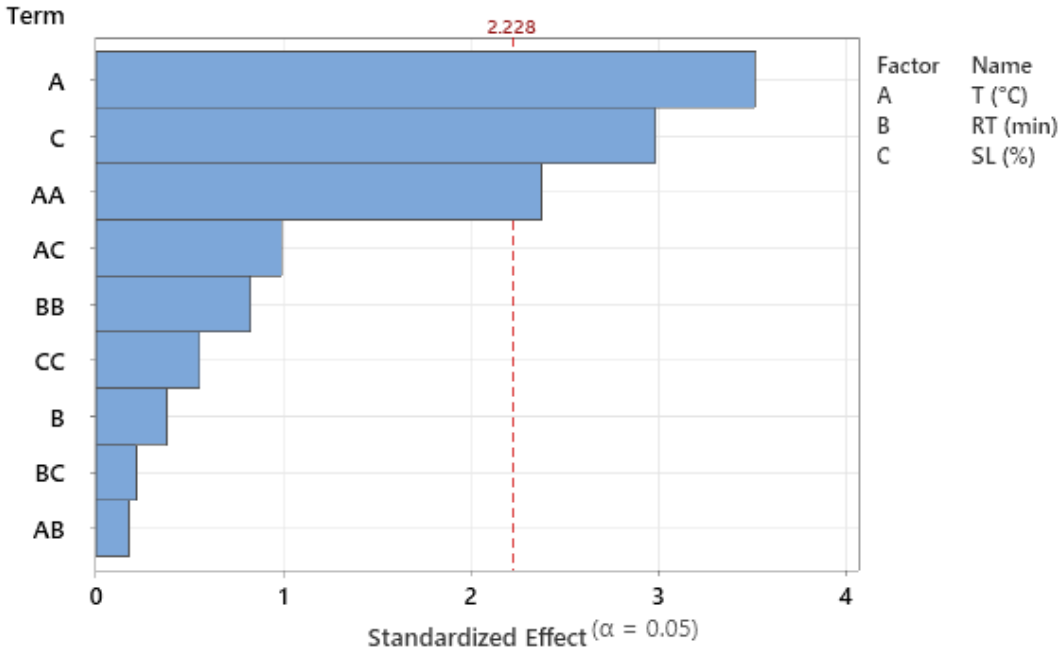

Figure 4.43 Pareto chart of the effects on ash yield.

The regression model was found significant with p = 0.038, and a correlation coefficient of R^2 = 0.74. The full regression model is shown next:

$$\boldsymbol{Ash\ yield\%} = \mathbf{177} - \mathbf{1.669}\,\boldsymbol{T} + \mathbf{0.462}\,\boldsymbol{RT} + \mathbf{5.60}\,\boldsymbol{SL} + \mathbf{0.00425}\,\boldsymbol{T} * \boldsymbol{T} - \mathbf{0.00332}\,\boldsymbol{RT} * \boldsymbol{RT} - \mathbf{0.0358}\,\boldsymbol{SL} * \boldsymbol{SL} - \mathbf{0.00064}\,\boldsymbol{T} * \boldsymbol{RT} - \mathbf{0.0143}\,\boldsymbol{T} * \boldsymbol{SL} - \mathbf{0.0047}\,\boldsymbol{RT} * \boldsymbol{SL}$$

The effect of process conditions on ash yield is visible in the contour plots in **Figure 4.44**. Temperature influenced AY considerably until it reached 200 °C. After this temperature, the ash yield range stays between 50 and 60 %. For AY to go below 50%, it is necessary to reduce the solid load below 16%.

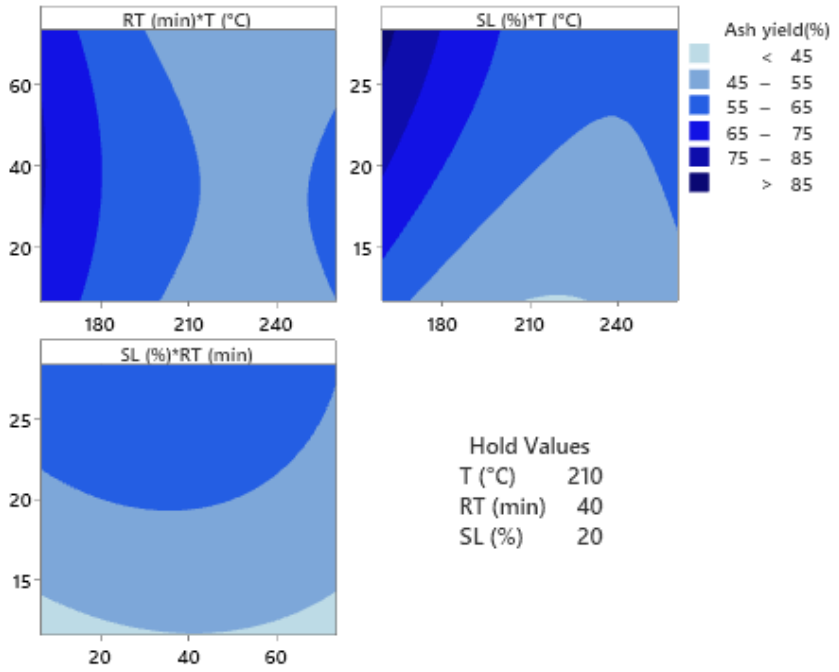

Figure 4.44 Contour plots of ash yield (%)

4.4.4 Equilibrium moisture content and humic acids

Besides the energy-related utilisation of hydrochar, there are other potential responses to evaluate the quality of hydrochar and how the HTC process conditions affect them. These qualities could have different behaviours than energetic responses and have distinct optimal zones. Therefore, it is interesting to add non-energetic responses to the multivariate optimization of HTC. Here, the assessed non-energetic responses are equilibrium moisture content (EMC) and the production of humic acids. The rationale for the importance of these two hydrochar characteristics is provided below, with a summary of the results responses for the complete DOE set, displayed in **Table 4.9**.

Table 4.9 Equilibrium moisture content (EMC) and Humic acids results for the complete DOE.

Temperature (°C)	Time (min)	SL (%)	EMC (%)	Humic acids in hydrochar (%)	Humic acids per solids in food waste (%)
180	20	15	4.5	27.6	13.2
240	20	15	2.4	25.2	13.1
180	60	15	4.3	23.4	12.4
240	60	15	2.7	22.9	11.3
180	20	25	8.2	25	16.6
240	20	25	3.8	20.6	11.4
180	60	25	4.8	18	11.4
240	60	25	3.8	19.7	11.2
159.5	40	20	8.6	12.3	10.9
260.5	40	20	2.7	31.4	15.8
210	6.4	20	3.8	23.8	13.7
210	73.6	20	4.6	19.5	10
210	40	11.6	2.9	29.2	13.8
210	40	28.4	5.2	17.9	11.4
210	40	20	2.9	23.7	13.5
210	40	20	4	20.1	10.6
210	40	20	3	24.1	13.7
210	40	20	4.5	21.1	12
210	40	20	3.9	18.4	9.9
210	40	20	3.1	22.3	12.4

Equilibrium moisture content (EMC)

EMC analyses the percentage of moisture that is hygroscopically re-adsorbed onto the hydrochar from the environment, in this case of known relative humidity (75%). EMC calculation is important to assess the storage and transport properties of hydrochar as it indicates the mass difference that could be saved, improving EMC property. In this case, lower EMC is desirable to save on transport costs as well as lower drying pre-treatment expenses associated with gasification or combustion end uses.

EMC values ranged from 2.44 to 8.47 %, with the lowest at (240/20/15) and the highest at (160/40/20). The pattern shows that the highest HTC temperatures promote the lowest EMC values, while it seems to increase when reaction time goes above 50 min. EMC appears to decrease at lower solid load. Low EMC values are associated with the hydrophobicity of hydrochar. HTC promotes hydrophobicity due to the removal of carboxyl and hydroxyl in phenol groups [163]. These reactions are enhanced by increasing temperature. However, hydrophobicity seems to decrease at longer reaction times. This could suggest that re-polymerization reactions could counter hydrophobicity properties, re-forming -OH groups.

Regarding the significance of factor effects, the temperature had a significant linear and quadratic effect ($p < 0.050$), while solid load had a significant linear effect. On the other hand, reaction time did not show any significant effect, the visualization of the significance test is illustrated in **Figure 4.45**.

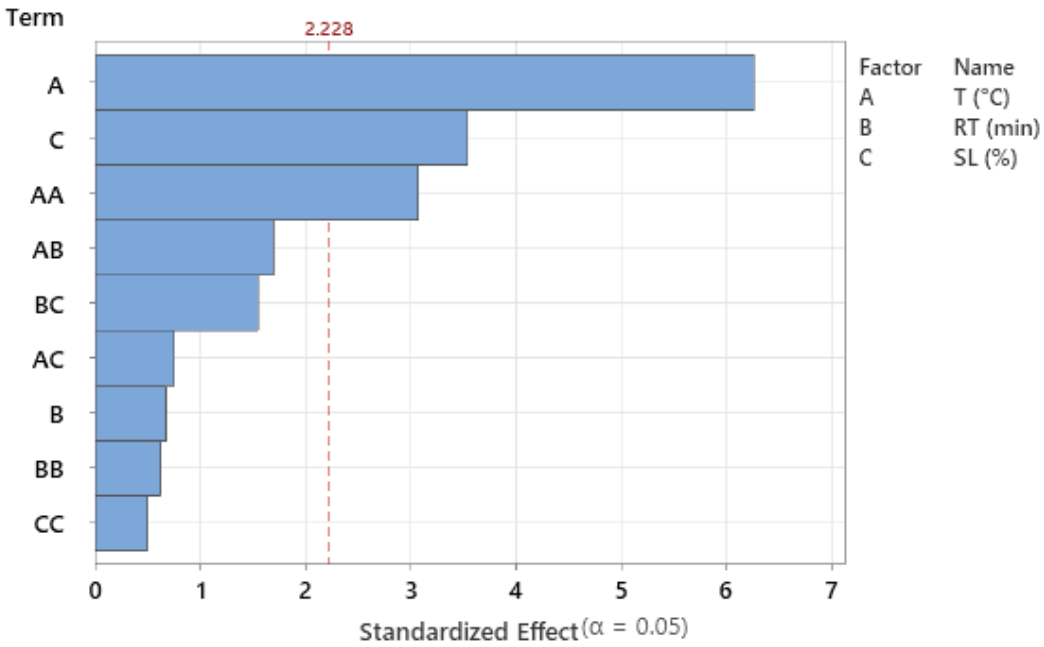

Figure 4.45 Pareto chart of the effects on EMC.

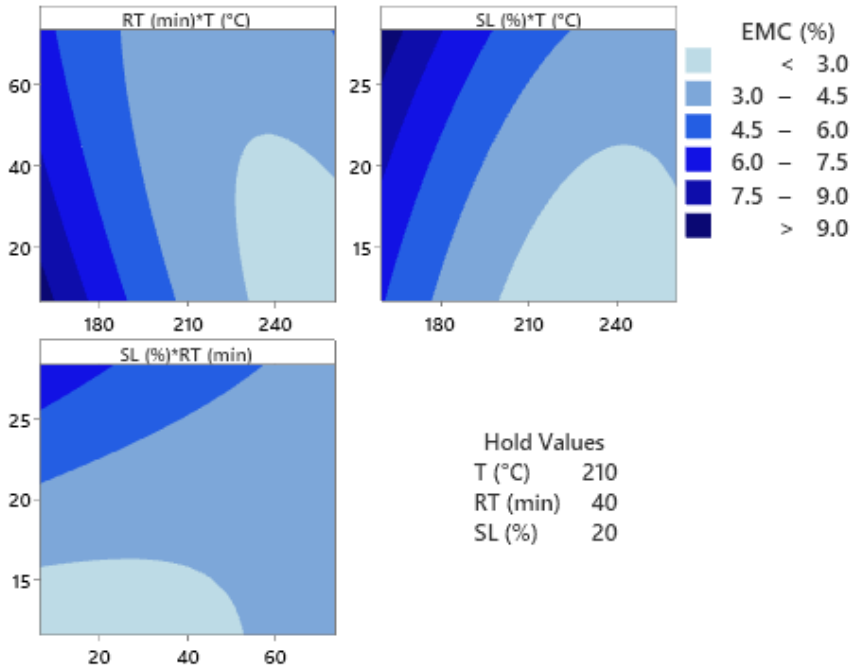

Figure 4.46 Contour plots of equilibrium moisture content (%).

4.4.5 Humic acids

Humic compounds are colloids found in soil generated from the biodegradation of plant biomass. This solid material is an organic arrangement of carbon with active cation exchange sites [164]. When these sites are occupied with protons it is called humic acid, a term used especially due to the separation technique of this material, where it precipitates in an alkali medium. However, these exchange sites are not always occupied by hydrogen cation when in soil, and it is recognized that this feature is seized by plants for nutrient transport and absorption [165]. Therefore, humic acids are collectively considered an interesting group of compounds for an advanced fertilization strategy in agriculture.

What follows is an exploratory experiment to evaluate the effect of humic acids fraction by HTC on food waste with the intent of expanding the valorisation of the technology for food waste treatment.

The highest humic yield in hydrochar was found at (260/40/20) with 31.4%, followed by (210/40/12) with 29.1% of hydrochar. This indicates that intense conditions could lead to the highest generation of humic acid material.

However, it was found that longer times had a negative effect on humic acids content, the longest time (210/73/20) yielding one of the lowest humic acids percentages (19.46%).

The generated contour plots suggest that the combination of high temperature, low solid load and short reaction times should result in high humic acids content (**Figure 4.47**). The Pareto chart (**Figure 4.48**) shows that only the linear effect of the solid load had statistical significance.

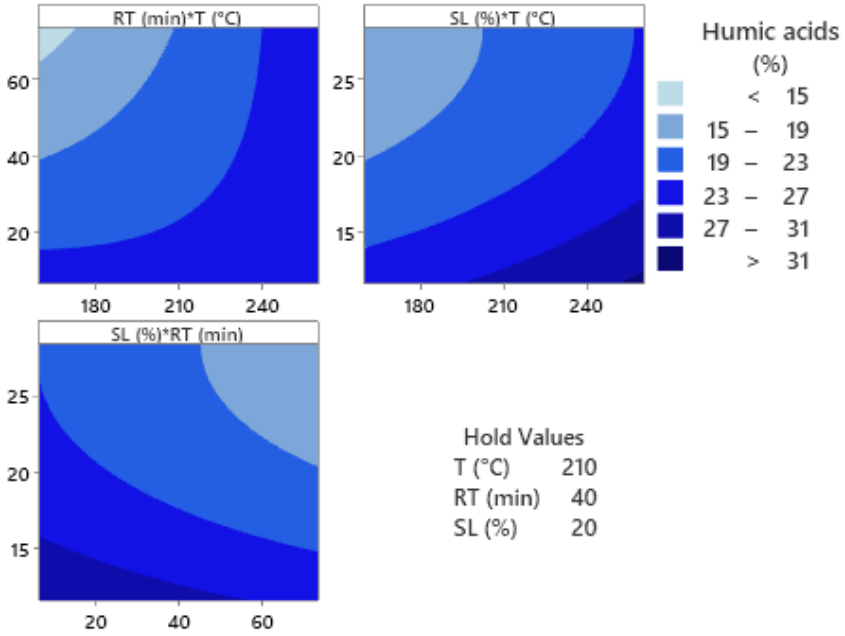

Figure 4.47 Contour plots of Humic acids in hydrochar (%).

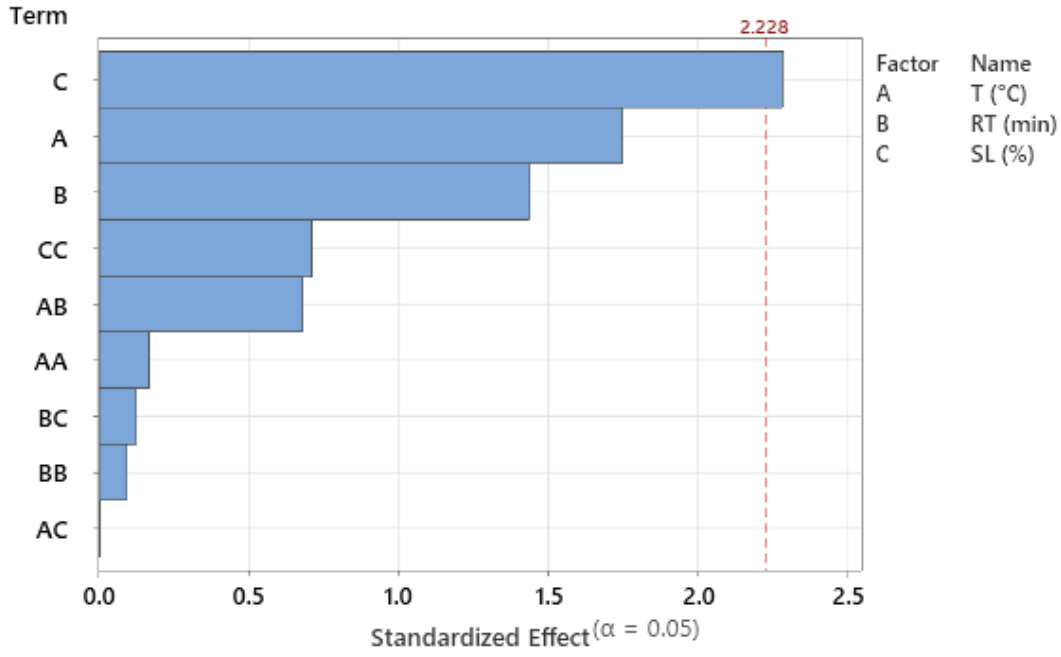

Figure 4.48 Pareto chart of the different effects for humic acids (%).

4.4.6 Summary and discussion

In this chapter was shown how the HTC successfully improves the characteristics of food waste and yielded a hydrochar with enhanced fuel qualities. For comparison, in **Table 4.10** are compiled the responses of previous HTC of food waste studies. The SY of this study ranged from 47.3 to 88.1 %, and removing the critical point the maximum was 66.2%. This SY was higher than most of the previous studies even with a wide range of temperatures. In the case of HHV, the maximum obtained was 33.7 (MJ/kg), which makes it the highest HHV reported to our knowledge. Similarly, the highest ED in the current work was 1.62 and was one of the highest in literature working with FW, even if the HHV of the original feedstock was particularly high in this work. In a similar manner, the energy yield (%) ranged from 62.8 to 88.1, making it the best performance in the literature, due to the combination of high HHV and SY, most likely due to the shorter time range used in this work.

Table 4.10 Composition and characteristics of hydrochars from HTC of food waste

Temperature	Yield (%)	HHV (MJ/kg)	EY (%)	ED	Reference
220 - 260 °C	-	19.55 - 29.77	26.95 - 23.57	1.85 - 2.82	[16]
180 - 220 °C	37 - 56	19.60 - 25.36	50 - 71	1.13 - 1.47	[22]
180 - 250 °C	39.5 - 72.5	19.5 - 25.6	-	-	[166]
180 - 250 °C	50.1 - 40.9	22.4 - 26.7	65.5 - 63.7	1.3 - 1.56	[112]
220 - 260 °C	59.83 - 45.27	24.37 – 27.64	59.98 - 45.29	1 -1	[161]
160 - 200 °C	52 - 58.4	23.3 - 29.6		5.5 - 7.3 #	[157]
180 – 280 °C	30.5 – 27.5	23.5 – 29.6	37.4 – 42.4		[114]
175 - 250 °C	40 - 44	21.6 - 26.7	-	1.18 - 1.46	[15]
200 - 260 °C	75 – 68.5	30.45 - 33.08	-	1.21 - 1.31	[6]
200 - 250 °C	23.8 - 28	31	-	1.83 - 1.95	[5]

based on LHV

The statistical results for the different responses of solid products evaluated previously are summarized in this subsection. The summary of the ANOVA for the different hydrochar quality responses including regression models and correlation coefficients is displayed in **Table 4.11**, **Table 4.12** and **Table 4.13** divided in energetic responses, mass yields and non-energetic responses. Later, the significance test of the individual effects for all responses are compiled in **Table 4.14**.

Regarding the energy responses, all regression models yielded statistical significance ($p < 0.050$). The response with the highest correlation coefficient was energy densification with 0.91. This was followed by HHV with 0.90, and both solid yield and energy yield (%) with 0.74.

Table 4.11 ANOVA of energetic responses of hydrochar

	Response			
	SY (%)	HHV (MJ/kg)	ED	EY (%)
R^2	0.74	0.90	0.91	0.74
R^2 *adj*	0.51	0.82	0.84	0.51
R^2 *pred*	0.00	0.54	0.56	0.00
F_0	3.24	11.06	12.17	3.24
F_{tab}	3.02	3.02	3.02	3.02
p-value	0.041	0.000	0.000	0.041
Model	175- 1.674 T + 0.469 RT + 5.87 SL + 0.00426 T*T - 0.00342 RT*RT- 0.0425 SL*SL - 0.00065 T*RT- 0.0143 T*SL- 0.0046 RT*SL	-37.6 + 0.526 T -0.126 RT + 0.593 SL - 0.001070 T *T + 0.000329 RT *RT - 0.0251 SL*SL + 0.000188 T *RT+ 0.00058 T *SL - 0.00363 RT*SL	-1.818 + 0.02602 T - 0.00642 RT + 0.0222 SL - 0.000053 T *T + 0.000014 RT *RT - 0.001056 SL *SL + 0.000010 T *RT+ 0.000025 T *SL - 0.000187 RT*SL	-17+0.012 T+0.226 RT+7.87 SL+0.00076 T*T - 0.00302 RT*RT- 0.1078 SL*SL - 0.00046 T*RT- 0.0135 T*SL+ 0.0050 RT*SL

Regarding the regression models for the mass yield responses of C, N and ash, CY showed no significance with p = 0.137 and a R^2= 0.66. On the other hand, NY and AY were found significant with R^2 values of 0.74 for both of the responses.

Table 4.12 ANOVA of mass yield of C, N and ash.

	CY (%)	NY (%)	AY (%)
R^2	0.66	0.74	0.74
R^2 *adj*	0.33	0.51	0.52
R^2 *pred*	0.00	0.00	0.00
F_0	2.07	3.25	3.31
F_{tab}	3.02	3.02	3.02
p-value	0.137	0.040	0.038
Model	153- 1.237 T + 1.07 RT + 4.09 SL + 0.00346 T*T - 0.00085 RT*RT+0.0175 SL*SL - 0.00355 T*RT- 0.0124 T*SL- 0.0154 RT*SL	74.7 - 0.670 T+ 0.586 RT+ 5.43 SL + 0.00224 T*T - 0.00416 RT*RT- 0.0364 SL*SL - 0.00093 T*RT- 0.0135 T*SL- 0.0032 RT*SL	177 -1.669 T+0.462 RT+5.60 SL + 0.00425 T *T - 0.00332 RT *RT - 0.0358 SL *SL - 0.00064 T*RT- 0.0143 T*SL- 0.0047 RT*SL

Regarding the non-energetic responses (**Table 4.13**), EMC showed a significant regression model (P = 0.002) and a R^2 = 0.87. However, the regression for humic acids had no significance and a low R^2 of 0.53.

Table 4.13 ANOVA of EMC and Humic acid (%).

	EMC (%)	Humic acids (%)
R^2	0.87	0.53
R^2 *adj*	0.75	0.10
R^2 *pred*	0.23	0.00
F_0	7.52	1.26
F_{tab}	3.02	3.02
p-value	0.002	0.360
Model	130.7 - 0.498 T - 0.557 RT - 1.31 MC + 0.000727 T *T + 0.000332 RT *RT + 0.00426 MC*MC + 0.000808 T *RT + 0.00144 T *MC + 0.00442 RT*MC	196 - 0.084 T - 0.59 RT - 4.47 MC + 0.00020 T *T + 0.00025 RT *RT + 0.0307 MC *MC + 0.00164 T*RT - 0.00003 T *MC + 0.0018 RT *MC

Table 4.14 displays the summary of the significance test for each of the effects considered in the quadratic regression model. Interestingly, solid load (SL) resulted in a highly relevant factor as it had a significant linear effect on all evaluated responses, except for O/C and H/C, although its only significant quadratic effect was on H/C. SL did not show significance in interaction effects. The effect of SL on responses affected by mass solubilisation (SY, and C-, N- and ash yield) was in a direct increase as SL increased. Meanwhile the energy-responses such as HHV, ED and EY had reached the highest point at mid SL, followed by a decrease as SL kept increasing. This proves that the moisture contained in food waste is a non-negligible factor that will determine the value of the response of interest. Therefore, adjusting solid load should be considered a process factor when optimizing an HTC process for food waste.

Table 4.14 p-values of all effects of all responses of the full DOE run set.

p-Value

Factor	Model	β_1 (T)	β_2 (RT)	β_3 (SL)	β_1^2	β_2^2	β_3^2	β_1*β_2	β_1*β_3	β_2*β_3
SY (%)	**0.040**	**0.006**	0.716	**0.015**	**0.041**	0.424	0.531	0.864	0.354	0.838
HHV (MJ/kg)	**0.000**	**0.000**	0.468	**0.047**	**0.011**	0.682	0.072	0.794	0.839	0.407
ED	**0.000**	**0.000**	0.433	**0.032**	**0.008**	0.712	0.094	0.751	0.849	0.351
EY (%)	0.200	0.415	0.877	**0.012**	0.650	0.427	0.095	0.891	0.326	0.804
H/C	0.270	0.300	0.576	0.820	0.915	0.269	**0.018**	0.710	0.592	0.313
O/C	**0.000**	**0.000**	0.422	0.064	**0.003**	0.887	0.549	0.978	0.519	0.655
C yield (%)	**0.040**	**0.022**	0.621	**0.002**	0.126	0.859	0.819	0.415	0.476	0.552
N yield (%)	0.137	0.452	0.937	**0.005**	0.184	0.266	0.534	0.775	0.311	0.867
Ash yield (%)	**0.038**	**0.006**	0.713	**0.014**	**0.039**	0.428	0.591	0.863	0.345	0.833
EMC (%)	**0.002**	**0.000**	0.515	**0.005**	0.071	**0.012**	0.547	0.120	0.468	0.153
Humic acids (%)	0.360	0.111	0.180	**0.046**	0.870	0.927	0.494	0.512	0.998	0.902

Temperature was another important factor. For energy responses, temperature exhibited significant linear effect for solid yield (p = 0.006), HHV (p = 0.000), ED (p = 0.000), ash yield and EMC. Also, it showed significant quadratic effect on solid yield (p = 0.047), HHV (p = 0.011), Energy densification (p = 0.009), ash yield and EMC. Temperature did not carry

significance in any of the interaction effects. Responses including SY, C yield, N yield, and ash yield decreased as temperature increased, whereas responses such as HHV, ED and EY increased with temperature. Interestingly HHV and ED had a deaccelerating pattern while EY displayed an accelerating pattern.

In contrast, reaction time carried no statistical significance on any of the effects. This indicates that reaction time has no major impact in the timespan selected for this work, which could be considered short in comparison to other HTC works. However, reaction time could have great importance in the energy analysis, via the time integrated rate of energy consumption during the HTC process. Hence, it is suggested that reaction time should be kept at a minimum.

After analysing the results of the parametric analysis and the effect on the different hydrochar quality responses, it was clear the different effects of parameters on different responses. Particularly, temperature and solid load showed important effects on practically all the responses evaluated, however, it was mostly the opposite effect. Therefore, this illustrates the necessity of incorporating optimisation in HTC studies.

4.5 Combustion of Hydrochar

4.5.1 Effect of HTC on DTG and TG curves

Hydrochar as solid fuel is the main utilisation proposal for hydrochar from food waste. Whereas by direct combustion or in blends with conventional coals. Thus, as part of incorporating hydrochar utilisation-linked responses into the optimisation test, investigating the role of HTC conditions on the combustion profiles of hydrochar is required for further advancing the HTC technology.

The combustion characteristics of hydrochar were investigated by thermogravimetric (TG) analysis. Derivative thermogravimetric (DTG) curves are useful for evaluating the combustion rates of samples at different temperatures and allow observing how HTC affect them. As the results are shown in **Figure 4.49**. The weight loss starts at just over 100 °C for most of the samples, attributed to the removal of moisture content. The weight loss continues as temperature increases; however, it is divided into two combustion zones. The first zone starts below 200 °C and finishes at 390 °C. Zone 2 starts at 400 °C and finishes between 590 and 600 °C. However, the combustion rates and the peaks' temperature were affected by HTC conditions.

Food waste as starting point displayed 5 DTG peaks, marked by arrows in **Figure 4.49**. The first peak was observed at 160 °C, and the second at 200 °C. This shows the presence of compounds of easy devolatilisation. The next two peaks were observed at 270 and 340 °C. These 4 DTG peaks were located in combustion zone 1, showing an accumulated weight loss of 65% and the maximum DTG (5.25 %/min). This first main peak is attributed to the devolatilisation and combustion of small size volatile matter. In contrast, Zone 2 showed only one DTG peak for food waste at 490 °C, attributed to the volatile matter of more complex carbon structures. These combustion zones were clearly divided by a valley where DTG fell to 0.6 %/min for food waste.

After HTC, the first two peaks observed in food waste disappeared and the first DTG peak moved to higher temperatures. Nonetheless, small shoulders remained at low temperatures for low-intensity runs. The main DTG peak for food waste was located at 270 °C. The main peak shifted to 320-350 °C for low and mid-intensity HTC. This pattern includes runs at 160, 180, and 210 °C disregarding the other factors, and also includes runs at 240 °C with short times. Interestingly, at high-intensity HTC conditions, the main peak shifted to a lower temperature between 220 and 230 °C. This pattern was observed in (240/60/X) and (260/40/20).

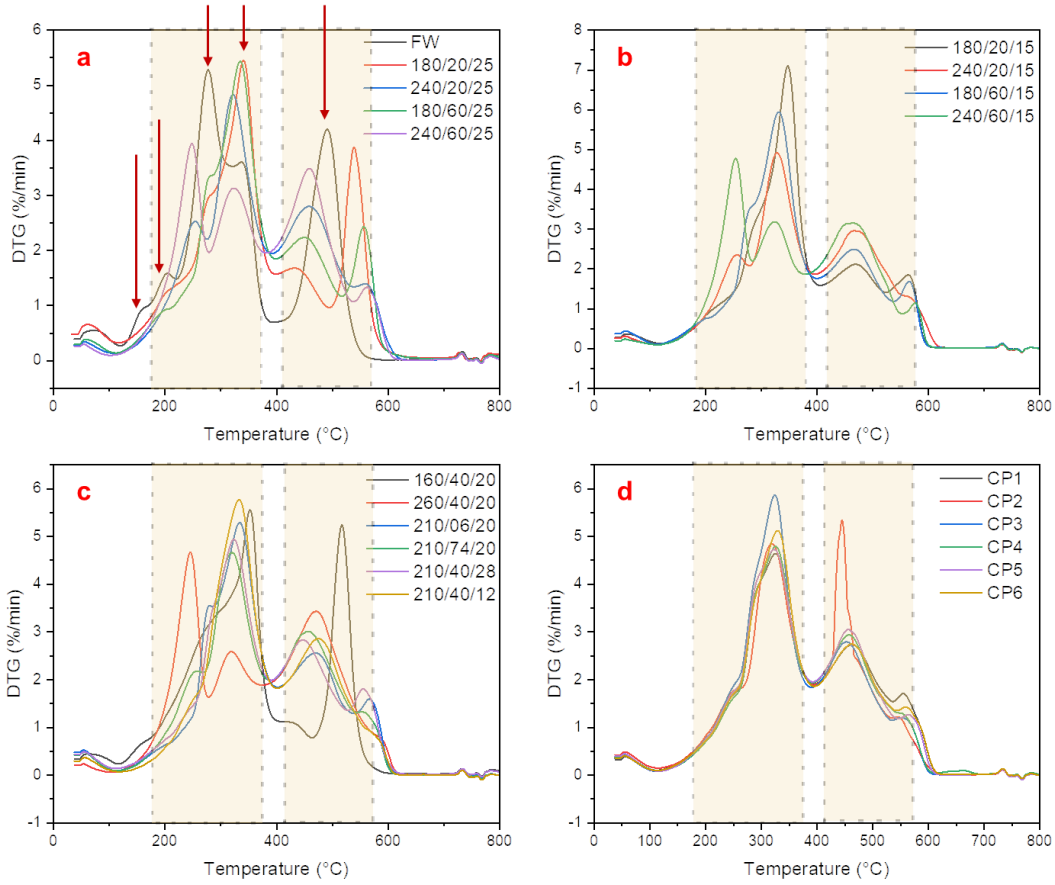

CP = centre point, FW = food waste, X/Y/Z = temperature/time/solid load

Figure 4.49 DTG curves of HTC of food waste.

Regarding combustion zone 2, the peak observed in the food waste sample was separated into visible peaks, one between 440-460 °C and the second one at 550-580 °C. Low-intensity conditions, particularly 160 and 180 C HTC reactions promoted an increase in the reactivity of the second peak. Whereas higher temperatures increased the reactivity of the peak at 450 °C. Also, high-intensity reactions decreased the depth of the valley between combustion zones from 0.6 %/min to 2 %/min in samples treated with HTC temperatures higher than 210 °C.

Similar behaviour on the main peak shifting has been reported previously for food waste [5,166]. These patterns seem counterintuitive, as high-intensity runs have lower VM but higher reactivity. Ischia et al. [166], argued that HTC produces two types of char from volatile matter in combustion zone 1, the first DTG peak of hydrochar is linked to a ‘secondary char’ temperature range of 230-240 °C, while the later peak at 320-350 °C was attributed to a ‘primary char’. The secondary char is a product of the re-condensation or re-polymerization of HTC intermediates with an amorphous structure that forms over the primary char [167]. Meanwhile, the primary char is referred to as the char formed in a solid-solid mechanism [168]. This could explain why the secondary char was not visible or showed low reactivity in low and mid-intensity hydrochar. Thus, the peak-shifting to 320-350 °C at low and mid-intensity HTC suggests that these conditions promote the formation of primary char while high-intensity conditions promote secondary char formation.

However, a distinctive peak in the primary char region remains for high-intensity HTC. Thus, the shifting of the main peak to a lower temperature at high-intensity conditions could indicate a separation of the previously formed char. The secondary char in our hydrochar could be associated with the lipid content. Li et al. [106] reported a peak shifting from 323 °C for lignocellulosic biomass, to 237 °C when triacylglycerides were added to the sample. They reported the increase of DTG at a lower temperature, as well as the higher presence of hydrocarbons from devolatilisation. However, in the current-work feedstock, the lipid was present in all samples. Therefore, high-intensity conditions could separate the lipids from the hydrochar matrix, they would not participate in the re-polymerization reactions and would be adsorbed onto the primary char surface in aliphatic hydrocarbons form. The three samples with a main peak in the secondary char (260/40/20), (240/60/25), and (240/60/15) also showed a viscous surface with a tarry or pitch-like appearance. Also, it is suggested that the high reactivity of secondary char would result in fuel segregation during the co-combustion of hydrochar and coal [168]. Thus, although high-intensity conditions would produce a higher energy content hydrochar, it would be of lower quality for combustion utilisation.

In this regard, it appears that mid-intensity conditions would benefit the combustion profiles of hydrochar. Hydrochar from mid conditions showed a DTG peak at higher temperatures for Zone 1, and a lower temperature peak for combustion 2. Hence, even though the combustion zones do not merge into one, it suggests lower fuel segregation.

4.5.2 Comprehensive index

For optimization purposes, a quantitative form of describing the combustion of hydrochar is necessary to compare among the DOE. There are numerical parameters to describe the combustion process using points on the DTG curve. These parameters are used in comprehensive indexes to numerically describe, evaluate and compare the combustion properties based on TGA curves. The used points are ignition temperature (T_i), burnout temperature (T_b), maximum weight loss rate (DTG_{max}), mean weight loss rate (DTG_{mean}), and temperature of maximum weight loss rate (T_{max}).

It has been argued that ignition temperature is not a physical property of fuel [19]. Hence, the intersection method was used to standardize the determination of ignition temperature through all samples. Because of the multi-peak DTG curves of hydrochar and food waste, in comparison to anthracite coal, burnout temperature was not determined by the intersection method. Instead, it was defined as the temperature where DTG fall below 0.5%/min, inspired by Sliz and Wilk [150].

Ignition temperature ranged from 205 to 292 °C throughout the experiment. The lowest T_i was 205 °C at 240/60/75 and the maximum was 292 °C at 180/20/85, this is linked to the peak-shifting explained in the previous section. Low and mid-intensity HTC moved the main peak in Z1 to a higher temperature, corresponding to primary char, whereas high-intensity conditions displayed a main peak of Z1 at a lower temperature, associated with a higher reactivity of secondary char. High-intensity runs showed a lower T_i than food waste. Burnout temperature (T_b) increased with the intensity of HTC conditions. Food waste displayed a T_b of 537 °C, increasing to 554 °C for (160/40/20) and 575 °C at (180/20/25). The rest of the runs ranged from 585 to 599 °C with a slight increasing pattern as conditions intensified. Although many samples coincided on their temperature of maximum DTG (T_m), DTG_{max} shows a slight, but unclear, decrease as HTC conditions increase severity. Run (180/20/15) displayed the highest DTG_{max} values with 7.1, considerably higher than the rest of the experiment. The second highest DTG_{max} was 5.94 (%/min) found at (180/60/15), suggesting that low temperature and low solid load benefit the reactivity of hydrochar. On the other hand, the mean weight loss (DTG_{mean}) showed little variation, ranging from 2.29 and 2.62 (%/min) for (210/40/28) and (210/40/12), respectively. Moreover, all runs with 15 %SL showed higher DTG_{mean} than their 25 %SL counterparts. This indicates that the SL has a crucial effect on the reactivity of char.

A larger S indicates a quicker and more aggressive combustion [106,161]. The results of the S are displayed in **Table 4.15**. According to Eq, S values are improved by high DTG_{max} and high DTG_{mean}. Also, S is punished by high T_i and T_b. Because of this, food waste showed the highest S values, reflecting the high reactivity of Z1, lowest T_i and T_b. Among hydrochars, the highest S was 4.14 at (240/60/15) and 4.08 at (260/40/20) due to the improved T_i caused by the modification of secondary char in Z1. Therefore, according to S, the reactivity decreased after the HTC reaction in comparison to food waste. However, among the hydrochars, the reactivity increased at low and high temperatures, showing a quadratic effect, with a considerable decrease at mid temperatures, as it is noticeable in **Figure 4.50**. Low solid load and long reaction times seemed to promote higher combustion reactivity.

Table 4.15 Combustion parameters of hydrochar

Sample (T/RT/SL)	T_i (°C)	T_m (°C)	T_b (°C)	DTG_{max} (%/min)	DTG_{mean} (%/min)	S (x 10^{-7})	H_f
Food waste	225	278	537	5.28	2.56	4.97	0.94
180/20/15	292	347	587	7.1	2.59	3.67	0.78
240/20/15	258	327	599	4.92	2.43	3	1.09
180/60/15	266	332	586	5.94	2.61	3.74	0.92
240/60/15	217	253	590	4.78	2.41	4.14	0.95
180/20/25	259	341	575	5.45	2.44	3.44	1.07
240/20/25	244	322	594	4.82	2.39	3.25	0.89
180/60/25	267	335	584	5.43	2.53	3.3	0.98
240/60/25	205	248	591	3.94	2.32	3.67	1.06
160/40/20	264	353	554	5.55	2.47	3.54	1.16
260/40/20	210	246	598	4.66	2.31	4.08	0.71
210/06/20	264	334	593	5.29	2.56	3.28	1
210/74/20	247	321	590	4.66	2.45	3.17	1.14
210/40/12	268	333	592	5.77	2.62	3.55	0.9
210/40/28	253	323	591	4.93	2.29	2.98	1.09
CP1	254	327	598	4.64	2.46	2.96	1.16
CP2	257	320	583	4.85	2.48	3.13	1.28
CP3	259	324	586	5.86	2.56	3.81	0.86
CP4	256	326	585	4.79	2.5	3.12	1.13
CP5	252	325	594	4.72	2.5	3.13	1.15
CP6	254	330	598	5.12	2.48	3.29	1.07

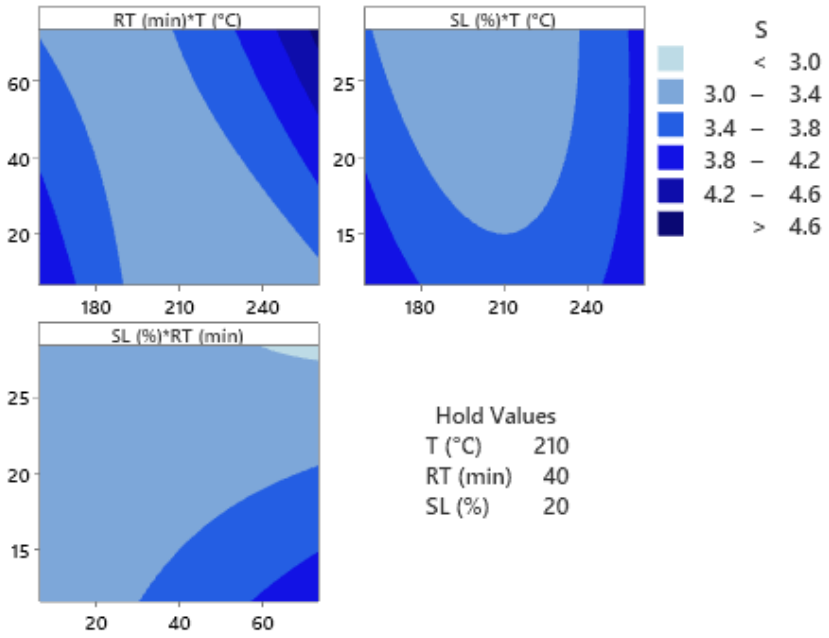

Figure 4.50 Contour plots of comprehensive combustion index

A second comprehensive index evaluated was the combustion stability (Hf). This index considers the temperature range where the combustion rate was higher than the maximum combustion rate. For the stability index, a lower value means a higher combustion stability. A quadratic effect of the three factor is visible on the contour plots **Figure 4.51**. Thus, lower values were found at both ends of the DOE range, with the highest values on the middle process conditions. The lowest value of Hf was 0.71 obtained at (260/40/20) in the sample of the highest temperature. Although low values were obtained at 240 and 180 °C. It is appreciable in the contour plots that the three factors had a quadratic effect

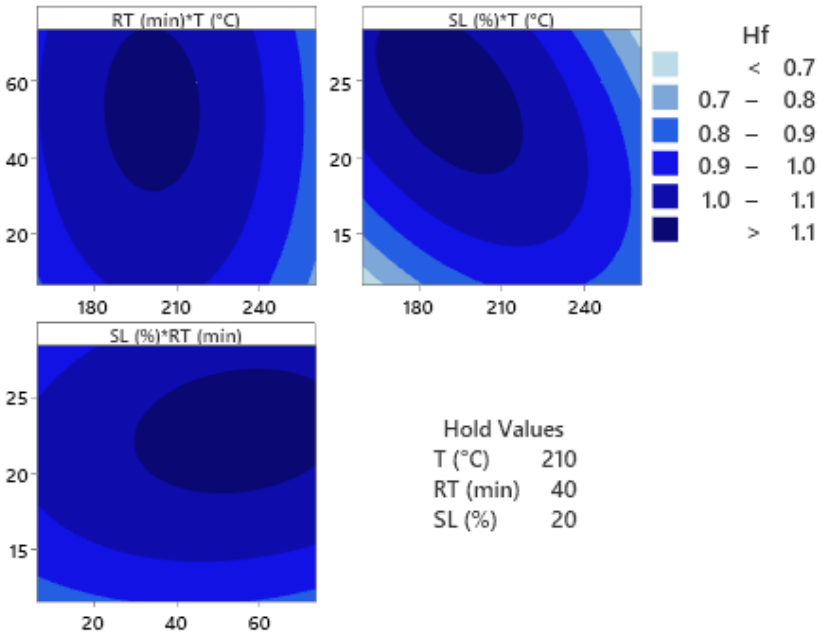

Figure 4.51 Contour plots of combustion stability index (H_f).

4.6 Optimization of individual responses

In order to evaluate optimal conditions for individual responses, the Derringer's desirability function is used. This will serve as a preamble to the multi-response optimization, and it will allow visualizing optimized conditions for individual responses and how they are compromised for the multi-response optimization. The individual optimization of all the hydrochar quality responses is compiled in **Table 4.16**.

Table 4.16 Individual optimization of hydrochar quality responses

Response 0	Criteria	Optimized value	Desirability (D)	T (°C)	RT (min)	SL (%)
Solid yield (%)	Maximise	88.1	1	159.6	34.2	28.4
HHV (MJ/kg)	Maximise	33.0	0.96	257.4	73.6	20.1
Energy densification	Maximise	1.60	0.97	258.4	73.6	20.1
Energy yield (%)	Maximise	86.6	0.94	159.5	47.8	27.6
C yield (%)	Maximise	95.9	1	159.5	40.3	28.4
N yield (%)	Minimise	66.3	1	202.3	6.4	11.6
Ash yield (%)	Minimise	40.6	1	216.6	6.4	11.6
EMC (%)	Minimise	2.4	1	210	35.6	11.6
Humic acids (%)	Maximise	31.5	1	260.4	6.4	11.6
S	Maximise	5.2	1	260.4	73.6	11.6
Hf	Minimise	0.5	1	260.4	6.4	28.4

The individual optimization of energy responses exhibited contrasting conditions. On one hand, solid yield (%) and energy yield (%) had the optimal results at the lowest temperature (159.5 °C), high solid load (28.4 and 27.7%, respectively), and mid reaction times (35.5 and 48.5 min) for optimized values of 81.99% solid yield and 86.61% of energy yield. This result was foreseeable because of the effect of temperature on the solubilisation, as well as being facilitated with a lower solid load. However, as mentioned before, this condition would result in a hydrochar of bad quality and the optimization considering multiple objectives is required. Other studies have found optimal conditions at their lowest temperature, Kannan et al. [31], reported an optimal condition for maximizing hydrochar yield (37%) at 180 °C and 120 min working with fish waste, and Stutzenstein et al. [32] 165 °C for 500 min with AD

digestate (50.37 %). In these studies, longer retention times are utilised compared to the current work. Long reaction times would cause the re-adsorption of initially solubilized materials. Nonetheless, if the temperature remains too low to initiate further decomposition reactions such as decarboxylation and dehydration, these will lead to a high SY of low quality hydrochar. Hence, slow reaction rate conditions (low temperature, low MC) and mid-RT are optimal for maximizing SY.

Regarding C, N, and ash yield (%), the optimized value for CY is calculated at 159.5 °C, 41.7 min and 28.4 %SL for 95 % of CY. These conditions include the lowest temperature for low solubilisation, and high solid load for low reaction rates. It also includes mid reaction times due to re-adsorption found at longer reaction times (> 40 min). In the case of N and ash yields (%) the optimization was set for minimizing values. It was found that both responses had similar optimal conditions with middle temperatures (202 and 216 °C), low reaction time (6.4 min) and low solid load (12 %), yielding optimized values of 66.3 and 40.3 (%) N and Ash yields, respectively. These conditions look for a significant solubilisation (mid temperature and low solid load), while minimizing the re-adsorption or re-polymerization conditions (higher temperatures and longer reaction times).

In the case of EMC (%), the objective was to find the conditions for minimizing the re-adsorption of moisture. The optimal conditions were 210 °C, 35 min, and 12 %SL for an optimized value of 2.44 % of moisture absorbed by the hydrochar. For humic acids (%), the optimized value was 31.45% humic acids in hydrochar at 260 °C, 6.4 min, and 12% SL.

For the optimisation of the comprehensive indices of combustion, it was found that maximum temperature (260 °C) and shortest time (6.4 °C) were optimal for both S and Hf indices. Possibly due to the increase of DTG_{mean} and increased reactivity of secondary char by high temperature and lower ignition temperature (t_i) benefiting higher values of S, and lower DTG_{max} temperature (t_p) for lower Hf. Whereas long reaction times always showed lower reactivity than the short time counterpart. Nonetheless, the optimal solid load for S was lowest SL due to high DTG_{max} at secondary char and in zone 2 (Z2). In the

case of H_f, higher SL showed lower higher t_p and higher DTG_{max}, due to less extend of carbonisation reaction into fixed carbon fraction in Z2.

The individual optimization showed how all the evaluated responses have different optimal conditions. By themselves, no response could indicate a proper optimization of HTC for food waste utilisation. In addition, most of the optimised conditions were on the margins of the DOE conditions due to the linear pattern of the main effects. Because most of optimisations fell on the margin of the DOE conditions makes the regression model to have less fidelity and to extrapolate the optimised values, instead of interpolating where the models are more useful.

In the next section is presented the multi-response optimization for hydrochar as a necessary step in the development and valorisation of HTC technology.

4.7 Multi-response optimization using desirability method

4.7.1 Hydrochar for solid fuel

The first multi-response optimization addresses the production of hydrochar for utilisation as solid fuel, mainly for combustion. The selected responses were solid yield (%), energy densification for heating value output, as well as minimising nitrogen yield (%) and equilibrium moisture content (%) for an hydrochar cleaner of nitrogen content and with less hygroscopicity, respectively. In addition, the comprehensive combustibility index (S) is included as a combustion indicator.

The optimisation was performed considering all response with the same level of importance, the composite desirability function (D) was 0.63. The optimized conditions were 260.4 °C, 46.4 min and 17.7 %SL, the results of the desirability analysis are shown in **Figure 4.52**. Under these conditions, the predicted responses are 55.6 % solid yield, 1.56 energy densification, 3.2 %EMC, meaning a 3.2 % of moisture regained at 75% relative humidity after 48 h, 4.13 S, and 78.9 % of nitrogen yield (NY%), or 21.1 % of nitrogen removed. Highest temperature improved most of the responses except SY, in this case SY was compromised with only 55 % this is a low value within the DOE. In contrast, long reaction time improved most of responses except for

SY, but in this case the rest of responses were compromised for a mid-reaction time improving SY, although the impact of RT on the responses was lesser than temperature. The optimal SL was 17.7 % is not the optimal point for none of the response, exhibiting a compromising of all responses. It is noteworthy that while in single-response optimisation the optimised process conditions tend to be the extremes values within the DOE, in the multi-response optimisation the optimised conditions were within the DOE area. This demonstrates the trade-off between response and the importance of the multi-response optimisation in HTC studies.

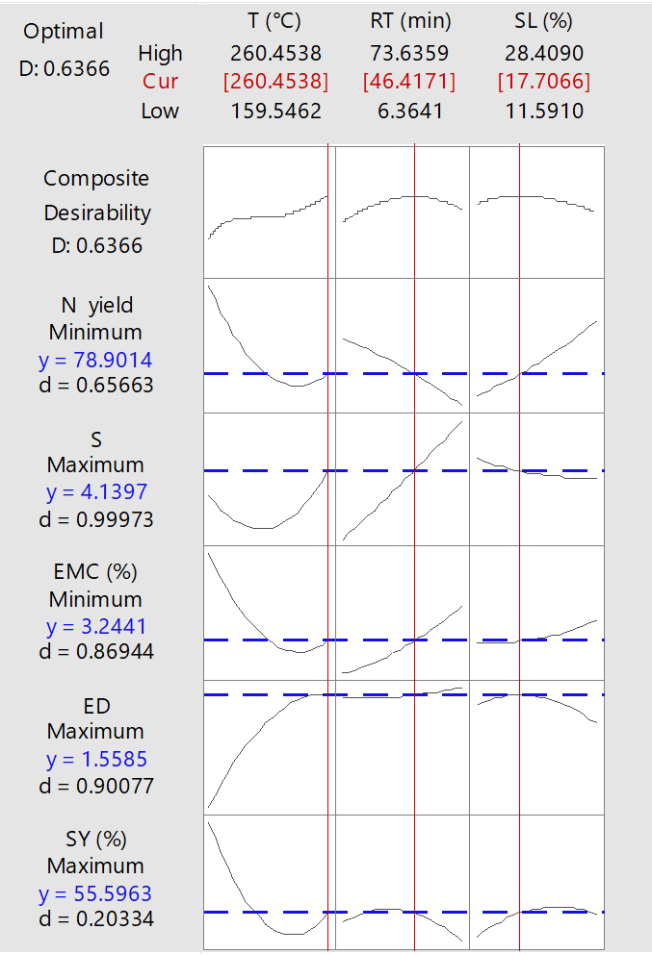

Figure 4.52 Multi-response by desirability analysis of hydrochar for solid fuel (Red font indicates the optimized process condition, blue font indicate the predicted response value).

Both the highest temperature and longest reaction time would increase the energy consumption during the HTC process. Thus, although these conditions

would maximize the evaluated responses, it would be sensible to perform an energy analysis and include it as another response in the optimization.

In **Table 4.17** are displayed previous HTC studies utilising DOE with different feedstocks. It is evident that the list is scarce and several of the studies do not make any optimisation attempts while others use graphical optimisation for one-response optimisation. Ronix [124] used the desirability function for a single-response optimisation, they reported a maximised surface area of 33.3 m^2/g while treating coffee husk with HTC conditions of 210 °C, 243 min, and 29 %SL. In addition, there are three previous studies that utilised desirability function for dual-response optimisations, two of them in the last year. Stutzenstein et al. [32] optimised the HTC of AD-digestate for a 36 % solid yield and a 0.8 O/C difference to feedstock, the optimal conditions were 165 °C, 500 min and a pH of 3.5. El Ouadrhiri et al. [33] treated date stone and found an optimised conditions of 200 °C, 120 min, and 20 mg of catalyst for optimised responses of 59.7 %SY and 75.8 %C yield. Finally, Sultana et al. [169] optimised the HTC of sewage sludge digestate and found a hydrochar with 70 %SY and 18.59 MJ/kg, with optimal conditions of 180 °C, 4 h and stirring at 600 rpm. This illustrates that the need for optimisation studies is necessary to progress the HTC development. Moreover, there is still a lack of multi-response optimisation and even less focused on a specific utilisation. Because of the difference between the feedstock in literature, it is complicated to do a direct comparison. Nonetheless, it is noteworthy that all optimisations found considered long reaction times, when is likely it would impact the viability of the process due to energy consumption.

Table 4.17 HTC optimisation studies utilising DOE.

Type of DEO	Feedstock	Variables	Responses	Optimized conditions	Optimized responses	Reference
2-level factorial with center points	Microalgae	T, RT, SL	SY, CY	-	-	[28]
Box-Behnken frational	Digested mail silage	T, RT, pH	Carbon content, CY	-	-	[29]
CCD	Olive stone	T, RT, SL	SY, HHV	-	-	[27]
CCRD	Sewage sludge	T, RT	SY, HHV, EY and ED	180/60 and 200/30	carbon recovery in liquid	[30]
CCD	Lignocellulosc biomass	T, RT, SL	SY, ED and EY	-	-	[170]
CCD	Palm shell	T, RT, SL	SY	-	-	[171]
CCD	Coffe husk	T, RT, SL	SY, BET	210/243/3.4:1	33.3 m^2/g	[124]
CCD	Shrimp waste	T, RT	SY	180/120	-	[31]
CCD	AD digestate	T, Rt, pH	SY, O/C ratios	165/500/3.5	36 %SY, 0.8 O/C difference	[32]
CCD	Bamboo	T, Rt, HCl	Levulinic acid	160/3h/0.37M	9.46% Levulic acid	[172]
CCD	Digested Sewage sludge	T, Rt, pH	Dewaterability and P release	170/1.93pH	48% SY, 70% P release	[173]
CCD	Date stone	T, Rt, catalyst dose	SY, C retention	200/120/20mg	59.71 %SY, 75.84 %C	[33]
Box-Behnken	Bark	T, Rt, Stirring speed	SY, HHV	180/4h/600rpm	69.89 %SY, 18.59 MJ/kg	[169]

4.8 Conclusion

Interestingly, solid load resulted in a highly relevant factor as it had significant linear effect on all the evaluated responses, although it did not show significance in interaction effects. This proves that the moisture contained in food waste is a non-negligible factor that will determine the value of the

response of interest. This is worth noting, as most modelling and mechanisms studies on HTC are conducted, or assumed to occur, in low solid load (<10%), while practical studies for treating wet wastes have considered minimizing the addition of water to increase environmental viability. Therefore, adjusting solid load should be considered a process factor when optimising an HTC process for food waste. Temperature exhibited significant linear effect for solid yield, HHV, energy densification, N yield, ash yield and EMC. Also, it showed significant quadratic effect on solid yield, HHV, energy densification, ash yield and EMC. In contrast, reaction time showed no significance on any of the effects. This indicates that reaction time has no major impact in the time range selected for this work, which could be considered short in comparison to other HTC works. However, reaction time could have great importance in the energy analysis, via the time-integrated rate of energy consumption during the HTC process. Hence, it is suggested that reaction time should be kept at a minimum.

The individual optimization of energy responses exhibited contrasting conditions. On one hand solid yield (SY) and energy yield (EY) had the optimal results at the lowest temperature, high solod load and mid reaction times. This result was foreseeable because of the effect of temperature on the solubilisation, as well as being facilitated with lower solid load. However, as mentioned before, this condition would result in a hydrochar of bad quality and the optimization considering multiple objectives is required. Regarding C, N and ash yield (%), optimized conditions include the lowest temperature for low solubilisation, and high solid load for low reaction rates. It also includes mid reaction times due to re-adsorption found at longer reaction times. In the case of N and ash yields (%) the optimization was set for minimizing values. These optimisation conditions aim for a significant solubilisation (mid-temperature and low solid load) and while minimizing the re-adsorption or re-polymerization conditions (higher temperatures and longer reaction times). The individual optimization showed how all the evaluated responses have different optimal conditions. By themselves, no response could indicate a proper optimisation of HTC for food waste utilisation.

The optimized conditions were 260.4 °C, 46.4 min and 17.7 %SL. Under these conditions, the predicted responses are 55.6 % solid yield, 1.56 energy densification, 3.2 % EMC, meaning a 3.2 % of moisture regained at 75% relative humidity after 48 h, 4.13 S, and 78.9 % of nitrogen yield (NY%), or 21.1 % of nitrogen removed. However, the downside of the optimized values is that is highly taxing on the energy efficiency of the process. Both the highest temperature and longest reaction time would increase the energy consumption during the HTC process. Thus, although these conditions would maximize the evaluated responses, it would be sensible to perform an energy analysis and include it as another response in the optimization. It is noteworthy that while in single-response optimisation the optimised process conditions tend to be the extremes values within the DOE, in the multi-response optimisation the optimised conditions were within the DOE area. This demonstrates the trade-off between response and the importance of the multi-response optimisation in HTC studies.

The combustion of food waste was divided into two combustion zones (Z1 and Z2) with two defined DTG (%/min) peaks. Both combustion zones were affected differently by HTC process conditions. In comparison to untreated FW, Z1 (associated with volatile matter) was separated into two peaks, the first peak at lower temperature was promoted in high-intensity hydrochars, while the second peak was higher in low-intensity hydrochars. The second peak of Z1 was reduced significantly in high-intensity hydrochars at the same time that the peak on Z2 grows. This indicates that the second peak of Z1 is an amorphous volatile matter that is transformed into fixed carbon at high-intensity process conditions. Meanwhile, the first peak of Z1 might be linked to a layer of lipids adsorbed onto the hydrochar surface.

Regarding the combustion combustibility index (S), a quicker and more aggressive combustion was found as the intensity of the process conditions increased. The combustion stability index (H_f) showed a quadratic effect with higher stability for low- and high-intensity hydrochars, mid-intensity conditions were detrimental H_f. Only the quadratic effect of temperature was significant for S, while no effect was significant for H_f.

Chapter 5. Multi-variable analysis of HTC process water: composition and bio-methanation capabilities

5.1 Introduction

Process water (PW) is the liquid fraction of the HTC outlet stream. Traditionally, it attracts less interest than the hydrochar product. Nonetheless, during the HTC reaction occurs a major transfer of the initial mass and C content into the liquid phase. For instance, in this study, the HTC reaction transferred up to 53% of the total mass and 74% of the total carbon into the process water under certain conditions. Thus, it could be inferred that neglecting this outlet stream would compromise the viability of the HTC process.

In this regard, two potential uses for the PW are to extract valuable compounds and energy recovery. Anaerobic digestion for methane production has been reported to be suitable for PW utilisation [135,174]. However, how HTC parameters affect the AD process, and its optimization is still in investigation. Therefore, this work evaluates the effect of process conditions on the product yields of different compounds and the effect on the bio-methanation capabilities of the process water using a DOE approach.

This chapter aims to comply with **Objective 3**: Assess how the process parameters of HTC affect the liquid product of HTC (also referred to as 'process water').

3a. Evaluate the effect of HTC parameters on the composition of process water.

3b. Evaluate the effect of HTC parameters on the bio-methane production capability of process water.

5.2 Composition

One important assessment of process water is to measure the amount of mass transferred into the liquid phase from the original feedstock. In this regard, three responses are measured to evaluate the solubilisation of mass

into PW: (i) total solids (g/kg PW) for an estimation of the total mass transferred and to use in the mass balance in later sections, (ii) total organic carbon (g/L) estimates the total solubilisation of C from the solid matrix (inorganic carbon values were negligible), and (iii) chemical oxygen demand (COD) (g/L), determines the potential oxidizing matter, which is also used as an indirect indicator of biodegradable matter. **Table 5.1** displays the results for the mentioned responses, as well as pH and ammonium. The pH is an indicator of H^+ activity present in the process water, hence is an indirect indicator of acid production during HTC. Ammonia is one of the most important N- containing compounds generated during HTC and could act as an inhibitor for anaerobic digestion. Ammonia is reported as total ammonia nitrogen (TAN) as it includes the concentration of ammonia and ammonium.

Table 5.1 Total solids, TOC, COD concentration and other responses in process water.

Temp. (°C)	Time (min)	SL (%)	TS (g/kg pw)	TOC (g/L)	COD (g/L)	TAN (mg NH_3-N/L)	pH
180	20	15	91.6	45.2	90.6	16.3	3.38
240	20	15	45	25.2	53.6	34	3.77
180	60	15	55.8	35	80.9	16.6	3.24
240	60	15	41.3	23	50.9	24	3.94
180	20	25	124.4	66	120.3	44.5	3.27
240	20	25	66.1	37.8	79.6	40.9	3.78
180	60	25	90.7	58	107.4	39	3.14
240	60	25	46.1	28.7	69	49	4.01
159.5	40	20	121	58	124.2	36.6	3.62
260.5	40	20	57.1	25	59.6	32.8	4.05
210	6.4	20	66	37.1	82.7	12.2	3.12
210	73.6	20	48.1	25.6	54.2	33.9	3.55
210	40	11.6	29.1	17.2	44.6	13.6	3.38
210	40	28.4	68.4	35.7	61.2	19.6	3.53
210	40	20	54.5	33	67	43	3.49
210	40	20	52.6	26.2	55	41.5	3.53
210	40	20	52.3	31.9	62.8	38.9	3.49
210	40	20	45.4	23.1	53.9	15	3.47
210	40	20	52.7	28.5	68.6	19.7	3.47
210	40	20	58.3	32.1	61.8	22.3	3.49

Overall, TS, TOC, and COD showed similar behaviour. The contour plots illustrate the pattern for TOC (**Figure 5.1**) and COD (**Figure 5. 2**). Low-intensity conditions promoted a higher concentration of TS, TOC, and COD. Concentrations decreased considerably at mid conditions and decreased slightly again as the process intensity keeps increasing. Run (180/20/25) yielded the highest values of TS of 124.4 g/kg PW and TOC of 66 g/L. Meanwhile, (160/40/20) showed the highest COD with 124.2 g/L. In contrast, the lowest concentration values were found at (210/40/12) with 29.1 g/kg TS, 17.2 g/L TOC, and 44.6 g/L COD. This was due to having the lowest SL (12%) which, unsurprisingly, yields low concentrations by having the lowest solid load. Also, it is directly linked to the solubilisation effect discussed previously for C% and SY% of hydrochar, where it was detected a re-adsorption or re-polymerisation process under severe process conditions, promoted by low solid load.

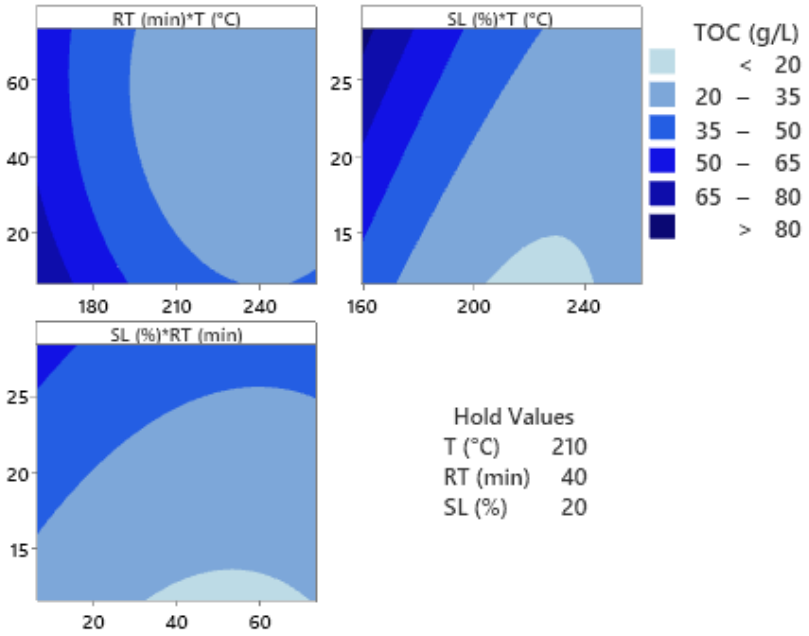

Figure 5.1 Contour plots of total organic carbon (TOC) (g/L) of process water.

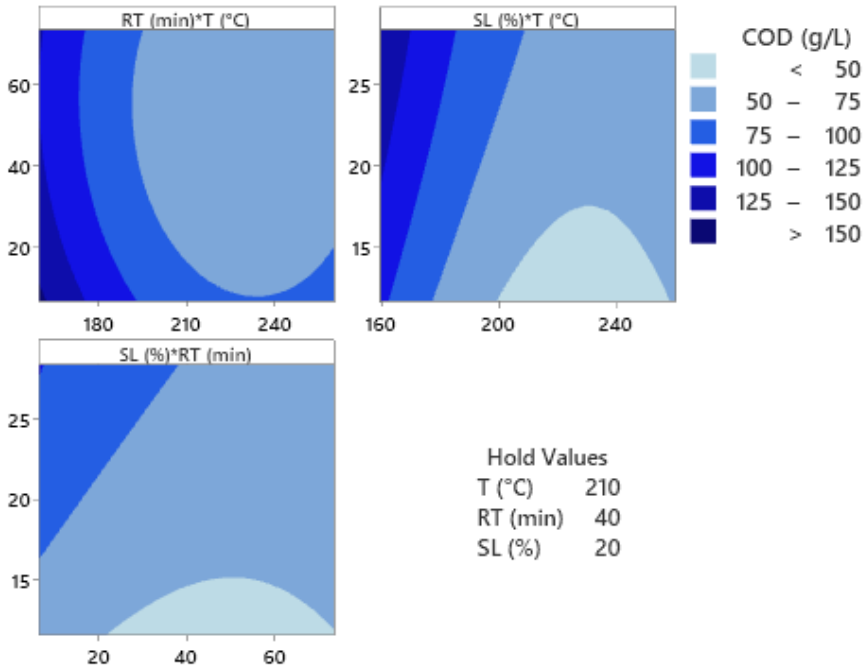

Figure 5. 2 Contour plots of chemical oxygen demand (COD) (g/L) of process water.

pH shows a major dependence on temperature. The pH increased from 3 to 4 linearly (**Figure 5.3**). Although RT and SL seemed to have a minor role, longer reaction times resulted in higher pH. This suggests a higher presence of acids at low temperatures.

TAN had two zones with high concentrations at low and high temperatures, visible by the saddle pattern in **Figure 5. 4**. Higher SL produced higher TAN concentrations than lower SL, although this was particularly noticeable at low temperatures. The effect of SL on TAN was less evident at mid and high T and RT. Run (240/60/25) yielded the highest TAN concentration with 49 mg/L, whereas (210/40/12) yielded the lowest concentration with 12.2 mg/L. In general, high SL and long RT seemed to promote the generation of TAN. Moreover, the quadratic effect of RT is an interesting result. Wang et al. [14] argued that N-$NH4^+$ is generated at low-temperature HTC by the hydrolysis and deamination of proteins and further reacts with sugar derivatives to form Maillard reaction compounds, explaining the concentrations at low temperature. Also, at 180 °C longer RT and lower SL would benefit the formation of Maillard products, explaining the low concentration of TAN. They

argued that as temperature increases, the Maillard reaction stalls and the generation of stable aromatic compounds is promoted, where nitrogen is incorporated in quaternary form, while deamination is enhanced. This re-absorption of nitrogen was observed in the hydrochar composition of the current work. However, a significant amount of nitrogen did not reabsorb into the hydrochar and continued the deamination process, increasing the concentration of TAN at high HTC temperatures.

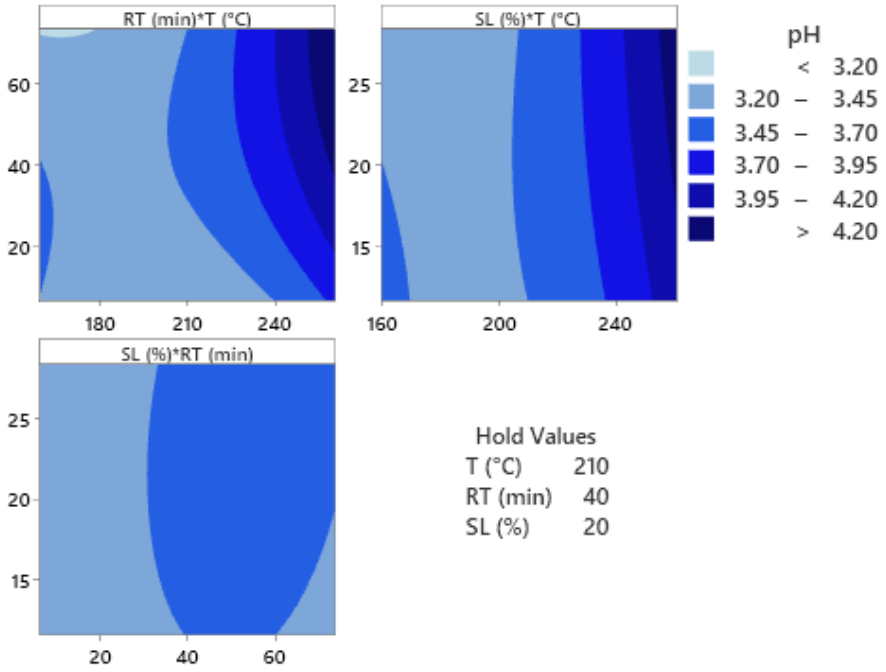

Figure 5.3 Contour plots of pH of process water.

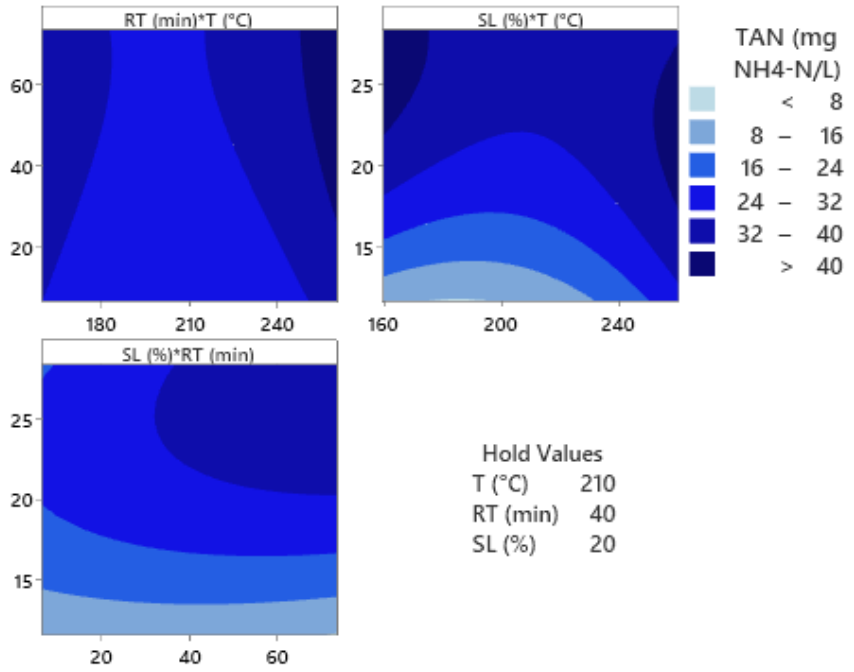

Figure 5.4 Contour plots of total ammonia nitrogen (TAN) (mg NH_4-N/L)

5.2.1 Gas chromatography analysis

Compounds analysed by gas chromatography were classified into three different groups: volatile fatty acids, N-compounds, and non-N cyclic compounds. The concentration of the analysed compounds is displayed in **Table 5.2**, **Table 5.3**, and **Table 5.4**, divided into the aforementioned groups.

Volatile fatty acids (VFA) are short-chain aliphatic carboxylic acids produced during the hydrolysis reactions of HTC. The VFA concentrations are shown in **Table 5.2**, where acetic acid had the highest yield, followed by glycolic and succinic, and levulinic acid. The sum of the VFA was grouped for a single response called total VFA (mg/L). Starting with total VFA, intense conditions yielded higher VFA concentrations. Run (240/60/25) displayed the highest VFA concentration with 13671 mg/L. Followed by (240/60/25) with 12654 mg/L. Runs with the highest temperature and solid load also showed total VFA values >10000. On the other side, the lowest runs were (180/20/15) and (160/40/20) with 3837 and 3936 mg/L, respectively. This indicates that intense process conditions and high SL promote the generation of VFA and, although

the initial HTC-hydrolysis produces a fraction of the VFA, their generation continues as process conditions increase. This was not expected from the pH results and could indicate the presence of other acid forms at low temperatures, which decrease as carbonisation progresses, such as carboxylic acids.

In addition, any of the individual VFA analysed saw their concentration decrease with process intensity. This could suggest that VFA do not take part in the re-polymerisation of hydrochar, or the generation rate overpowers the re-polymerisation rate. Therefore, VFA generation continues from the degradation of already solubilised compounds.

The ANOVA showed a significant fit for the regression model ($P < 0.05$) with an $R^2 = 0.98$. The significance test showed that temperature had a significant linear and quadratic effect. Reaction time had a significant quadratic effect. The solid load had a linear significant effect. Also, the 2-way interaction effect of temperature and reaction time showed statistical significance. The regression model is shown next:

$$\boldsymbol{Total\ VFA}\left(\frac{\boldsymbol{mg}}{\boldsymbol{L}}\right) = -\mathbf{54311} + \mathbf{411.5}\,\boldsymbol{T} + \mathbf{293.8}\,\boldsymbol{RT} + \mathbf{335}\,\boldsymbol{SL} - \mathbf{0.826}\,\boldsymbol{T} * \boldsymbol{T} - \mathbf{1.356}\,\boldsymbol{RT} * \boldsymbol{RT} - \mathbf{8.71}\,\boldsymbol{SL} * \boldsymbol{SL} - \mathbf{0.802}\,\boldsymbol{T} * \boldsymbol{RT} + \mathbf{2.04}\,\boldsymbol{T} * \boldsymbol{SL} - \mathbf{0.65}\,\boldsymbol{RT} * \boldsymbol{SL}$$

A higher concentration of VFAs was found at higher HTC process conditions. However, intense process conditions also showed higher pH than lower process conditions. Although the process water was still acidic (pH around 4), this result is counterintuitive. One possible explanation could be the presence of large compounds with acidic groups that are generated during the hydrolysis at low temperature (for instance, carboxylic acids), and participate in the re-polymerization of hydrochar at higher process conditions, causing an increase in pH. This hypothesis is supported by the behaviour of COD and TOC, which decrease with process intensity.

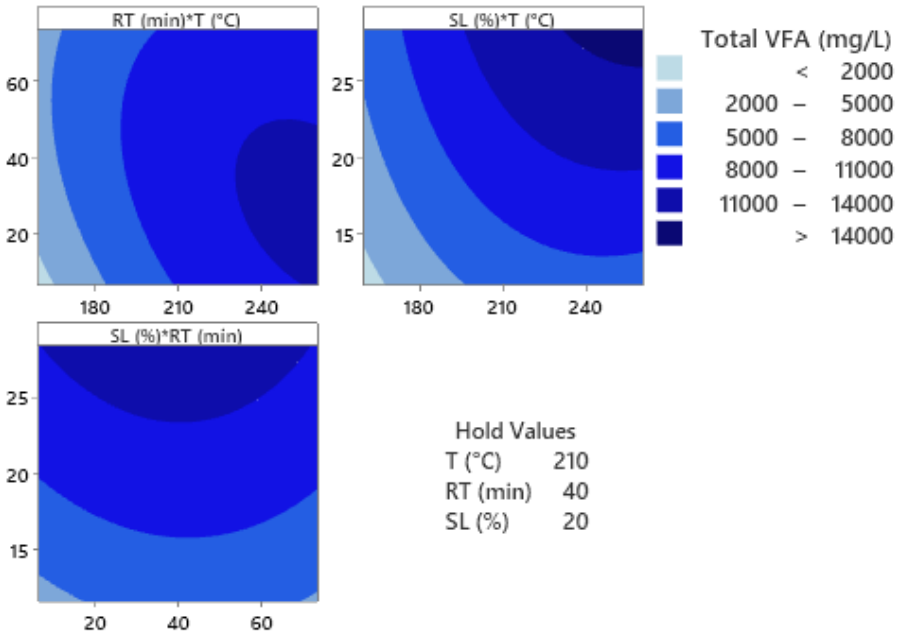

Figure 5.5 Contour plot of total volatile fatty acids

N-compounds group also showed high concentrations, particularly pyrrolidinone (**Table 5.3**). Pyrrolidinone varied insignificantly from 2,129 to 2,173 mg/L. The two runs with the lowest intensity did not reveal the presence of pyrrolidinone, (160/40/20) and (180/20/25). Thus, it could be inferred that pyrrolidinone is not generated during the initial hydrolysis and is a product of further Maillard reactions.

Other N-compounds analysed were 2-methyl-pyrazine, 2,5-dimethylpyrazine, ethylpyrazine, 2,3-dimethylpyrazine, 2,3,5-trimethylpyrazine. These compounds were found in low concentrations, ranging from 7 to 170 mg/L. Nonetheless, it was observed that within individual compounds, the high intensity of the HTC process causes a higher concentration of pyrazine compounds.

Another interesting compound group is the phenolic compounds. Generally, phenolic compounds were found in low quantities (**Table 5.4**). These could be associated with the low content of lignin in food waste feedstock. The concentration of total phenolic compounds yielded a minimal variation from 95 to 113 mg/L, with higher concentration at higher process conditions. All individual compounds followed this trend, indicating that even if the

concentrations are low, for reasons associated with the feedstock composition, there is a generation of phenolic compounds due to the HTC process, which increases with process intensity.

Table 5.2 Volatile fatty acids concentration in process water (mg/L)

Temperature (°C)	Time (min)	SL (%)	Acetic acid	Isobutyric acid	Butyric acid	isovaleric acid	Crotonic acid	Malonic acid	Levulinic acid	Succinic acid	glutaric acid	Glycolic acid	Valeric acid	Total VFAs
180	20	25	4579.24	7.27	7.66	66.36	0.00	22.65	150.95	330.59	34.38	2624.21	7.48	7830.79
240	20	25	5105.78	26.64	48.26	185.49	3.22	22.46	497.00	539.75	133.49	7105.48	3.43	13671.02
180	60	25	4242.09	0.00	10.98	117.05	0.00	22.87	268.37	416.27	50.46	2994.40	18.83	8141.32
240	60	25	3502.98	22.92	77.95	246.13	2.82	22.46	647.88	677.70	178.42	7271.69	3.72	12654.68
180	20	15	2298.42	0.00	7.04	36.87	0.00	22.51	61.65	125.82	22.59	1258.12	4.65	3837.66
240	20	15	4029.29	29.49	45.82	190.46	3.08	22.76	291.70	298.21	58.42	4075.87	4.71	9049.81
180	60	15	2886.19	9.39	9.23	79.54	0.00	22.49	143.83	271.91	29.97	1550.60	4.82	5007.96
240	60	15	2995.93	34.08	81.88	258.53	2.87	22.73	310.11	414.26	105.63	3466.27	4.90	7697.18
159.5	40	20	2725.88	86	6.12	40.53	0.00	22.74	37.73	176.82	16.89	899.84	2.93	3936.34
260.4	40	20	3943.53	27.24	108.44	314.37	2.47	0.00	479.06	630.70	154.27	5275.85	6.06	10941.99
210	6.4	20	3496.63	9.13	10.85	80.78	1.06	22.68	222.01	461.54	64.23	3057.52	12.36	7438.79
210	73.6	20	3180.61	29.21	40.64	252.83	1.93	22.49	345.25	548.93	119.62	4027.55	8.25	8577.31
210	40	28.4	4150.07	17.05	26.42	145.52	4.38	22.58	516.67	647.26	119.59	6215.26	13.07	11877.87
210	40	11.6	2894.51	11.43	14.47	106.84	0.51	22.70	190.45	261.13	45.43	2420.73	6.88	5975.08
210	40	20	3966.14	14.78	24.20	110.68	3.36	22.69	373.79	455.54	89.62	4530.35	8.64	9599.78
210	40	20	3632.40	20.80	33.36	164.22	3.85	22.71	356.47	582.02	107.41	5469.86	8.11	10401.22
210	40	20	4415.56	11.79	21.84	118.01	2.23	22.74	339.29	498.90	97.67	4430.94	9.08	9968.05
210	40	20	3516.18	17.41	27.11	151.28	5.67	22.73	379.04	491.03	95.26	5019.48	9.69	9734.87
210	40	20	4116.62	16.85	28.15	138.40	4.49	22.53	340.03	513.36	87.56	4569.69	9.70	9847.38
210	40	20	4553.21	16.38	23.28	126.97	1.80	22.47	361.44	464.40	76.10	3712.96	7.85	9366.86

Table 5.3 Protein derived N-compounds concentration in process water (mg/L)

Temperature (°C)	Time (min)	SL (%)	2-Methyl-pyrazine	pyrrolidinone	2,5-dimethylpyrazine	ethylpyrazine	2,3-dimethylpyrazine	2,3,5-trimethylpyrazine
180	20	25	67.48	0.00	26.87	4.59	7.45	16.58
240	20	25	176.66	2135.58	21.16	7.33	10.47	30.72
180	60	25	69.44	2135.21	26.90	4.26	7.83	16.65
240	60	25	155.05	2133.72	157.36	5.83	9.00	26.59
180	20	15	46.37	2140.94	17.81	3.39	6.83	0.00
240	20	15	5.42	2129.79	42.48	2.23	7.14	18.30
180	60	15	66.88	2132.07	28.60	4.16	7.21	16.26
240	60	15	135.88	2148.07	148.95	5.68	9.12	26.42
159.5	40	20	25.01	0.00	13.68	2.59	6.71	16.02
260.4	40	20	137.15	2168.91	152.43	5.29	9.64	26.87
210	6.4	20	99.53	2142.08	37.09	5.32	8.00	17.64
210	73.6	20	85.19	2161.09	51.26	3.70	7.84	19.12
210	40	28.4	110.91	2173.06	73.18	4.90	7.61	19.52
210	40	11.6	84.75	2130.13	38.97	4.48	8.25	18.79
210	40	20	112.09	2134.10	63.05	4.79	8.44	19.52
210	40	20	112.72	2149.40	67.47	4.71	8.59	19.77
210	40	20	115.70	2126.69	61.96	4.99	8.03	20.26
210	40	20	96.65	2128.68	51.87	3.91	7.86	17.05
210	40	20	93.88	2138.29	59.47	4.76	8.44	19.22
210	40	20	128.02	2128.14	76.09	6.31	8.43	19.95

Table 5.4 Cyclic compounds concentration in Process water (mg/L)

Temperature (°C)	Time (min)	SL (%)	Cyclo-pentanone	5-hexenoic acid	2-Methyl-2-cyclopenten-1-one	3-Methyl-2-cyclopentenone	2,3-Dimethyl-2-cyclopenten-1-one	Benzoic acid	Phenol	P-cresol	Hydro-cinnamic acid	Total phenolic compounds
180	20	25	1.90	12.86	4.31	43.53	0.00	3.28	24.17	13.48	54.82	95.75
240	20	25	14.23	25.55	146.64	38.89	18.86	4.03	26.84	14.03	56.56	101.47
180	60	25	2.08	11.33	7.34	43.79	0.00	3.53	24.23	13.87	54.97	96.61
240	60	25	24.18	19.08	219.88	36.49	26.58	3.79	28.02	14.40	57.61	103.82
180	20	15	0.00	4.95	3.04	40.56	0.00	3.42	0.00	13.56	54.66	71.64
240	20	15	10.56	12.20	85.35	37.93	16.18	3.93	28.90	13.38	56.58	102.78
180	60	15	1.35	8.00	4.12	43.70	0.00	3.15	24.13	13.57	54.99	95.84
240	60	15	17.87	9.42	143.69	50.15	22.53	4.39	28.28	13.69	56.94	103.30
159.5	40	20	1.18	4.54	2.90	40.42	0.00	2.96	23.62	13.34	54.71	94.63
260.4	40	20	29.36	25.13	175.20	65.93	33.43	4.75	32.83	14.01	58.14	109.73
210	6.4	20	2.04	22.16	7.29	45.16	0.00	2.97	24.55	13.41	54.81	95.75
210	73.6	20	3.94	19.19	47.19	41.94	11.54	4.44	26.35	13.67	56.01	100.46
210	40	28.4	4.25	35.11	43.00	48.43	10.87	3.29	25.27	13.72	55.51	97.79
210	40	11.6	3.09	14.32	16.23	41.68	10.15	20.27	24.85	13.48	55.32	113.91
210	40	20	4.51	16.43	41.96	42.76	10.59	3.45	25.81	13.94	55.73	98.94
210	40	20	5.72	27.57	56.54	43.78	12.97	3.65	26.50	13.73	56.27	100.15
210	40	20	3.83	19.02	35.97	44.82	10.30	3.22	26.23	13.97	55.81	99.22
210	40	20	3.52	27.35	34.72	44.51	10.57	3.43	26.34	13.68	55.53	98.98
210	40	20	3.34	25.39	33.28	42.98	10.84	3.81	25.83	13.89	55.76	99.30
210	40	20	5.52	19.22	45.80	42.10	11.41	2.84	24.50	14.02	55.56	96.91

5.3 Biochemical methane potential

The production of biomethane from process water by anaerobic digestion is one of the uses proposed for this HTC product stream. While the biomethanation of PW from HTC has been explored before, works with experimental utilisation of PW from food waste are scarce. Thus, this section evaluates how HTC process parameters affect the biomethane production capability of PW.

Final biochemical methane potential (BMP_{final}), for the cumulative biomethane produced (mL CH_4/g COD), and depletion time, for the time to reach the final production (days) and deplete the substrate, were used as the responses to evaluate the effect of HTC parameters, using a significance test. The results of these responses are displayed in **Table 5.5**.

Table 5.5 Final biomethane production and residence time (mean values).

Temperature (°C)	Time (min)	SL (%)	BMP_{final} (mL CH_4/g COD)	Substrate depletion (days)
Food waste			435.4 ± 46.4	16 ± 0
180	20	25	261.5 ± 0.49	28 ± 1.4
240	20	25	193.8 ± 1.9	22 ± 2.8
180	60	25	235.9 ± 10.8	23 ± 1.4
240	60	25	205.3 ± 2.4	9.5 ± 0.7
180	20	15	234.2 ± 16.9	24.5 ± 4.9
240	20	15	198.7 ± 7.9	18 ± 4.2
180	60	15	202.3 ± 6.7	18 ± 0
240	60	15	206.2 ± 16.2	12 ± 1.4
210	40	20	215.9 ± 12.9	25.5 ± 1.73

The BMP_{final} in food waste was considerably higher in comparison to any of the PW runs with 435.4 ± 46.4 mL CH_4/g VS. More than 170 mL CH_4/g VS than the highest process waters. The BMP test of the FW sample was calculated based on volatile solids instead of COD because it was a solid feedstock, opposite to process water. The BMP plot of food waste is displayed in **Figure 5.6** and it shows an abrupt start of CH_4 production since day 1. This production continues and then shows a decelerating pattern,

reaching a plateau of cumulated CH_4 on day 11. The easily biodegradable matter present in food waste caused a negligible lag phase due to a rapid start and steady production until depleting the substrate. Also, there was no inhibitory effect in food waste feedstock.

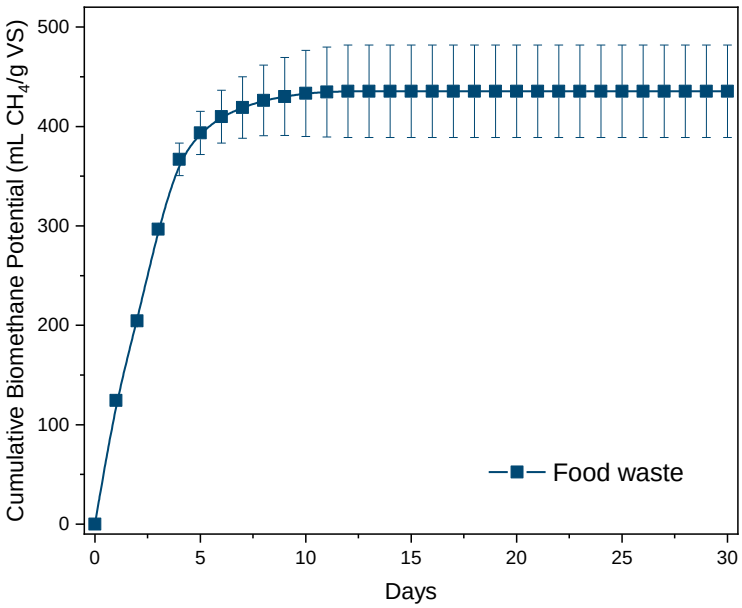

Figure 5.6 Biochemical methane potential (BMP) of food waste (N = 2).

The BMP plots of the DOE are shown in **Figure 5.7**. In comparison to food waste BMP, biomethane production with process waters exhibits various steps and plateaus, which could indicate the use and depletion of a substrate type before switching to a less bioavailable substrate. Low temperature yielded the highest biomethane production at the end of the experimental time. The highest methane production was observed at (180/20/25) with 261.5 ± 0.49 mL CH_4/g COD, followed by (180/60/25) and (180/20/15) with 235.9 ± 10.8 and 234.2 ± 16.9 mL CH_4/g COD, respectively. This trend agrees with that reported by Lucian et al. [20] for OFMSW HTC process water. They found the highest production at 180 °C and 1 h with 205 mL CH_4/g COD and the lowest at 250 °C and 6 h for 166 mL CH_4/g COD. However, the results obtained in this work were higher.

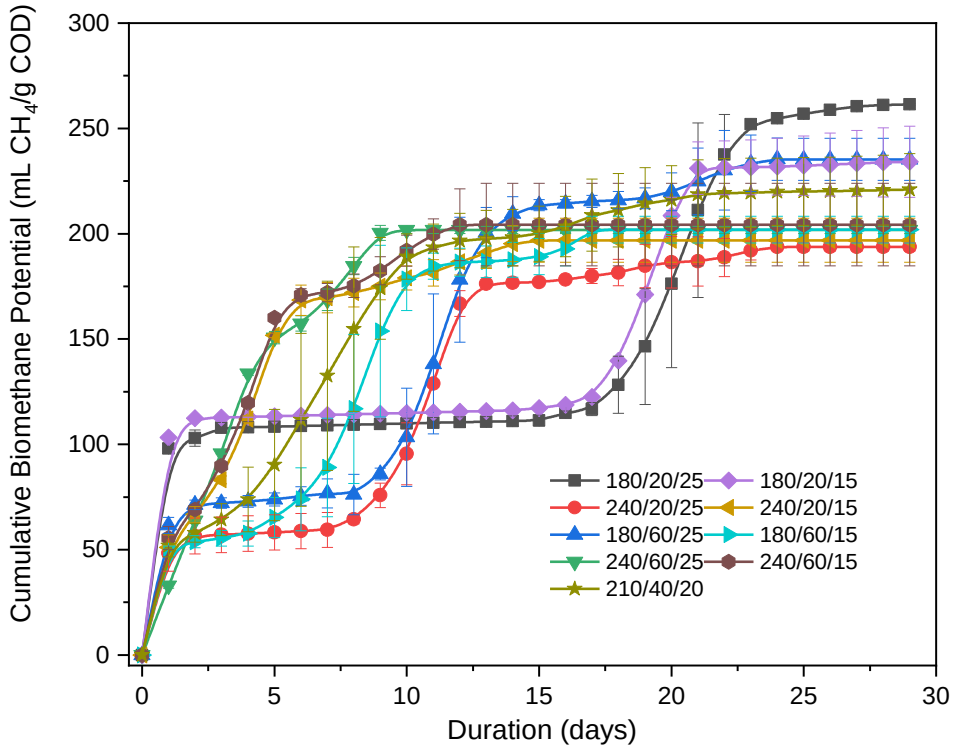

Figure 5.7 Biochemical methane potential (BMP) produced from the anaerobic digestion of the process water from the DoE runs (N = 2).

The smaller BMP-DOE allows a regression model with linear and interaction effects, not including quadratic effects, although it maintains the orthogonality of the model. The results of the significant test are displayed in **Table 5.6**. The regression model was significant for both responses BMP_{final} ($p = 0.001$) and depletion time ($p = 0.000$). Regarding the individual effects, temperature showed a significant linear effect for both responses. Temperature also exhibited a significant interaction effect in T*RT and T*SL for BMP_{final}. Reaction time had a significant linear effect for depletion time ($p = 0.000$). The SL linear effect was significant for BMP final ($p = 0.032$) and had high importance for depletion time ($p = 0.053$). No process interaction was significant for depletion time. Triple interactions were not significant for any of the responses.

$$BMP_{final}\left(mL\frac{CH4}{g}COD\right) = 230 - 0.104\,T - 3.71\,RT + 12.43\,SL + 0.0157\,T*RT - 0.0546\,T*SL + 0.004\,RT*SL - 0.000055\,T*RT*SL - 0.84$$

$$Substrate\ depletion\ (days) = 65.6 - 0.231\,T - 1.231\,RT - 1.18\,SL + 0.00552\,T*RT + 0.00792\,T*SL + 0.0688\,RT*SL - 0.000354\,T*RT*SL + 6.06$$

Table 5.6 Significance test of BMP_{final} (mL CH_4/g COD) and depletion time (days), p < 0.05 = significant.

		Prob > Ftab						
Factor	Model	β1 (T)	β2 (RT)	β3 (SL)	β1* β2	β1* β3	β2* β3	β1* β2* β3
BMPfinal	**0.001**	**0**	0.067	**0.032**	**0.003**	**0.012**	0.762	0.95
Depletion time	**0**	**0**	**0**	0.053	0.15	0.15	0.373	0.107

5.3.1 Effect of HTC process parameters on BMP test profile

Process parameters had different effects on the methane production profile. Low-temperature runs displayed the longest plateaus. The first plateau for the runs (180/20/25) and (180/20/15) lasted 15 days after the initially abrupt biomethane production during the first two days, possibly due to HTC-hydrolysis products, i.e., sugars and amino acids. This could indicate two possibilities: 1) at low temperature there are two or three different types of compounds with considerably different biodegradability. For example, sugars and Maillard compounds. Thus, the AD-hydrolysis stage of the less biodegradable second compound group caused the plateau. Or 2) the presence of an inhibitory compound, generated during the HTC process at low temperature (180 °C), as it was not present in the raw food waste run.

Lower SL decreased BMP_{final} by around 10 % from (180/20/25) to (180/20/15) due to the reduction of SL from 25 to 15 %. Nonetheless, lower SL meaning only affected the second substrate group, not the production of the first compound group nor the duration of the intermediary plateau. Thus, the higher solubilisation at higher SL only impacted the second substrate.

As process intensity increases, the abrupt initial biomethane production, BMP_{final} and duration of lag phases decreased. This is observable in the runs

maintaining low temperature with longer reaction times such as (180/60/25), increasing RT from 20 to 60 min resulted in a decrease of the initial production by half and shortened the plateau time by half, in comparison with short time runs. This could be an indication that longer reaction times enhanced the degradation of the second compound group and simultaneously promoted the generation of Maillard compounds, which reduced the initial sugar concentration. Moreover, a second intermediary plateau appears, further suggesting the modification and separation of the second compound group seen at (180/20/X). These patterns are even more patent at (180/60/15).

The high-temperature runs yielded lower biomethane production in general. They ranged from 185.30 ± 0.03 to 192.52 ± 19.57 mL CH_4/g COD, a considerable reduction against low-temperature runs. Nevertheless, the bioavailability seems to be greatly improved in the most severe conditions. Both (240/60/25) and (240/60/15) showed a great reduction of the intermediary plateau times, to the point that the AD behaviour resembles a decelerating pattern. Also, it is noted that high-temperature runs reached the final production as early as 9.5 days into the process (i.e. 240/60/25), a considerably shorter time in comparison with the low temperature runs that reached final production after around 25 days. This could be an important response when selecting the optimal conditions.

The centre points exhibited a mid-production of 224.16 ± 9.87 mL CH_4/g COD, which locates them in the middle between the minimum and maximum production, indicating a direct proportionality with the intensity of the process.

Interestingly, run (240/20/25) not only had the lowest final biomethane production but also preserved relatively high intermediary plateau times. This suggests that reaction time and solid load play a major role in the biomethanation capability of the PW. It also indicates that the high temperature of HTC by itself does not improve the biomethane capabilities of PW from food waste and should be accompanied by longer reaction times. In contrast, between (240/60/25) and (240/60/15) there were minor differences, probably the most interesting one was reaching the final production on day 11 for (240/60/25) and day 13 for (240/60/15).

5.3.2 Evaluation of inhibitory behaviour during BMP tests

Regarding the possibility of inhibitory compounds generated during HTC of food waste, various compound groups are recognized and could be present in this feedstock. Among the possible inhibitory compounds from food waste transformation, we can mention ammonia, phenolic compounds, lignin-related compounds, N-aromatics, and long-chain fatty acids (LCFA) [175]. Lignin-related compounds could be discarded by their low proportion present in our feedstock (6 %). Also, lignin compounds, along with other phenolic compounds were found to increase with more severe HTC process conditions, according to the GC analysis. These high-severity PW also showed higher digestibility than milder process conditions. Thus, it is not intuitive to assume that an inhibitory effect or intermediate lag phase was caused by phenolic and lignin-related compounds. Ammonia and N-aromatic are plausible inhibitory agents due to the protein degradation during HTC and the high protein content in our feedstock. However, nitrogen solubilisation increased with the severity of the process, along with the increase of N-aromatics found in the GC analysis. Therefore, although the N-compounds are present in the PW, their content would not be reduced as HTC intensity increases. Thus, it does not explain the decrease of the plateau time with intense process conditions. Regarding LCFAs, their presence is probably due to the high content of lipids in the FW feedstock and will not be degraded by temperatures in the range of the HTC process (180 – 260 °C). However, longer reaction times could promote the sedimentation of LCFAs on the hydrochar surface. Nonetheless, the appearance of free fatty acids in hydrothermal conditions has been reported at over 220 °C [107]. Thus, fatty acids may be in the form of triglycerides at 180 °C runs. Therefore, the long plateaus present in low-temperature runs are likely to be due to the AD-hydrolysis stage of complex molecules, and not by inhibition.

To summarize, low-intensity conditions (low temperature, short reaction times, and high SL) promote the solubilisation of organic matter into PW and lead to higher total methane production. Nonetheless, low-intensity conditions showed an AD profile with considerable mid-process plateau,

associated with a hydrolysis stage of complex solubilised organic matter after the depletion of an initial easily digestible substrate. Moreover, high-intensity conditions improved the digestibility of PW reducing the mid-reaction plateaus towards a decelerating pattern, similar to that found in raw food waste.

5.3.3 Kinetics of biomethane production

Kinetic parameters were used numerically to understand the AD of FW-PW and to develop a simulation with fidelity. The results of the kinetic parameters and their correlation coefficient are displayed in **Table 5.7.**

Table 5.7 Kinetic parameters of BMP runs.

Sample	Model	$BMP_{max}1$	R_m1	λ1	$BMP_{max}2$	R_m2	λ2	R^2
Food waste	Logistics	931.84	205.75	0.04				0.9881
180/20/25	Double logistics	109.72	105.65	0.00	258.55	76.82	19.05	0.9978
240/20/25	Double logistics	57.16	159.75	0.67	188.56	48.60	8.84	0.9945
180/60/25	Double logistics	70.38	1925.47	0.97	221.60	56.79	9.83	0.9891
240/60/25	Double logistics	39.67	164.73	0.93	205.07	31.62	0.91	0.9920
180/20/15	Double logistics	113.23	334.22	0.61	236.47	55.46	17.01	0.9961
240/20/15	Double logistics	196.12	30.12	0.02	176.19	0.00	16.35	0.9776
180/60/15	Double logistics	52.27	321.38	0.34	199.72	40.06	5.71	0.9952
240/60/15	Double logistics	37.71	126.47	0.68	204.65	31.85	0.91	0.9872
210/40/20	Double logistics	45.30	136.94	0.42	209.67	29.74	3.22	0.9919

BMP_{final} parameter indicates the final product during the experiment, while the BMP_{max} estimates the predicted maximum production. However, in this experiment, the methane production reached a maximum plateau during the experimental time. Thus, $BMP_{max,2}$ should be similar to BMP_{final}, while $BMP_{max,1}$ should fit the first plateau value. **Table 5.7** displays the fitting curve of the logistic model over the BMP experimental line along with the correlation coefficient. The logistics model fitted the majority of BMP lines

with $R^2 > 0.99$, two runs were fitted with $R^2 > 0.98$ and only one with $R^2 > 0.97$. The kinetic model described adequately the behaviour of two biomethane production phases for the three kinetic parameters. Therefore, the double-logistics equation can be used successfully for modelling the biomethane production via AD from HTC-PW of food waste.

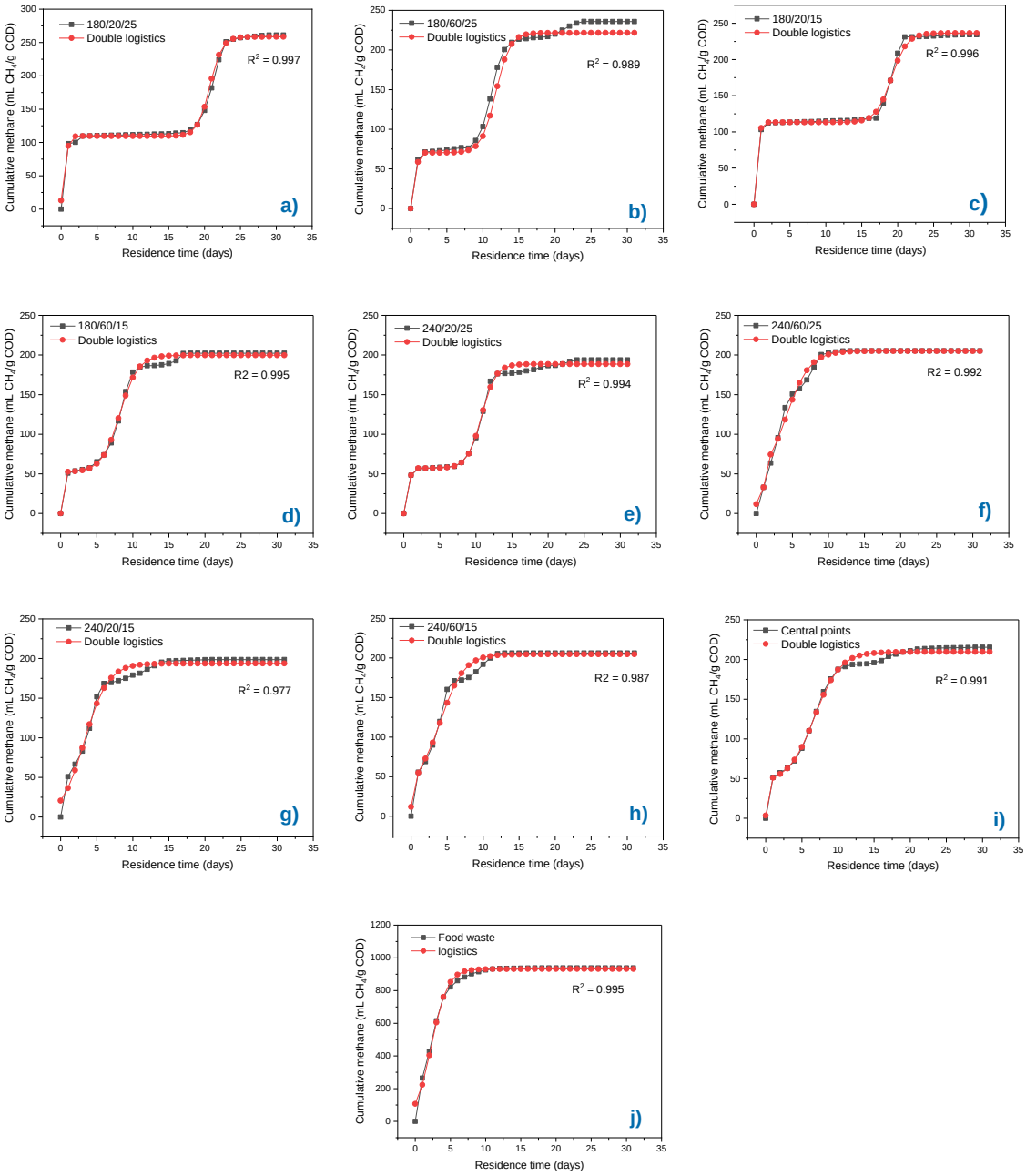

Figure 5.8 Logistics model fitting for BMP profiles.

Although the double logistics equations fitted the BMP line with a high correlation coefficient and adequate kinetic parameters, especially for low-intensity runs (**Figure 5.8a and c**). There was a lack of fit for a third biomethane production stage. This third stage was not covered by the double logistics models. Instead, $BMP_{max,2}$ either stayed on the second phase

plateau (**Figure 5.8b**) or neglected the second plateau and reached the plateau at depletion time (**Figure 5.8d-i**). Therefore, the double-logistics equation could be used to model the AD of HTC-PW of food waste for determining BMP_{final} under most of the analysed process conditions. However, for future work, the parametrization and fitting of a multi-sigmoidal equation for biomethane productions should be considered.

5.4 Conclusion

Low-intensity conditions (low temperature, short reaction times, and high solid load) promote hydrolysis during HTC while maintaining low carbonisation reactions. This caused high solubilisation of organic matter into PW which is reflected in a high concentration of TS, TOC, and COD. For TS and TOC, the linear effect of the three factors was significant and only the quadratic effect of temperature. COD had similar effects with exception of the linear effect of RT. Lower SL produced higher total ammonia nitrogen (TAN) concentrations than high SL, although this was particularly noticeable at low temperatures. The effect of SL on TAN was less evident at mid and high T and RT. However, none of the effects showed significance. The linear effect of RT and SL were significant for pH while temperature was insignificant.

The concentration of VFA increased with more severe process conditions, although pH was lower at low-intensity conditions. This could indicate the presence of other acids at low temperatures, such as carboxylic acids, which could be transformed as the HTC reaction progresses, while VFAs keep being generated. None of the individual VFA analysed saw their concentration decrease as process conditions intensified. This could suggest that VFA do not take part in the re-polymerisation of hydrochar, or the generation rate overpowers the re-polymerisation rate. Therefore, VFA generation continues from the degradation of already solubilised compounds. The highest yielding VFA was acetic acid, followed by glycolic,

succinic and levulinic acid. Pyrrolidinone had the highest concentration among N-compounds, and it did not appear at low-intensity runs. Pyrazine and phenolic compounds were found at low concentrations and showed to increase with higher process conditions.

The high solubilisation of organic matter into PW led to a higher biomethane potential. Nonetheless, low-intensity conditions showed an AD profile with considerable mid-reaction plateaus with higher BMP_{final} (mL CH_4/g COD). Whereas, high-intensity conditions reached a lower BMP_{final} than milder conditions while improving the digestibility of PW, reducing the mid-reaction plateaus towards a decelerating pattern, similar to that found in raw food waste, shortening the substrate depletion time considerably. The temperature was the main effect governing the BMP, with a significant linear effect and interaction with RT and SL. The linear effect of SL was also significant.

The double logistic equation fsuccessfully fitted the BMP curves with high R^2 values. Therefore, the double-logistics equation could be used to model the AD of HTC-PW of food waste for determining BMP_{final} under most of the analysed process conditions. However, for future work, the parametrization and fitting of a multi-sigmoidal equation for biomethane productions should be considered. Also, for future work, the utilisation of a full DOE for both HTC and BMP test would allow the optimisation of the biomethanation of HTC process water and bring further insight into the effect of the HTC process on the methanation capabilities of process water, enhancing its utilisation prospects.

Chapter 6. Energy analysis of hydrothermal carbonization of food waste

6.1 Introduction

Energy analysis is a crucial assessment for the feasibility of the HTC process. The energetic analysis is intended to understand the energy flows of the process, locate inefficacies, and estimate energy recovery, providing necessary insight for the implementation of HTC in a larger process for the valorisation of food waste. In previous chapters, it was shown that various responses are enhanced by long reaction times and high temperatures, and in literature, several studies have reported optimal HTC reaction times of multiple hours and high temperatures. However, these conditions increase the energy consumption of the HTC process and have a toll on the viability of the overall process. Therefore, in this chapter, after performing the energy analysis, the energy efficiency of the HTC process was included in the multi-response optimisation and utilised as a viability response.

This chapter aims to comply with **Objective 4**: Perform an energy analysis of different energy streams and how the process parameters affect energy efficiency.

4a. Evaluate the effect of HTC parameters on the energy efficiency processing food waste process.

4b. Evaluate the impact of implementing biomethanation of process water on the energy efficiency of the HTC process.

4c. Evaluate the impact of the drying stage on the energy efficiency of the HTC process.

4d. Perform an optimisation test including energy efficiency responses.

6.2 Mass Balance

The mass balance considers the percentage of mass in each of the three product streams of HTC. The results include the mass yield in hydrochar, free process water separated by vacuum filtration, moisture contained in hydrochar after filtration, and the mass lost in gas form. **Figure 6.1** shows the results of all HTC runs.

In general, higher hydrochar yields were obtained at lower intensity conditions when reactions that lead to mass solubilization, such as hydrolysis, are not promoted. Another factor causing a higher hydrochar yield was a high SL, those runs with 25% SL showed high hydrochar yield, and run (210/40/29) had the highest hydrochar yield. A more detailed explanation of this trend was discussed in **Chapter 4.4.1**. The mass yield of gas exhibited small variation, from 3 to 6% with the lowest at (160/40/20) and the highest at (260/40/20), suggesting a higher production of non-condensable gases, particularly CO_2, at high temperatures, although the production remains minimal.

A more interesting result was the water retention of hydrochar. The runs with higher SL produced the highest hydrochar yield. However, they retained high quantities of moisture in the hydrochar, particularly at low temperatures. For instance (180/20/25) and (180/60/25) retained over 35% of moisture in the hydrochar, while it decreased to >24% when increasing the temperature in (240/20/25) and (240/60/25). This suggests that dewaterability was improved by high temperatures. The lowest moisture retention in hydrochar was obtained at (240/60/15) with 9.8%, due to the combination of low SL and high temperature, which enhanced the carbonisation process. It was followed by (210/40/12) with 9.9% and (260/40/20) with 10%. Corroborating the relation of water retention with temperature and SL.

In contrast, (160/40/20) displayed the lowest dewaterability, the retained water represented 59% of the mass yield due to the low temperature (160 °C). At this temperature, the carbonisation process has not properly started. Instead, a gel-like matrix was formed impeding the dewatering of the hydrochar, possibly due to caramelisation reactions. In addition, (210/40/28)

showed a high water-retention of 44% mass yield. This could suggest that at the lowest MC, the high solid load reduced the HTC reaction rate and the carbonisation degree. Thus, even if high SL and low temperature had the highest energy efficiency because of their high solid yield, the low dewaterability of hydrochar could negatively affect the overall process efficiency.

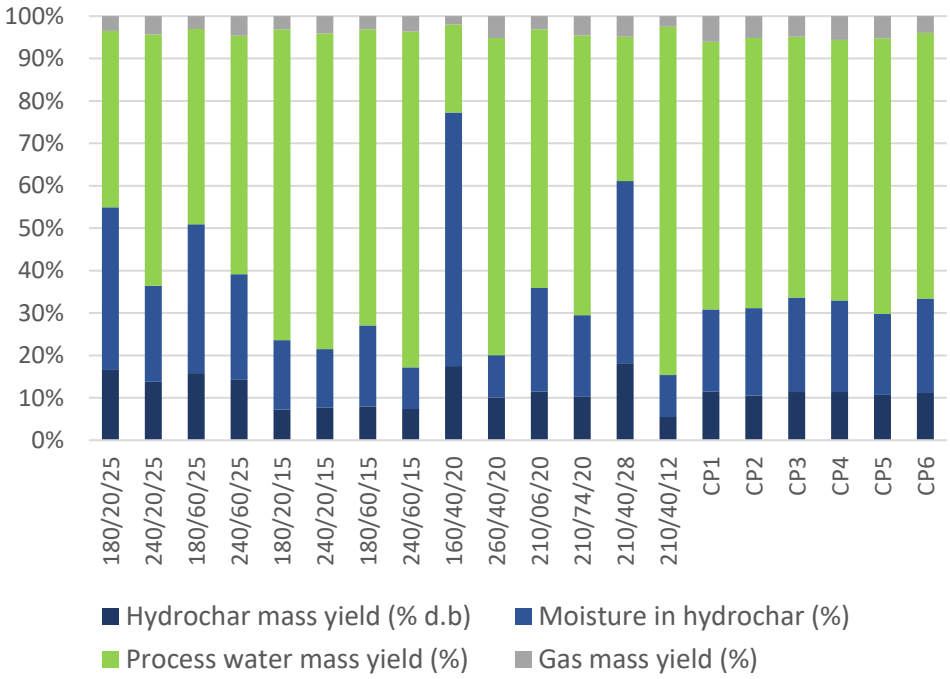

Figure 6.1 Mass balance of HTC runs.

6.3 Energy analysis

The energy analysis consists of the energy balance, including the analysis of the energy streams, and the energy efficiency analysis, for major insight into the process.

6.3.1 Energy streams

For the energy analysis, three scenarios were proposed to evaluate the HTC system (Scenario 1, 2 and 3). Different energy streams are considered in the scenarios to assess the impact of specific stages. Nonetheless, all three

consider the following assumptions, for outputs: $Q_{th,Hyc}$ is the thermal energy of hydrochar, $Q_{th,biogas}$ is the thermal energy in the biogas produced by anaerobic digestion of HTC process waters; for inputs: the thermal energy in food waste ($Q_{th,FW}$), the thermal energy for heating the feedstock, or sensible heat to reach the reaction temperature ($Q_{th,pHt}$), the electric consumption of the reactor during HTC reaction ($W_{el,HTC}$), the electric consumption for a filter press separation ($W_{el,press}$) and the thermal energy for hydrochar drying ($Q_{th,dry}$) to 8% MC as proposed by from Lucian et al. [20]. To calculate energy recovery ($Q_{th,Rec}$), was assumed a total ideal equal to $Q_{th,pHt}$, with the assumption of two heat exchanges with 50% efficiency each. Thus $Q_{th,Rec} = 0.25Q_{th,PHt}$ as described in Mahmood [8]. **Table 6.1** displays the results of all energy streams used for the energy analysis.

Run (210/40/28) showed the highest value of $Q_{th,FW}$ with 1319.9 kJ and lowest at (210/40128) with 538.5 kJ due to high solid yield. Pre-heating energy ($Q_{th,pht}$), reached the highest value at (260/40/20) with 182.1 kJ and lowest at (160/40/20) with 104.1, dependent on the reaction temperature. The energy consumption during HTC reaction ($Q_{el,HTC}$) is directly linked to reaction time and the highest value was 1325.4 kJ for (210/73/20), more than ten-fold the lowest value 114.6 kJ at (210/06/80). This considerable difference indicates that the process efficiency will be highly affected by the reaction time. The energy consumption by the press filter varied from 2 to 6.5 kJ, these values will be negligible under all conditions for the overall process analysis. The drying energy ($Q_{th,dry}$) varied from 369.8 to 58.2 at (160/40/20) and (260/80/20), respectively. The drying energy assessed the impact of enhancing dewaterability on the efficiency of the process. Therefore, the three factors govern the values of different energy inputs, and the optimal energy efficiency should involve the combination of the three.

Table 6.1 Energy streams of HTC process.

Temp. (°C)	Time (min)	SL (%)	Energy inputs				Energy outputs			
			$Q_{th,FW}$ (kJ)	$Q_{th,pht}$ (kJ)	$W_{el,HTC}$ (kJ)	$W_{el,press}$ (kJ)	$Q_{th,dry}$ (kJ)	$Q_{th,hyc}$ (kJ)	$Q_{th,biogas}$ (kJ)	$Q_{th,rec}$ (kJ)
180	20	15	697	125.6	240	2.6	100.4	427.6	133.3	31.4
240	20	15	696.9	174.2	360	2.8	82.8	534.6	69.12	43.5
180	60	15	696.9	125.6	720	2.8	116.8	469.8	99.9	31.4
240	60	15	696.9	174.2	1080	2.6	58.3	506.5	72.2	43.5
180	20	25	1161.6	114.2	240	5.9	234.7	897.6	107.57	28.5
240	20	25	1161.5	158.4	360	4.9	136.1	875.5	78.6	39.6
180	60	25	1161.6	114.2	720	5.6	214.4	888.6	97.2	28.5
240	60	25	1161.7	158.4	1080	5.1	150.1	960.4	69.4	39.6
159.5	40	20	929.5	104.1	480	6.2	369.8	803.1	54.1	26
260.5	40	20	929.5	182.1	720	3.6	58.2	741.2	74.2	45.5
210	6.4	20	929.2	143.1	114.6	4.1	149	756.3	97.9	35.8
210	73.6	20	929.3	143.1	1325.4	3.7	116.5	689	64.7	35.8
210	40	11.6	538.5	154.5	720	2	60	351.1	65.2	38.6
210	40	28.4	1319.9	131.6	720	6.5	263.1	1082.4	41	32.9
210	40	20	929.4	143.1	720	4.1	116.9	756.6	79.9	35.8
210	40	20	929.3	143.1	720	3.8	125	712.9	65.5	35.8
210	40	20	929.2	143.1	720	4.1	135	772.6	72.6	35.8
210	40	20	929.2	143.1	720	4	131.2	734.5	62.8	35.8
210	40	20	929.3	143.1	720	3.8	115.5	701.4	84.1	35.8
210	40	20	929.3	143.1	720	4	135.4	680.7	72.6	35.8

For energy outputs, Run (210/40/28) showed the highest $Q_{th,hyc}$ value of 1082.4 kJ, due to the combination of medium process conditions and the highest solid load. However, the run (210/40/12) yielded the lowest values with 351.1 kJ. Therefore, the solid load is the main factor for hydrochar

energy output, overpowering the heating values of the hydrochar, which is temperature-related. Energy from biogas from process water ($Q_{th,biogas}$) ranged from 41.0 to 133.3 kJ. Low-intensity HTC conditions promoted higher $Q_{th,biogas}$, particularly runs at 180 °C and short times (20 min). This could be because at 180 °C, solid solubilisation is promoted at a high rate, while re-polymerization reactions do not commence until higher temperatures. Lower temperatures (160 °C) showed poor dewaterability, which resulted in low amounts of free PW and lower energy from biogas, mainly due to lower organic matter in PW. Longer reaction times and higher temperatures affected negatively the energy extracted from process water. Runs with lower SL yielded slightly higher energy from biogas than its counterpart. Energy recovery ($Q_{th,rec}$) depended on ($Q_{th,pHt}$) and ranged from 26 to 45.5 kJ.

6.3.2 Energy efficiency

The energy efficiency (η) of the three scenarios was assessed to evaluate the hydrochar production, process water utilisation and the impact of the dewaterability factor on the process efficiency. For this, 3 scenarios were created, each scenario adds energy streams to assess their impact on the overall energy efficiency of the process. The energy efficiency of the complete DOE run on the three scenarios is shown in **Table 6.2**. Scenario 1 assesses the process with hydrochar as the only energy product. Here, neither the biogas from process water nor the energy consumption from drying are considered. Scenario 2 assesses the inclusion of bio-methane obtained from anaerobic digestion of process waters into the overall process. Scenario 3 assessed the effect of HTC on the separation of the process water, or dewaterability, and how it impacts the energy efficiency of the process. Hence, a drying stage for the hydrochar is included.

Also, an estimation of the Energy Return of Investment (EROI) is presented in Table 3, considering the process in scenario 3. For the EROI estimation, only the usable energy for the process is considered, excluding energy from the feedstock. Also, hydrochar and biogas are considered for energy outputs.

Table 6.2 Energy efficiency (η) of scenarios 1, 2 and 3.

Temp. (°C)	Time (min)	SL (%)	Energy efficiency (η)			EROI
			Scenario 1	Scenario 2	Scenario 3	
180	20	15	43.2	55.6	50.82	1.2
240	20	15	47	52.5	49.16	0.97
180	60	15	32.5	38.9	36.16	0.59
240	60	15	28.2	31.8	30.92	0.44
180	20	25	61.1	67.9	58.85	1.69
240	20	25	54.5	59	54.57	1.45
180	60	25	46	50.7	45.78	0.94
240	60	25	41.7	44.5	41.85	0.74
159.5	40	20	54.8	58.1	46.74	0.89
260.5	40	20	43	46.9	45.47	0.85
210	6.4	20	66.7	74.7	66.42	2.08
210	73.6	20	30.2	32.9	31.35	0.47
210	40	11.6	27.6	32.1	30.84	0.44
210	40	28.4	51.4	53.1	47.37	1
210	40	20	44.2	48.5	45.58	0.85
210	40	20	41.8	45.3	42.38	0.78
210	40	20	45.1	49	45.61	0.84
210	40	20	43	46.4	43.22	0.8
210	40	20	41.1	45.7	42.96	0.8
210	40	20	40	43.9	40.84	0.75

The schematic for scenario 1 is shown in **Figure 6.2**, and the energy efficiency is denominated as $\eta 1$. The Run (210/6.4/20) showed the highest $\eta 1$ of 66.7%, linked to the shortest reaction time, followed by (180/20/25) with 61.1%, which could be associated with an adequate hydrochar yield and HHV, combined with a short reaction time. On the other hand, the lowest value was 27.6% $\eta 1$ at (240/60/15). The second-lowest $\eta 1$ in scenario 1 was 28.2% obtained at (240/60/15) due to the combination of low hydrochar yield, high temperature, and long reaction time. Therefore, reaction time significantly impacted the energy efficiency of the process, while it did not show a significant effect on composition or solid fuel characteristics.

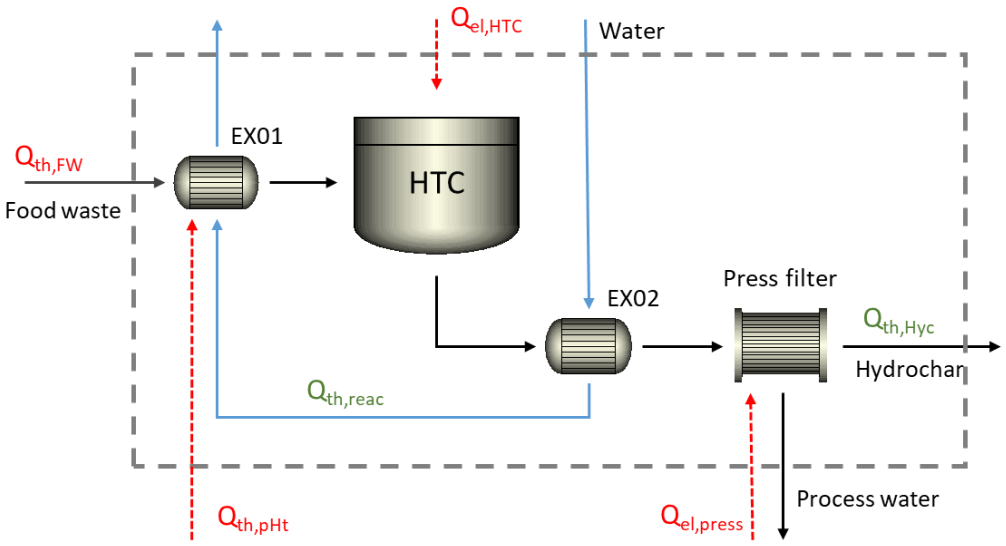

Figure 6.2 Schematic of scenario 1.

The schematic of scenario 2 is shown in **Figure 6.3**. This scenario includes the separation of the process water via filter press and AD biomethane production with the energy efficiency denominated $\eta 2$. The highest $\eta 2$ were in the same runs as in scenario 1, (210/06/20) and (180/20/25), although $\eta 2$ values increase to 74.7 and 67.9%, respectively. The lowest $\eta 2$ was in runs (240/60/15) and (210/40/12) with 31.8 and 32.1%, respectively, the same highest and lowest runs as in scenario 1. Although the implementation of AD in the HTC process did not alter the overall process behaviour, it caused an increase in the $\eta 2$ in a range from 1.7 to 12.4%, with an average increase of 4.7%. The highest increase was at (180/20/15), from 43.2 to 55.6%. Run (210/06/20) showed an increase of 8%, due to the combination of high biogas energy and short energy consumption.

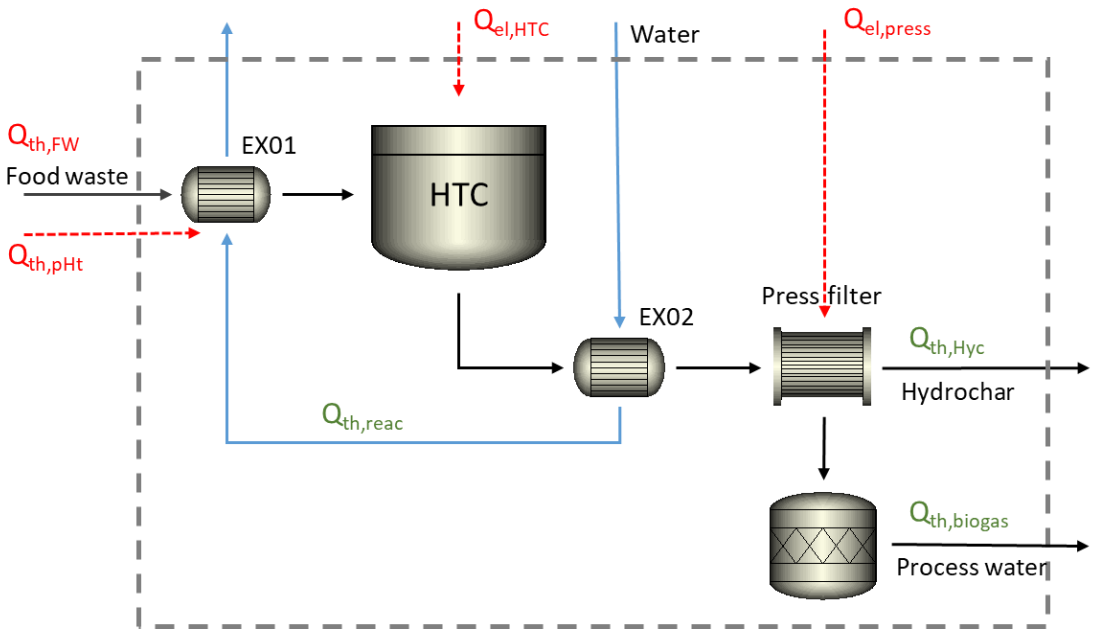

Figure 6.3 Schematic of scenario 2.

Scenario 3 introduced a drying stage for hydrochar that considers the experimental separation of process water, the remaining moisture in wet hydrochar is reduced to 8% MC with a dryer, consuming thermal energy. A diagram of the process scheme is displayed in **Figure 6.4**. Overall, implementing a drying stage decreases the $\eta 3$ of the HTC process by a mean of 4%, ranging from 0.9 to 11.4 %. The same runs presented the highest and lowest $\eta 3$ as in previous scenarios, (210/06/20) was the highest with 66.4% $\eta 3$, which means the energy recovered from process water via biogas met the demand for the hydrochar drying stage. Several runs had an energy production from process water sufficient to meet the drying stage demand, visible in **Figure 6.5**. All low SL (high-MC) runs showed a positive balance between energy from process water and drying energy, whereas high-SL runs were negative. Mid-SL showed equivalence between these two energy streams throughout different process conditions, thus heavily impacted by SL.

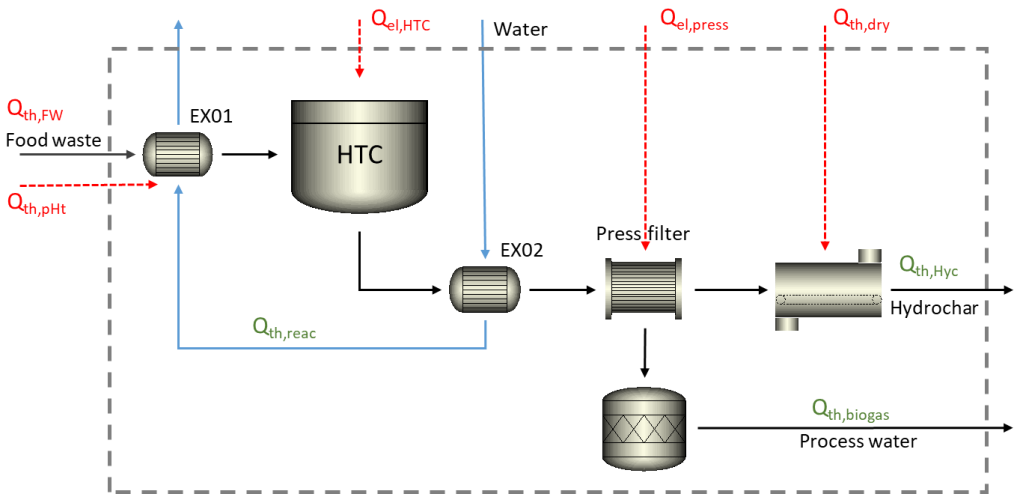

Figure 6.4 Schematic of scenario 3.

Lucian et al. [20] reported an energy efficiency analysis for an HTC process with a setup similar to scenario 3. They reported a η of 59 % for 180 °C 1 h, 60 % for 220 °C 3 h, and 42 % for 250 °C 6 h working with OFMSW. In that study, they reported lower energy output than in the current work, expected because of the difference between OFMSW and a cleaner FW. However, the energy consumption during HTC was determined based on the heating of the reactor vessel, meanwhile the energy consumed maintaining the HTC-reaction temperature appears to have been neglected, resulting in little difference between 1 h at 180 °C (236 kWh/ton OFMSW) and 6 h at 250 °C (349 kWh/ton OFMSW). Hence, their energy consumption might be very significantly underestimated. Mahmood et al. [8] reported a η of 86.7% working with food waste. However, the energy recovered from process water was calculated as thermal energy from combustion based on its elemental composition using a correlation for bio-oils. This assumption might not be only overestimated but technically unfeasible.

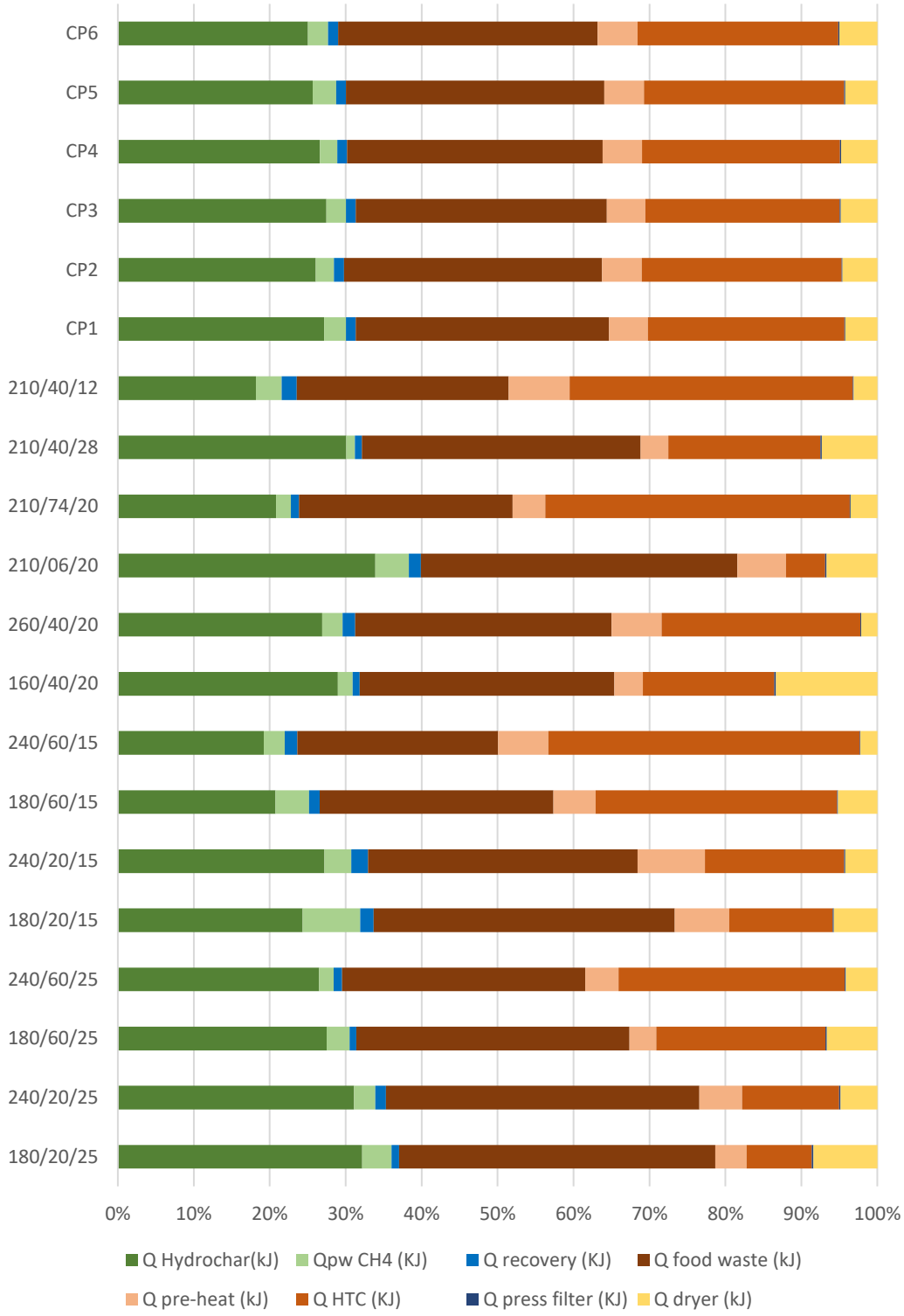

Figure 6.5 Energy yield by energy streams.

Regarding EROI, several runs produced more energy in hydrochar and biogas than the energy consumed in their production. This assessment neglects the energy contained in food waste. The highest EROI was in run

(210/06/20) with 2.08, meaning that more than double the energy invested was produced. Other favourable process conditions were (180/20/25) with 1.69, (240/20/25) with 1.45 and (180/20/15) with 1.20. In Run (210/74/20), the EROI is 1. The rest of the evaluated runs were energetically unfavourable. McGaughy and Reza [6] reported an EROI as high as 4.91 for 200 °C and 2.94 for 260 °C, working with a simplified thermodynamic simulation using food waste. Although this could be an overestimation, it indicates that there is room for improving the overall process. Mahmood et al. [8] reported an EROI of 4 at 250 °C while working with food waste. However, energy from process water was calculated as thermal energy from bio-oil. Also, energy lost to the environment was considered as energy output, increasing the EROI with non-usable energy.

In general, η in the three scenarios showed the same pattern. These patterns did not change with the inclusion of biogas from PW and the drying stage of hydrochar. The contour plots of $\eta 3$ are displayed in **Figure 6.6**. Contour plots show that RT and SL are the main factors affecting η, whereas temperature showed a minor effect. Interestingly, RT was insignificant in all previous responses that evaluated hydrochar composition and solid fuel characteristics. RT was highly significant even at the short window used in this study.

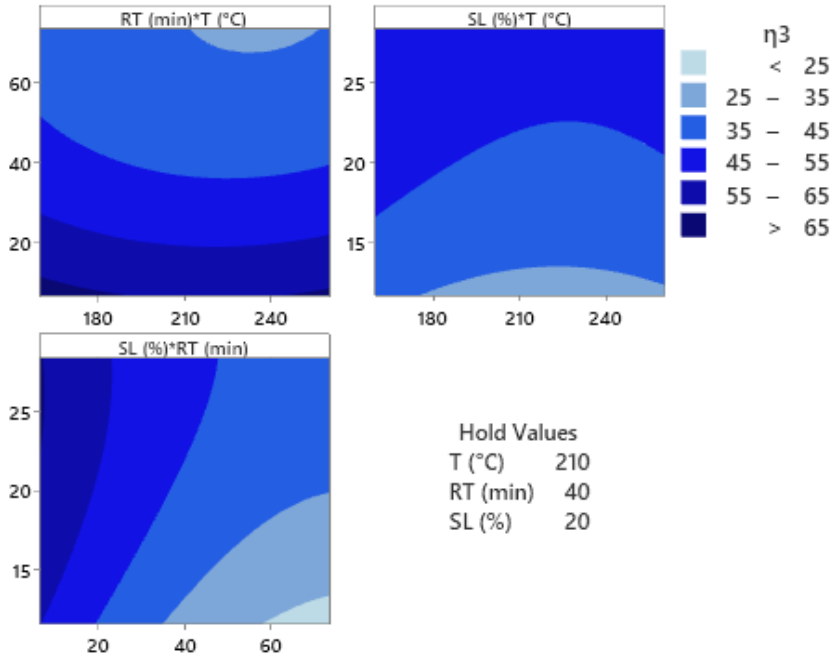

Figure 6.6 Contour plots of energy efficiency of scenario 3.

A significance test was performed to evaluate the effect of the HTC factors over the η in the three scenarios and EROI. The results are summarized in **Table 6.3**. The regression model was significant for all responses ($p < 0.000$) and they all presented correlation coefficients (R^2) over 0.95. The linear effect of the three factors (T, RT and SL) was significant for η1, η2 and EROI. Linear temperature was not significant for η3, suggesting that the effect of temperature on η decreased when considering the drying stage. This was unexpected as temperature enhances the dewaterability of hydrochar. Similarly, the quadratic effect of temperature was significant only for η1 and η2. For EROI, the quadratic effect of temperature was particularly low. The quadratic effect of RT was significant for η2, η3 and EROI, although it was also important for η 1. The quadratic effect of MC showed high importance in η1, η2 and η3, although it did not reach statistical significance. In contrast, none of the interaction effects showed significance.

Table 6.3 Significance test of individual effects of HTC factors on energy efficiency.

		Prob > F_{tab}									
Response	*Model*	*β1 (T)*	*β2 (RT)*	*β3 (SL)*	*β1* β1*	*β2* β2*	*β3* β3*	*β1* β2*	*β1* β3*	*β2* β3*	R^2
EF1	**0**	**0.023**	**0**	**0**	**0.044**	0.058	0.122	0.536	0.273	0.868	0.95
EF2	**0**	**0.001**	**0**	**0**	**0.013**	**0.004**	0.1	0.884	0.537	0.491	0.97
EF3	**0**	0.097	**0**	**0**	0.103	**0.009**	0.088	0.756	0.86	0.348	0.96
EROI	**0**	**0.05**	**0**	**0**	0.31	**0**	0.473	0.704	0.834	0.318	0.96

6.4 Multi-response optimisation HTC products considering energy efficiency.

The optimisation test was carried out with Minitab 19 software, based on Derringer's desirability method, as it has the capacity to optimize with multi-objective and multi-variable. The optimisation takes into consideration the fuel quality parameters of hydrochar and the energy efficiency of the different scenarios presented in the last section. The idea of optimisation is to find the process conditions where it is possible to achieve the hydrochar with the best qualities while maintaining the maximum energy efficiency possible.

The optimisation consisted of maximizing energy efficiency (η) of scenario 3, solid yield (SY), HHV, comprehensive combustibility index (S), equilibrium moisture content (EMC), and nitrogen yield. All responses were set with an importance of 1. The results are displayed in **Figure 6.7**. The optimised conditions were 260 °C, 32.86 min and 19.23 %SL for optimised results of 47.6 % η, 56 %SY, 2.8 %EMC, 3.8 S,a HHV of 31.8 MJ/kg. This result shows that only including energy efficiency into the optimisation test reduced the RT from 46.4 to 32.8 min in comparison with the optimisation performed in

chapter 4.7.1, although SL remains similar and temperature stays the same. However, the optimal energy efficiency of 47.6 % is low within the DOE.

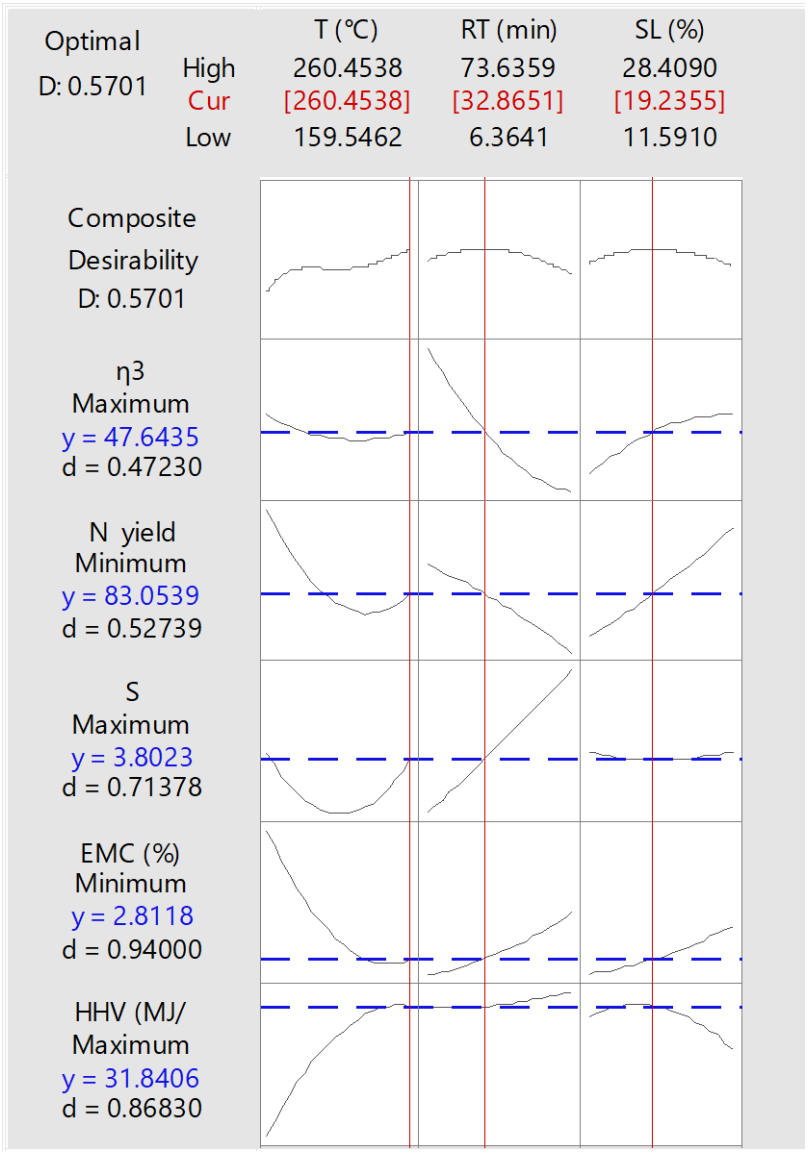

Figure 6.7 Desirability analysis for energy efficiency of scenario 3 and hydrochar quality

Because of the low energy efficiency in the optimisation test, there were carried out following optimisation test incrementing the importance of η in comparison to the other responses within the optimisation. This is a crucial tool for decision making with the desirability function. The results of the following optimisation test are displayed in **Table 6. 4**. Incrementing the

importance level from 1 to 5 increased the optimal energy efficiency from 47.6 to 66.3 %. At the same time the optimal conditions varied, in particular reaction time went from 33 to 7 min. This is due to the fact that RT was the main factor affecting the energy efficiency as it increases rapidly when energy consumption during reaction is kept at minimum. It is noted that solid load only changed from 19 to 20 % incrementing the importance of η, while temperature remained unchangeable. Also noteworthy, solid yield, HHV, and EMC were barely affected by the change of conditions. Therefore, the energy efficiency increased considerably while maintaining and hydrochar with high SY and HHV, and good hygroscopic values. On the other hand, N yield, and S were affected by the change of importance. The change on N yield represented a decrease of nitrogen removal from 17 to 10 %, and the value of S was also affected considerably. Thus, this shows the flexibility of the desirability function for decision making, and the right optimisation depends on meeting all the goals of the user.

Table 6.4 Optimisation with different importance value for energy efficiency

Importance value of η3	**1**	**2**	**3**	**4**	**5**	**Criteria**
Variable	**Opt. Value**	**Opt. Value**	**Opt. Value**	**Opt. Value**	**Opt. Value**	
T (°C)	260.5	260.5	260.5	260.5	260.5	
RT (min)	32.9	19.9	12.5	7.7	7.0	
SL (%)	19.2	19.4	20.1	20.4	20.6	
Response						
η3	47.6	55.8	61.7	65.6	66.3	maximise
N yield (%)	83.1	85.8	88.0	89.4	89.7	minimise
S	3.8	3.5	3.4	3.3	3.3	maximise
EMC (%)	2.8	2.5	2.5	2.5	2.5	minimise
HHV (MJ/Kg)	31.8	31.7	31.5	31.4	31.4	maximise
SY (%)	56.9	56.6	56.1	55.6	55.6	maximise

Although the inclusion of energy yield (%) is becoming a standard in more HTC research publications, energy efficiency assessments are still scarce. Moreover, to the author's knowledge, this is the first multi-response

optimisation of the HTC process considering energy efficiency and hydrochar quality. Therefore, it is proposed that direct utilisation-responses are necessary to be analysed along with viability-responses, such as energy efficiency, to advance the development of the HTC technology. For instance, the combustibility or the devolatilisation capabilities of the hydrochar.

6.5 Conclusion

The linear effect of the three factors (T, RT and SL) was significant for $\eta 1$, $\eta 2$ and EROI. Linear temperature was not significant for $\eta 3$, suggesting that the effect of temperature on η decreased when considering the drying stage. This was unexpected as temperature enhances the dewaterability of hydrochar. Similarly, the quadratic effect of temperature was significant only for $\eta 1$ and $\eta 2$. For EROI, the quadratic effect of temperature was particularly low. The quadratic effect of RT was significant for $\eta 2$, $\eta 3$ and EROI, although it was also important for $\eta 1$. RT was the main factor when evaluating energy efficiency. The quadratic effect of SL showed high importance in $\eta 1$, $\eta 2$ and $\eta 3$, although it did not reach statistical significance. In contrast, none of the interaction effects showed significance.

Scenario 1 considered the energy efficiency of an HTC process only with heat recovery and process water separation. highest energy efficiency ($\eta 1$) was 66.7%, which could be associated with an adequate hydrochar yield and HHV, combined with a short reaction time. Therefore, reaction time significantly impacted the energy efficiency of the process, while it did not show a significant effect on composition or solid fuel characteristics. The three factors showed a significant linear effect on $\eta 1$, as well as the quadratic effect of temperature.

Scenario 2 included the energy recovery from biomethane from process water. The highest $\eta 2$ were in the same runs as in scenario 1, mid-temperature and SL with the shortest RT although maximum $\eta 2$ values increase to 74.7%. Although the implementation of AD in the HTC process did not alter the overall process behaviour, it caused an increase in the $\eta 2$ in a range from 1.7 to 12.4%, with an average increase of 4.7%. All factors had

a significant linear effect on $\eta 2$, also the quadratic effect of temperature and RT.

implementing a drying stage decreases the $\eta 3$ of the HTC process by a mean of 4%, ranging from 0.9 to 11.4 %. The same run (210/40/06) presented the highest $\eta 3$ with 66.4%, which means the energy recovered from process water via biogas met the demand for the hydrochar drying stage, including the mechanical separation and the thermal drying to 10% moisture content. The energy recovered by biomethanation was enough to cover drying energy. All low SL runs showed a positive balance between energy from process water biomethanation and drying energy consumption, whereas high-SL runs were negative. When considering the drying stage, the temperature did not show significance in any of its effects, while reaction time had significance on its linear and quadratic effect, SL had a significant linear effect.

The multi-response optimisation successfully found optimal conditions of 260 °C, 7 min and 20 %SL for a high energy efficiency of 66% while maintaining a high quality of hydrochar. This was achieved by incrementing the importance of energy efficiency within the desirability function in comparison to other responses. Thus, this shows the flexibility of the desirability function for decision making, and the right optimisation depends on meeting all the goals of the user.

Chapter 7. Conclusions

For an easier reading of the conclusions, they are classified by objectives, which are linked to specific chapters.

***Objective 1**. Perform a design of experiments for the understanding of the implementation of HTC as a pre-treatment of food waste for the conversion into energy-dense hydrochar.*

Interestingly, solid load resulted in a highly relevant factor as it had significant linear effect on all the evaluated responses, although it did not show significance in interaction effects. This proves that the moisture contained in food waste is a non-negligible factor that will determine the value of the response of interest. This is worth noting, as most modelling and mechanisms studies on HTC are conducted, or assumed to occur, in low solid load (<10%), while practical studies for treating wet wastes have considered minimizing the addition of water to increase environmental viability. Therefore, adjusting solid load should be considered a process factor when optimising an HTC process for food waste. Temperature exhibited significant linear effect for solid yield, HHV, energy densification, N yield, ash yield and EMC. Also, it showed significant quadratic effect on solid yield, HHV, energy densification, ash yield and EMC. In contrast, reaction time showed no significance on any of the effects. This indicates that reaction time has no major impact in the time range selected for this work, which could be considered short in comparison to other HTC works. However, reaction time could have great importance in the energy analysis, via the time-integrated rate of energy consumption during the HTC process. Hence, it is suggested that reaction time should be kept at a minimum.

The individual optimization of energy responses exhibited contrasting conditions. On one hand solid yield (SY) and energy yield (EY) had the optimal results at the lowest temperature, high solid load and mid reaction times. This result was foreseeable because of the effect of temperature on the solubilisation, as well as being facilitated by lower solid load. However, as mentioned before, this condition would result in a hydrochar of bad quality

and the optimization considering multiple objectives is required. Regarding C, N and ash yield (%), optimized conditions include the lowest temperature for low solubilisation, and high solid load for low reaction rates. It also includes mid reaction times due to re-adsorption found at longer reaction times. In the case of N and ash yields (%) the optimization was set for minimizing values. These optimisation conditions aim for a significant solubilisation (mid-temperature and low solid load) and while minimizing the re-adsorption or re-polymerization conditions (higher temperatures and longer reaction times). The individual optimization showed how all the evaluated responses have different optimal conditions. By themselves, no response could indicate a proper optimisation of HTC for food waste utilisation.

The optimized conditions were 260.4 °C, 46.4 min and 17.7 %SL. Under these conditions, the predicted responses are 55.6 % solid yield, 1.56 energy densification, 3.2 %EMC, meaning a 3.2 % of moisture regained at 75% relative humidity after 48 h, 4.13 S, and 78.9 % of nitrogen yield (NY%), or 21.1 % of nitrogen removed. However, the downside of the optimized values is that is highly taxing on the energy efficiency of the process. Both the highest temperature and longest reaction time would increase the energy consumption during the HTC process. Thus, although these conditions would maximize the evaluated responses, it would be sensible to perform an energy analysis and include it as another response in the optimization. It is noteworthy that while in single-response optimisation the optimised process conditions tend to be the extremes values within the DOE, in the multi-response optimisation the optimised conditions were within the DOE area. This demonstrates the trade-off between response and the importance of the multi-response optimisation in HTC studies.

***Objective 2**. Evaluate the thermogravimetric properties of hydrochar and the effect of the process variables. For the assessment of utilising the hydrochar in thermochemical processes such as incineration or gasification.*

The combustion of food waste was divided into two combustion zones (Z1 and Z2) with two defined DTG (%/min) peaks. Both combustion zones were affected differently by HTC process conditions. In comparison to untreated FW, Z1 (associated with volatile matter) was separated into two peaks, the first peak at lower temperature was promoted in high-intensity hydrochars, while the second peak was higher in low-intensity hydrochars. The second peak of Z1 was reduced significantly in high-intensity hydrochars at the same time that the peak on Z2 grows. This indicates that the second peak of Z1 is an amorphous volatile matter that is transformed into fixed carbon at high-intensity process conditions. Meanwhile, the first peak of Z1 might be linked to a layer of lipids adsorbed onto the hydrochar surface.

Regarding the combustion combustibility index (S), a quicker and more aggressive combustion was found as the intensity of the process conditions increased. The combustion stability index (H_f) showed a quadratic effect with higher stability for low- and high-intensity hydrochars, mid-intensity conditions were detrimental H_f. Only the quadratic effect of temperature was significant for S, while no effect was significant for H_f.

***Objective 3**. Assess how the process parameters of HTC affect the liquid product of HTC (also referred to as 'process water').*

Low-intensity conditions (low temperature, short reaction times, and high solid load) promote hydrolysis during HTC while maintaining low carbonisation reactions. This caused high solubilisation of organic matter into PW which is reflected in a high concentration of TS, TOC, and COD. For TS and TOC, the linear effect of the three factors was significant and only the quadratic effect of temperature. COD had similar effects with exception of the linear effect of RT. Lower SL produced higher total ammonia nitrogen (TAN) concentrations than high SL, although this was particularly noticeable at low temperatures. The effect of SL on TAN was less evident at mid and high T and RT. However, none of the effects showed significance. The linear

effect of RT and SL were significant for pH while temperature was insignificant.

The concentration of VFA increased with more severe process conditions, although pH was lower at low-intensity conditions. This could indicate the presence of other acids at low temperatures, such as carboxylic acids, which could be transformed as the HTC reaction progresses, while VFAs keep being generated. None of the individual VFA analysed saw their concentration decrease as process conditions intensified. This could suggest that VFA do not take part in the re-polymerisation of hydrochar, or the generation rate overpowers the re-polymerisation rate. Therefore, VFA generation continues from the degradation of already solubilised compounds. The highest yielding VFA was acetic acid, followed by glycolic, succinic and levulinic acid. Pyrrolidinone had the highest concentration among N-compounds, and it did not appear at low-intensity runs. Pyrazine and phenolic compounds were found at low concentrations and showed to increase with higher process conditions.

The high solubilisation of organic matter into PW led to a higher biomethane potential. Nonetheless, low-intensity conditions showed an AD profile with considerable mid-reaction plateaus with higher BMP_{final} (mL CH_4/g COD). Whereas, high-intensity conditions reached a lower BMP_{final} than milder conditions while improving the digestibility of PW, reducing the mid-reaction plateaus towards a decelerating pattern, similar to that found in raw food waste, shortening the substrate depletion time considerably. The temperature was the main effect governing the BMP, with a significant linear effect and interaction with RT and SL. The linear effect of SL was also significant.

The double logistic equation successfully fitted the BMP curves with high R^2 values. Therefore, the double-logistics equation could be used to model the AD of HTC-PW of food waste for determining BMP_{final} under most of the analysed process conditions. However, for future work, the parametrization and fitting of a multi-sigmoidal equation for biomethane productions should be considered.

***Objective* 4**. *Perform an energy analysis of different energy streams and how the process parameters affect the energy efficiency.*

The linear effect of the three factors (T, RT and SL) was significant for η1, η2 and EROI. Linear temperature was not significant for η3, suggesting that the effect of temperature on η decreased when considering the drying stage. This was unexpected as temperature enhances the dewaterability of hydrochar. Similarly, the quadratic effect of temperature was significant only for η1 and η2. For EROI, the quadratic effect of temperature was particularly low. The quadratic effect of RT was significant for η2, η3 and EROI, although it was also important for η1. RT was the main factor when evaluating energy efficiency. The quadratic effect of SL showed high importance in η1, η2 and η3, although it did not reach statistical significance. In contrast, none of the interaction effects showed significance.

Scenario 1 considered the energy efficiency of an HTC process only with heat recovery and process water separation. highest energy efficiency ($\eta 1$) was 66.7%, which could be associated with an adequate hydrochar yield and HHV, combined with a short reaction time. Therefore, reaction time significantly impacted the energy efficiency of the process, while it did not show a significant effect on composition or solid fuel characteristics. The three factors showed a significant linear effect on $\eta 1$, as well as the quadratic effect of temperature.

Scenario 2 included the energy recovery from biomethane from process water. The highest $\eta 2$ were in the same runs as in scenario 1, mid-temperature and SL with the shortest RT although maximum $\eta 2$ values increase to 74.7%. Although the implementation of AD in the HTC process did not alter the overall process behaviour, it caused an increase in the $\eta 2$ in a range from 1.7 to 12.4%, with an average increase of 4.7%. All factors had a significant linear effect on $\eta 2$, also the quadratic effect of temperature and RT.

implementing a drying stage decreases the $\eta 3$ of the HTC process by a mean of 4%, ranging from 0.9 to 11.4 %. The same run (210/40/06) presented the

highest $\eta 3$ with 66.4%, which means the energy recovered from process water via biogas met the demand for the hydrochar drying stage, including the mechanical separation and the thermal drying to 10% moisture content. The energy recovered by biomethanation was enough to cover drying energy. All low SL runs showed a positive balance between energy from process water biomethanation and drying energy consumption, whereas high-SL runs were negative. When considering the drying stage, the temperature did not show significance in any of its effects, while reaction time had significance on its linear and quadratic effect, SL had a significant linear effect.

The multi-response optimisation successfully found optimal conditions of 260 °C, 7 min and 20 %SL for a high energy efficiency of 66% while maintaining a high quality of hydrochar. This was achieved by incrementing the importance of energy efficiency within the desirability function in comparison to other responses. Thus, this shows the flexibility of the desirability function for decision making, and the right optimisation depends on meeting all the goals of the user.

Objective 5. *Propose recommendations for future work in the areas of developing HTC technology and its application for food waste.*

After proving the usefulness of RSM for multi-responses optimisation based on a design of experiments. It will be of great use if a DOE is populated with responses based on direct utilisation of hydrochar, for example, combustion, fertilizer or adsorbent. Also, responses related to logistics are scarce and would be of great value to increase the attractiveness of HTC technology, such as pelletisation or briquetting for improved storage and transport. In addition, expanding the experiment of equilibrium moisture content would add to the storage capabilities of hydrochar. Moreover, complying with standards directed at solid fuel for industrial or domestic use would increase the economic viability of hydrochar as a solid fuel product.

Comprehensive indices are conceptually useful for quick and practical estimations of combustion or gasification performance. Also, they are

commonly used in the thermogravimetric analysis of published papers. However, existent indices are generated for coal samples, which have a different DTG curve than biochar or hydrochar. Coal DTG curves present only one peak and combustion zones. Thus, when applied to hydrochar samples, the indices are not capable to discern between VM and FC peaks, or considering the fuel segregation by the separation of peaks. Therefore, generating comprehensive indices for hydrochars and biochars would be of great use in thermogravimetric studies.

The generation of empirical models based on experimental data would overcome the limitations of the black-box approach for HTC mechanism modelling. This would advance greatly the understanding of hydrochar and the ability to build robust simulations, which would accelerate exponentially the development of HTC technology and its application on food waste.

The utilisation of a full DOE with quadratic terms for both HTC and BMP test would allow the experimental optimisation of the biomethanation of HTC process water and bring further insight into the effect of the HTC process on the methanation capabilities of process water, allowing the development of better simulations, thus, enhancing its utilisation prospects.

For gasification utilisation of hydrochar, key in the implementation of hydrochar in the synthetic fuel route, there is a lack of experimental data. Whereas on the syngas composition and how it is affected by HTC conditions, type of gasifier and gasification conditions. Most of the work done so far relies heavily on TGA and needs to be projected to gasification rigs. Models including this experimental data would be highly useful to develop plant designs based on the gasification of hydrochar.

Research combining the logistics of food waste recollection for de-centralized HTC process plants and hydrochar distribution is crucial information for the technology and this area of research has not been properly developed.

An important work to do with HTC of food waste is to develop a DOE considering food components as factors, for insight on how the proportion of biomolecules affects the hydrochar. There are plenty of reports on

carbohydrates, whereas it is limited work with protein, lipids and the interaction of the three of them in HTC. Elucidating the interaction between the main components of food waste would allow a degree of prediction necessary when working with such heterogeneous material as food waste.

Chapter 8. References

[1] WEC. Worl Energy Trilemma Index 2021. 2021.

[2] UN. The Sustainable Development Goals Report 2021. 2021.

[3] FAO. Global food loss and food waste - Extent, causes and prevention. Rome: 2011. https://doi.org/10.4337/9781788975391.

[4] Kaushik R, Parshetti GK, Liu Z, Balasubramanian R. Enzyme-assisted hydrothermal treatment of food waste for co-production of hydrochar and bio-oil. Bioresour Technol 2014;168:267–74. https://doi.org/10.1016/j.biortech.2014.03.022.

[5] Saqib NU, Baroutian S, Sarmah AK. Physicochemical, structural and combustion characterization of food waste hydrochar obtained by hydrothermal carbonization. Bioresour Technol 2018;266:357–63. https://doi.org/10.1016/j.biortech.2018.06.112.

[6] McGaughy K, Toufiq Reza M. Hydrothermal carbonization of food waste: simplified process simulation model based on experimental results. Biomass Convers Biorefinery 2018;8:283–92. https://doi.org/10.1007/s13399-017-0276-4.

[7] Funke A, Ziegler F. Heat of reaction measurements for hydrothermal carbonization of biomass. Bioresour Technol 2011;102:7595–8. https://doi.org/10.1016/j.biortech.2011.05.016.

[8] Mahmood R, Parshetti GK, Balasubramanian R. Energy, exergy and techno-economic analyses of hydrothermal oxidation of food waste to produce hydro-char and bio-oil. Energy 2016;102:187–98. https://doi.org/10.1016/j.energy.2016.02.042.

[9] Pham TPT, Kaushik R, Parshetti GK, Mahmood R, Balasubramanian R. Food waste-to-energy conversion technologies: Current status and future directions. Waste Manag 2015;38:399–408. https://doi.org/10.1016/j.wasman.2014.12.004.

[10] Chen X, Lin Q, He R, Zhao X, Li G. Hydrochar production from watermelon peel by hydrothermal carbonization. Bioresour Technol 2017;241:236–43. https://doi.org/10.1016/j.biortech.2017.04.012.

[11] Idowu I, Li L, Flora JRV, Pellechia PJ, Darko SA, Ro KS, et al. Hydrothermal carbonization of food waste for nutrient recovery and reuse. Waste Manag 2017;69:480–91. https://doi.org/10.1016/j.wasman.2017.08.051.

[12] Feng Y, Sun H, Han L, Xue L, Chen Y, Yang L, et al. Fabrication of hydrochar based on food waste (FWHTC) and its application in aqueous solution rare earth ions adsorptive removal: Process, mechanisms and disposal methodology. J Clean Prod 2019;212:1423–33. https://doi.org/10.1016/j.jclepro.2018.12.094.

[13] Oliver-Tomas B, Hitzl M, Owsianiak M, Renz M. Evaluation of hydrothermal carbonization in urban mining for the recovery of phosphorus from the organic fraction of municipal solid waste. Resour Conserv Recycl 2019;147:111–8.

https://doi.org/10.1016/j.resconrec.2019.04.023.

[14] Wang T, Zhai Y, Zhu Y, Peng C, Xu B, Wang T, et al. Influence of temperature on nitrogen fate during hydrothermal carbonization of food waste. Bioresour Technol 2018;247:182–9. https://doi.org/10.1016/j.biortech.2017.09.076.

[15] Akarsu K, Duman G, Yilmazer A, Keskin T, Azbar N, Yanik J. Sustainable valorization of food wastes into solid fuel by hydrothermal carbonization. Bioresour Technol 2019;292:121959. https://doi.org/10.1016/j.biortech.2019.121959.

[16] Bhakta Sharma H, Panigrahi S, Dubey BK. Food waste hydrothermal carbonization: Study on the effects of reaction severities, pelletization and framework development using approaches of the circular economy. Bioresour Technol 2021;333:125187. https://doi.org/10.1016/j.biortech.2021.125187.

[17] Gupta D, Mahajani SM, Garg A. Effect of hydrothermal carbonization as pretreatment on energy recovery from food and paper wastes. Bioresour Technol 2019;285:121329. https://doi.org/10.1016/j.biortech.2019.121329.

[18] Ismail TM, Yoshikawa K, Sherif H, Abd El-Salam M. Hydrothermal treatment of municipal solid waste into coal in a commercial Plant: Numerical assessment of process parameters. Appl Energy 2019;250:653–64. https://doi.org/10.1016/j.apenergy.2019.05.042.

[19] Li XG, Lv Y, Ma BG, Jian SW, Tan HB. Thermogravimetric investigation on co-combustion characteristics of tobacco residue and high-ash anthracite coal. Bioresour Technol 2011;102:9783–7. https://doi.org/10.1016/j.biortech.2011.07.117.

[20] Lucian M, Volpe M, Merzari F, Wüst D, Kruse A, Andreottola G, et al. Hydrothermal carbonization coupled with anaerobic digestion for the valorization of the organic fraction of municipal solid waste. Bioresour Technol 2020;314:123734. https://doi.org/10.1016/j.biortech.2020.123734.

[21] Wang T, Zhai Y, Zhu Y, Gan X, Zheng L, Peng C, et al. Evaluation of the clean characteristics and combustion behavior of hydrochar derived from food waste towards solid biofuel production. Bioresour Technol 2018;266:275–83. https://doi.org/10.1016/j.biortech.2018.06.093.

[22] Wilk M, Śliz M, Gajek M. The effects of hydrothermal carbonization operating parameters on high-value hydrochar derived from beet pulp. Renew Energy 2021;177:216–28. https://doi.org/10.1016/j.renene.2021.05.112.

[23] Hantoro R, Septyaningrum E, Siswanto BB, Izdiharrudin MF. Hydrochar Production through the HTC Process: Case Study of Municipal Solid Waste Samples in East Java, Indonesia. Solid Fuel Chem 2020;54:418–26. https://doi.org/10.3103/S036152192006004X.

[24] Tradler SB, Mayr S, Himmelsbach M, Priewasser R, Baumgartner W, Stadler AT. Hydrothermal carbonization as an all-inclusive process for food-waste conversion. Bioresour Technol Reports 2018;2:77–83. https://doi.org/10.1016/j.biteb.2018.04.009.

[25] Toptas Tag A, Duman G, Yanik J. Influences of feedstock type and process variables on hydrochar properties. Bioresour Technol 2018;250:337–44. https://doi.org/10.1016/j.biortech.2017.11.058.

[26] Román S, Libra J, Berge N, Sabio E, Ro K, Li L, et al. Hydrothermal carbonization: Modeling, final properties design and applications: A review. Energies 2018;11:1–28. https://doi.org/10.3390/en11010216.

[27] Álvarez-Murillo A, Román S, Ledesma B, Sabio E. Study of variables in energy densification of olive stone by hydrothermal carbonization. J Anal Appl Pyrolysis 2015;113:307–14. https://doi.org/10.1016/j.jaap.2015.01.031.

[28] Heilmann SM, Davis HT, Jader LR, Lefebvre PA, Sadowsky MJ, Schendel FJ, et al. Hydrothermal carbonization of microalgae. Biomass and Bioenergy 2010;34:875–82. https://doi.org/10.1016/j.biombioe.2010.01.032.

[29] Mumme J, Eckervogt L, Pielert J, Diakité M, Rupp F, Kern J. Hydrothermal carbonization of anaerobically digested maize silage. Bioresour Technol 2011;102:9255–60. https://doi.org/10.1016/j.biortech.2011.06.099.

[30] Danso-Boateng E, Shama G, Wheatley AD, Martin SJ, Holdich RG. Hydrothermal carbonisation of sewage sludge: Effect of process conditions on product characteristics and methane production. Bioresour Technol 2015;177:318–27. https://doi.org/10.1016/j.biortech.2014.11.096.

[31] Kannan S, Gariepy Y, Vijaya Raghavan GS. Optimization of the conventional hydrothermal carbonization to produce hydrochar from fish waste. Biomass Convers Biorefinery 2018;8:563–76. https://doi.org/10.1007/s13399-018-0323-9.

[32] Stutzenstein P, Bacher M, Rosenau T, Pfeifer C. Optimization of Nutrient and Carbon Recovery from Anaerobic Digestate via Hydrothermal Carbonization and Investigation of the Influence of the Process Parameters. Waste and Biomass Valorization 2018;9:1303–18. https://doi.org/10.1007/s12649-017-9902-4.

[33] El Ouadrhiri F, Elyemni M, Lahkimi A, Lhassani A, Chaouch M, Taleb M. Mesoporous Carbon from Optimized Date Stone Hydrochar by Catalytic Hydrothermal Carbonization Using Response Surface Methodology: Application to Dyes Adsorption. Int J Chem Eng 2021;2021. https://doi.org/10.1155/2021/5555406.

[34] Mohr A, Raman S. Lessons from first generation biofuels and implications for the sustainability appraisal of second generation biofuels. Effic Sustain Biofuel Prod Environ Land-Use Res 2015;63:281–310. https://doi.org/10.1016/j.enpol.2013.08.033.

[35] Strezov V, Patterson M, Zymla V, Fisher K, Evans TJ, Nelson PF. Fundamental aspects of biomass carbonisation. J Anal Appl Pyrolysis 2007;79:91–100. https://doi.org/10.1016/j.jaap.2006.10.014.

[36] Reißmann D, Thrän D, Bezama A. Hydrothermal processes as treatment paths for biogenic residues in Germany: A review of the technology, sustainability and legal aspects. J Clean Prod 2018;172:239–52. https://doi.org/10.1016/j.jclepro.2017.10.151.

[37] Reza MT, Lynam JG, Uddin MH, Coronella CJ. Hydrothermal carbonization: Fate of inorganics. Biomass and Bioenergy 2013;49:86–94. https://doi.org/10.1016/j.biombioe.2012.12.004.

[38] Swain PK, Das LM, Naik SN. Biomass to liquid: A prospective challenge to research and development in 21st century. Renew Sustain Energy Rev 2011;15:4917–33. https://doi.org/10.1016/j.rser.2011.07.061.

[39] Widjaya ER, Chen G, Bowtell L, Hills C. Gasification of non-woody biomass: A literature review. Renew Sustain Energy Rev 2018;89:184–93. https://doi.org/10.1016/j.rser.2018.03.023.

[40] Libra JA, Ro KS, Kammann C, Funke A, Berge ND, Neubauer Y, et al. Hydrothermal carbonization of biomass residuals: A comparative review of the chemistry, processes and applications of wet and dry pyrolysis. Biofuels 2011;2:71–106. https://doi.org/10.4155/bfs.10.81.

[41] Brosowski A, Thrän D, Mantau U, Mahro B, Erdmann G, Adler P, et al. A review of biomass potential and current utilisation – Status quo for 93 biogenic wastes and residues in Germany. Biomass and Bioenergy 2016;95:257–72. https://doi.org/10.1016/j.biombioe.2016.10.017.

[42] Milbrandt A, Seiple T, Heimiller D, Skaggs R, Coleman A. Wet waste-to-energy resources in the United States. Resour Conserv Recycl 2018;137:32–47. https://doi.org/10.1016/j.resconrec.2018.05.023.

[43] Peters JF, Banks SW, Bridgwater A V., Dufour J. A kinetic reaction model for biomass pyrolysis processes in Aspen Plus. Appl Energy 2017;188:595–603. https://doi.org/10.1016/j.apenergy.2016.12.030.

[44] FAO. Food wastage footprint. 2013.

[45] FAO. Food Wastage Footprint: Fool cost-accounting. 2014.

[46] Kaltschmitt M, Bridgwater A V. Biomass gasification and pyrolysis. State of the art and future prospects. 1997.

[47] Demirbas A. Biorefinery technologies for biomass upgrading. Energy Sources, Part A Recover Util Environ Eff 2010;32:1547–58. https://doi.org/10.1080/15567030902780394.

[48] Huiru Z, Yunjun Y, Liberti F, Bartocci P, Fantozzi F. Technical and economic feasibility analysis of an anaerobic digestion plant fed with canteen food waste. Energy Convers Manag 2019;180:938–48. https://doi.org/10.1016/j.enconman.2018.11.045.

[49] Ramzan N, Ashraf A, Naveed S, Malik A. Simulation of hybrid biomass gasification using Aspen plus: A comparative performance analysis for food, municipal solid and poultry waste. Biomass and Bioenergy 2011;35:3962–9. https://doi.org/10.1016/j.biombioe.2011.06.005.

[50] Bhutto AW, Qureshi K, Abro R, Harijan K, Zhao Z, Bazmi AA, et al. Progress in the production of biomass-to-liquid biofuels to decarbonize the transport sector-prospects and challenges. RSC Adv 2016;6:32140–70. https://doi.org/10.1039/c5ra26459f.

[51] IEA. World Energy Outlook 2021 - revised version October 2021 2021.

[52] IEA. World Energy Outlook 2016. 2016. https://doi.org/10.1111/j.1468-0319.1987.tb00425.x.

[53] Baliban RC, Elia JA, Floudas CA. Biomass and natural gas to liquid transportation fuels: Process synthesis, global optimization, and topology analysis. Ind Eng Chem Res 2013;52:3381–406. https://doi.org/10.1021/ie3024643.

[54] EIA. International Energy Outlook 2021. 2021.

[55] Arvidsson M, Haro P, Morandin M, Harvey S. Comparative thermodynamic analysis of biomass gasification-based light olefin production using methanol or DME as the platform chemical. Chem Eng Res Des 2016;115:182–94. https://doi.org/10.1016/j.cherd.2016.09.031.

[56] Haro P, Trippe F, Stahl R, Henrich E. Bio-syngas to gasoline and olefins via DME - A comprehensive techno-economic assessment. Appl Energy 2013;108:54–65. https://doi.org/10.1016/j.apenergy.2013.03.015.

[57] Doherty W, Reynolds A, Kennedy D. The effect of air preheating in a biomass CFB gasifier using ASPEN Plus simulation. Biomass and Bioenergy 2009;33:1158–67. https://doi.org/10.1016/j.biombioe.2009.05.004.

[58] Damartzis T, Michailos S, Zabaniotou A. Energetic assessment of a combined heat and power integrated biomass gasification-internal combustion engine system by using Aspen Plus®. Fuel Process Technol 2012;95:37–44. https://doi.org/10.1016/j.fuproc.2011.11.010.

[59] Sansaniwal SK, Pal K, Rosen MA, Tyagi SK. Recent advances in the development of biomass gasification technology: A comprehensive review. Renew Sustain Energy Rev 2017;72:363–84. https://doi.org/10.1016/j.rser.2017.01.038.

[60] Molino A, Larocca V, Chianese S, Musmarra D. Biofuels production by biomass gasification: A review. Energies 2018;11:1–31. https://doi.org/10.3390/en11040811.

[61] Sansaniwal SK, Rosen MA, Tyagi SK. Global challenges in the sustainable development of biomass gasification: An overview. Renew Sustain Energy Rev 2017;80:23–43.

https://doi.org/10.1016/j.rser.2017.05.215.

[62] Keche AJ, Gaddale APR, Tated RG. Simulation of biomass gasification in downdraft gasifier for different biomass fuels using ASPEN PLUS. Clean Technol Environ Policy 2015;17:465–73. https://doi.org/10.1007/s10098-014-0804-x.

[63] Matas Güell B, Sandquist J, Sørum L. Gasification of Biomass to Second Generation Biofuels: A Review. J Energy Resour Technol 2012;135. https://doi.org/10.1115/1.4007660.

[64] Gómez-Barea A, Leckner B. Modeling of biomass gasification in fluidized bed. Prog Energy Combust Sci 2010;36:444–509. https://doi.org/10.1016/j.pecs.2009.12.002.

[65] Pala LPR, Wang Q, Kolb G, Hessel V. Steam gasification of biomass with subsequent syngas adjustment using shift reaction for syngas production: An Aspen Plus model. Renew Energy 2017;101:484–92. https://doi.org/10.1016/j.renene.2016.08.069.

[66] van Steen E, Claeys M. Fischer-Tropsch catalysts for the biomass-to-liquid process. Chem Eng Technol 2008;31:655–66. https://doi.org/10.1002/ceat.200800067.

[67] Hamelinck CN, Faaij APC, den Uil H, Boerrigter H. Production of FT transportation fuels from biomass; technical options, process analysis and optimisation, and development potential. Energy 2004;29:1743–71. https://doi.org/10.1016/j.energy.2004.01.002.

[68] Titirici MM, Thomas A, Antonietti M. Back in the black: Hydrothermal carbonization of plant material as an efficient chemical process to treat the CO2 problem? New J Chem 2007;31:787–9. https://doi.org/10.1039/b616045j.

[69] Brown AB, McKeogh BJ, Tompsett GA, Lewis R, Deskins NA, Timko MT. Structural analysis of hydrothermal char and its models by density functional theory simulation of vibrational spectroscopy. Carbon N Y 2017;125:614–29. https://doi.org/10.1016/j.carbon.2017.09.051.

[70] Goudriaan F, Peferoen DGR. Liquid fuels from biomass via a hydrothermal process. Chem Eng Sci 1990;45:2729–34. https://doi.org/10.1016/0009-2509(90)80164-A.

[71] Kruse A, Dinjus E. Hot compressed water as reaction medium and reactant. Properties and synthesis reactions. J Supercrit Fluids 2007;39:362–80. https://doi.org/10.1016/j.supflu.2006.03.016.

[72] Weber K, Quicker P. Properties of biochar. Fuel 2018;217:240–61. https://doi.org/10.1016/j.fuel.2017.12.054.

[73] Smith AM, Whittaker C, Shield I, Ross AB. The potential for production of high quality bio-coal from early harvested Miscanthus by hydrothermal carbonisation. Fuel 2018;220:546–57. https://doi.org/10.1016/j.fuel.2018.01.143.

[74] Mihajlović M, Petrović J, Maletić S, Isakovski MK, Stojanović M,

Lopičić Z, et al. Hydrothermal carbonization of Miscanthus × giganteus: Structural and fuel properties of hydrochars and organic profile with the ecotoxicological assessment of the liquid phase. Energy Convers Manag 2018;159:254–63. https://doi.org/10.1016/j.enconman.2018.01.003.

[75] He C, Giannis A, Wang JY. Conversion of sewage sludge to clean solid fuel using hydrothermal carbonization: Hydrochar fuel characteristics and combustion behavior. Appl Energy 2013;111:257–66. https://doi.org/10.1016/j.apenergy.2013.04.084.

[76] Basso D, Patuzzi F, Castello D, Baratieri M, Rada EC, Weiss-Hortala E, et al. Agro-industrial waste to solid biofuel through hydrothermal carbonization. Waste Manag 2016;47:114–21. https://doi.org/10.1016/j.wasman.2015.05.013.

[77] Cai J, Li B, Chen C, Wang J, Zhao M, Zhang K. Hydrothermal carbonization of tobacco stalk for fuel application. Bioresour Technol 2016;220:305–11. https://doi.org/10.1016/j.biortech.2016.08.098.

[78] Machado NT, de Castro DAR, Santos MC, Araújo ME, Lüder U, Herklotz L, et al. Process analysis of hydrothermal carbonization of corn Stover with subcritical H2O. J Supercrit Fluids 2018;136:110–22. https://doi.org/10.1016/j.supflu.2018.01.012.

[79] Sabio E, Álvarez-Murillo A, Román S, Ledesma B. Conversion of tomato-peel waste into solid fuel by hydrothermal carbonization: Influence of the processing variables. Waste Manag 2016;47:122–32. https://doi.org/10.1016/j.wasman.2015.04.016.

[80] Codignole Luz F, Volpe M, Fiori L, Manni A, Cordiner S, Mulone V, et al. Spent coffee enhanced biomethane potential via an integrated hydrothermal carbonization-anaerobic digestion process. Bioresour Technol 2018;256:102–9. https://doi.org/10.1016/j.biortech.2018.02.021.

[81] Zhuang X, Zhan H, Huang Y, Song Y, Yin X, Wu C. Denitrification and desulphurization of industrial biowastes via hydrothermal modification. Bioresour Technol 2018;254:121–9. https://doi.org/10.1016/j.biortech.2018.01.061.

[82] Smith AM, Singh S, Ross AB. Fate of inorganic material during hydrothermal carbonisation of biomass: Influence of feedstock on combustion behaviour of hydrochar. Fuel 2016;169:135–45. https://doi.org/10.1016/j.fuel.2015.12.006.

[83] Escala M, Zumbühl T, Koller C, Junge R, Krebs R. Hydrothermal carbonization as an energy-efficient alternative to established drying technologies for sewage sludge: A feasibility study on a laboratory scale. Energy and Fuels 2013;27:454–60. https://doi.org/10.1021/ef3015266.

[84] Briesemeister L, Wittmann T, Gaderer M, Spliethoff H. Study of a decentralized entrained-flow gasification plant in combination with biomass from hydrothermal carbonization for CHP. 22nd Eur. Biomass Conf. Exhib., 2014, p. 458–61.

[85] Funke A, Ziegler F. Hydrothermal carbonization of biomass: A summary and discussion of chemical mechanisms for process engineering. Biofuels, Bioprod Biorefining 2010;4:160–77. https://doi.org/10.1002/bbb.198.

[86] Erlach B, Harder B, Tsatsaronis G. Combined hydrothermal carbonization and gasification of biomass with carbon capture. Energy 2012;45:329–38. https://doi.org/10.1016/j.energy.2012.01.057.

[87] Gai C, Chen M, Liu T, Peng N, Liu Z. Gasification characteristics of hydrochar and pyrochar derived from sewage sludge. Energy 2016;113:957–65. https://doi.org/10.1016/j.energy.2016.07.129.

[88] Feng Y, Yu T, Chen D, Xu G, Wan L, Zhang Q, et al. Effect of Hydrothermal Treatment on the Steam Gasification Behavior of Sewage Sludge: Reactivity and Nitrogen Emission. Energy and Fuels 2018;32:581–7. https://doi.org/10.1021/acs.energyfuels.7b03304.

[89] Gai C, Guo Y, Liu T, Peng N, Liu Z. Hydrogen-rich gas production by steam gasification of hydrochar derived from sewage sludge. Int J Hydrogen Energy 2016;41:3363–72. https://doi.org/10.1016/j.ijhydene.2015.12.188.

[90] Álvarez-Murillo A, Ledesma B, Román S, Sabio E, Gañán J. Biomass pyrolysis toward hydrocarbonization. Influence on subsequent steam gasification processes. J Anal Appl Pyrolysis 2015;113:380–9. https://doi.org/10.1016/j.jaap.2015.02.030.

[91] Gunarathne DS, Mueller A, Fleck S, Kolb T, Chmielewski JK, Yang W, et al. Gasification characteristics of hydrothermal carbonized biomass in an updraft pilot-scale gasifier. Energy and Fuels 2014;28:1992–2002. https://doi.org/10.1021/ef402342e.

[92] Tremel A, Stemann J, Herrmann M, Erlach B, Spliethoff H. Entrained flow gasification of biocoal from hydrothermal carbonization. Fuel 2012;102:396–403. https://doi.org/10.1016/j.fuel.2012.05.024.

[93] Islam MA, Kabir G, Asif M, Hameed BH. Combustion kinetics of hydrochar produced from hydrothermal carbonisation of Karanj (Pongamia pinnata) fruit hulls via thermogravimetric analysis. Bioresour Technol 2015;194:14–20. https://doi.org/10.1016/j.biortech.2015.06.094.

[94] Briesemeister L, Kremling M, Fendt S, Spliethoff H. Air-Blown Entrained Flow Gasification of Biocoal: Gasification Kinetics and Char Behavior. Energy and Fuels 2017;31:9568–75. https://doi.org/10.1021/acs.energyfuels.7b01611.

[95] Feng Y, Yu T, Ma K, Xu G, Hu Y, Chen D. Effect of Hydrothermal Temperature on the Steam Gasification Performance of Sewage Sludge: Syngas Quality and Tar Formation. Energy and Fuels 2018;32:6834–8. https://doi.org/10.1021/acs.energyfuels.8b00696.

[96] Lane DJ, Truong E, Larizza F, Chiew P, De Nys R, Van Eyk PJ. Effect of Hydrothermal Carbonization on the Combustion and

Gasification Behavior of Agricultural Residues and Macroalgae: Devolatilization Characteristics and Char Reactivity. Energy and Fuels 2018;32:4149–59. https://doi.org/10.1021/acs.energyfuels.7b03125.

[97] Hardi F, Imai A, Theppitak S, Kirtania K, Furusjö E, Umeki K, et al. Gasification of Char Derived from Catalytic Hydrothermal Liquefaction of Pine Sawdust under a CO2 Atmosphere. Energy and Fuels 2018;32:5999–6007. https://doi.org/10.1021/acs.energyfuels.8b00589.

[98] Briesemeister L, Kremling M, Fendt S, Spliethoff H. Air-Blown Entrained-Flow Gasification of Biocoal from Hydrothermal Carbonization. Chem Eng Technol 2017;40:270–7. https://doi.org/10.1002/ceat.201600192.

[99] Ulbrich M, Preßl D, Fendt S, Gaderer M, Spliethoff H. Impact of HTC reaction conditions on the hydrochar properties and CO2 gasification properties of spent grains. Fuel Process Technol 2017;167:663–9. https://doi.org/10.1016/j.fuproc.2017.08.010.

[100] Sevilla M, Fuertes AB. Chemical and structural properties of carbonaceous products obtained by hydrothermal carbonization of saccharides. Chem - A Eur J 2009;15:4195–203. https://doi.org/10.1002/chem.200802097.

[101] Titirici MM, Antonietti M, Baccile N. Hydrothermal carbon from biomass: A comparison of the local structure from poly- to monosaccharides and pentoses/hexoses. Green Chem 2008;10:1204–12. https://doi.org/10.1039/b807009a.

[102] Sevilla M, Fuertes AB. The production of carbon materials by hydrothermal carbonization of cellulose. Carbon N Y 2009;47:2281–9. https://doi.org/10.1016/j.carbon.2009.04.026.

[103] Falco C, Baccile N, Titirici MM. Morphological and structural differences between glucose, cellulose and lignocellulosic biomass derived hydrothermal carbons. Green Chem 2011;13:3273–81. https://doi.org/10.1039/c1gc15742f.

[104] Falco C, Perez Caballero F, Babonneau F, Gervais C, Laurent G, Titirici MM, et al. Hydrothermal carbon from biomass: Structural differences between hydrothermal and pyrolyzed carbons via 13C solid state NMR. Langmuir 2011;27:14460–71. https://doi.org/10.1021/la202361p.

[105] Jia X, Li M, Zhu J, Jiang Y, Wang Y, Wang Y. Enhancement split-phase hydrogen production from food waste during dark fermentation: Protein substances degradation and transformation during hydrothermal pre-treatments. Int J Hydrogen Energy 2019;44:17334–45. https://doi.org/10.1016/j.ijhydene.2018.12.199.

[106] Li Y, Liu H, Xiao K, Jin M, Xiao H, Yao H. Combustion and Pyrolysis Characteristics of Hydrochar Prepared by Hydrothermal Carbonization of Typical Food Waste: Influence of Carbohydrates, Proteins, and Lipids. Energy and Fuels 2020;34:430–9.

https://doi.org/10.1021/acs.energyfuels.9b02940.

[107] Ravber M, Knez Z, Škerget M. Hydrothermal degradation of fats, carbohydrates and proteins in sunflower seeds after treatment with subcritical water. Chem Biochem Eng Q 2015;29:351–5. https://doi.org/10.15255/CABEQ.2015.2193.

[108] Teri G, Luo L, Savage PE. Hydrothermal treatment of protein, polysaccharide, and lipids alone and in mixtures. Energy and Fuels 2014;28:7501–9. https://doi.org/10.1021/ef501760d.

[109] Cheng F, Cui Z, Chen L, Jarvis J, Paz N, Schaub T, et al. Hydrothermal liquefaction of high- and low-lipid algae: Bio-crude oil chemistry. Appl Energy 2017;206:278–92. https://doi.org/10.1016/j.apenergy.2017.08.105.

[110] Kruse A, Funke A, Titirici MM. Hydrothermal conversion of biomass to fuels and energetic materials. Curr Opin Chem Biol 2013;17:515–21. https://doi.org/10.1016/j.cbpa.2013.05.004.

[111] Chen X, Ma X, Peng X, Lin Y, Wang J, Zheng C. Effects of aqueous phase recirculation in hydrothermal carbonization of sweet potato waste. Bioresour Technol 2018;267:167–74. https://doi.org/10.1016/j.biortech.2018.07.032.

[112] Picone A, Volpe M, Giustra MG, Bella G Di, Messineo A. Hydrothermal carbonization of lemon peel waste: Preliminary results on the effects of temperature during process water recirculation. Appl Syst Innov 2021;4. https://doi.org/10.3390/asi4010019.

[113] Zheng C, Ma X, Yao Z, Chen X. The properties and combustion behaviors of hydrochars derived from co-hydrothermal carbonization of sewage sludge and food waste. Bioresour Technol 2019;285:121347. https://doi.org/10.1016/j.biortech.2019.121347.

[114] Mazumder S, Saha P, McGaughy K, Saba A, Reza MT. Technoeconomic analysis of co-hydrothermal carbonization of coal waste and food waste. Biomass Convers Biorefinery 2020. https://doi.org/10.1007/s13399-020-00817-8.

[115] Bamminger C, Marschner B, Jüschke E. An incubation study on the stability and biological effects of pyrogenic and hydrothermal biochar in two soils. Eur J Soil Sci 2014;65:72–82. https://doi.org/10.1111/ejss.12074.

[116] Busch D, Stark A, Kammann CI, Glaser B. Genotoxic and phytotoxic risk assessment of fresh and treated hydrochar from hydrothermal carbonization compared to biochar from pyrolysis. Ecotoxicol Environ Saf 2013;97:59–66.

[117] Chu Q, Xue L, Singh BP, Yu S, Müller K, Wang H, et al. Sewage sludge-derived hydrochar that inhibits ammonia volatilization, improves soil nitrogen retention and rice nitrogen utilization. Chemosphere 2020;245:125558. https://doi.org/10.1016/j.chemosphere.2019.125558.

[118] Liu X, Cheng Y, Liu Y, Chen D, Chen Y, Wang Y. Hydrochar did not

reduce rice paddy NH3 volatilization compared to pyrochar in a soil column experiment. Sci Rep 2020;10:1–9. https://doi.org/10.1038/s41598-020-76213-z.

[119] Subedi R, Kammann C, Pelissetti S, Taupe N, Bertora C, Monaco S, et al. Does soil amended with biochar and hydrochar reduce ammonia emissions following the application of pig slurry? Eur J Soil Sci 2015;66:1044–53. https://doi.org/10.1111/ejss.12302.

[120] Ekpo U, Ross AB, Camargo-Valero MA, Fletcher LA. Influence of pH on hydrothermal treatment of swine manure: Impact on extraction of nitrogen and phosphorus in process water. Bioresour Technol 2016;214:637–44. https://doi.org/10.1016/j.biortech.2016.05.012.

[121] Ekpo U, Ross AB, Camargo-Valero MA, Williams PT. A comparison of product yields and inorganic content in process streams following thermal hydrolysis and hydrothermal processing of microalgae, manure and digestate. Bioresour Technol 2016;200:951–60. https://doi.org/10.1016/j.biortech.2015.11.018.

[122] Mihajlović M, Petrović J, Stojanović M, Milojković J, Lopičić Z, Koprivica M, et al. Hydrochars, perspective adsorbents of heavy metals: a review of the current state of studies. Zaštita Mater 2016;57:488–95.

[123] Raulino GSC, Vidal CB, Lima ACA, Melo DQ, Oliveira JT, Nascimento RF. Treatment influence on green coconut shells for removal of metal ions: Pilot-scale fixed-bed column. Environ Technol (United Kingdom) 2014;35:1711–20. https://doi.org/10.1080/09593330.2014.880747.

[124] Ronix A, Pezoti O, Souza LS, Souza IPAF, Bedin KC, Souza PSC, et al. Hydrothermal carbonization of coffee husk: Optimization of experimental parameters and adsorption of methylene blue dye. J Environ Chem Eng 2017;5:4841–9. https://doi.org/10.1016/j.jece.2017.08.035.

[125] Erlach B, Wirth B, Tsatsaronis G. Co-Production of Electricity, Heat and Biocoal Pellets from Biomass: A Techno-Economic Comparison with Wood Pelletizing. Proc World Renew Energy Congr – Sweden, 8–13 May, 2011, Linköping, Sweden 2011;57:508–15. https://doi.org/10.3384/ecp11057508.

[126] Stemann J, Erlach B, Ziegler F. Hydrothermal carbonisation of empty palm oil fruit bunches: Laboratory trials, plant simulation, carbon avoidance, and economic feasibility. Waste and Biomass Valorization 2013;4:441–54. https://doi.org/10.1007/s12649-012-9190-y.

[127] Jimenez J, Latrille E, Harmand J, Robles A, Ferrer J, Gaida D, et al. Instrumentation and control of anaerobic digestion processes: a review and some research challenges. Rev Environ Sci Bio/Technology 2015;14:615–48.

[128] Xu F, Li Y, Ge X, Yang L, Li Y. Anaerobic digestion of food waste – Challenges and opportunities. Bioresour Technol 2018;247:1047–58. https://doi.org/10.1016/j.biortech.2017.09.020.

[129] Abbasi T, Tauseef SM, Abbasi SA. Anaerobic digestion for global warming control and energy generation - An overview. Renew Sustain Energy Rev 2012;16:3228–42. https://doi.org/10.1016/j.rser.2012.02.046.

[130] Van DP, Fujiwara T, Tho BL, Toan PPS, Minh GH. A review of anaerobic digestion systems for biodegradable waste: Configurations, operating parameters, and current trends. Environ Eng Res 2020;25:1–17. https://doi.org/10.4491/eer.2018.334.

[131] Rezaee M, Gitipour S, Sarrafzadeh M-H. Different pathways to integrate anaerobic digestion and thermochemical processes: Moving toward the circular economy concept. Environ Energy Econ Res 2020;4:57–67.

[132] Pecchi M, Baratieri M. Coupling anaerobic digestion with gasification, pyrolysis or hydrothermal carbonization: A review. Renew Sustain Energy Rev 2019;105:462–75. https://doi.org/10.1016/j.rser.2019.02.003.

[133] Wirth B, Reza T, Mumme J. Influence of digestion temperature and organic loading rate on the continuous anaerobic treatment of process liquor from hydrothermal carbonization of sewage sludge. Bioresour Technol 2015;198:215–22. https://doi.org/10.1016/j.biortech.2015.09.022.

[134] Erdogan E, Atila B, Mumme J, Reza MT, Toptas A, Elibol M, et al. Characterization of products from hydrothermal carbonization of orange pomace including anaerobic digestibility of process liquor. Bioresour Technol 2015;196:35–42. https://doi.org/10.1016/j.biortech.2015.06.115.

[135] Brown AE, Finnerty GL, Camargo-Valero MA, Ross AB. Valorisation of macroalgae via the integration of hydrothermal carbonisation and anaerobic digestion. Bioresour Technol 2020;312:123539. https://doi.org/10.1016/j.biortech.2020.123539.

[136] Aragón-Briceño C, Ross AB, Camargo-Valero MA. Evaluation and comparison of product yields and bio-methane potential in sewage digestate following hydrothermal treatment. Appl Energy 2017;208:1357–69. https://doi.org/10.1016/j.apenergy.2017.09.019.

[137] Mannarino G, Sarrion A, Diaz E, Gori R, De la Rubia MA, Mohedano AF. Improved energy recovery from food waste through hydrothermal carbonization and anaerobic digestion. Waste Manag 2022;142:9–18. https://doi.org/10.1016/j.wasman.2022.02.003.

[138] De la Rubia MA, Villamil JA, Rodriguez JJ, Mohedano AF. Effect of inoculum source and initial concentration on the anaerobic digestion of the liquid fraction from hydrothermal carbonisation of sewage sludge. Renew Energy 2018;127:697–704. https://doi.org/10.1016/j.renene.2018.05.002.

[139] Lohri CR, Zabaleta I, Rohr M, Baier U, Zurbrügg C. Improving the Energy-Related Aspects of Biowaste Treatment in an Experimental Hydrothermal Carbonization Reactor. Waste and Biomass

Valorization 2018;9:429–42. https://doi.org/10.1007/s12649-016-9746-3.

[140] Mäkelä M. Experimental design and response surface methodology in energy applications: A tutorial review. Energy Convers Manag 2017;151:630–40. https://doi.org/10.1016/j.enconman.2017.09.021.

[141] Kleijnen JPC. Sensitivity analysis and optimization in simulation: design of experiments and case studies. Winter Simul Conf Proc 1995:133–40. https://doi.org/10.1109/wsc.1995.478715.

[142] Montgomery DC. Design and Analysis of Experiments. John Wiley & Sons; 2013.

[143] Khuri AI, Mukhopadhyay S. Response surface methodology. Wiley Interdiscip Rev Comput Stat 2010;2:128–49. https://doi.org/10.1002/wics.73.

[144] Costa NR, Lourenço J, Pereira ZL. Desirability function approach: A review and performance evaluation in adverse conditions. Chemom Intell Lab Syst 2011;107:234–44. https://doi.org/10.1016/j.chemolab.2011.04.004.

[145] Van Soest PJ. Collaborative Study of Acid-Detergent Fiber and Lignin. J Assoc Off Anal Chem 2020;56:781–4. https://doi.org/10.1093/jaoac/56.4.781.

[146] Van Soest PJ, Robertson JB, Lewis BA. Methods for Dietary Fiber, Neutral Detergent Fiber, and Nonstarch Polysaccharides in Relation to Animal Nutrition. J Dairy Sci 1991;74:3583–97. https://doi.org/10.3168/jds.S0022-0302(91)78551-2.

[147] Anderson S. Soxtec: Its Principles and Applications. Oil Extr Anal 2019:11–24. https://doi.org/10.1201/9780429104527-2.

[148] Channiwala SA, Parikh PP. A unified correlation for estimating HHV of solid, liquid and gaseous fuels. Fuel 2002;81:1051–63. https://doi.org/10.1016/S0016-2361(01)00131-4.

[149] Chen WH, Lin BJ, Colin B, Chang JS, Pétrissans A, Bi X, et al. Hygroscopic transformation of woody biomass torrefaction for carbon storage. Appl Energy 2018;231:768–76. https://doi.org/10.1016/j.apenergy.2018.09.135.

[150] Śliz M, Wilk M. A comprehensive investigation of hydrothermal carbonization: Energy potential of hydrochar derived from Virginia mallow. Renew Energy 2020;156:942–50. https://doi.org/10.1016/j.renene.2020.04.124.

[151] Zhang Y, Guo Y, Cheng F, Yan K, Cao Y. Investigation of combustion characteristics and kinetics of coal gangue with different feedstock properties by thermogravimetric analysis. Thermochim Acta 2015;614:137–48. https://doi.org/10.1016/j.tca.2015.06.018.

[152] Madsen RB, Jensen MM, Mørup AJ, Houlberg K, Christensen PS, Klemmer M, et al. Using design of experiments to optimize derivatization with methyl chloroformate for quantitative analysis of

the aqueous phase from hydrothermal liquefaction of biomass. Anal Bioanal Chem 2016;408:2171–83. https://doi.org/10.1007/s00216-016-9321-6.

[153] Zwietering HM, Jongenburger I, Rombouts FM, Riet VK. Modeling of the Bacterial Growth Curve. Appl Environ Microbiol 1990;56:1875–81.

[154] Pramanik SK, Suja FB, Porhemmat M, Pramanik BK. Performance and kinetic model of a single-stage anaerobic digestion system operated at different successive operating stages for the treatment of food waste. Processes 2019;7. https://doi.org/10.3390/pr7090600.

[155] Lipovetsky S. Double logistic curve in regression modeling. J Appl Stat 2010;37:1785–93. https://doi.org/10.1080/02664760903093633.

[156] Zeki B. Food Processing Engineering Technology Guide. 2012.

[157] Gupta D, Mahajani SM, Garg A. Investigation on hydrochar and macromolecules recovery opportunities from food waste after hydrothermal carbonization. Sci Total Environ 2020;749:142294. https://doi.org/10.1016/j.scitotenv.2020.142294.

[158] Solomon PR. Relation between coal aromatic carbon concentration and proximate analysis fixed carbon. Fuel 1981;60:3–6. https://doi.org/10.1016/0016-2361(81)90023-5.

[159] Schobert H. Chemistry of fossil fuels and biofuels. Cambridge University Press; 2013.

[160] Lin Y, Ge Y, Xiao H, He Q, Wang W, Chen B. Investigation of hydrothermal co-carbonization of waste textile with waste wood, waste paper and waste food from typical municipal solid wastes. Energy 2020;210. https://doi.org/10.1016/j.energy.2020.118606.

[161] Sharma HB, Dubey BK. Co-hydrothermal carbonization of food waste with yard waste for solid biofuel production: Hydrochar characterization and its pelletization. Waste Manag 2020;118:521–33. https://doi.org/10.1016/j.wasman.2020.09.009.

[162] Volpe M, Fiori L. From olive waste to solid biofuel through hydrothermal carbonisation: The role of temperature and solid load on secondary char formation and hydrochar energy properties. J Anal Appl Pyrolysis 2017;124:63–72. https://doi.org/10.1016/j.jaap.2017.02.022.

[163] Schafer HNS. Factors affecting the equilibrium moisture contents of low-rank coals. Fuel 1972;51:4–9. https://doi.org/10.1016/0016-2361(72)90029-4.

[164] Senn TL, Alta RK. A review of Humus and Humic Acids. 1973.

[165] Dhanapal S, Sathish Sekar D. Enhanced in Vitro Propagation of Musa Accuminata Induced By Humic Acid From Coal Extract As Compared With Commercially Available Humic Acid Products. Int J Res Eng Technol 2014;03:300–7. https://doi.org/10.15623/ijret.2014.0307051.

[166] Ischia G, Fiori L, Gao L, Goldfarb JL. Valorizing municipal solid waste via integrating hydrothermal carbonization and downstream extraction for biofuel production. J Clean Prod 2021;289:125781. https://doi.org/10.1016/j.jclepro.2021.125781.

[167] Lucian M, Volpe M, Gao L, Piro G, Goldfarb JL, Fiori L. Impact of hydrothermal carbonization conditions on the formation of hydrochars and secondary chars from the organic fraction of municipal solid waste. Fuel 2018;233:257–68. https://doi.org/10.1016/j.fuel.2018.06.060.

[168] Gao L, Volpe M, Lucian M, Fiori L, Goldfarb JL. Does hydrothermal carbonization as a biomass pretreatment reduce fuel segregation of coal-biomass blends during oxidation? Energy Convers Manag 2019;181:93–104. https://doi.org/10.1016/j.enconman.2018.12.009.

[169] Sultana A, Novera TM, Islam MA, Limon SH, Islam MA. Multi-response optimization for the production of Albizia saman bark hydrochar through hydrothermal carbonization: characterization and pyrolysis kinetic study. Biomass Convers Biorefinery 2021. https://doi.org/10.1007/s13399-020-01182-2.

[170] Mäkelä M, Benavente V, Fullana A. Hydrothermal carbonization of lignocellulosic biomass: Effect of process conditions on hydrochar properties. Appl Energy 2015;155:576–84. https://doi.org/10.1016/j.apenergy.2015.06.022.

[171] Nizamuddin S, Mubarak NM, Tiripathi M, Jayakumar NS, Sahu JN, Ganesan P. Chemical, dielectric and structural characterization of optimized hydrochar produced from hydrothermal carbonization of palm shell. Fuel 2016;163:88–97. https://doi.org/10.1016/j.fuel.2015.08.057.

[172] Sweygers N, Somers MH, Appels L. Optimization of hydrothermal conversion of bamboo (Phyllostachys aureosulcata) to levulinic acid via response surface methodology. J Environ Manage 2018;219:95–102. https://doi.org/10.1016/j.jenvman.2018.04.105.

[173] Lühmann T, Wirth B. Sewage sludge valorization via hydrothermal carbonization: Optimizing dewaterability and phosphorus release. Energies 2020;13:1–16. https://doi.org/10.3390/en13174417.

[174] Wirth B, Mumme J. Anaerobic Digestion of Waste Water from Hydrothermal Carbonization of Corn Silage. Appl Bioenergy 2013;1. https://doi.org/10.2478/apbi-2013-0001.

[175] Chen Y, Cheng JJ, Creamer KS. Inhibition of anaerobic digestion process: A review. Bioresour Technol 2008;99:4044–64. https://doi.org/10.1016/j.biortech.2007.01.057.

Appendix

Appendix A. Complete data of proximate and ultimate analysis of food waste and hydrochar

Temp. (°C)	Time (min)	SL (%)	VM (%)	FC (%)	Ash (%)	C (%)	H (%)	S (%)	N (%)
Food waste			81.0	13.6	0.7	47.4	7.6	0.1	2.2
			86.5	4.5		47.5	7.7	0.1	2.4
180	20	15	81.7	14.6	1.3	61.3	7.3	0.0	3.5
			82.0	11.7		62.2	7.2	0.0	3.5
240	20	15	73.6	22.9	1.8	67.9	7.9	0.1	3.5
						67.9	8.3	0.1	3.4
180	60	15	76.2	19.1	1.5	62.6	7.0	0.0	4.0
			77.7	16.3		61.3	6.9	0.0	3.9
240	60	15	75.4	22.2	1.4	70.1	7.4	0.0	3.6
						70.3	7.4	0.0	3.4
180	20	25	76.8	18.0	1.5	57.1	7.3	0.0	3.8
			76.4	20.1	0.8	57.6	6.7	0.0	3.7
240	20	25	72.5	24.5	1.5	67.8	6.9	0.1	3.8
						65.4	6.8	0.0	3.4
180	60	25	74.2	21.7	1.2	61.0	6.9	0.2	3.9
			73.3	21.6		58.4	6.8	0.1	3.7
240	60	25	71.2	24.9	2.0	67.2	7.7	0.0	3.6
						67.6	7.9	0.0	3.5
159.5	40	20	79.8	13.9	2.3	51.3	6.6	0.1	3.2
			77.9	8.6		49.8	6.3	0.0	3.1
260.5	40	20	72.0	25.5	1.2	70.9	8.0	0.0	3.6
			72.4	22.5		71.1	9.1	0.0	3.7
210	6.4	20	74.5	21.9	1.0	63.6	8.2	0.1	3.8
			78.0	15.9		63.7	8.7	0.1	3.5
210	73.6	20	72.2	22.7		65.4	8.4	0.0	3.2
						65.4	8.4	0.0	3.2
210	40	11.6	72.6	24.2	1.2	66.9	6.8	0.0	3.4
			73.6	23.0	0.9	67.3	7.1	0.0	3.2
210	40	28.4	71.2	24.3	1.8	63.9	7.2	0.1	3.6
						62.5	6.4	0.1	3.5
210	40	20	72.2	24.5	1.0	64.4	8.5	0.0	3.2
			75.6	19.0		64.9	7.9	0.0	3.4
210	40	20	71.2	24.3	1.6	65.9	8.4	0.0	3.2
			72.9	21.1		65.3	8.2	0.0	3.3
210	40	20	73.2	23.6	0.9	66.9	8.5	0.1	3.7

			78.8	15.8		64.8	8.2	0.1	3.7
210	40	20	71.2	25.5	0.8	65.9	7.8	0.1	3.3
			72.2	22.2		66.0	7.0	0.0	3.3
210	40	20	72.5	24.3	0.7	65.3	7.8	0.0	3.4
						65.3	7.7	0.0	3.3
210	40	20	73.8	23.4	0.3	65.2	6.7	0.0	3.8
			73.2	23.3	1.2	64.8	6.8	0.0	3.6

Appendix B. Descriptive statistic of data used in DOE.

Variable	Mean	SE Mean	StDev	Variance	CoefVar	Sum of Squares	MSSD
FC (%)	20.778	0.778	3.479	12.101	16.74	8864.138	15.606
VM (%)	76.851	0.697	3.118	9.725	4.06	118306.004	13.003
Ash(%)	1.847	0.135	0.604	0.365	32.69	75.191	0.128
C (%)	65.797	0.991	4.433	19.649	6.74	86959.104	31.004
H (%)	7.699	0.157	0.702	0.493	9.12	1194.977	0.405
O (%)	23.38	1.20	5.36	28.70	22.92	11476.49	43.84
N (%)	3.5885	0.0489	0.2189	0.0479	6.10	258.4533	0.0493

Variable	Mean	SE Mean	StDev	Variance	CoefVar	Sum of Squares	MSSD
SY (%)	56.90	2.00	8.93	79.75	15.70	66256.01	88.59
HHV (MJ/Kg)	28.825	0.634	2.834	8.034	9.83	16770.250	11.502
ED	1.3950	0.0311	0.1392	0.0194	9.98	39.2884	0.0283
EY (%)	78.49	1.44	6.44	41.50	8.21	123986.49	26.75
H/C	1.4062	0.0251	0.1125	0.0126	8.00	39.7858	0.0103
O/C	0.2721	0.0198	0.0886	0.0079	32.57	1.6296	0.0117
Ash yield(%)	56.73	1.98	8.84	78.19	15.59	65847.08	87.01
N yield (%)	84.40	2.27	10.17	103.40	12.05	144429.70	112.72
C yield (%)	76.18	1.47	6.57	43.16	8.62	116877.77	32.16
Humic acids (%)	22.301	0.972	4.346	18.892	19.49	10305.401	22.394
EMC (%)	4.180	0.365	1.633	2.668	39.08	400.165	3.624